Experimental studies on analysis, performance, emissions and combustion characteristics of Carbon blends as fuel in a CI Engine

A Thesis

Submitted by

ARUN KUMAR WAMANKAR

(Roll Number: 511ME128)

In Partial Fulfillment of the
Requirement for the Degree

of

DOCTOR OF PHILOSOPHY

Under the Supervision of

PROF. S. MURUGAN

Associate Professor

Department of Mechanical Engineering
National Institute of Technology,
Rourkela -769008
India
November 2015

Department of Mechanical Engineering
National Institute of Technology,
Rourkela –769008
India

CERTIFICATE

This is to certify that the thesis entitled "**Experimental studies on analysis, performance, emissions and combustion characteristics of Carbon blends as fuel in a CI Engine**" being submitted by **Mr. Arun Kumar Wamankar (511ME128)** for the award of Ph.D. degree is a record of bonafide research carried out by him in the Mechanical Engineering Department, National Institute of Technology, Rourkela, under my guidance and supervision. To the best of my knowledge, the results presented in this thesis have not been submitted to any other University or Institute for the award of any degree or diploma.

Supervisor
Prof. S. Murugan
Associate Professor
Department of Mechanical Engineering
National Institute of Technology
Rourkela- 769008

ACKNOWLEDGEMENT

I would like to express my heartfelt and sincere thanks to my supervisor **Prof. S. Murugan, Associate Professor,** Department of Mechanical Engineering for giving me an opportunity to work in this interesting research work. As my supervisor, he constantly forced me to remain focused on achieving my goal. His observations and comments helped me to establish the overall direction of the research, and to move forward with the investigations in depth. I am also thankful for his valuable guidance, inspiration, constant encouragement, heartfelt good wishes, and support through all the phases my research work.

I am ever grateful to **Prof. R.K. Sahoo**, Director who motivated me to do research work in NIT Rourkela, and given me a support all time during study. I also sincerely thank **Prof. S. S. Mohapatra**, Head, Department of Mechanical Engineering for their valuable advice to complete my research work successfully.

I take this opportunity to sincerely acknowledge and thank my Doctoral Scrutiny Committee Chairman **Prof. K.P. Maity** and members, **Prof. R.K. Sahoo**, Mechanical Engineering Department, **Prof. K.C. Patra**, Civil Engineering Department, and **Prof. Mithilesh Kumar**, Metallurgical and Materials Engineering Department, who have provided encouraging and constructive feedback and suggestions whenever required. And also, I thank to **Prof. Ashok Kumar Satapathy,** Department of Mechanical Engineering, for his valuable advice and support to complete my research work. I also thank many anonymous reviewers from various Journals, for their valuable comments which have helped me to improve the quality of manuscript during publications of the research article.

I would like to thank our technical staff members **Mr. N.P. Barik**, **Mr. Ramkrishna Mandal**, and **Mr. Chandra Sekhar Mohanty,** and other administrative staff who have been kind enough to help in their respective roles. I also thank my all research colleagues and friends for providing support and friendship that I needed.

I would like to thank my parents, brother, sisters, brother-in-law's, especially, to my wife Mrs. Padmaja, son Samarth and daughter Eashita for their great support, patience and unconditional love during my good and bad times. Above all, I owe it all to Almighty God for granting me the wisdom, health and strength to undertake this research task and enabling me to its completion.

(Arun Kumar Wamankar)

ABSTRACT

Pyrolysis is a method to convert organic substances into useful energy by thermal decomposition. In pyrolysis, the organic substances are thermally degraded to get value added products, which are principally pyrolysis oil, pyrogas, and carbon black or char. Recently, many pilot and demonstrated pyrolysis plants have been installed in many countries. In a practical pyrolysis plant, four principal products are obtained; they are Tyre pyrolysis oil (TPO), pyrogas, carbon black (CB) and steel wire. The CB obtained from a tyre pyrolysis plant possesses a considerable amount of energy, which can be used as an alternative energy source for heat and power applications.

Carbon black (CB) is one of the products obtained from a tyre pyrolysis plant [M/S Agrwal & Agrwal Co. Rourkela] and disposed in large quantities in plant sites or open land, causing a severe environmental pollution. Reuse and recycling are better options to derive energy or value added products from waste substances and to minimize the disposal problems. The CB is a sloid fuel possesses a considerable heating value of 32.8 MJ/kg in it. In this investigation, the possibility of using it as a solid alternative fuel as coal, charcoal water slurry fuel and orange skin powder for CI engines has been explored. For this purpose, two different fuels; (i) Carbon black-diesel slurry (Carbodiesel) with a heating value of 42.7-40.7 MJ/kg, and (ii) Carbon black-water-diesel (CBWD) emulsion with heating value range of 41.77-40.1 MJ/kg, were prepared by adopting methods as well as the CB was taken at different proportions from 5% to 20% on the volume basis. The net heating value of diesel is 43 MJ/kg. The CB powder was mixed with diesel at 80^{o}C and continuously stirred about 15 minutes using a mechanical stirrer to get a slurry, and tested at different load conditions in a single cylinder, air cooled, direct injection (DI), diesel engine with developing power of 4.4 kW at 1500 rpm. A small capacity 4.4 kW direct injection Diesel engine was selected, which is widely used in agriculture, small and medium scale industries for energy applications. Since, this is an early stage of investigation, a small powered diesel engine which is used for irrigation purpose in India.

Initially, the CB was doped with diesel by following a certain sequential processes (fuel prepration process), and the mixture was commonly referred to as Carbodiesel. The mixture containing on the volume basis 5% CB was denoted as Carbodiesel5. Similarly, on the volume basis 10%, 15% and 20% CB in Carbodiesel were denoted as Carbodiesel10,

Carbodiesel15 and Carbodiesel20 respectively. All the four Carbodiesels were tested as alternative fuels in a DI diesel engine. The brake thermal efficiency for all the Carbodiesels was found to be lower than that of diesel at all load. This may be due to the lower calorific value and poor air-fuel mixing in the combustion chamber of Carbodiesels. And also, the heat release rate was marginally lower for the all Carbodiesels compared to that of diesel at full load due lower incomplete combustion. The NO emission of the all Carbodiesel is higher compared to diesel. This may be probably due to the lower heat release rate as a results inferior combustion. The results indicated that, Carbodiesel10 gave better performance and lower emissions compared to those of Carbodiesel15 and Carbodiesel20 at full load. A maximum 10% of diesel can be replaced by Carbodiesel10, when it is used as a fuel in the diesel engine, without any major modification in the engine. After the comparison of Carbodiesel5, Carbodiesel10, Carbodiesel15 and Carbodiesel20 with Diesel, on the basis of experimental results and 10% diesel replacement with CB, I have chosen Carbodiesel10 as an optimum blend which was further used as a fuel the investigations.

Secondly, Carbodiesel10 was chosen as optimum which was tested in the same engine at different injection timings of two advanced and retarded injection timings for a maximum of 3 degree crank angle (^{o}CA) at a regular interval of 1.5^{o}CA, from the original injection timings of 23^{o}CA bTDC. Based on the thickness of shim the interval of injection timing was changed to 1.5^{o}CA for each shim. There are 3 shim provided by manufacture (23^{o}CA original injection timing), in which only 2 shim can be removed for changing the injection timing. Hence, the maximum change of the injection timing was 3^{o}CA. More importantly optimising injection timing will help to further optimise other engine parameters when compared to the standard injection timing of 23^{o}CAbTDC, and other injection timings tested for Carbodiesel10, the advanced injection timing of 26^{o}CAbTDC exhibited the brake thermal efficiency higher by about 5.9% than that of diesel at full load. This may be due to more fuel accumulated in combustion chamber, lower ignition delay and earlier fuel injected in chamber. The carbon monoxide (CO) and unburnt hydrocarbon (HC) emissions for the Carbodiesel10 at 26^{o}CABTD advanced injection timing was found to be lower by about 36.2% and 40.6% compared to that of original injection timing. This may be due to the higher cylinder temperature and increased oxidation between the carbon and oxygen molecules, and the conversion into carbon dioxide and earlier strat of combustion relative to the TDC. The heat release rate was also found to be higher by about 1% than that of original injection timing at full load, may be due to more accumulation of air mixture in the delay period.

After the analysis of the results, it was understood that a few problems occurred because CB is solid fuel, which were mainly (i) long-time stability problem, (ii) poor spray formation and (iii) higher NO emission. Research works indicated that a solid fuel can be used with water in the form of emulsion, which can reduce the nitric oxide (NO) emission. Therefore, as a next third technique, four different emulsions of CB-water-diesel were prepared with the help of a surfactant, by varying the percentages of the CB. The CB obtained from a pyrolysis plant was dried in direct sunlight for one day, to remove the moisture in it. The CB was then crushed manually by hammering, to get it in the form of powder. Then, the powder was further classified by a sieve to get a fine powder size of 40m. At first, diesel was mixed with water proportionally with the help of a surfactant Tween-20. Further, the CB powder was mixed diesel + water + surfactant with the emulsion at room temperature and continuously stirred for 15 min to get the emulsion. Surfactant process is used to mix two liquid of different density and surface tension. Surfactants are compounds that lower the surface tension of liquid that decrease the interfacial tension between two liquids. It is normal water. Initially, diesel was mixed with the water proportionally with the help of a surfactant Tween-20. The purpose of additing water with the CB is to increase fluidity and surface tension.An emulsion containing on the volume basis 5% CB was denoted as CBWD5. Similarly, on the volume basis 10%, 15% and 20% CB in the emulsion were denoted as CBWD10, CBWD15 and CBWD20, respectively. The emulsions were tested in the same engine. For all the CBWD emulsions the heat release rate, and cylinder pressure were found to be lower compared to than that diesel. This may be due to lower heating value, lower cetane number, higher density fuel and improper air-fuel mixing combustion. The NO emission was found to be lower in the range between 16% - 42% for all the emulsions, compared to that of diesel at full load. This may be due to lower combustion temperature caused by the lower heat release rate in the premixed combustion. The NO emission of the all Carbodiesels are higher compared to that of diesel. This may probably be due to the lower heat release rate as a results inferior combustion.

The CBWD10 emulsion was chosen as an optimum emulsion based on the performance and emissions of the engine tested at different loads. Further, more the engine was operated different injection timings. Based on the thickness of shim the interval of injection timing was changed to 1.5^{o}CA for each shim. There are 3 shim provided by manufacture (23^{o}CA original injection timing), in which only 2 shim can be removed for changing the injection

timing. Hence, the maximum change of the injection timing was 3^{o}CA. The brake thermal efficiency at full load for the CBWD10 emulsion operated at 26^{o}CAbTDC were higher by about 1.3% and 2.3% than that of diesel, and the CBWD10 emulsion at the original injection timing respectively. At advanced injection timing the peak pressure is reached closer to TDC, which results in higher effective pressure to do work, which leads to the higher brake thermal efficiency. Retarded injection timings brake thermal efficiency is lower than that of original injection timing because lower heat release rate and in complete combustion. The NO emission was found to be lower by about 21% compared to that of diesel at full load. This may be due to presence of water in the emulsion and the lower incylinder temperature.

Further, as a fourth technique the combined effect of compression ratio, nozzle opening pressure and injection timing were studied for the engine run on the CBWD10 emulsion. The CBWD10 emulsion was tested in the same diesel engine subjected to different compression ratios viz; 16.5, 17.5 and 18.5, injection timings viz; 23, 24.5 and 26^{o}CAbTDC and nozzle opening pressures viz; 200, 220 and 240 bar. Compression ratio was changed by changing the clearance volume by inserting gaskets of different thicknesses between the cylinder and cylinder head. Compression ratios below 16.5 led to a poor power output, and ratios above 18.5 were not possible, due to engine structural constraints. An increase of fuel nozzle opening pressure was required to enhance the fuel atomization at the nozzle outlet, resulting in more distributed vapor phase, which improves mixing. Further, increase in the nozzle opening pressure, results in a lower maximum heat release rate due to lesser air entrainment, since the fuel droplets are finer and they do not find air to form a homogeneous mixture. Initially, the nozzle opening pressure of the engine was kept as 200 bar (as set by the manufacturer), The nozzle opening pressure was varied from 200 bar to 240 bar in intervals of 20 bar, and the nozzle opening pressure was varied by tightening or loosening the screw of the injector, to a maximum possible (i.e. 240 bar and 180 bar respectively). Lower nozzle opening pressure was not chosen as viscosity of fuel was higher. The engine exhibited an improved combustion, performance and lower emissions, when the engine were operated with a higher compression ratio of 18.5 with the advanced injection timing of 26^{o}CA bTDC, and 220 bar nozzle opening pressure. At 18.5 compression ratio, the heat release rate was found to be higher by about 9% and the BTE was also found to be higher by about 5.1% than that diesel, at full load. This may be improve the combustion and attributed to the greater accumulation of fuel, because of the ignition delay as the injection of fuel take place earlier in the compression process. And also air-fuel takes a shorter duration for proper formation in

combustion process and resulting in improved brake thermal efficiency. The CO and HC emissions were reduced by about 46.2% and 35% respectively for the CBWD10 emulsion at 18.5 compression ratio with the advanced injection timing of 26^{o}CA bTDC, and 220 bar nozzle opening pressure at full load respectively. This may be due to increase better and more complete combustion of the fuel and improved fuel atomizing characterstics in the cylinder chamber.

An attempt was also made to improve the engine performance by inducing more turbulence in the combustion chamber. In the next technique, the CBWD10 emulsion was tested with a modification of the piston arrangement. The CBWD10 emulsion fuelled engine ran successfully with the internal jet piston without any noise. The maximum heat release rate for the CBWD10 with the internal jet piston was found to be higher by about 1.9% than that of the original piston engine. This may be due to the shorter ignition delay and better mixture formation of fuel and air as a results higher turbulence motion of air in the combustion chamber by the internal jets. The turbulence due to internal jet piston resulted in improvement in brake thermal efficiency using the CBWD10 which was 1.3% higher compared to that of base engine. The CO and HC emissions were reduced by about 23.5% and 7.2% respectively for the CBWD10 emulsion with the internal jet piston compared to that of the engine run with the conventional piston. This may be due to better mixture formation of the air and fuel by the jets, which leads to complete combustion.

The experimental results of the engine run on the CBWD10 emulsion were also validated with a two zone model, using a MATLAB software program. Using the two zone combustion model, the combustion parameters such as ignition delay, heat release rate, heat transfer and fuel spary, and the chemical equilibrium such as CO, HC and NO, formation composition were determined theoretically. The combustion and emission parameters as calculated from the model showed a minor deviation from the experimental results. The cylinder pressure values showed a deviation of around 8.3%, Simulation results of cylinder pressure is closer to the experimental value due to the proper combustion of the fuel which is find out with the validation work. While deviation of heat release rate and mass fraction of fuel burnt were approximately 2.3% and 13.24% respectively. Due to higher carbon percentage mass fraction burned were lower for CB blends and CBWD emulsion. The NO, CO, HC and smoke emissions showed mean deviations of 3.4%, 21.5%, 3.8 and 3.8% respectively from the theoretical results.

From this investigation, it is summarised that the CB can be used as alternative fuel for CI engine at low percentage when doped with diesel, the emissions were high compared to the CBWD emulsions. Further investigations are required to reduce emissions and also investigate durability tests when the engine is run on CBWD10 emulsion.

Key words: Carbodiesel, CBWD emulsion, injection timing, nozzle opening pressure, compression ratio, Internal jet piston, combustion, performance and emission.

CONTENTS

LIST OF FIGURES

LIST OF TABLES

NOMENCLATURE

Symbol	Discription
a	length of crank
A_f	arrhenius constant
B	bore diameter
BDC	bottom dead centre
BSEC	brake specific energy consumption
BTE	brake thermal efficiency
CA	Crank angle
CB	carbon black
CBWD	carbon black-water-diesel
C_D	discharge coefficient
CI	compression ignition
CO	carbon monoxide
CR	compression ratio
C_p	specific heat at constant pressure
cst	centistroke
Cv	specific heat at constant volume
CV	calorific value
DI	direct injection
E	internal energy
EGT	exhaust gas temperature
h	enthalpy
HC	hydrocarbon
IJP	internal jet piston
Kg	kilo gram
l	length of connecting rod
m	mass of fuel/air
ML	Mili liter
$\dot{m}$	rate of mass transfer
n	number of moles
p	pressure

Q_L	heat loss
$\dot{Q}$	heat generated
R_{mol}	molar gas constant
SMD	sauter mean diameter
Symbol	**Discription**
T	temperature
TDC	top dead centre
TPO	tyre pyrolysis oil
V	instantaneous volume of cylinder
Vc	clearance volume
Vs	stroke volume
W	work done
X	instantaneous position of piston
$\frac{dp}{d\theta}$	rate of pressure rise
γ	ratio of specific heat
θ	crank angle
^{o}CAbTDC	degree crank angle before top dead centre
^{o}C	degree centigrade
Subscript	
a	air zone
b	burning zone
cyl	of the cylinder
f	dissociation
inj	formation
inst	instantaneous
t	per second (time)
1	at state 1
2	at state 2

CHAPTER 1
INTRODUCTION

1.1 General

According to a report released by the Intergovernmental Panel on Climate Change (IPCC) in 2015, since year 1880 the average global temperature on Earth has increased by about 0.8^{o}C per decade [1], as a result of global warming. The main cause for global warming is the increased greenhouse gases (GHGs) resulting from human activity; primarily, the burning of fossil fuels, and other sources. In the current scenario, global warming cannot be totally avoided, but can be controlled to a certain extent. In the last two decades, different methods have been adopted to reduce the accumulation of GHGs in the atmosphere. These include; introduction of emission control devices, improving energy efficiency, introduction of a variety of cleaner and greener fuels, waste reduction and conversion of waste to energy. This chapter presents the concept of GHGs, their concentration in the atmosphere, the principle of their effect; global warming and ozone depletion, sources of global warming, methods to reduce anthropogenic gases, solid waste management, disposal of waste tyres; application of waste tyres, merits and demerits of waste tyres, solid fuels for IC engines, and the organization of this thesis.

1.2 Greenhouse gases (GHGs)

1.2.1 Basic information

The greenhouse effect is the natural process of the global warming of the earth. The primary GHGs in the earth's atmosphere are water vapor, carbon dioxide (CO_2), methane (CH_4), nitrous oxide (NO_x), and ozone [2]. GHGs greatly affect the temperature of the earth. The CO_2 enters the atmosphere through the burning of fossil fuels, solid waste, trees and wood products, and also as a result of certain chemical reactions. CH_4 is emitted during the production and transport of coal, natural gas, oil, livestock and other agricultural practices, and by the decay of organic waste in municipal solid waste landfills. The NO_x is emitted during agricultural and industrial activities, as well as during the combustion of fossil fuels and solid waste. Industrial processes, refrigeration, and the use of a variety of consumer products contribute to the emissions of fluorinated gases. Figure 1.1 portrays the GHGs present in the atmosphere in 2013 [3].

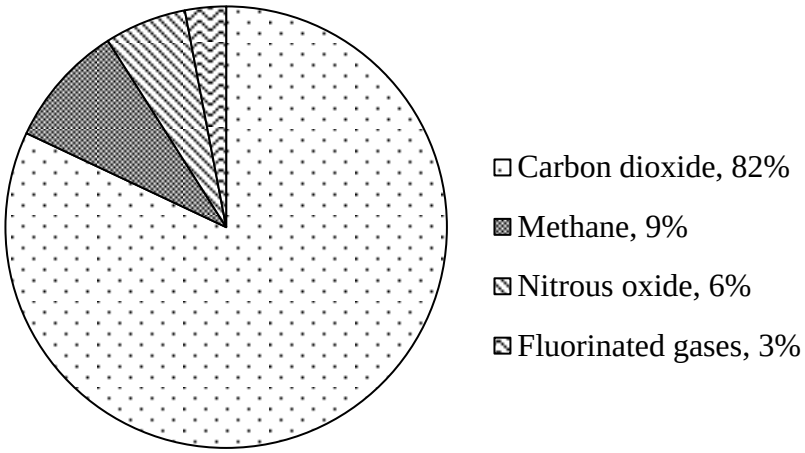

Figure 1.1 GHGs present in the atmosphere

It is apparent from the figure that, CO_2 is the major component of in the GHGs, which can be controlled to some extent in combustion devices. Figure 1.2 depicts the top 10 countries which emit CO_2 in the world during 2013.

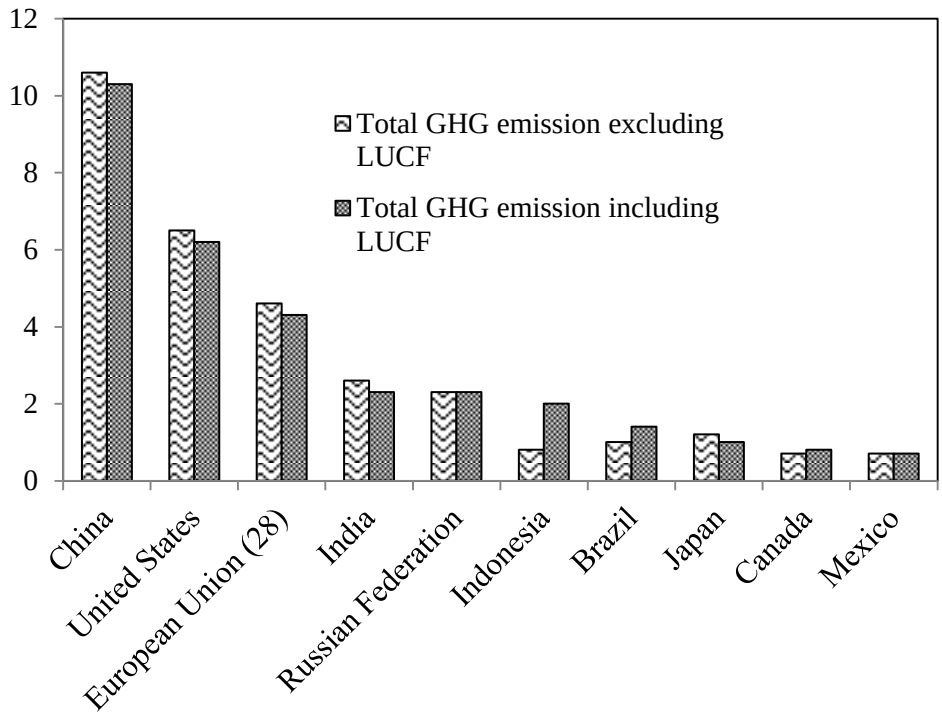

Figure 1.2 Top 10 countries that emit the highest CO_2 emission

LUCF refers to emissions stemming from land use change and forestry.

1.2.2 Greenhouse effect

The greenhouse effect is a process in which energy from the sun readily penetrates into the lower atmosphere and onto the surface of the earth. Without the greenhouse effect, radiation from the Sun in the form of visible light would travel to the Earth and be changed into heat, only to be lost in space. This principle is illustrated in Fig. 1.3.

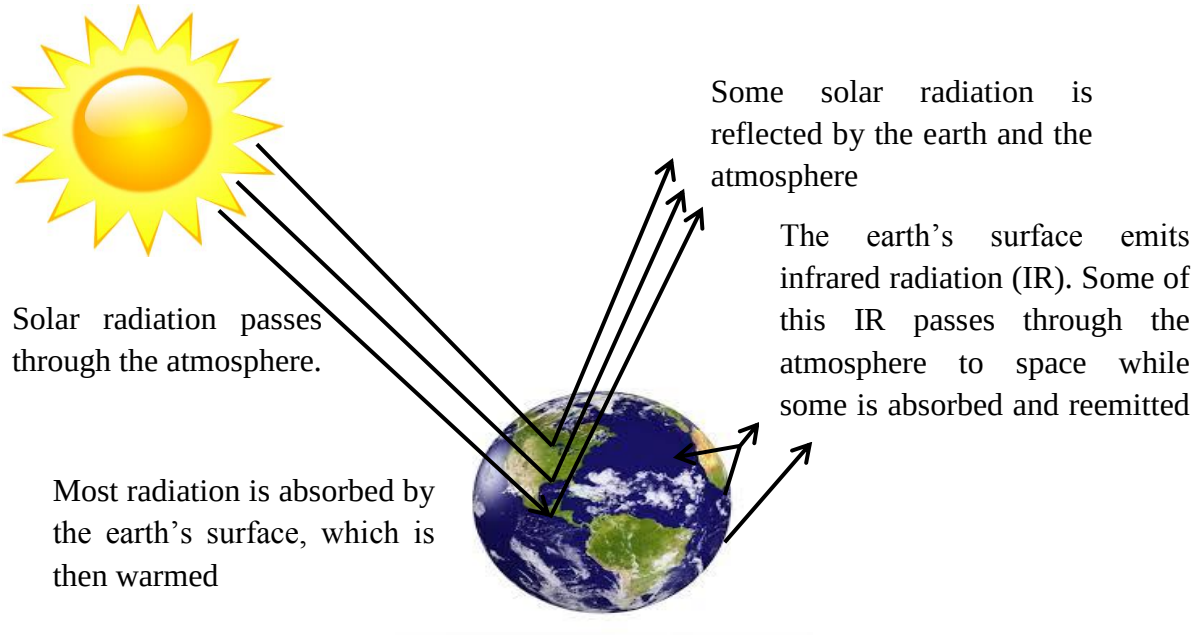

Figure 1.3 Radiation balance and the role of the greenhouse effect

The GHGs that are present in the atmosphere trap the heat radiated from the sun and warm up the planet. Due to the continuous accumulation of these gases in the atmosphere, the overall warming of the earth's surface also increases every year. This is called "global warming."

1.2.3 Global warming and Ozone depletion

As mentioned earlier, due to the accumulation of the GHGs in the atmosphere the earth's surface is warmed up. The relative measure of how much heat is trapped by the GHGs in the atmosphere is referred to as the global warming potential (GWP). The GWP of different gases are listed in Table 1.1. The term 'ozone hole' refers to the depletion of the protective layer over the earth's surface. Ozone (O_3) in the atmosphere absorbs ultraviolet radiation from the sun, thereby protecting living organisms that exist below the dangerous radiation. People, plants, and animals living under the ozone layer are harmed by the solar radiation that reaches the earth's surface, where it causes health problems from eye damage to skin cancer [4].

Table 1.1 Details of Greenhouse (GHG) gases

Greenhouse gases	**Chemical formula**	**Pre-industrial concentration**	**Concentration in 2015**	**Atmospheric lifetime (years)**	**Anthropogenic sources**	**Global warming potential (GWP)***
Carbon dioxide	CO_2	278000 ppbv	362000 ppbv	Variable	Fossil fuel combustion, land conversion, cement production	1
Methane	CH_4	700 ppbv	1792 ppbv	12.2+/- 3	Fossil fuels, Rice paddles, waste dump, livestock	21
Nitrous oxide	N_2O	275 ppbv	343 ppbv	120	Fertilizer industrial processes combustion	310
CFC-12	CCL_2F_2	0	0.612 ppbv	102	Liquid coolants, foams	6200-7100
HCFC-22	$CHCIF_2$	0	0.128 ppbv	12.1	Liquid coolants	1300-1400
Perfluoro- methane	CF_2	0	0.080 ppbv	50000	Production of aluminium	6500
Sulphur hexa-fluoride	SF_6	0	0.039 ppbv	3200	Dielectric fluid	23900

Note: pptv=1 part per trillion by volume; ppbv=1 part per billion by volume; ppmv= 1 part per million by volume

* = variation

Ozone depletion occurs when chlorofluorocarbons (CFCs) formerly found in aerosol spray cans and refrigerants are released into the atmosphere. These gases, through several chemical reactions, cause the ozone molecules to break down, reducing the ozone's ultraviolet (UV) radiation-absorbing capacity [5]. The ozone depleting potential (ODP) is the ratio of the calculated degradation of the ozone layer for each mass unit of a gas emitted into the atmosphere, relative to the calculated depletion of the reference gas CFC 11 (ODP = 1.0). The class I ODP substances are classified into 8 groups of refrigerants and chemicals, which are identified by the Environmental Protection Agency (EPA). It is reported that the GWP and ODP increase every year in the world.

1.2.4 Sources of global warming

The increase in the accumulation of GHGs is caused by anthropogenic (that is, resulting from human activities) or natural events. The different sources that cause global warming are illustrated in Fig. 1.4.

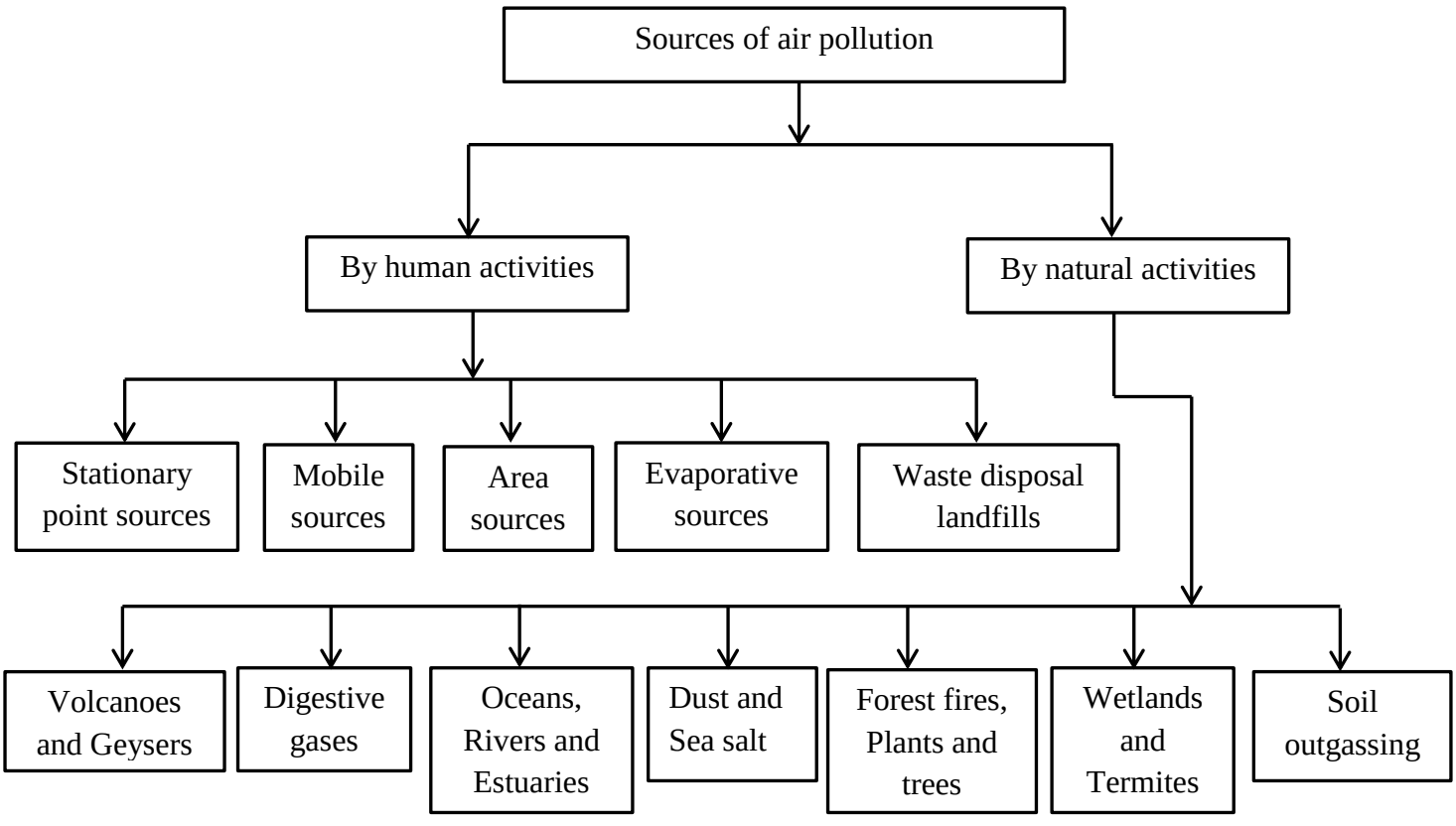

Figure 1.4 Sources of air pollution

The GHGs produced by anthropogenic activities can be controlled by appropriate mechanisms. Important human activities which can be controlled are described below.

1.2.4.1 Burning fossil fuels

The oxidation of carbon in organic matter and the combustion of carbon-based fuels produce CO_2, which is the most significant GHG emission, and is directly affected by anthropogenic activity. Fossil fuel combustion releases stored organic matter and reduces the ability of natural ecosystems to store carbon. The concentration of CO_2 is increasing at a rate of about 2–3 ppm/year and is projected to reach a range between 535 to 983 ppm by the end of the 21st century [6].

The largest human activity based source of CO_2 emissions is the combustion of fossil fuels. In 2011, it was estimated that combustion emitted about 33.2 billion tonnes of CO_2 worldwide [7]. The three majorly used fossil fuels are coal, natural gas and crude oil. Coal is the most carbon intensive fossil fuel. For every tonne of coal burned, approximately 2.5 tonnes of CO_2 are produced [8]. It is the largest fossil fuel source of CO_2 emissions. Coal is responsible for 43% of CO_2 emissions from fuel combustion, 36% is produced by oil and 20% from natural gas [8].

1.2.4.2 Cement manufacture

The cement industry produces around 5% of global man-made CO_2 emissions. When calcium carbonate is heated, it produces lime and carbon dioxide. CO_2 is also produced by the burning of fossil fuels that provide power to the cement manufacturing process. It is estimated that the cement industry produces around 5% of global man-made CO_2 emissions, of which 50% is produced from the chemical process itself, and 40% from the burning of fuel to power that process [9]. The increase in CO_2 emission from the year 2000 to 2014 is shown in Figure 1.5. It can be observed from the figure that the CO_2 emission has increased by about 12.2% from that of year 2000.

1.2.4.3 Farming and forestry

The use of change in land mainly through deforestation leads to more anthropogenic CO_2 emissions. Agricultural activities, wetland changes, pipeline losses, and vented subsurface landfill emissions, all lead to higher atmospheric concentrations of methane. The use of fertilizers can also lead to higher nitrous oxide (N_2O) concentrations.

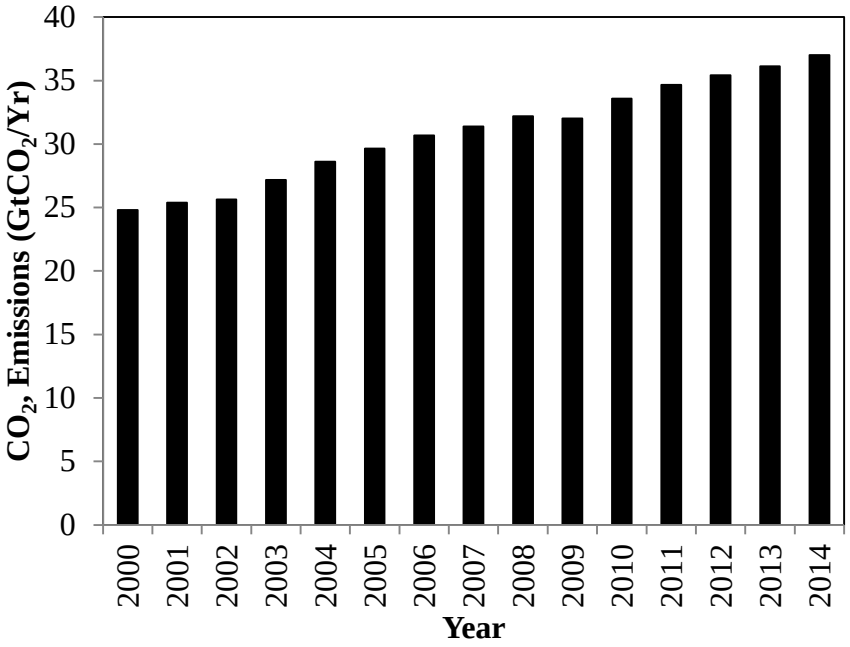

Figure 1.5 CO_2 emission increased by fossil fuel and from cement industries

1.2.4.4 Agriculture

Agricultural activities such as irrigation, livestock digestion, manure use, and paddy rice farming also contribute to the GHGs emissions. Various management practices for agricultural soils can lead to the production and emission of nitrous oxide. Smaller sources of emissions include rice cultivation, which produces CH_4, and burning crop residues, which produce CH_4 and N_2O.

1.2.4.5 Livestock

According to the United Nations (UN), livestock produces methane gas which is responsible for 18% of the world's GHGs emissions. This includes the effect of deforestation in order to create grazing land. Methane (CH_4) is produced by the enteric fermentation in the digestive tracts of ruminant animals such as cattle, goats, and sheep; and manure management [6].

1.2.4.6 Aerosols

Aerosols directly scatter and absorb solar radiation. The scattering of radiation causes atmospheric cooling, whereas absorption can cause atmospheric warming. Aerosols (particles suspended in the atmosphere), particularly sulphate aerosols from fossil fuel combustion, exert a cooling influence by reduced sunlight. The use of Chlorofluorocarbons (CFCs) in

refrigeration systems and the use of CFCs and halons in fire suppression systems and manufacturing processes have increased [10].

1.2.4.7 Disposed site

Waste disposal landfills create microbes, and chemical reactions act upon the waste and generate landfill gas that contains methane (CH_4) and carbon dioxide (CO_2) as well as small amounts of ammonia, mercaptans and other sulphides. These gases escapes from the landfill and is released into the atmosphere.

1.3 Methods to reduce GHGs

Different methods used for reducing or controlling anthropogenic gases are given below;

(i) Reduction of fossil fuel consumption. Many strategies have been applied for reducing CO_2 emissions from higher consumption of energy in homes, businesses, industry, and transportation.

(ii) Provision of efficient insulation of buildings.

(iii) Use of more fuel-efficient vehicles.

(iv) Using more efficient electrical appliances

(iv) Harnessing power from renewable sources of energy and the use of greener and cleaner fuels.

(v) Reducing personal energy use by turning off lights and electronics when not in use.

(vi) Effective solid waste management systems.

1.4 Solid waste management

The different methods of solid waste management are illustrated in Figure 1.6. Although wastes are available in the form of solids, liquids and gases, solid waste is available in a large quantity compared to liquid and gaseous wastes. Solid waste is the unwanted or useless solid material from various sources, such as domestic, industrial, and commercial, organic material, glass, metal, plastic paper etc. The management of solid waste reduces it's adverse impacts on the environment and human health, and supports economic development and improved quality of life. The solid waste disposed, is considerably larger than the waste liquids disposed every year. The disposal of solid waste affects the soil, air and water. The anthropogenic gases released from organic solid wastes are also one of the reasons for the increase in CO_2 emission. Therefore, it is essential to reduce or minimise the waste to control the anthropogenic gases.

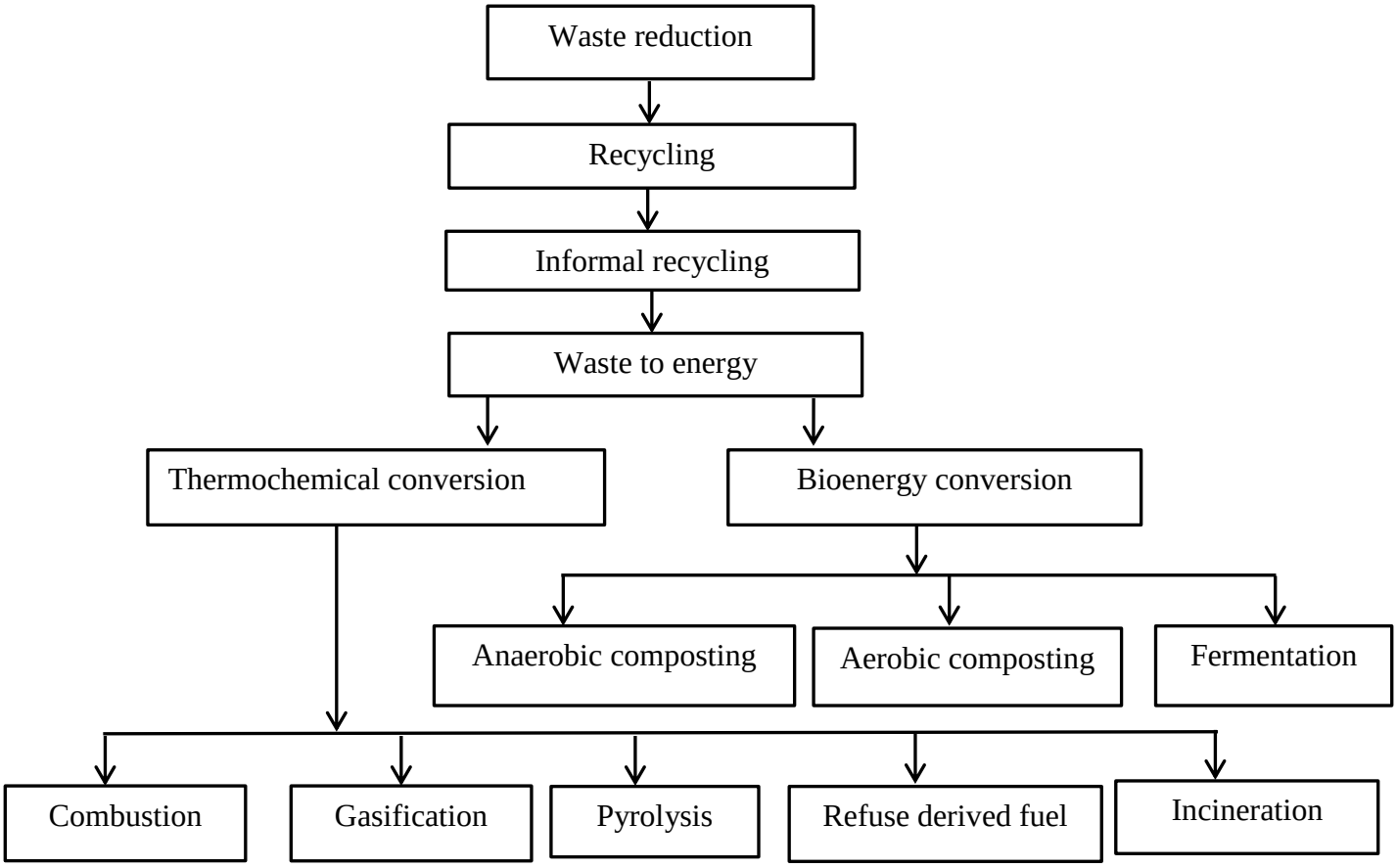

Figure 1.6 Solid waste management

1.4.1 Waste reduction

It eliminates the production of waste at the source of usual generation and reduces the demands for large scale treatment and disposal facilities. Some of the ways to reduce wastes include manufacturing products with less packaging, encouraging the public to choose reusable products, such as reusable plastic and glass containers, backyard composting and sharing, and donating any unwanted items rather than discarding them [11].

1.4.2 Recycling

Recycling refers to the removal of items from the waste stream to be used as raw materials in the manufacture of new products. Recycling occurs in three stages: in the first stage waste is sorted from the dumped sites; in the second stage, the recyclables are collected, and in the final stage, the recyclables are used to create raw materials. These raw materials are then used in the manufacturing of new products.

1.4.3 Waste to energy

'Waste to energy' is a popular term used worldwide nowadays, because it offers the following solutions; (i) minimisation of disposal problem (ii) production of energy and chemicals (iii) reduction of some of the GHGs. An organic waste originated from different wastes is generally used in this 'Waste to Energy' process. There are many varieties of organic substances available in the form of municipal, industrial and agriculture wastes in the world. In addition to these, biomass wastes can also be converted into useful energy. For instance, Murugan and Sai Gu [12] listed different organic wastes and biomass substances through which energy can be obtained by following any one of the 'Waste to Energy' processes. Tables 1.2 and Table 1.3 give the details of commonly available wastes in India for energetics and biomass sources respectively.

1.5 Different process of waste to energy

1.5.1 Biochemical conversion

Energy can also be extracted from organic wastes through different bio-chemical processes. The energy content of the primary source can be converted, through bio-decomposition of waste, into energy-rich fuels which can be utilized for different purposes. The biochemical conversion processes include anaerobic digestion, and fermentation [13]. Biochemical conversion is carried out at lower temperatures and lower reaction rates than other conversion processes. The process produces bio-ethanol and biodiesel from biomass or organic wastes; these are used as biofuels in CI engines in a dual fuel mode and as pure biofuels [14].

1.5.1.1 Anaerobic digestion

In anaerobic digestion, an absence of oxygen encourages bacteria to break down food and other natural solid wastes. In this process, the organic substance of the wastes is segregated and fed into a closed container (Biogas digester) where, in the presence of methanogenic bacteria and under anaerobic conditions, it undergoes bio-degradation producing methane-rich biogas. The process waste produces biogas and liquid slurry. The biogas is used on a small scale to produce power in IC engines by running them on a dual fuel or single fuel mode [15, 16]. Biogas mainly consists of CH_4 and CO_2. Biogas provides a clean fuel for both SI (petrol) and CI (diesel) engines. It can be used to run CI engines on a dual fuel mode, where the gas is mixed with the incoming air and ignited by a pilot diesel fuel. Biogas can be used in light and heavy duty vehicles and small power generation units. Light duty vehicles

can normally run on biogas without any modifications, whereas, heavy duty vehicles without closed loop control may have to be adjusted, if they run on biogas [17].

1.5.1.2 Aerobic digestion

Aerobic digestion means composting with oxygen. Organic matter is turned into biologically decomposed waste by micro-organisms living in the composting material (biomass) in a controlled condition [16].

1.5.1.3 Fermentation

Dark fermentation and photo-fermentation are the two methods that can convert the organic substrates into hydrogen in the absence or presence of light, respectively. This is possible because of the processing activity of diverse groups of bacteria. These technologies can be used as valuable options for waste water treatment [16].

1.5.2 Thermochemical conversion

Thermochemical conversion is a process in which the energy content of solid waste is extracted and utilized, by performing a thermal treatment process at high temperature. In a thermochemical conversion, the biomass is subjected to high temperature, and depending on the quantity of oxygen supplied, processes such as combustion, gasification and pyrolysis occur. Fuels such as producer gas, pyrolysis oil, and syngas, can be produced through thermochemical conversion methods.

1.5.2.1 Combustion

Combustion is an exothermic chemical reaction characterized by large heat generation and luminescence. When a fuel is burnt, the heat-generating oxidation reaction, where carbon, hydrogen, oxygen, combustible sulfur, and the nitrogen contained in it react with air or oxygen, is known as combustion. It proceeds by gas phase reaction, surface reaction, or both, following processes such as fusion, evaporation, and pyrolysis. In an actual combustion reaction, complex phenomena such as evaporation, mixture, diffusion, convection, heat conduction, radiation, and luminescence advance at a very high velocity take place. A gaseous fuel burns directly in a gas phase as premixed combustion or diffused combustion. A liquid fuel burns as an inflammable gas in the gas phase after surface evaporation, which is called as evaporation combustion [19].

Table 1.2 Commonly available wastes in India for energetics [12]

Type	**Quantity**	**Projected year**
Wheat, MT/year	15.4	2012
Rice, MT/year	13.1	2012
Sugarcane, MT/year	–	–
Vegetable seeds, MT/year	–	–
Sesame seed, MT/year	0.6–0.7	2012
Castor seed, MT/year	2.29	2012
Rapeseed and mustard, MT/year	6.6	2012
Linseed, MT/year	0.152	2012
Sunflower, MT/year	0.147	2012
Soybean, MT/year	12.2	2012
Ground nut, MT/year	5.12	2012
Food grain, MT/year	16–17	2012
Food and fruit processing industry waste, MT/year	4.5	2012
Waste food and garbage, MT/year	–	2012
Animal wastes (Cow dung, poultry etc.), MT/year	1200	2012
Oil cakes (non-edible), MT/year	2.842	2006
Oil cakes (edible), MT/year	–	–
Jute, MT/year	10.8	2012
Plastic bag and plastic wastes, MT/year	5.9	2012
Waste papers (household, printing, publishing, industries etc.), MT/year	2.75	2011
Waste wood from construction and demolition, MT/year	0.25–0.3	2014
Waste rubber and waste tire, MT/year	0.6	2012
Municipal waste water, million litres/day	12,145	2012
Waste cooking oil		
Spent wash, KL/year	400	2012
Waste cotton, textile and processing wastes	–	–
Tannery waste	–	–
Tannery solid waste, MT/year	–	–
Tannery sludge generation, MT/year	0.3	2012
Leather waste	–	–
Tannery,m^3/day/120MLD	52,500	2012
Paper andpulp,m^3/day	1600	2012
Dairy industry, million litres/day	50–60	2012
Municipal waste water, ML/day	12,145	2012
Spent wash, KL/year	400	2006
Press mud, MT/year	9	2012
Willow dust, ton/year	30,000	2012

Note: ML = mili liter, KL = Kilo liter

Table 1.3 Different biomass sources that are significantly available in India [18]

Name of the crop	Annual production (Thousand MT)	Type of residue	Total available residue (Thousand MT)
Banana	80,000	Residue	240,000
Wheat	78,000	Stalks	117,000
Sugarcane	276,250	Bagasee	91,162.5
Maize	18,500	Stalks	37,000
Rice	145,050	Husk	29,010
Wheat	78,000	Pod	23,400
Bajra	7690	Stalks	15,380
Millets	12,410	Stalks	14,892
Sugarcane	276,250	Top and leaves	13,812.5
Ginger	273,333	Stalks	13,667
Cassava	6060	Starch from roots	10,908
Cassava	6060	Starch from roots	10,908
Maize	18,500	Cobs	5550
Arhar	1950	Stalks	4875
Cassava	6060	Solid waste	3636
Cassava	6060	Solid waste	3636
Cotton	3000	Husk	3300
Coconut	13,125.2	Shell	2887.544
Bajra	7690	Cobs	2537.7
Bajra	7690	Husk	2307
Barley	1200	Stalks	1560
Dry chilly	800.1	Stalks	1200.15
Urad dal	750	Stalks	825
Arhar	1950	Husk	585.3
Cumin seed	200	Stalks	310
Coriander	250	Stalks	287.5
Areca nut	330	Husk	264
Rice	145,050	Stalk	217.575
Rice	145,050	Straw	217.575
Coffee	300.3	Husk	150.15
Urad dal	750	Husk	150
Garlic	598	Sheath	149.5

1.5.2.2 Gasification

Gasification is a process that converts an organic substance or fossil fuel based carbonaceous materials into carbon monoxide (CO), hydrogen (H_2) and carbon dioxide (CO_2). This is carried out by allowing the material to react at high temperatures above 700°C, without combustion, with a controlled amount of oxygen. The resulting gas mixture is called syngas or producer gas, and is itself a fuel. The advantage of gasification is that using the syngas is potentially more efficient than direct combustion of the original fuel, because it can be

combusted at higher temperatures. The producer gas (syngas) obtained by the process of gasification can have an end use for a thermal application or for a mechanical/electrical power generation; like any other gaseous fuel, producer gas has the control for power compared to that of solid fuel [20].

1.5.2.3 Pyrolysis

Pyrolysis is the thermal decomposition of an organic material in the absence or with a small amount of oxygen, to convert it directly into a gas. This process is used in the chemical industry to produce charcoal, activated carbon and methanol, from wood. It is also used to produce, coke from coal, and to convert biomass into syngas and biochar. Anhydrous pyrolysis can also be used to produce liquid fuel from plastic waste, with a higher cetane value and lower sulphur content than those of diesel diesel [21]. In the pyrolysis of waste tyres, in addition to energy and chemicals, steel wire is also obtained as a by-product.

Depending on the operating conditions, the pyrolysis process can be divided into three types: (i) Conventional, or slow pyrolysis (ii) Fast pyrolysis, and (iii) Flash pyrolysis [22].

(i) Conventional or slow pyrolysis

Slow pyrolysis is the simplest pyrolysis process, which has been used for the last thousands of years for char production at low temperatures and low heating rates. In this process, the vapour residence time is too high, i.e. 5 min to 30 min, and components in the vapour phase continue to react with each other resulting in the formation of solid char and other liquids [23]. But, there are some technical limitations which have made it less suitable for a good quality bio-oil production, as cracking of the primary product takes high residence time and extra energy input, and could adversely affect the bio-oil yield and quality.

(ii) Fast pyrolysis

In this type of process, an organic substance is rapidly heated to a high temperature in the absence of oxygen. In this process, the products obtainable are (i) 60%–75% pyrolysis oil (ii) 15%–25% carbon black or char depending on the feedstock and 10%–20% gas depending on the feedstock used. The production of liquid is usually done from organic substances at a low temperature, a high heating rate and short resident time. The important parameters that influence fast pyrolysis are high heat transfer and heating rate, very short vapour residence time, rapid cooling of vapours and aerosol for high bio-oil yield, and precision control of

reaction temperature [24]. Fast-pyrolysis is receiving a great attention in the production of liquid fuels and a range of value added chemicals [25]. Pyrolysis oil can be easily and economically transported and stored.

(iii) Flash pyrolysis

It is a promising process for the production of solid, liquid and gaseous fuels. The process can be characterized by rapid devolatilization in an inert atmosphere, high heating rate of the particles, high reaction temperatures between 450°C and 1000°C, and very short gas residence time of less than one second [26]. However, this process has some technological limitations like poor thermal stability, corrosiveness of the oil, solids in the oil, increase of oil viscosity over time by the catalytic action of char, dissolution of alkali concentrated in the char, and the production of pyrolytic water. The pyrolysis process has a few drawbacks over other processes. The fuel obtained from this process has a high oxygen content which reduces its calorific value. It also contains many reactive components that can form higher molecular weight species. These components result in an increase in the viscosity and decrease in volatility, which is unfavourable for fuelling diesel engines [25].

1.5.2.4 Refuse derived fuel (RDF)

It is a fuel produced by shredding and dehydrating solid waste with a waste conversion technology. The fuel consists largely of combustible components of municipal waste, such as plastics and biodegradable wastes [27].

1.5.2.5 Incineration

It is a waste treatment process that involves the combustion of organic substances contained in waste materials. Incineration is a high-temperature waste treatment process. Incineration of waste materials converts the waste into ash, flue gas, and heat. Incineration removes water from hazardous sludge, reduces its mass and volume, and converts it to ash that can be safely disposed on land, or in some waters, or underground pits. This method has many advantages like; reducing the volume of waste, rendering it harmless, reducing transportation costs and the production of GHGs [11].

1.5.2.6 Hydrogen production from waste

Energy specializes in providing solutions to waste disposal issues and utilizing these to generate hydrogen for use as a substitute to hydrocarbon fuels. It utilizes a small-scale waste

gasification system to obtain hydrogen from waste. This includes the conversion of organic-containing solid, liquid and gaseous wastes into synthesis gas as an intermediate step and then to hydrogen gas. Hydrogen can be produced from different wastes, forestry and agricultural residues, and animal, municipal and industrial wastes. Hydrogen has the potential to provide energy for stationary energy conversion devices such as fuel cells, as well as for transportation. This wide application of hydrogen can replace conventional fuels to a certain extent in minor applications [28, 29].

1.6 Disposal of waste tyres

Waste tyres and plastics are the major sources of wastes disposed in the municipal and industrial areas in the world. Billions of waste tyres are available all over the world. They cannot be burnt or disposed as they are in open lands. Dumping of these wastes in open land releases a certain amount of methane during their decomposition and hence, they are also sources of GHG emissions. It is estimated that approximately 1.5 billion new tyres are produced annually in the world [30].

1.6.1 Reuse of waste tyres

Waste tyres can be reused in different ways, which are illustrated in Figure 1.7.

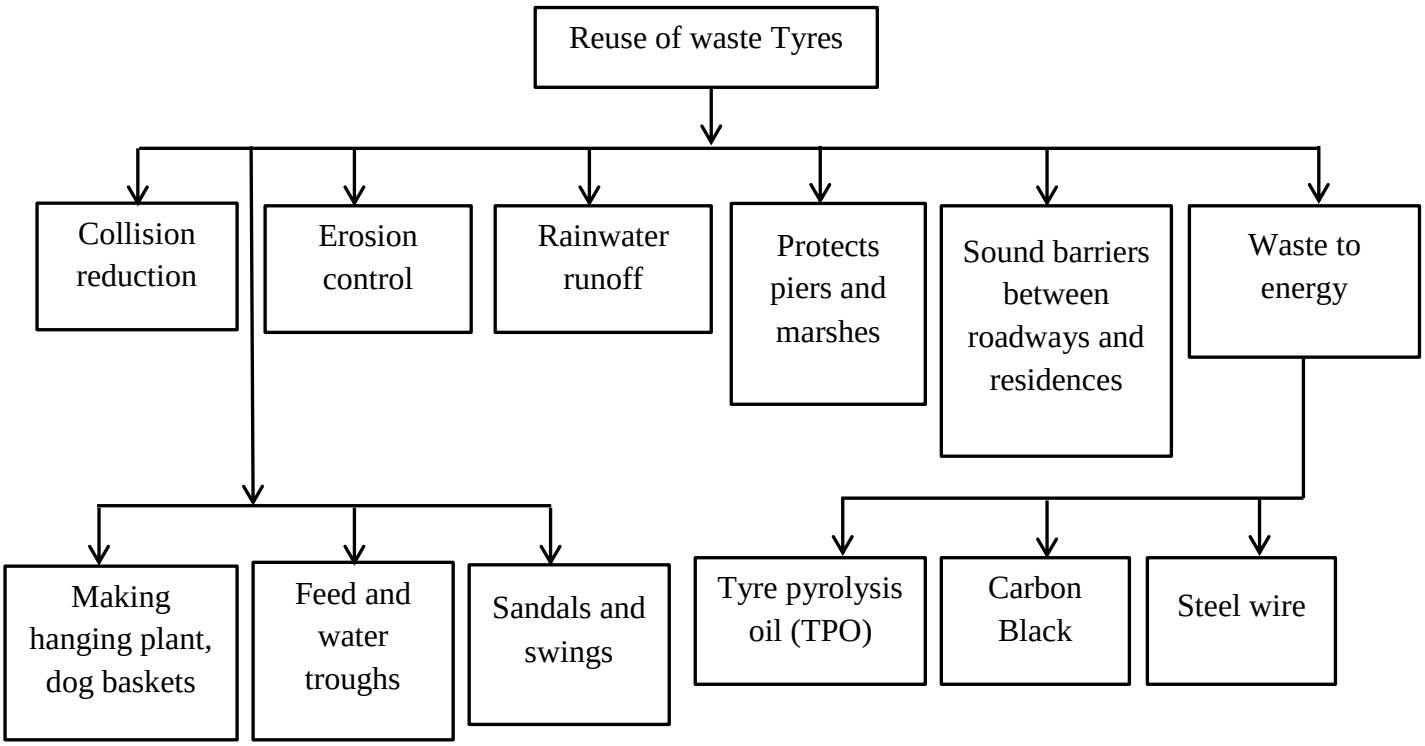

Figure 1.7 Reuses of waste tyre

1.6.2 Applications of waste Tyres

The main applications of each category are given below:

1.6.2.1 Tyre-derived fuel

- Cement industry
- Paper/pulp industry
- Utility boilers
- Industrial boilers

1.6.2.2 Ground rubber applications

- Rubber modified asphalt
- Molded and extruded products
- New tire manufacturing
- Athletic and recreational applications
- Horticultural applications
- Animal bedding
- Surface modification
- Cut, punched and stamped rubber products

1.6.2.3 Civil engineering applications

- Landfill construction and operation
- Building of retaining walls
- Erosion control
- Shoring up embankments
- Backfill for water and bridge abutments
- Sub-grade insulation for roads

1.6.3 Pyrolysis of waste Tyres

Pyrolysis is a method to convert organic substances into useful energy by thermal decomposition. In pyrolysis, the organic substances are thermally degraded to get value added products, which are principally pyrolysis oil, pyrogas, and carbon black or char. Several studies have been documented on the production and characterisation of pyrolysis products obtained from the pyrolysis of tyres, adopting different processes [31, 32], reactors [33, 34], feed stocks [32-34], etc. Documents are also available on the research works related to the of study the effects of varying the heating rate, heat input [35], condenser water cooling rate [32], etc.

Recently, many pilot and demonstrated pyrolysis plants have been installed in many countries. In a practical pyrolysis plant, four principal products are obtained; they are Tyre pyrolysis oil (TPO), pyrogas, carbon black (CB) and steel wire. Tyre pyrolysis oil (TPO) is used as a secondary heat source in burners, while pyrogas is used as a secondary heat source

in the pyrolysis reactor itself, to reduce fuel consumption. Steel wire is used in steel manufacturing. The remaining CB is impure and can not be used in industrial applications, like charcoal. Hence, it is dumped in the open land. This causes an environmental threat, and is a less economic aspect of the pyrolysis process. The energy contained in CB can be recovered by an appropriate method, so that the waste can be minimised. Pyrolytic CB, only a less percentage is used in coating of electrical insulation cables, road pavement and production of colour pigments.

1.7 Solid fuels in IC Engines

A solid fuel is an organic material that originates from a variety of sources, such as decomposed hydrocarbons present in the industrial, municipal and agricultural sectors, and used as a fuel to produce heat, which is usually released through combustion. Solid fuels have been used by humanity for many years to create fire. They are mainly classified into two categories, (i) natural fuels, such as wood, coal, etc. and (ii) manufactured or artificial fuels, such as charcoal, coke, briquettes, etc. Coal is one of the solid fuels, the fuel source which enabled the industrial revolution, used in fired furnaces, to run steam engines, and is a major component of electricity generation. According to the International Energy Agency (IEA) 41% of the world's electricity is generated by burning coal. In addition to the continuous improvement in the clean coal technology, possibilities of producing solid alternative fuels from different organic wastes have been explored in recent years. The merits and demerits of solid fuels are given below:

1.7.1 Merits

- They are easy to transport.
- They are convenient to store without any risk of spontaneous explosion.
- Their cost of production is low.
- They possess moderate ignition temperature.
- Availability in large quantities.

1.7.2 Demerits

- Their ash content is high.
- A large proportion of their heat is wasted.
- They burn with clinker formation.
- Their combustion operation cannot be controlled easily.

In the late half of the 1800s, before petroleum–based fuels were introduced, solid fuels such as coal, slurry and charcoal were tested and used in IC Engines [36]. When Rudolf Diesel

was developing his engine, one of the fuels he used was coal dust mixed with water. Fine particles of coal (carbon) were dispersed in water and injected and burned in an early diesel Engine [36]. Many investigations were also carried out to use solid fuels such as charcoal [37], coal [38-40], orange powder [41], carbon nanotubes [42, 43] etc. as fuels in compression ignition (CI) Engines.

1.8 Present Investigation

It is understood that the CB obtained from a tyre pyrolysis plant possesses a considerable amount of energy, which can be used as an alternative energy source for heat and power applications. Hence, the present investigation is aimed to run a single cylinder, four stroke, air cooled, direct injection (DI) diesel Engine using CB as an alternative fuel, by adopting different techniques.

The main objectives of the present work are as follows:

i. To characterise the CB obtained from a tyre recycling plant for its suitability as a solid alternative fuel.
ii. To carry out preliminary investigation with carbon black diesel slurry (diesel doped with CB) in a stationary DI diesel Engine.
iii. To make attempts to prepare carbon black-water-diesel (CBWD) emulsion with the conventional diesel fuel and characterise, it for its suitability as a fuel for compression ignition (CI) Engines.
iv. To carry out experimental investigation with emulsions without and with Engine modification
v. To improve the engine efficiency and reduce some of the exhaust emissions from the Engine fuelled with an optimum emulsion.
vi. To validate the experimental results using a mathematical model for optimum emulsion.

1.9 Organization of thesis

Chapter 1

This chapter explains the source of GHG emissions, global warming potential and ozone deflection, waste management and disposal of waste tyres. A description of the type of solid fuels and their utilisation as alternative fuels in compression ignition (CI) engines are also given.

Chapter 2 Literature review

In this chapter, the fundamentals of combustion behaviour and emission formation in CI engines are explained. Further, a comprehensive review of research works pertaining to the

production, characterization and utilisation of some of the solid fuels in the form of slurry, blend and emulsion as alternative fuels in CI engines is presented with illustrations. The various issues related to the combustion, performance and emission parameters of the CI engine fuelled with the solid fuel are discussed in this chapter. The review also includes the NO_x emission reduction strategies adopted in emulsion fuelled engines.

Chapter 3 Fuel preparation and characterization

This chapter details the methods and materials involved in the production of CB obtained from waste tyres. The production of Carbodiesel fuel (CB doped with diesel) and the CBWD emulsion from the CB. The chapter also discusses the characterization of Carbodiesel fuel and the CBWD emulsion which were considered in this study. The test results obtained from the Thermogravimetric analyser (TGA), CHNS and Scanning electron microscope (SEM) instruments are also analysed and discussed. The chapter also discusses the characterization and rheological behaviour of a CBWD emulsion considered in this study. The XRD analysis of CB and study of the Zeta potential of CBWD10 emulsion are also discussed in this chapter.

Chapter 4 Experimental setup and methodology

In this chapter, the necessary engine experimental setup and other accessories are described systematically. The method of determining the uncertainty of the experimentation is also included at the end of this chapter. The details on the various methodologies adopted, and the modifications involved in the engine experimental setup are also discussed in this chapter. The methods of calculating the important combustion, performance and emissions parameters are discussed. The details of various methodologies adopted, and the modifications involved in the engine are also discussed in this chapter. The methods of calculating the important combustion, performance and emissions parameters are discussed.

Chapter 5 Results and discussion

Detailed discussions on the comparative analysis of the combustion, performance and emission results obtained from the experimental investigation from a diesel engine fuelled with different Carbodiesels and the CBWD emulsions under various operating conditions are given in this chapter. This chapter also discusses the sample validation of the experimental results by theoretical modelling using MATLAB programming for the prediction of a few

combustion and emission parameters of the diesel engine fuelled with an optimum emulsion (CBWD10).

Chapter 6 Conclusions

The summary of the findings from the experimental investigations carried out in this study is given in this chapter. It also mentions the important conclusions of the investigation, and the scope for future work.

CHAPTER 2
LITERATURE REVIEW

2.1 General

Before carrying out any research work in a particular area, it is necessary to understand the basics and the recent developments in that area. This will be helpful to identify a problem to be resolved through research. A review of research collection of articles and published documents is the first step of the research work in any field. This chapter initially presents the fundamentals of a compression ignition (CI) Engine, spray formation of the fuel, the combustion concept, and emissions from the CI Engine. Further, the chapter presents a review of the various research works related to the production of different solid fuels that have been obtained from coal, char coal, and other organic substances obtained from municipal and agricultural wastes. The chapter also includes a review of the characterisation of solid fuels and their utilisation with diesel and other fuels in DI diesel Engines. The efforts that have been proposed worldwide to reduce the oxides of nitrogen (NO_x) and smoke emissions from CI Engines fuelled with the slurry, emulsion and its blends are also reviewed and presented.

2.2 Some basic concepts of CI Engines

Spark ignition (SI) engines are used to run, motorcycle, outboard motors, pressure washers, snowmobiles, small passenger cars and light vehicles, while CI Engines are used to run heavy commercial vehicles, military vehicles, marine, locomotive engine and stationary electric power plants. The CI Engines are preferred than SI engines because of their higher thermal efficiency and longevity. The CI engines are well suited for today's transport, power, and miscellaneous applications such as automotive, ships, aircraft, industrial power, railways power, etc. used. CI Engines are expected to dominate in the market, in spite of new technologies such as, electric vehicles and fuel cell vehicles, MPFI engines. The demand for CI engines in the world in the year 2015, is forecasted and given in Fig. 2.1 [44].

From this data, we can understand the requirement of diesel engines to be used in transport and power sectors in the World. China has a maximum share of demand of diesel engines which accounts about 25% of the total demand. Similarly, Asia/Pacific, Western Europe, North America and other regions have a maximum share of demand of diesel engine are accounts about 22%, 23%, 11% and 19% of the total global demand.

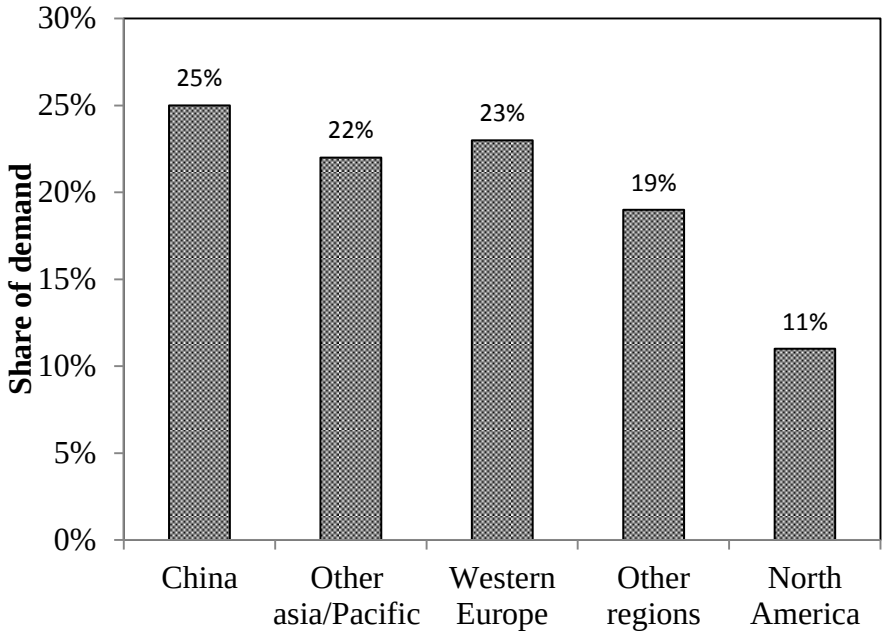

Figure 2.1 Demand of diesel engines in the world for the year 2015 [44]

2.2.1 Two stroke and four stroke CI Engine

A two stroke engine completes the whole process of conversion of heat into power in two strokes, up and down movements of the piston during only one crankshaft revolution. In a two-stroke Engine, the end of the combustion stroke and the beginning of the compression stroke happen simultaneously, with the intake and exhaust functions occurring at the same time.

A four stroke CI Engine comprises four strokes namely suction, compression, expansion or power, and exhaust. These, four strokes are complete in two revolutions of the crank shaft. In suction stroke, the piston moves from the top dead centre (TDC) to bottom dead centre (BDC). The inlet valve opens and air is drawn into the cylinder and during this time the exhaust valve is closed. During compression stroke, the inlet and exhaust valve are closed and piston moves from the bottom dead centre (BDC) to top dead centre (TDC). In this stroke, the pressure and temperature reach the maximum point due to compression. During power stroke, the both inlet and outlet valve are closed, and the hot gases expand adiabatically, in the cylinder pushing the piston down, and hence work is done. In the exhaust stroke, the piston again moves upward from the BDC reaching the TDC. During this period, the exhaust valve opens, while the inlet valve is closed. The upward movement of the piston pushes the combustible gases out through the exhaust valve, and the cycle is completed.

2.2.2 DI and IDI Engines

Based on the method of introducing injected fuel into the combustion chamber, CI engines are divided into two types which are: (i) direct injection (DI) and (ii) Indirect injection (IDI) compression ignition Engines.

(i) DI Engines

In DI Engines, fuel is directly injected into the combustion chamber, right into the top of the piston. DI Engines operate at higher injection pressures, and therefore more complete atomization occurs. These Engines do not require a pre-chamber to ensure proper diffusion of the fuel into the air. Generally, there are three types of the DI Engine which are follows [36, 45]

(i) Quiescent chamber with a multi-hole nozzle

(ii) Bowl-in-piston chamber with swirl and multi-hole nozzle

(iii) Bowl-in-piston chamber with swirl and single-hole nozzle

Figure 2.2 (a) and (b) show the different types of DI Engines.

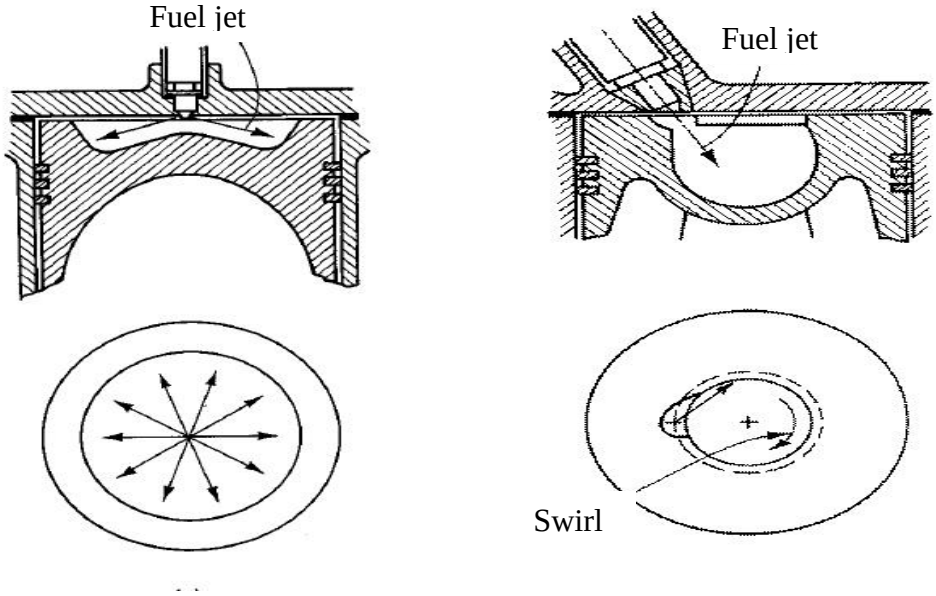

(a) Quiescent chamber (b) Swirl in chamber

Figure 2.2 DI Engines [36]

(ii) IDI Engines

In IDI diesel engines, fuel is first injected into the pre-chamber, where it rapidly mixes with oxygen and ignition occurs. As the flame front expands in the pre-chamber, it forces the fuel to enter the combustion chamber rapidly, effectively mixing the fuel with air in the cylinder

and atomization is achieved. Generally, there are two common types of IDI Engines; they are, Engines with a

(i) Swirl prechamber

(ii) Turbulent prechamber

Figure 2.3 (a) and (b) show the different types of IDI Engines [36, 45].

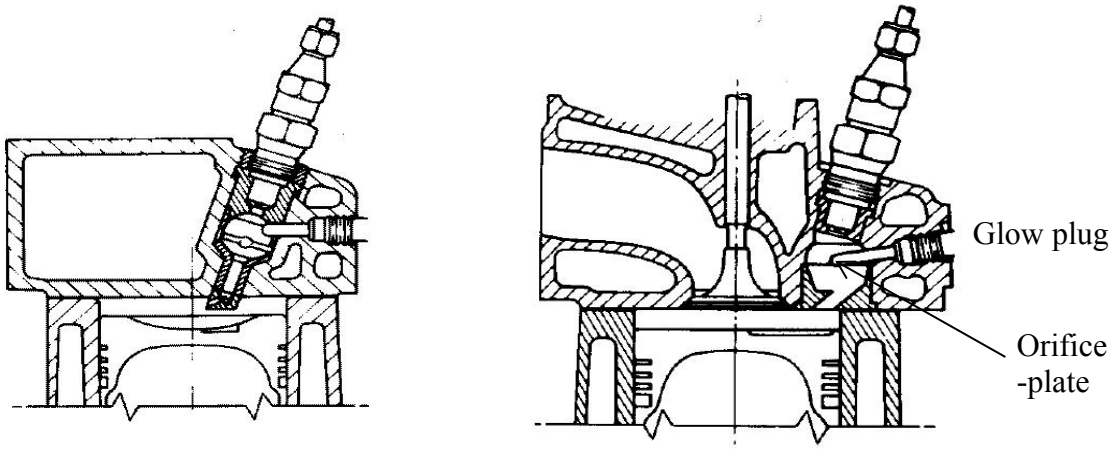

(a) Turbulent (b) Swirl pre-chamber

Figure 2.3 IDI Engines [36]

Table 2.1 provides comparisons of the characteristics between the DI and IDI system of the Engines and Table 2.2 lists the merits and demerits of the ID and IDI systems of the Engines.

2.3 CI Engine combustion

Combustion is a process in which chemical reaction takes place between carbon and hydrogen in combination with oxygen, and generates heat energy. In CI Engines, initially air is compressed through a high compression ratio 16:1 to 20:1, raising its temperature and pressure to a high value. Then, fuel is injected through one or more jets into this highly compressed air, and mixed in the combustion chamber during the combustion process [36].

The combustion process proceeds by the following stages in CI Engines, which is illustrated in Fig. 2.4 [36, 45].

Table 2.1 Characteristics of the DI and IDI Engines

S.No.	Description	DI	IDI
1	Fuel injection	Inside the combustion chamber	Small pre chamber above the cylinder, where the fuel is injected
2	Combustion chamber	One (main Combustion chamber)	Two (one is the pre- combustion and the other, the main combustion chamber)
3.	Orifices	One	One or more
4.	Size	largest	Small
5.	Compression ratio	12-18	20-24
6.	Chamber	Open, Bowl-in-piston, Deep bowl-in-piston	Swirl pre-chamber, Single/multi orifice pre-chamber
7.	Air-flow pattern	Quiescent, medium swirl, high swirl	Very high swirl, very turbulent in pre-chamber
8.	Number of nozzle holes	Multi/Single	Single
9.	Injection pressure	Very high	low

Table 2.2 Merits and demerits of the ID and IDI Engines

S.No.	Types of Engine	Merits	Demerits
1.	DI engines	Cold starting is easier	Tend to be noisy
		More economical	More prone to blockages due to small injection holes
		Smaller combustion space	Slower swirling, particularly at low engine speeds
		Better thermal efficiency	Lower power output
2.	IDI engines	The injection pressure required is low, so the injector is cheaper to produce	Fuel efficiency is lower
		High rate of swirl over wide range of engine speed	Higher compression ratio required to aid starting
		The injection direction is of less importance	Glow plugs are needed for a cold engine start
		Higher engine speeds can be reached, since burning continues in the pre-chamber	The heat and pressure of combustion is applied to one specific point on the piston as it exits the pre-combustion chamber or swirl chamber, such engines are less suited to high specific power outputs than direct injection diesels

(i) Ignition delay (ab)

Fuel is injected directly into the cylinder at the end of the compression stroke. The liquid fuel atomizes into small drops and penetrates into the combustion chamber. The fuel mixes with the air at high-temperature high-pressure. There is an interval of time in the degree crank angle between the start of injection and start of combustion, which is called as ignition delay. The ignition delay takes place in two stages: (i) physical delay and (ii) chemical delay. In physical delay, atomization of liquid fuel jet, evaporation of fuel droplets and mixing of fuel vapour with air occur. In chemical delay, the reaction starts slowly and then accelerates until inflammation or ignition takes place [36].

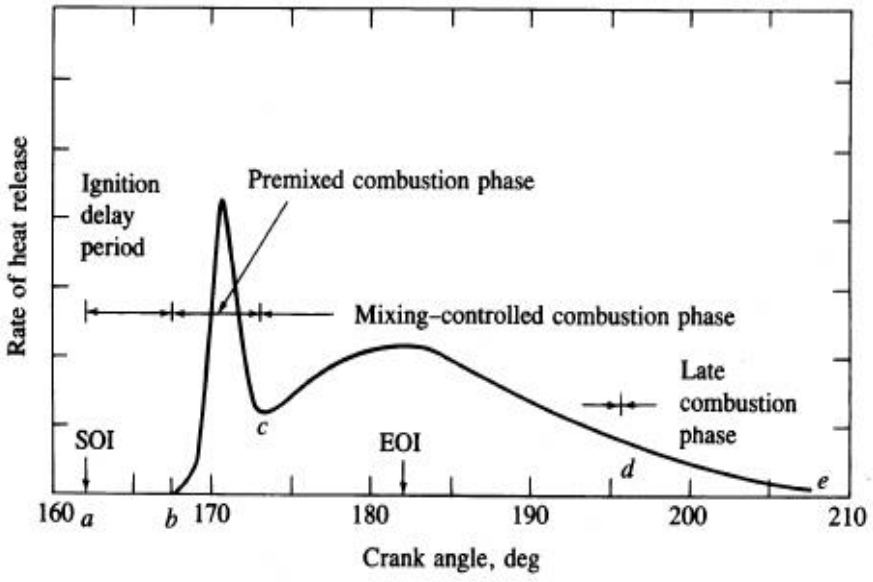

Figure 2.4 Four stages of combustion in CI Engines

(ii) Premixed combustion phase (bc)

The combustion of the fuel which has mixed with the air to within the flammability limits during the ignition delay period occurs rapidly in a few crank angles. This depends on the atomization of fuel and its quality. As a result, the peak heat release rate in the premixed combustion is generally higher than that of the subsequent stages. The consequence of the high heat release rate is more effective during this period [36].

(iii) Mixing controlled combustion phase (cd)

The rapid combustion period is followed by the third stage, viz, controlled combustion. The temperature and pressure in the second stage are already quite high. Hence, the fuel droplets injected during the second stage burn faster with a reduced ignition delay as soon as they find the necessary oxygen, and any further pressure rise in controlled by the injection rate.

(iv) Late combustion phase (de)

Heat release proceeds at a lower rate later part of the expansion stroke (no additional fuel injected during this phase), and this is referred to as late combustion. Combustion of any unburned liquid fuel and soot occurs during this phase [36].

2.4 Spray formation

Fuel spray formation is an important factor in CI Engines, as its shape and composition strongly affect the ignition and flame propagation processes [46]. In a CI Engine, the fuel is sprayed directly through the nozzle into the cylinder and the air-fuel mixture ignites spontaneously. Spray formation directly impacts the combustion quality. Larger droplets provide a higher penetration into the chamber but smaller droplets are required for quick mixing and evaporation of the fuel. The spray formation of the droplet size depends on various factors, such as injection pressure, air density, fuel viscosity and the size of the orifice. A larger spray cone angle may place the fuel on top of the piston, and outside the combustion bowl in open chamber diesel Engines. This condition will result in an excessive incomplete combustion because of depriving the fuel access to the air available in the combustion bowl (chamber). Wide cone angles may also cause the fuel to be sprayed on the cylinder walls, rather than inside the combustion bowl where it is required. As the spray angle is one of the variables that influences the rate of mixing of air into the fuel jet near the outlet of the injector, it can have a significant impact on the overall combustion process [46].

2.5 Emissions from CI Engines

CI engines generate undesirable emissions during combustion process; that are classified into types of emissions; (i) exhaust emissions and (ii) evaporative emissions [47]. Exhaust emissions are the combustible gases which are released into the atmosphere through the exhaust manifold of the CI Engine. The exhaust emissions are commonly seen in both stationary and locomotive engines. These emissions include hydrocarbon (HC), oxide of carbon (CO and CO_2), oxides of nitrogen (NO and NO_2), oxides of sulphur (SO_2 and SO_3), particulate matter and soot, and smoke.

Evaporative emissions are the gaseous emissions that are diurnal, permeation, hot soak, running loss, refueling and crankcase [47]. The type of exhaust and evaporative emissions, their nature and causes are tabulated in Table 2.3 and Table 2.4 respectively.

Table 2.3 Exhaust emissions [47]

Emission	Characteristics	Causes	Consequences/effects
Unburnt hydrocarbon (HC)	Partially burned fuel, Toxic gas	Poor ignition fuel, Improper ignition timing, Improper air-fuel ratio and low cylinder compression	Asthma, liver disease, lung disease, and cancer
Carbon monoxide (CO)	Colorless, odorless, and tasteless gas, density slightly less than air	Insufficient amount of air in the air-fuel mixture	Toxic to humans, carbon monoxide reduces the blood's ability to carry oxygen
Oxides of nitrogen (NO_x)		High temperature and pressure inside the engine, Insufficient oxygen	Acid rain, destroys resistance to respiratory infection
Particulate matter	Finely divided solids or liquids such as dust, fly ash, soot, smoke, aerosols, fumes, mists	Improper air-fuel mixing, rich mixture, fuel quality	The rough surface of particles makes them irritant with other toxins in the environment, and increase the hazards of particle inhalation
Sulfur oxides (SOx)		High temperature, Oil combustion from the oxidation of sulfur contained in the fuel	Acid rain, air pollution, heart disease, emphysema, bronchitis
Aldehydes	Odorous oxygenated hydrocarbons	Alcohol fuel	Pungent smell of the engine exhaust
Smoke	Visible emissions, blue, white and black	Due to incomplete combustion	More irritating and cause nuisance

Table 2.4 Evaporative emissions [47]

Emission	Causes
Diurnal	Due to temperature changes throughout the day. As the day gets warmer, the fuel in the tank heats up and begins to evaporate
Permeation	Due to fuel that works its way through the material used in the fuel system
Hot soak	Due to residual heat from the equipment just after the engine is shut off
Running loss	Due to diurnal except that the heating is caused by engine operation
Refuelling	Due to filling time from pumped to the tank
Crankcase	Vapours released from the crankcase of an engine

The exhaust emissions are higher in percentage than those of non-exhaust or evaporative emissions. Therefore, the exhaust emissions must be within the standards, when a CI Engine is operated with an alternative fuel. The latest EPA (US), Euro and Bharat (India) standards for stationary diesel Engines are listed in Table 2.5.

Table 2.5 Emission standards for diesel Engines, by USA with Euro and Bharat [48-50]

Emissions	**kW < 8**			**8 ≤ kW < 19**		
Standards	**EPA(US)-420-B-16-022**	**Euro-III**	**Bharat-II**	**EPA(US)-420-B-16-022**	**Euro-III**	**Bharat-II**
CO, g/kWh	8.0	8.0	8.0	6.6	4.0	6.6
NMHC+ NO_x, g/kWh	7.5	7.5	7.5	7.5	1.1	7.5
NO_x, g/kWh	-		9.2	-	7.0	9.2
PM, g/kWh	0.75	0.4	0.8	0.6	0.15	0.8

2.6 Production and characterisation of solid fuels

Solid fuels have been used by humanity for many years to create fire. Solid fuel refers to various types of organic material that originates from a variety of sources, such as decomposed hydrocarbons in solid form from the industrial, municipal and agricultural sectors, and used as a fuel to produce energy and provide heat, usually released through combustion. According to the International Energy Agency (IEA), 41% of the world's electricity is generated by burning coal. In addition to continuous improvement in clean coal technology, the possibilities of producing solid alternative fuels from different organic wastes are explored.

Generally, energy from the solid organic materials can be recovered from direct combustion. The direct combustion of fuel pellets is harmful to the environment. However, when solid fuels are processed or recycled to replace the existing fossil fuels, the GHG emissions can be reduced.

As mentioned in the Introduction chapter, apart from direct combustion, energy can be recovered from organic materials by pyrolysis and gasification, anaerobic digestion and fermentation [13, 15, 16, 20, 21]. Some researchers have made attempts to directly use solid fuels in the form of slurry or emulsion in IC Engines [51]. Preparation of fuel and its characterisation is very important, because an effective combustion occurs in a combustion

device based on its physical and chemical properties of the fuel, stoichiometric air supply, and combustion geometry.

2.6.1 Coal

Before the introduction of liquid and gaseous fuels widely, coal was used as the main source of energy apart from biomass, for the production of electricity and/or heat, and also for industrial purposes, such as refining metals for several years, because of its abundant availability. Due to the decomposition over several years under the earth, dead plant matter forms as peat and then is converted into lignite, sub-bituminous coal, bituminous coal, and lastly anthracite, in stages. Ever since the industrial revolution began in the 18th Century, the use of coal was gradually and considerably reduced due to the increase in air pollution. But, coal is still considered as a potential fuel for heat and power applications. However, towards the end of the 1950s, the Soviet Union started developing new ways to utilize coal sludge for power generation. Two major problems of sludge transportation and combustion were solved during a series of experiments and research. Pulverized coal was mixed with water to produce coal-water slurry (CWS). It was suggested that the CWS could be used in place of oil and gas in heat and power applications. During the last 30 years, the US Department of Energy (DOE) has been researching the use of coal/water fuels in boilers, gas turbines and diesel engines. It was reported that when coal based slurry or fuel was used as a fuel in a low speed diesel engine, it provided a thermal efficiency equal to that obtained in a gas combined cycle gas turbine that run on natural gas as a primary fuel.

Chen et al. [52] prepared different slurries from biomass char, a low rank coal char and sub-bituminous coals. The slurries were prepared by mixing them with water after milling and including a range of additives, such as polyacrylic acid, charged copolymers D101 and D102, and sucrose. The effect of the solid type, particle size distribution, and additives, on the preparation of highly loaded slurries with the desired rheological behaviour, was systematically examined, in terms of the apparent viscosity and yield stress. It was reported that, for low rank coals such as lignite, thermal and densification treatment would be essential to achieve the solid loading of slurry fuel.

Dincer et al. [53] investigated the effects of different chemicals that were used as dispersing agents and stabilisers on the stability and viscosity of coal water slurry (CWS). In the investigation, they used Anionic type of chemicals-polyisoprene sulphonic acid soda

(Dynaflow-K), a derivative of carboxylic acid (AC 1320) and naphthalene sulfonate formaldehyde condensate (NSF) as dispersing agents. In the same study, they used the sodium salt of carboxymethyl cellulose (CMC-Na) as a stabiliser. They used bituminous coal (thermal code no. 434) of Turkish origin, with a medium volatile matter as a sample. They reported that the polymeric anionic dispersing agent such as Dynaflow, showed a greater effect on the viscosity and stability of coal water slurry.

Gu Tian-ye et al. [54], reported that when the proportion of coal was more than 30% in the coal water slurry (CWS), all its properties had improved, and it met the requirements for use as a fuel. Coalification, porosity, surface oxygenic functional groups, zeta potential and grindability had a great effect on the performance of blended coal CWS. They also reported that this led to some differences in the performance between the slurry made from single coal and that made from blended coal. They affirmed that, coal blending might effectively reduce the concentration of the oxygen functional groups and enhance the absorbing ability of the coal surface for anionic additives, which would enhance the slurryability. The zeta potential of a coal surface was related to the coal rank and particle size. It was reported that the use of a dispersant could increase the absolute value of the zeta potential, which would give a well dispersed and low viscous CWS. It was reported that, the addition of coals having different properties could effectively enhance the slurryability.

In an investigation carried out by Kihm et al. [55], the droplet size characteristics near the tip of intermittent sprays of diesel fuel injected from an electronically controlled accumulator injection system were studied. The Sauter Mean Diameter (SMD) was measured at a low obscuration without multi- scattering bias. The investigation results revealed that the spray tip SMD increased with the ambient gas density and axial measurement location, and fell inversely with injection pressure. The dependence of SMD on the nozzle orifice diameter was negligible for fully developed sprays. The results indicated that the droplet SMD of diesel sprays was always smaller than those of CWS and spray tip SMD. The results also indicated that the spray-tip SMDs increased with the distance downstream from the orifice exit and decreased with injection pressure.

Khodakov [56] reviewed and analysed the possibility of coal water fuel (CWF) as an alternative fuel for power generation. He also discussed different prospective fields of its application. He mentioned that CWF became especially popular as a subject of research in

the early 1970s. In his report, he also stated that a technology was developed for utilizing coal slurry, in which coal was enriched, hydraulically extracted, and transported from a colliery. Further, he confirmed that many researchers and process engineers working at research centres owned by public and private companies were assigned with the task of developing industrial-grade technologies for obtaining the CWF that would be an alternative to petroleum products. After the year 2000, research works on the utilisation of CWF became fewer in number, and have now ceased almost completely. This is because, first the technical problems related to the development and utilization of CWF was not resolved and, the second, this kind of fuel turned out to be economically inefficient even at very high prices compared to petroleum. Industrially developed countries have chosen the path of developing technologies for using renewable energy carriers [56].

Edward T. Mchale [57] studied the atomization and combustion behaviour of a diesel engine run on coal-water fuel (CWF). The properties of CWF that influence mainly the rheology and particle size distribution were analysed. He reported that the relationship between the atomization process and the CWF viscosity was an important issue. The water evaporating at the outset of the process might affect ignition. The heat of vaporization of water in a 70% CWF was close to the sensible heat required to raise the coal to its ignition temperature. He also reported that the results of the study were consistent. Furthermore, he concluded that, if the first stage of the process was conducted at a stoichiometric ratio near about 0.8, then the NO_x emissions could be reduced by about 50% for the entire process [57].

Wei Yuchi [58] studied the effects of coal characteristics on the properties of CWS such as slurryability, rheological behavior, and static stability, by using sixteen Chinese coals with different coal ranks from lignite to anthracite. He also provided the correlations between the CWS properties and 18 parameters from 40 coal properties, by the multivariate progressive regression method. He reported that the carbon content and grindability index of coal showed a positive correlation with slurryability, while the content of air equilibrium moisture and the surface area determined by the Mercury Porosimeter, gave negative effects. He also reported that the rheological behavior of CWS was positively correlated with the ash content, content of soluble ions, and pore volume determined by the Mercury Porosimeter, while the zeta potential properties of the coal surface negatively impacted the rheological behavior. The content of soluble ions showed a positive effect on the static stability of CWS, while the content of the inordinate had a negative influence.

Ajay and Yiannis [59] studied the combustion of single coal-water fuel, consisting of either micronized or pulverized bituminous coal powder, and of carbon black and diesel. They conducted the study with pre-dried agglomerates of known initial size and weight. They reported that the influence of the ground coal on the char combustion was found to be weak, and on an average the agglomerates of both coal grinds burned at equivalent rates. They also indicated that, from a coal water fuel (CWF) combustion perspective, there was no advantage in micronizing coal. Further, they confirmed that the coal water fuel could provide an excellent medium for their utilization, if ultrafine coal would be already available, as a by-product of coal cleaning operations. They concluded that the micronized CWF was found to burn hotter in the last stages of char combustion, which might impede extinction and increase carbon conversion. They also concluded that carbon black with calcium magnesium acetate (CMA) agglomerates ignited faster than pulverised bituminous powder.

Shengxiang Deng and Jiemin Zhou [60] experimentally investigated the droplets of coal tar/water emulsion for their unsteady burning behavior. They analysed coke residues by the Scanning Electron Microscope (SEM). They reported that, the ignition delays of the emulsions were found to be longer than those of ordinary coal tar (CT) droplets of the same size, but the peak temperature of the emulsions occurred much earlier. They also observed a steeper temperature rise with the emulsions in the combustion history, which evidenced not only soot reduction, but also the extent of the burnout of the cenospheres. They further reported that, the latter was an important aspect in the reduction of emissions. They also found that the emulsion droplet's swelling was found to be bigger, compared to that of coal tar (CT). They also pointed out that, the coke particles formed from the emulsions were more porous, with thinner and more fragile shells. The CT residues were harder and more resistant to burning. The excess burnout time or the ratio of the burnout time of the emulsions depended on the water concentration, and indicated that a longer oxidation time was required for the coke particles, from coal tar than from the emulsions. They concluded that, in the entire test carried out with the emulsions, the first swelling happened before the ignition of the droplet, while abundant release from little droplets occurred after the swelling. The occurrence of micro-explosions before the ignition of the droplet was a crucial factor in the production of well-defined shell structures in the solid residues. The droplet combustion occurred with a greater intensity during the later stages of the droplet's lifetime, and affected the molecular structure of the residue during the solidification phase. The carbonaceous

residue of CT was found to be denser and more regular compared to the softer, more fragile amorphous cenospheres of the emulsions.

Burgess and Ghaffari [61] in a study, examined coal water slurry (CWS), methanol (CMS) and a water-methanol mixture (CWMS). They measured the temperatures and combustion times for a range of droplet sizes. They reported that the fine coal particles and water evaporation were the causes of the micro explosive dispersion of part of a CWS droplet, which occurred in the pre-ignition period, if the slurry was made from a low swelling coal. If the droplet was larger than the minimum size, during the flame period, the CMS and CWMS droplets of all sizes were disrupted. They also reported that, the overall combustion time for methanol-containing slurries was found to be shorter than that of CWS. The CWS droplets could ignite heterogeneously or, if there was a sufficient time for a build-up of coal volatiles, in the gas phase. The large droplets of water based slurries of low-swelling coals micro explode in the pre-ignition period, and disperse considerable amount of coals in the process, thus reducing the overall burn-out times. The methanol based slurries also dispersed a large amount of coal, but in a less violent and more sustained way during the flame period. They concluded that, there was a minimum droplet diameter for the micro explosion, which was a function of the swelling number of coal, and decreased rapidly with increased temperature.

Ken D. Kihm and Paul Deignan [62] conducted experiments to measure the dynamic surface tension of coal-water slurry (CWS) mixtures containing various types of surfactants and with different coal loadings. They characterized the interfacial characteristics of CWS mixtures by measuring both the static and dynamic surface tensions. During experimentation they measured the dynamic surface tension using a maximum air bubble pressure technique. They used coal with 55pm volume mean diameter (VMD) and five different surfactants; one non-ionic alkyl phenol ethoxylate (NP-l00), and four anionic surfactants; branched dodecyl benzene sulfonic acid (DDBS-hard), linear dodecyl benzene sulfonic acid (DDBS-soft), a sodium salt of a branched alkyl benzene sulfonic acid (1223H), and a sodium salt of sulfonated fatty acid (1840X) for preparing the CWS. They prepared 40% and 50% CWS mixtures, with the surfactant concentrations ranging from 0.1 to 5.0% in weight. They also measured the static surface tension using a Du Nouy ring tensiometer to determine the Critical Micelle Concentration (CMC). They analysed the results, and concluded that the CMC of the CWS mixtures was considerably higher than that of an aqueous solution, due to the absorption of a surfactant by coal particles. When the CMC was met, the static surface

tension values of CWS mixtures were identical to those of the corresponding aqueous solutions. The dynamic surface tension of the CWS mixtures showed an increase with the increase in coal weight concentration. It was believed that, this was primarily because of the increase in interfacial surfaces, and the increase in the absorption of the surfactant with the increasing coal concentration.

The effects of particle size, solid concentration, pH and temperature on the rheological properties of coal water slurry (CWS) were investigated by Xinzhi Chen et al. [63]. They used Brookfield R/S (Remote/Sensing) with a Rheometer to investigate the rheological behaviour of the CWS samples. The sample was prepared from the solid residue of the plasma pyrolysis of coal. The Rheometer was calibrated by using the Newtonian standard solution (4900 mPas at 25^{o}C). They concluded from the results that, the rheological behavior of CWS suspension can be shear thinning, depending on the solid content as well as the operating conditions. The apparent viscosity of the CWS increases with the decreasing particle size. Alkaline suspension favoured storage and transport. The relation between viscosity and temperature was not simply linear, and a more suitable cubic model was proposed. After sedimentation for 12 days, the volume ratio of the clear liquid to the initial volume of 55% wt% suspension was found to be about 2%.

2.6.2 Carbon Nanotubes

Sadhik Basha and Anand [42] proposed a Carbon Nanotube (CNT) blended water-diesel emulsion as an alternative fuel in a diesel engine. They prepared the CNT blended water-diesel emulsion by using a mechanical homogenizer and ultrasonicator. The CNT was taken in mass fraction of 25 ppm and 50 ppm and dispersed in the distilled 5% water, using the ultrasonicator set at a frequency of 40 kHz, 120W for 30 min. Then the surfactant mixture was prepared by mixing the two surfactants (Span 80 and Tween 80) with 2% by volume with an HLB value of 8. The 93% diesel was mixed with the surfactant mixture by a mechanical homogenizer at a constant speed of 2500 r/min for 15 min at a room temperature of 30^{o}C. The prepared CNT blended water-diesel emulsion fuels were kept in the 200 ml graduated scale test tube under static conditions. It was observed that the CNT was completely dispersed in the distilled water during ultrasonication. This possibly led to the encapsulation of CNT in the water droplet present in the continuous oil layer (diesel fuel). Figure 2.5 shows the preparation method.

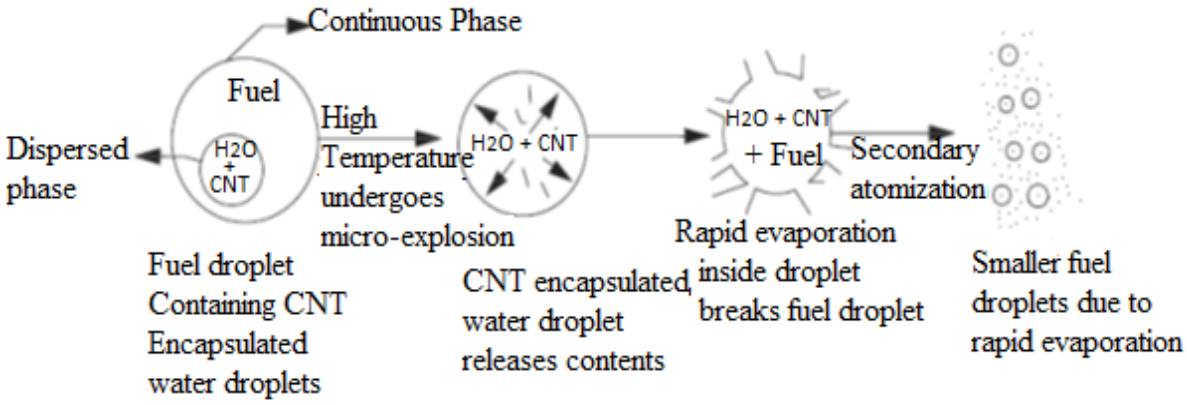

Figure 2.5 Schematic of micro-explosion phenomenon of CNT blended water–diesel emulsion fuel [42]

Tewari et al. [43] prepared a carbon nano tube (CNT) – biodiesel emulsion using a suitable surfactant. The biodiesel used for the preparation of the emulsion was obtained from honge oil.

Sadhik Basha and Anand [64] produced biodiesel from the raw Jatropha oil by standard transesterification process, and subsequently, two different nanoparticles; Alumina, CNT, and Alumina–CNT were blended with biodiesel in mass fractions of 25 and 50 ppm with the aid of an ultrasonicator to prepare the nanoparticles blended biodiesel fuel.

2.6.3 Charcoal based slurries

Fawziet et al. [65] explored the possibilities of different emulsions obtained from oil, water and charcoal, by analysing their characteristics. In their study, they prepared fuel oil-water emulsions with calorific values ranging from 33.9 to 42.3 MJ/kg and fuel oil-water charcoal emulsions with the calorific values ranging from 30.6 to 37.8 MJ/kg. These emulsions had relatively low sulphur and wax contents, and underwent the water gas shift reaction during combustion. They reported that the presence of a surfactant in the emulsions acted as an inhibitor of the corrosion activity of the water and fuel oil. Further, they classified the prepared emulsion into two types; stable and unstable. They described the stability of emulsion as a function of the zeta potential, dynamic viscosity, and density. For higher values of the zeta potential (104-115 mV), the emulsions were considered as stable during storage and handling, while for lower values the emulsions were unstable due to the separation of water and/or charcoal. They also reported that the physico-chemical properties of the

emulsions showed compatibility between some of the oil - water emulsions, oil - water charcoal emulsions and customary boiler fuels.

Vaghela Kalpesh and Dabhi Shyam [66] reviewed different research works related to the utilization of charcoal as an alternative fuel for CI engines. They reported that the charcoal diesel slurry could be prepared by the emulsification process, by using the proper surfactant, and used in CI engines. Some external energy like shaking or stirring may be required to obtain a homogeneous mixture. A non-ionic type surfactant may produce a more stable mixture as compared to other kinds of emulsifiers and better viscosity could be achieved.

2.6.4 Biomass fuels other than Coal/Charcoal slurries

Purushothaman and Nagarajan [41] have prepared orange skin power-diesel slurry in different proportions, and examined the physical and chemical properties. The solution was prepared from de-moisturized and finely ground orange skin powder less than 100-150 μm size mixed with diesel. The orange skin powder 30% mixed with 70% diesel (i.e. 300 g powder + 700 g diesel) on mass basis, and after 15–20 days the mixture was filtered to form orange skin powder diesel solution (OSPDS) and only 63% (630 g) was obtained. They reported that diesel loss increased with the increased percentage of mixture because the powder absorbed by the diesel was in the form of a precipitate.

Table 2.6 gives the comparison of important fuel properties between the solid based slurries, emulsion and diesel. The numerical value refers to the percentage of nanoadditive alumina, CNT in the blend fuel and orange skin powder.

Table 2.6 Fuels properties between the solid based slurries and emulsion and diesel

Fuels	**Properties**					
	Density @ 15 °C kg/m^3	**Kinematic viscosity @ 40 °C (cSt)**	**Flash point (°C)**	**Fire point, (°C)**	**Cetane number**	**Net calorific value (MJ/kg)**
Diesel [43]	840	2-3	56	65	46	43
D2S5W25CNT [42]	848.2	3.38	55	-	46	40.7
D2S5W50CNT [42]	848.9	3.42	54	-	47	40.9
HOME [43]	880	5.6	170	-	-	36.2
HOME25CNT [43]	898	5.7	166	-	-	34.6
HOME50CNT [43]	900	5.8	164	-	-	35.10
JBD [64]	895	5.25	85	-	53	38.88
JBD25A [64]	896	5.31	84	-	54	39.22
JBD50A [64]	897	5.35	82	-	56	39.53
JBD25CNT [64]	895.5	5.29	83	-	55	39.5
JBD50CNT [64]	897.9	5.33	81	-	57	39.78
JBD25A25CNT [64]	895.2	5.35	81	-	57	39.99
30% OSPDS [41]	851	4.1	70	83	-	40.9
D2S15W [41]	858.5	4.9	62	-	43	38.8
D2S15W25A [41]	859.1	4.94	63	-	48	39.3
D2S15W50A [83]	859.3	4.98	65	-	50	39.8
D2S15W100A [83]	859.6	5.01	66	-	50	39.9

2.7 Utilisation of solid fuel in CI engines

The utilisation of different solid fuels in the form of slurries or emulsions in CI engines has been reviewed and published by the researcher in the Journal of Renewable and Sustainable Energy Reviews, Elsevier Publications. The important points extracted from the review which are related to the use of such fuels in CI engines are given in Table 2.7.

Table 2.7 Review on the engine performance, combustion and emission results obtained from different diesel engine configurations fuelled with different solid fuels in the form of slurries or emulsions

[(+) indicates higher than diesel, (-) indicates lower than diesel]

S.No	Researcher Name	Reference	Type of fuel used	Type of engine and its capacity	Engine behaviour in comparison with that of diesel engine		
					Performance	Emission	Combustion
1	Guiyang Zhang et al	[67]	coal liquefaction (DCL)	Heavy-duty, 6 cylinder, turbocharged, intercooled, 246/2100 rated power/speed (kW/r/min), with exhaust gas recirculation (EGR).	BTE 8.5% (+) and 4% (-) at full load with the EGR system. BSFC showed an opposite trend to the BTE.	When EGR increased, 70% NO_x decreased, about 60% soot increased.	When 0-50% increased EGR, the maximum in-cylinder pressure, rate of heat release about the 25% and 6% mean gas temperature decreased.
2	Zhang Qiang et al	[68]	diesel-water coal slurries	8 kW, 1500 r/min diesel engine generating unit with a built - in electronic control unit.	Similar performance.	NOx and black smoke emissions not appeared.	Not reported.
3	Zhang Qiang, Ren Lan-zhu, Tian Ying	[69]	diesel CWS blends	Single cylinder, air cooled, diesel engine with 1200 rpm.	BSFC 20% (-) and BTE 17% (+) with the increase of fuel injection timings from 17^{o}CA to 18^{o}CA.	Smoke 22% (-) HC emissions 11% (+) NO_x (-) decreased first and then increased, CO emissions increased first and then decreased at full load.	Combustion duration - shortest at advance angle of 18^{o}CA.

S.No	Researcher Name	Reference	Type of fuel used	Type of engine and its capacity	Engine behaviour in comparison with that of diesel engine		
					Performance	Emission	Combustion
4	Stuart	[39]	CWS	DI, four stroke, bore - 229mm, stroke - 267 mm, Speed 1000 rpm pancake-shaped combustion chamber.	Higher indicated BTE.	Not reported	Combustion characteristics of a CWS were improved by replacing a small amount of the water with diesel.
5	Seshadri et al.	[70]	CWS	Modified positive displacement fuel injection system of a diesel engine.	Injection pressure of about 30 MPa or higher, than sprays were found to be similar for the CWS, diesel and water. The spray tip penetration as a function of time was found to be similar for the CWS, diesel and water-diesel emulsion.	Not reported	Not reported
6	Urban et al.	[71]	CWS	Medium-speed, two-stroke, 900 rpm, 160 kW, manufactured by Electro-Motive Division of General Motors Corporation.	BTE 85% (+)	NOx - 50% (-) HC - 50% (+) at full load. PM - 40% (+)	Ignition delay - reduced Pre combustion air temperature of about 1000 K was required to achieve the maximum combustion efficiency with the CWS in a medium speed engine.

S.No	Researcher Name	Reference	Type of fuel used	Type of engine and its capacity	Engine behaviour in comparison with that of diesel engine		
					Performance	Emission	Combustion
7	Uzkan et al.	[38]	CWS and diesel fuel	Two-cylinder, four stroke, 645 Electro-Motive Diesel (EMD), 900 rpm speed with 1850 psi full load.	The injection timing of the pilot fuel played an important role in the CWS combustion. The CWS amount and timing, decreased the pilot fuel amount moved the CWS combustion to later crank angles. This reduced the CWS combustion (as well as engine thermal) efficiency.	The pilot amount (diesel) is decreased to a low load, as the exhaust smoke increased.	The cylinder pressure and temperature were low (1050 psi) at part load, in comparison with the full load operation of the engine (1850 psi). As the pilot timing was changed toward the top dead centre (TDC) for the same pilot and the CWS amounts, the cumulative heat release increased to the peak and then decreased.
8	Kishan et al.	[72]	CWS	Two-stroke, four cylinder, conventional open chamber, direct-injection, 1390 kW rated power, 120 to 900 rpm speed.	Higher indicated thermal efficiencies for the specific injection timings due to faster burning rates. Lower equivalence ratios or smaller particle sizes resulted in higher BTE.	Not reported.	Increasing the inlet air temperature improved the ignition and combustion characteristics of the CWS.

S.No	Researcher Name	Reference	Type of fuel used	Type of engine and its capacity	Engine behaviour in comparison with that of diesel engine		
					Performance	Emission	Combustion
9	Rao et al	[73]	CWS	Cooper-Bessemer JS-1 single-cylinder, four stroke, with a speed range of 300-450 rpm and 150 psi bmep.	Higher manifold air temperature (MAT) improved the ignition process and BTE, resulting in better performance and reduced SFC.	Low CO emission. The high manifold air temperature increased NO_x emission. But air temperatures below 93°C, CWS generated lower NO_x. Larger hole nozzles generated lower NO_x, both with CWS and DF-2 fuels.	High injection pressures (up to 15,000 psi.) resulted in the good atomization of CWS, and in combination with the heated combustion air resulted in short ignition delays.
10	Hsu	[40, 74]	micronized coal-water slurry (MCWS)	GE 7FDL two cylinder, four stoke, DI diesel engine, 229 mm bore, 267 mm stroke, 1050 rpm speed, 195 kW rated maximum output power.	The engine was able to run with 50% coal in the slurry at 1050 rpm without major changes in the engine parameters.	Not reported	The maximum heat release rate resulted in a higher maximum cylinder pressure. The peak cylinder pressure became higher when about 95% of the CWS fuel was burned.
11	Hsu	[75]	CWS	GE 7FDL two cylinder, DI diesel engine, 1050 rpm speed, 195 kW full rated power with new accumulator-based injection system.	Improved pumping system was required to achieve better performance results at full load.	Not reported	New accumulator based injector system through reduced ignition delay.

S.No	Researcher Name	Reference	Type of fuel used	Type of engine and its capacity	Engine behaviour in comparison with that of diesel engine		
					Performance	Emission	Combustion
12	Hsu et al.	[76]	CWS	GE 7FDL two cylinder, DI diesel engine, 229 mm bore, 267 mm stroke and 1050 rpm speed, 195kW maximum rated power.	Engine was able to give 99.5% combustion efficiency. Holding the cylinder pressure below 17 MPa and the BTE was close to that of diesel.	NO_x - 26% (-) due to water content in CWS fuel.	Higher injection pressure yielded better engine combustion results when the engine was operated at 85 MPa.
13	Hsu et al.	[77]	CWS	GE 7FDL two cylinder, DI diesel engine, 229 mm bore, 267 mm stroke and 1050 rpm speed with high speed camera	The 8 μm fuel size faster burn at the average cylinder temperature was low with lower quality combustion.	Not reported.	The combustion of coal fuel ended with burnt the wall-attached fuel off the piston bowl and within the range tested (less than 89 MPa), and higher injection pressure provided more dehydrated coal fuel at ignition time.
14	Siebers, T. M. Dyer	[78]	CWS	A single-event, constant-volume combustion bomb designed and fabricated by Volkswagen Research in West Germany.	The combustion was designed to closely simulate the combustion processes occurring near TDC in various types of piston engines.	Not reported.	The ignition delay of the CWS fuel was dependent on temperature and pressure. Ignition delay- (longer) Heat release rate- (lower)

S.No	Researcher Name	Reference	Type of fuel used	Type of engine and its capacity	Engine behaviour in comparison with that of diesel engine		
					Performance	Emission	Combustion
15	Hsu	[79]	CWS	GE 7FDL two cylinder, DI diesel engine, 229 mm bore, 267 mm stroke and 1050 rpm speed, 195 kW rated power.	The completion of the first phase coal fuel locomotive track test marked a major milestone in the development of used coal fuel.	Not reported	The electronic controlled test engine yielded 99.5% combustion efficiency.
16	Benedek et al.	[80]	CWS	Cooper-Bessemer 33-cm (13-in.) bore, 400 rpm, single cylinder research engine.	Not reported	NO_x - 19% (-) CO - lower	Not reported.
17	Dodge et al.	[81]	Micronized coal-water slurries (MCWS)	Single cylinder, four stroke Cooper JS-1 diesel engine with 300-450 rpm speed range with high injection pressures varying from 40 to 140 MPa.	The cone angles and fuel-air mixing increased rapidly with the relatively constant cone angles of diesel. At high injection pressures the CWS mixed with air more slowly, and the sprays penetrated more rapidly than diesel at the same injection pressures.	Not reported.	Increasing the injection pressure reduced the drop sizes in the CWS sprays, while the increasing injection pressure reduced the drop sizes in the diesel fuel sprays more gradually.

S.No	Researcher Name	Reference	Type of fuel used	Type of engine and its capacity	Engine behaviour in comparison with that of diesel engine		
					Performance	Emission	Combustion
18	Sadhik Basha and Anand	[42]	Carbon nanotubes (CNT) blended, water diesel emulsion, and diesel fuels	Single-cylinder, four-stroke, mechanical-injection type, air-cooled, DI diesel engine developing a power of 4.4 kW at 1500 rpm constant speed.	The BTE of the CNT blended water–diesel emulsions was 11.5% (+), for water-diesel emulsion at the full load 2.4% (+).	NO_x (CNT blended water–diesel emulsions)- 27.6% (-) Water-diesel emulsion the NOx- 22% (-) at full load.	The cylinder pressure for the CNT blended water–diesel emulsions by about 5.6% (-). Heat release rate- 3.3% (-) at the full load.
19	Sadhik Basha and Anand	[82]	CNT blended Jatropha Methyl Ester (JME) emulsions, JME and JME-water emulsion	Single-cylinder, four-stroke, air-cooled, DI diesel engine developing a power of 4.4kW at a constant speed of 1500 r/min.	BTE- 2-4% (+) CNT blended JME emulsion fuels in comparison with neat JME and JME-water emulsion.	The NOx and smoke emissions were found to be lower by about 17% than those of neat JME and JME-water emulsion at full load.	The cylinder pressure and heat release rate 5-7% (-) for the CNT blended JME emulsion compared to that of the neat JME and JME-water emulsion.
20	Tewari et al	[43]	Multi walled carbon nanotubes (MWCNTs) blended biodiesel, HOME and diesel.	Single cylinder, four stroke, DI diesel engine at 1500 rpm speed, 5.2 kW rated power.	The BTE HOME-MWCNT blended fuels were 2-5% (+) compared to that of HOME.	NO_x- 4-29% (+) for HOME-MWCNT blended fuels compared to that of HOME and 6-25% (+) compared to that of diesel. .	Ignition delay- reduced higher premixed combustion fraction and higher peak temperatures.

S.No	Researcher Name	Reference	Type of fuel used	Type of engine and its capacity	Engine behaviour in comparison with that of diesel engine		
					Performance	Emission	Combustion
21	Sadhik Basha and Anand	[83]	Water–diesel emulsion fuel, Alumina nanoadditive blended water-diesel emulsion fuels and diesel.	Single-cylinder, four-stroke, naturally aspirated, mechanical-injection type, air-cooled, DI diesel engine developing a power of 4.4 kW at a constant speed of 1500 r/min	The BTE 28.9% for D2S15W100A, whereas it is 28.3, 27.9, 26.9 and 25.2% for D2S15W50A, D2S15W25A, D2S15W, and neat diesel, at the full load.	NO_x for D2S15W100A about 33.5% (-) . By about 11% lower compared to that of D2S15W emulsion.	Alumina nanoparticles blended water–diesel emulsion of the cylinder peak pressure 5.7% and heat release rate 13-20.3% higher compared to water diesel emulsion.
22	Sadhik Basha and Anand	[64]	Alumina and CNT nanoparticles blended biodiesel fuel	Single cylinder, air cooled, DI diesel engine with 4.4 kW rated output power with 1500 rpm speed	The BTE for the JBD25A25CNT 16% (+) than biodiesel at the full load.	Smoke 14.9% (-) than that of Jatropha biodiesel fuel.	Cylinder peak pressure for the JBD25A25CNT 5.3% (-) compared to that of JBD fuel and heat release rate 15.7% (-) at the full load.
23	Valentin Soloiu et al	[37]	Biomass charcoal diesel slurries	Yanmar NF-19, single cylinder, air-cooled, DI engines, 1200 rpm speed, 7.8 bmep, and Omega combustion chamber.	BSFC- 4.8% (+).	NOx- 30% (-). The engine was operated with retarded injection timing the NO_x level decreased.	Charcoal slurry fuel-2.1ms (longer). Net heat release for charcoal slurry-35 J/^{o}CA (+).

S.No	Researcher Name	Reference	Type of fuel used	Type of engine and its capacity	Engine behaviour in comparison with that of diesel engine		
					Performance	Emission	Combustion
24	Patton R et al.	[84]	Charcoal based slurry and coal based slurry	Not mentioned	Charcoal-based water slurries reduced engine abrasion problems compared to coal based slurry.	Not reported.	Potential supply of charcoal was adequate to supply 75% of current diesel fuel consumption.
25	Piriou et al	[51]	Solid biomass	Reciprocating engines	The main technical barrier is related to fuel metering and conveying to the engine combustion chamber. It is actually very difficult to feed a powdered solid fuel at high frequency while keeping a constant metering of dust. Computer controlled injection system for conventional fuels will certainly help in injecting such type of fuels.	Not reported.	The combustion fine biomass particles can occur quickly enough to fit in the cycle of an internal combustion engine running at high speed.

S.No	Researcher Name	Reference	Type of fuel used	Type of engine and its capacity	Engine behaviour in comparison with that of diesel engine		
					Performance	Emission	Combustion
26	Purushothaman et al.	[41]	Orange Skin Powder Diesel Solution (OSPDS) and diesel.	Single cylinder, air cooled, 4.4 kW rated power, 1500 rpm DI diesel engine.	30% OSPDS was optimum for better performance at full load. BTE 1.1% was found higher at 235 bar than that of other fuel injection pressures 215 and 255 bar. BTE of 30% OSPDS 1.2% (-) at the full load.	NOx 26% (+), HC 66% (-) and CO 39% (-) with 30% OSPDS at 235 bar than that of diesel at a full load.	The cylinder pressure with 30% OSPDS at 235 bar fuel injection pressure, 2.8% (+). The peak heat release rate, for 30%OSPDS at 235 bar is 15 J/^{o}CA (+).
27	Harish Reddy et al.	[85]	Orange peel powder diesel solution (OPPDS)	Single cylinder, 4 stroke, 1500 rpm constant speed and 3.7 KW rated power, DI engine.	Not reported	CO_2 13.3% (-) at 20% load, 16.1% (-) at 80% load for both 20% and 30% OPPDS. HC and CO emission 53.3% (-) and 16.7% (-). NOx- 9-26% (-).	Not reported.

2.8 Tyre pyrolysis process

Alsaleh and Sattler [86] suggested that the waste tires are excellent materials for recovery of energy, as well as solid, liquid, and gaseous by products, via pyrolysis process: made predominantly from the petroleum product rubber, they have a high heating value, as well as high volatile content and medium sulfur content. They reported that the temperature is the predominant factor influencing the distribution of gas, liquid, and solid phase pyrolysis products, and their physical and chemical properties. Other influential factors include heating rate, particle size, feedstock composition, pyrolysis time, tyre residence time, carrier gas flow rate, volatiles residence time, presence of steam in the carrier gas, and presence of a catalyst in the tyre.

Martinez JD et al. [87] reported the most common pyrolysis reactors include fixed bed, rotary kiln, and fluidized bed. The fixed bed reactors (FBR) are usually used for slow pyrolysis in a batch process characterized by low heating rates, long solid and vapor residence times, and often low temperature. Pyrolysis involves heating a feedstock to temperatures more than 400°C without oxygen in order to volatilize and decompose the feedstock, producing oil, gas, and carbon black. Pyrolysis time is related to particle size in general, larger particles require longer residence times to achieve the same degree of conversion.

Williams [32] proposed that the oil resulting from pyrolysis may be used directly as a fuel, upgraded to a higher quality fuel, or used to produce chemicals. The gases typically consist of hydrocarbons and hydrogen with a high heating content, so that the gases can serve as a fuel for the pyrolysis process. The solid char consists of carbon black filler along with pyrolysis char.

Sharuddin et al. [88] explored the pyrolysis method, the waste management becomes more efficient, less capacity of landfill needed, less pollution and also cost effective. Moreover, with the existence of pyrolysis method to decompose plastic into valuable energy fuel, the dependence on fossil fuel as the non-renewable energy can be reduced and this solves the rise in energy demand.

Nhlanhla et al. [89] reported that the pyrolysis is identified as an endothermic process that induces the thermal decomposition of feed materials without the addition of any reactive gases, such as air or oxygen. The thermal efficiency of this process is approximately 70%, and can be increased up to 90% with the use of pyrolysis products as fuel. The thermal energy used to drive the pyrolysis reaction is applied indirectly by thermal conduction

through the walls of the containment reactor. They also suggested that the pyrolysis generally occurs at temperatures between 400 and 800°C. As the temperature changes, the product distribution are also altered. Lower pyrolysis temperatures usually produce more liquid products while higher temperatures favour the production of gases. The pyrolysis process yields a gaseous fraction of mainly non-condensable gases, a solid fraction mainly composed of carbon, metal and others inert material as well as an oily fraction mainly composed of organic substances condensable at ambient temperature and pressure. The composition of the pyrolysis products is influenced by the process operating conditions such as, feed size, operating temperature and pressure, residence time, heating rate and the presence of catalytic medium.

The following are the summary of the review on the characterisation and utilisation of different solid fuels as alternative fuels for CI engines;

- Many of the research works carried out in the past show that the slurries or emulsions obtained as coal, charcoal, carbon nanotube, nanoadditive blended, carbon black, orange skin powder and solid biomass seem to obtain energy from, and can be utilized in the form of slurry in CI engine.
- The physical properties of the solid fuel as the particle size, viscosity, density and slurryability directly affected the engine parameters. The nanoparticle size of the solid fuel gave a better performance.
- The CWS, Charcoal water slurry, CBWS, OSPDS exhibit lower BTE compared to that of diesel in a CI engine without any engines modification. But, minor engine modification such as injection timing, and injection pressure improved the BTE of the engine.
- Nanoadditive blended and nanoparticles blended water–diesel emulsion gave higher BTE than that of diesel while the CO, NOx and smoke emission were lower.
- From the literature review, undertaken in this work, no use of Carbon black as possible alternatives energy source has been found for heat and power applications.

CHPATER 3
FUEL PREPARATION AND CHARACTERISATION

3.1 General

In this research work, two different categories of fuels, carbon black (CB) based slurry (Carbodiesel) and CB based emulsions (CBWD) were considered as alternative fuels for DI diesel engines. The methods of preparing CB based slurries and emulsions, and characterisations were described with the necessary schematic diagrams and photographs, in this chapter. Also, analysis of CB using SEM, TGA/DTA, FT-IR and spray analysis for the emulsion are also described in this chapter with the necessary illustrations. The viscosity of the carbon black-water-diesel emulsion (CBWD) increases with the solid concentration in the emulsion, but the stability of the suspension will become poorer, if the viscosity is reduced. Therefore, before utilization of the CBWD emulsion in combustion devices, a preliminary investigation is essential to study its rheological behaviour. This chapter discusses the the rheological behaviour of the CBWD emulsion.

3.2 Materials

Raw carbon black (RCB) is one of the value added products obtained in a tyre pyrolysis process, and the others are tyre pyrolysis oil (TPO), pyrogas and steel [90]. The schematic diagram of the pyrolysis process followed in the tyre recycling plant in India is shown in Fig. 3.1.

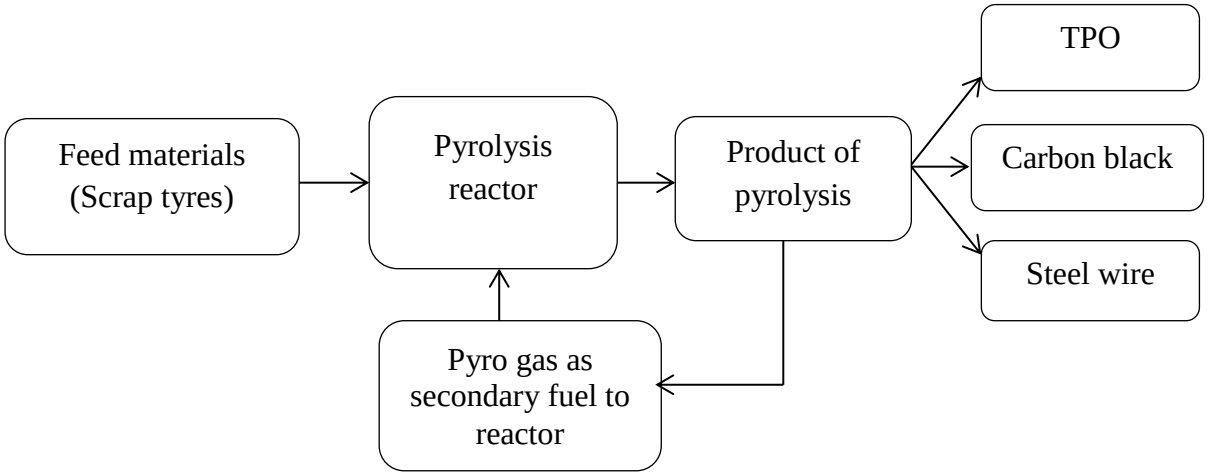

Figure 3.1 Block diagram of tyre pyrolysis process

The general procedure of the pyrolysis process is as follows; the discarded waste tyres are fed into an externally heated reactor unit. The fed tyres are heated in the absence of oxygen. The process is carried out in a temperature range of 450-500^{o}C. The volatile vapour evolved in the reactor is condensed in a water cooled condenser. The condensed liquid, referred to as tyre pyrolysis oil (TPO), is collected in a separate oil tank. Some of the non-condensable volatile vapour is returned to the reactor unit, and used as a secondary gaseous fuel, to preheat the reactor. A solid waste, CB, is collected from the reactor unit after the process is complete. The percentages of the various product yields of the tyre pyrolysis process are 45% TPO, 15% pyrogas, 30% CB and 10% steel wire. This 30% CB is obtained as a waste from the total input. This CB is impure and disposed in the open land.

Figure 3.2 shows the photographic view of Agrwal Tyre pyrolysis plant, Rourkela which are growing the CB and oil and the process indicating feed stock to the end product through the pyrolysis process [91, 92].

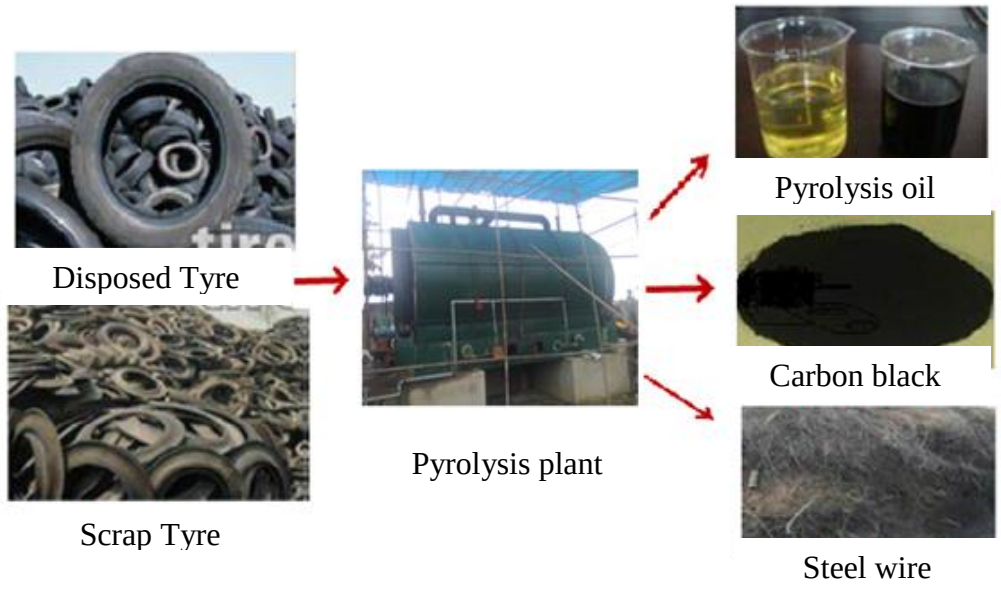

Figure 3.2 Pyrolysis process and its products [88]

The CB is used as reinforcing filler in rubber, especially in tyres or as activated carbon because of its high carbon content [93]. A sample of raw Carbon black (RCB) before pre-treatment was dried, and ground. The RCB was screened using a sieve, to get the maximum particle size of 40μ for determining the initial particle size distribution. The RCB with a particle size of 40μ was leached in concentrated sulphuric acid (70 wt.%), and treated for the removal of heavy metals and other contaminants. The treated carbon black (CB) sample was dried for further analysis.

3.3 Analysis of CB

The CB was pelletized and analysed for the presence of inorganic components using Rigaku's Philips Ultima IV *X-ray diffraction* instrument (XRD). Proximate, and ultimate analyses were used to determine the elemental composition, moisture, while the Bomb calorimeter was used to determine the calorific value of the sample. The element composition of CB is tabulated in Table 3.1. The important proximate and ultimate analyses of CB are compared with those of some of the solid fuels given in Table 3.2.

Table 3.1 Element of CB

Material	**Elements**
Carbon black	C, S, Si, Zn, Fe

Table 3.2 Proximate and ultimate analysis

Properties	Coal [40]	Charcoal [37]	CB [94]
Density, kg/m^3	673-913	400	860
Calorific value, MJ/kg	35.6	29.2	32.8
C, wt%	84.15	94	86.4
H, wt%	5.15	NA	2.86
N, wt%	1.26	NA	<0.3
S, wt%	0.59	NA	0.02
O, wt%	6.39	6	1
Ash content, %	0.36	10.241.77	10.24

3.4 XRD analysis of CB

X-ray diffraction (XRD) is an analytical technique which is specifically used for the phase analysis of a crystalline structure. It relies on the dual wave or particle nature of X-rays to obtain information about the structure of materials, which are usually crystalline in nature. It can be utilized to analyse different qualities or properties of single or polycrystalline materials. It can help in the identification of fine-grained minerals, such as clays and mixed layer clays that are difficult to determine optically. It can also help in the identification of the atomic or molecular structure of the crystalline material [95]. A schematic diagram of the XRD principle is shown in Fig. 3.3.

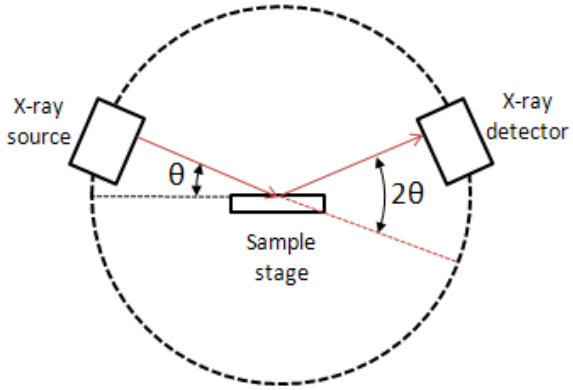

Figure 3.3 XRD principle

X-ray diffraction works on the principle of Bragg's Law, which states that $n\lambda = 2d \sin\theta$, where *d* is the diffraction spacing between planes, θ is the incident angle, *n* is any integer, and λ is the wavelength of the beam incident on the nanoparticles. The XRD analysis requires a large volume of sample, and is a time-consuming technique. A crystallographer can produce a 3-D picture of the density of electrons within the crystal by measuring the angles and intensities of the diffracted X-ray beams. X-rays are directed at the sample, and the diffracted rays are collected after detection, processed and then counted to make the calculations. From the intensity, the chemical bonds can also be determined [95]. In order to characterize the inorganic residue, the CB sample is analysed using the X-ray diffraction technique. This was carried out in a Siemmens-5000 X-ray diffractometer which is available in the Physics department laboratory at NIT, Rourkela. Figure 3.4 shows the photographic view of the multipurpose X-ray diffraction instrument (Rigaku's Philips Ultima IV).

Figure 3.4 Multipurpose X-ray diffraction instrument (Rigaku's Philips Ultima IV)

The XRD sample was prepared by placing a few grams of powder on the glass holder of the XRD analysis. The XRD was operated at 40V and 30A, using copper filtered Cu-Kα radiation with a wavelength of 1.541 Å. The diffraction pattern was obtained by scanning the sample at an interval angle of 2θ from 10º to 80° and a rate of 2/0.02 (degrees/s). The technical specifications of the XRD are given in Annexure 1.

The spectra obtained for CB are shown in Fig. 3.5. For the CB powder sample a significant overlap of the diffraction profile was seen. From the figure it is cleared that the concentration of C element is highest in comparision to the other elements. The XRD spectrum of the CB sample exhibits the presence of Zn, Si, S and Fe inorganic residues. Sulphur is one of the most common impurities in CB which is introduced with the tyre rubber feedstock during tyre manufacturing [93]. Other inorganic contaminants such as Si, Zn and Fe are also added to the raw materials of the tyre during tyre manufacturing; they are used in the form of trace metals, and cracking catalyst residues. These metal traces might also be formed in the pyrolysis reactor. The presence of Zn, S impurity is also observed in the XRD spectra. This is because, during pyrolysis at high temperature, zinc starts decomposing to form ZnS by chemically reacting with the sulphur presence in the sample.

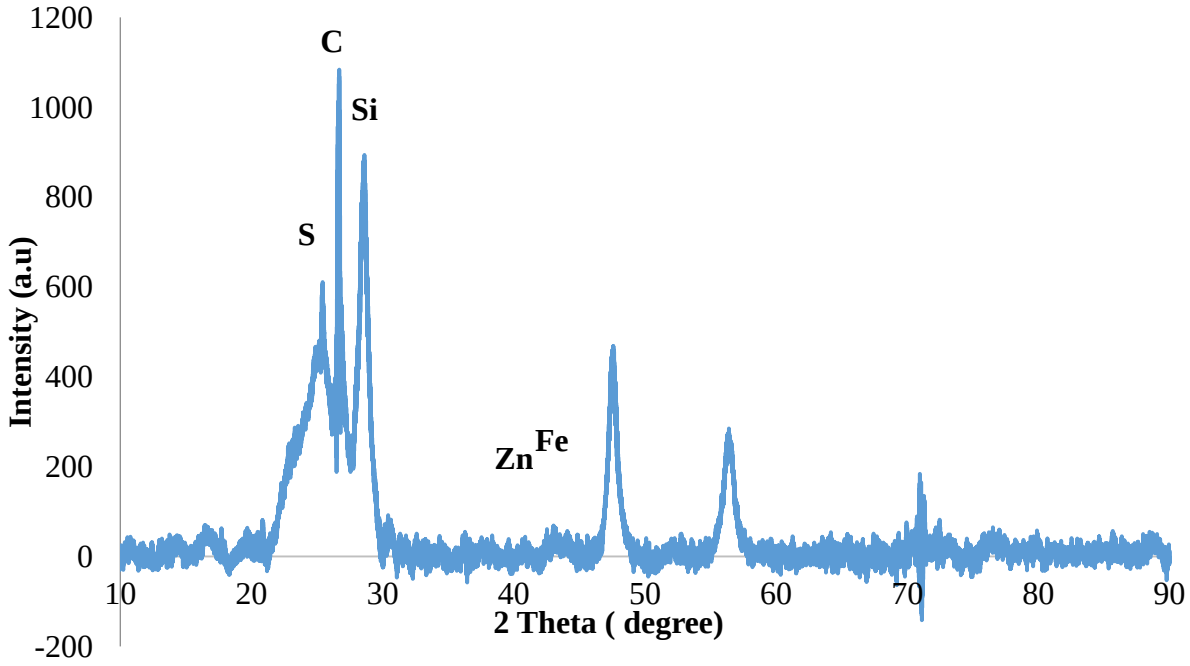

Figure 3.5 XRD spectra of CB

3.4.1 Carbon black leaching

The treatment of CB was done using concentrated sulphuric acid (70wt.%). The treatment was carried out at a reaction temperature of 60ºC, and reaction time of 90 minutes. The

reaction was carried out in a 500ml beaker placed on a hotplate magnetic stirrer maintained at 60ºC. The initial XRD analysis showed a high concentration of zinc oxide (ZnO), iron oxide (FeO) and sulphur present in the RCB. The concentrated sulphuric acid at elevated temperatures can react with the focus compounds to form water soluble salts and gaseous compounds that can be easily isolated from the solid phase. After the reaction the mixture was cooled. Further it was filtered, washed with deionised water to neutralise the solids, and finally, the solids were dried at 110^{o}C for 24 hours [96].

3.5 SEM analysis of CB

It is necessary to understand the structure of the CB, if it has to be used in a combustion device. A sample of CB obtained from the TPO plant and the CB after grinding was initially found to have fine powder particles of 40µ size. Figure 3.6 shows the photographic views of the coal powder, Charcoal powder and CB from pyrolysis of tyres.

Figure 3.6 Photographic view of the (a) coal powder, (b) Charcoal powder and (c) CB powder

The objective of this investigation is to use the different slurries and emulsion obtained from the CB powder in a stationary diesel engine. The hole size of the injector nozzle of the test engine was 0.25mm which was larger than 40µ. After grinding the CB into powder form, the CB powder was tested by a scanning electron microscope (SEM) to study the structure of the CB powder. The principle of SEM is that, when a material is irradiated with a high energy electron beam, the sample will emit X-rays. The X-rays have energies that are characteristics of the elements being irradiated. This permits the identification of the elements present in any

solid that can be viewed by the SEM. The image of the CB obtained by the SEM is shown in Fig. 3.7.

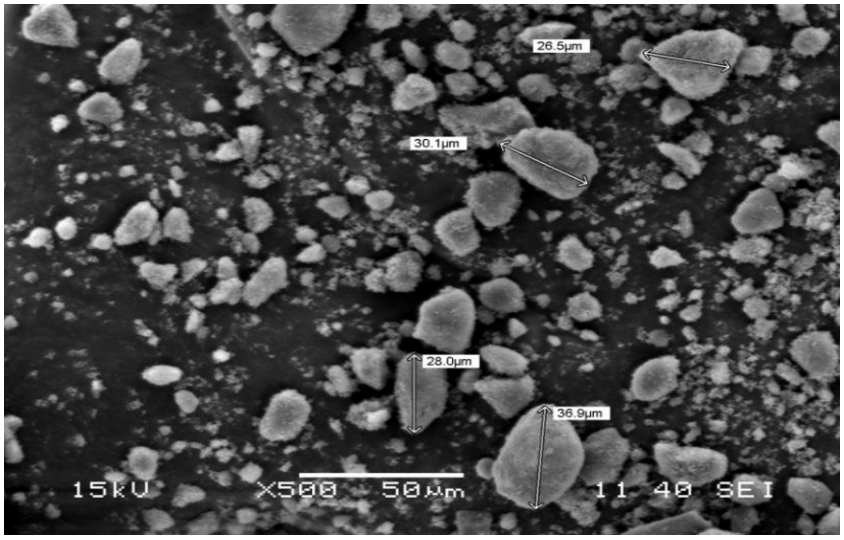

Figure 3.7 Image of the CB by the SEM [88]

Mostly circular crystal filaments and some semicircular crystal filaments are seen in the image. The image also confirms the average particle size of the CB powder as 40µ, which is favourable for solid particle combustion [92].

3.6 TGA and DTA analysis

The thermal gravimetric analysis (TGA) is a method weight changes (mass) as a function of temperature under a controlled atmosphere. It is used to predict as vaporization, absorption and desorption and chemical properties such as decomposition, chemisorptions, and oxidation of organic substance in an oxygen free or inert atmosphere. Differential thermal analysis (DTA) is a method to find the difference in temperature and heat flows between the sample and reference. It is used to ensure whether the sample is exothermic or endothermic. Figure 3.8 depicts the TGA and DTA curves obtained for the CB in an oxygen environment.

The thermo gravimetric/differential thermal analysis (TG/DTA) was carried out for the CB sample using a SHIMADZU DTG-60/60H instrument. The technical specifications of the instrument are given in Annexure 2. A known weight of the sample was heated in a silica crucible at a constant heating rate of 10^{o}C /min operating in a stream of oxygen atmosphere with a flow rate of 40 mL/min from 35^{o}C to 1000^{o}C. The TGA curves represent mass loss percent vs. temperature, and DTA curves are their derivatives with respect to temperature. It

can be observed from the figure that, the CB oxidized about 75% of its original mass at 650^{o}C, with an elevated exothermic reaction around 450^{o}C from the lignin oxidation. It can also be observed that, about 80% of the CB oxidized between 450 and 700^{o}C. It can also be observed, from the figure that an increased oxidation reaction occurred at 450^{o}C, with a higher exothermic reaction from the CB [92].

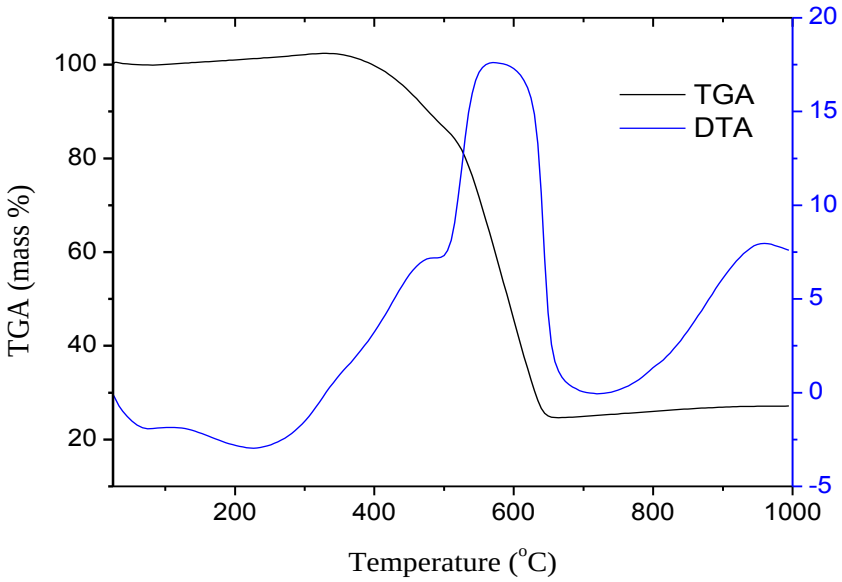

Figure 3.8 TGA/DTA analysis of CB

3.7 Fuel preparation and characterisation

3.7.1 CB based slurries

3.7.1.1 Carbodiesel

In this investigation, Carbodiesel from the CB was prepared adopting a sequence of processes. A block diagram of the process involved in the preparation of Carbodiesel is shown in Figure 3.9, and the photographic views of diesel and Carbodiesel are illustrated in Figure 3.10 and Figure 3.11 respectively.

In this study, CB was dried in direct sunlight for one day, to remove the moisture in it. The CB was powdered with the help of a hammer. Then, the powder was further classified by a sieve to get a fine powder size of 40 µ. This was done because, the injector nozzle diameter is 0.25mm which is greater than 40 size of CB particle. The CB was taken at different proportions from 5% to 20% on the volume basis. The CB powder was mixed with diesel at 80^{o}C and continuously stirred about 15 minutes using a mechanical stirrer to get a slurry, with a 0.15kWh unit electricty consumption. For stirring operation, the power consumed was approximately 0.04 kW. Finally, the slurry was cooled and filtered to get a Carbodiesel.

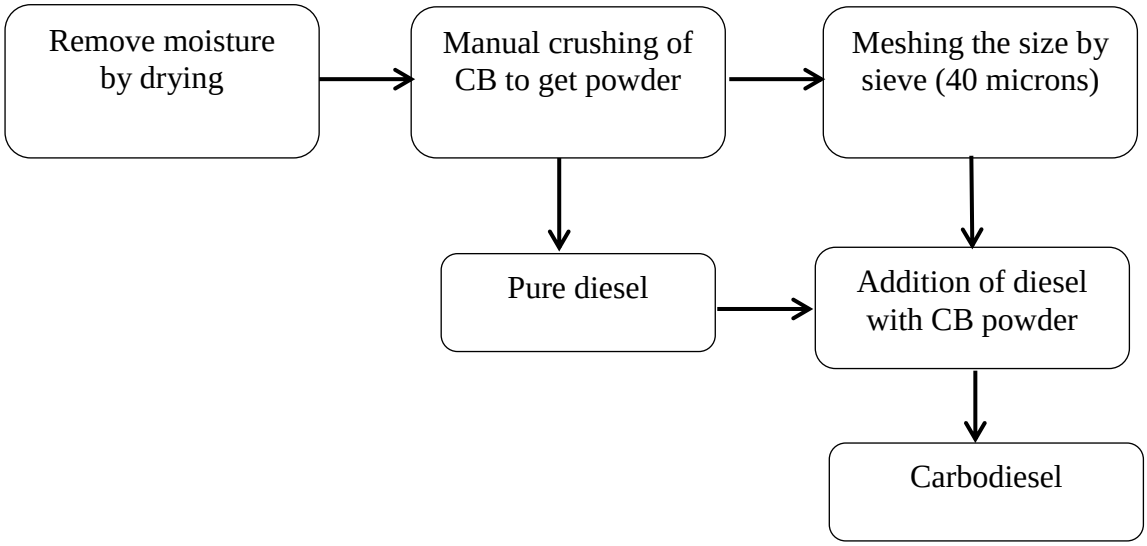

Figure 3.9 Carbodiesel preparation process [92]

Figure 3.10 Pure diesel

Figure 3.11 Carbodiesel

The Carbodiesel obtained from the CB and diesel in different proportions, and the notations are given in Table 3.3. The Carbodiesel5 fuel cost are given in Annexure 3.

The steps involved to get 5% volume of CB are as follows:

We know that, Vol. = Mass/ρ (3.1)

Where, ρ = density of CB

$1\ m^3 = 1000$ litre

1 litre $= 1/1000\ m^3$

250 ml $= \{(1\times10^{-3})/4\}\times860\ kg/m^3$

$= 0.215$ kg

$= 215$ gm

50 ml $= 215/5$

$= 43$ gm

43 gm of CB is equal of 5% volume of CB

Similarly, 86, 129 and 172 gm of CB is equal of 10, 15 and 20% volume of CB

Table 3.3 Carbodiesel5, Carbodiesel10 Carbodiesel15 and Carbodiesel20 [92]

Carbon black %	**Diesel %**	**Name of Fuel**
5	95	Carbodiesel5
10	90	Carbodiesel10
15	85	Carbodiesel15
20	80	Carbodiesel20

3.7.1.2 Ultimate analysis of Carbodiesels

The chemical compositions of different Carbodiesels are compared with those of diesel and are given in Table 3.4.

Table 3.4 Ultimate analysis of Carbodiesels [92]

Sl. No	**fuel type**	**C %**	**H %**	**N %**	**S %**
1.	Carbodiesel5	79.7	8.3	9.5	2.1
2.	Carbodiesel10	81.2	8.4	7.2	2.5
3.	Carbodiesel15	80.6	8.9	7.6	2.6
4.	Carbodiesel20	79.9	8.7	7.4	2.9
5.	Diesel	84.3	9.4	1.3	0.8

3.7.1.3 Fuel properties of Carbodiesels

The comparison of various physical properties of Carbodiesel5, Carbodiesel10, Carbodiesel15 and Carbodiesel20 are given in Table 3.5.

Table 3.5 Properties of Carbodiesels [92]

Properties	**Carbodiesel5**	**Carbodiesel10**	**Carbodiesel15**	**Carbodiesel20**
Density, kg/m^3	833.0	833.9	839.2	841.0
Viscosity, cSt	2.8	2.9	3.02	3.08
Ash content,%	0.003	0.004	0.006	0.008
Carbon Residues,%	0.08	0.1	0.14	0.2
Flash point,^{o}C	62	64	67	68
Fire point, ^{o}C	67	71	73	77
Pour point, ^{o}C	< -12	< -12	< -12	< -12
Cetane Number	49	48	46	45
Calorific Value, MJ/kg	42.7	42.3	41.9	40.7

3.7.1.4 FT-IR analysis

The Fourier Transform Infrared Spectroscopy (FTIR) offers a quantitative and qualitative analysis of the organic and inorganic samples. The spectra produce a profile of the sample, a distinctive molecular finger print that can be used to screen and scan samples of many different components. It identifies chemical bonds in a molecule by producing an infrared absorption spectrum. The FTIR is an effective analytical instrument for detecting the functional groups, and characterizing covalent bonding formation. The FTIR test was carried out in a Perkin Elmer Spectrum equipment, which has a scan range of 400-4000 cm^{-1} with a resolution of 1.0 cm^{-1}. The technical specifications of the instrument are given in the Annexure 4. Figure 3.12 shows the photograph of the Penkin Elmer spectroscopy used in the study.

Figure 3.12 Penkin Elmer spectroscopy

The results of the FTIR analysis for Carbodiesels are depicted in Figure 3.13. The variation of the percentage transmittance with wave length gives the information about the position of various bond vibrations, distinguished by several modes such as stretching, distortion, bending etc. It can also determine the quality of a sample, and the amount of a component in a mixture. It is evident from the figure 3.13 that the 5% CB line is not following the trends of all of the other data lines. It might be contributed to the experimental error during analysis.

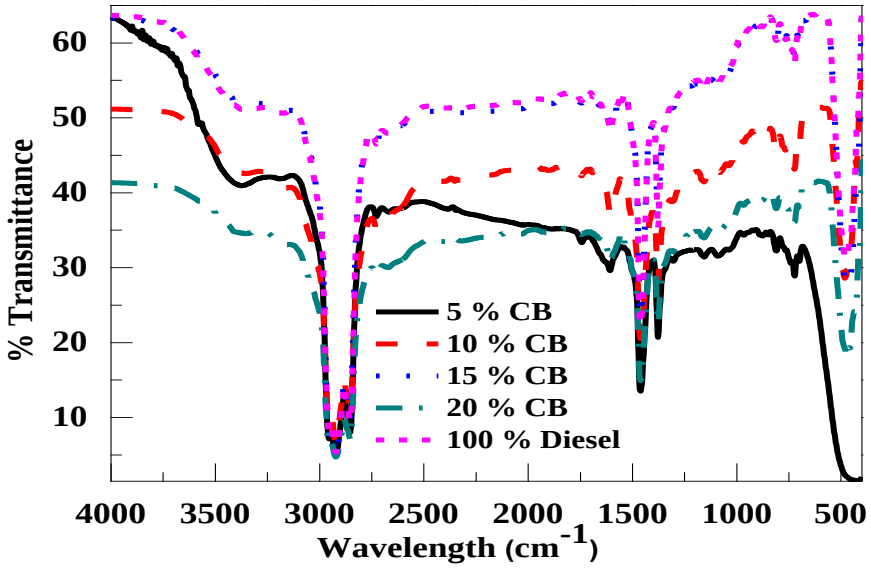

Figure 3.13 FT-IR analysis

Table 3.6 Various bonds present in CB diesel blends and diesel

Wave number cm^{-1}	Wavelength µm	Bond	Product
2922.99	3.0 – 3.7	C-H	All blends and diesel
2833.26	3.0 – 3.7	C-H	All blends and diesel
1742.56	5.4 – 6.1	C=O	All blends and diesel
1606.10	5.9 – 6.3	C=N	All blends and diesel
1461.02	6.8 – 7.7	C-H	All blends and diesel
1376.73	13 – 14	C-Cl	All blends and diesel
808.56	8.3– 12.5	C-C	CB15, CB10
1742.56	5.4 – 6.1	C=O	diesel, CB10
1155.92	7.4 – 10	C-F	Diesel
808.91	11.9– 12.3	Nitrate	Diesel
480.17	v17 – 21	C-I	Diesel

Table 3.6 gives the various bonds present in different Carbodiesels and diesel. It can be observed from the table that the Carbodiesels have strong bonds of carbon with the hydrogen,

oxygen, nitrogen and chlorine etc. The stretching vibrations exist in the functional groups leading to an increase or decrease in bond length.

3.7.2 CB based emulsion

3.7.2.1 Emulsion principle

Generally, emulsions are prepared out of two immiscible fluids like oil and water, one being dispersed into another, presence of surface-active compounds. Emulsion is a thicker (more viscous) liquid or fluid than the oil or water they contain. They are used as intermediate or end products such as the food (salad dressing), ice cream, chemicals, cosmetics, pharmaceutical, paints, oil and coating industries [97].

There are two main types of emulsion. Figure 3.14 shows the picture of types of emulsion.
(a) Oil in water emulsion-oil droplets in water (Examples- milk, ice cream, salad cream)
(b)Water in oil emulsion-water droplets in oil (Examples- margarine, butter, skin cream)
In figure 3.14, white droplets are showing water droplet and black droplets are showing oil droplet

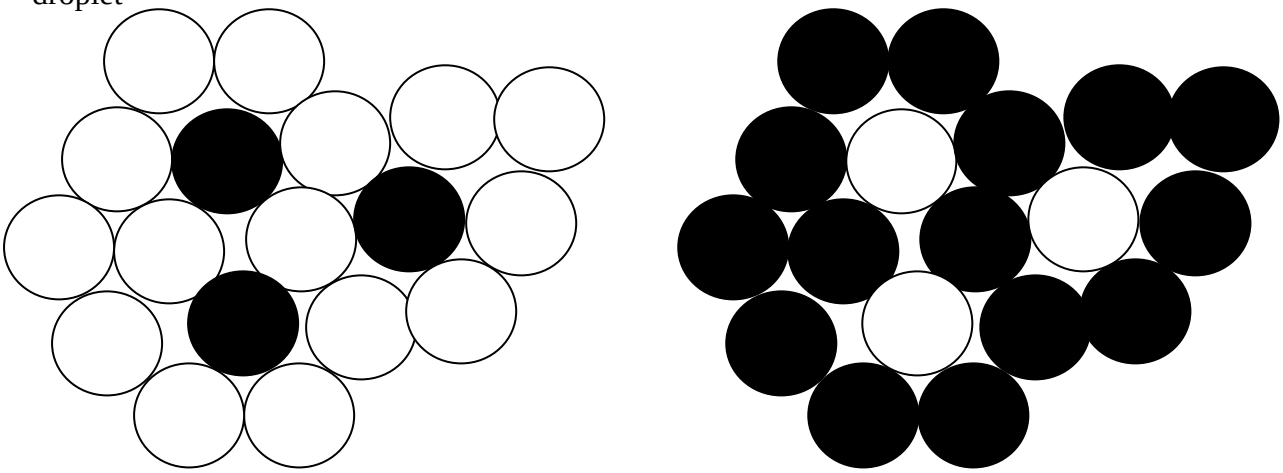

(a) Oil-in-Water emulsion (b) Water-in-Oil emulsion

Figure 3.14 (a) and (b) types of emulsion

An oil-in-water emulsion, wherein the oil is the dispersed phase, and water is the dispersion medium. Water-in-oil emulsion, where in water is the dispersed phase and oil is the external phase. Emulsion does not depend on the actual amounts of oil and water present in an emulsion [98]. Formulating a water-in-oil emulsion is inherently more difficult than an oil-in-water emulsion.

An emulsion is an unstable mixture through thermodynamic point of view, because there is a natural phenomenon for a liquid/liquid system to separate and reduce its interfacial area and, its interfacial energy. Produce the better stability of the emulsion are required some important properties such as droplet size, time, temperature, pH value of the water, nature of liquid etc. Proper droplet size distribution and small size of droplets gave the better stability of the emulsion compared to big droplet size. Surface film is require to water droplets at the oil/water interface as results the adsorption of high-molecular-weight polar molecules that are interfacially active [99]. These surface films produce the good stability of an emulsion by increasing the interfacial viscosity. Temperature can also affect stability of emulsion. Temperature affects the physical properties of oil, water, interfacial films, and surfactant solubilities in the oil and water phases. The pH value of the water also affects the stability of the emulsion. Adding inorganic acids and bases strongly influences their ionization in the interfacial films and radically changes the physical properties of the films. The pH of water affects the rigidity of the interfacial films. Acid or low pH generally produces water-in-oil emulsion and basic or high pH produces oil-in-water emulsion [100].

3.7.2.2 Emulsion mechanism

Emulsion can be stabilized by increasing the repulsion between the dispersed phase by increasing the electrostatic repulsion or steric repulsion. Emulsifiers are amphiphiles that reduce the interfacial tension between the two phases and contribute to the stabilization of dispersed droplets with electrostatic or steric effects. In the process of emulsion preparation mostly droplet formation and coalescence occurs simultaneously. Depending on the time scale of droplet formation, adsorption has to be fast enough to ensure stabilization before droplet coalescence. Therefore, efficiency of emulsifiers during emulsification depends on a good fit of adsorption kinetics to the process of droplet generation, efficient lowering of surface tension and stabilization. Emulsifier is a substance that stabilizes emulsion, stopping them separating between them.

Emulsifier molecules have two different ends:

A hydrophilic end - 'water-loving' - that forms chemical bonds with water but not with oils

A hydrophobic end - 'water-hating' - that forms chemical bonds with oils, but not with water

Hydrophilic-lipophilic balance (HLB) of an emulsifier is important for the emulsification process. Different emulsifiers have different HLB values, which can predict their ability to

stabilize various kinds of emulsions. Emulsifier (surfactants) with the HLB values ranging between 4 and 8 are used to prepare the water-in-oil type of emulsions and the HLB values between 8 and 16 are used to prepare the oil-in-water emulsions [101]. The different types of surfactants which are used for the emulsification process are given in Annexure 5.

3.7.2.3 CBWD emulsion

Preparing an emulsion is a complex phenomenon because it involves diesel, water and surfactant or emulsifier. The selection of a surfactant or emulsifier is important before starting the emulsification process. Emulsification process is used to mix two liquids of different densities and surface tension. It can also be defined as the mixing of one substance with another, which is hydroscopic in nature. Surfactants are compounds that lower the surface tension of a liquid that decreases the interfacial tension between two liquids. Surfactants may act as detergents, wetting agents, emulsifiers, foaming agents and dispersants. In this investigation, the role of the surfactant is that of an emulsifier. For the emulsification process a suitable surfactant has to be chosen for the two liquids to be emulsified. This depends on the HLB value and ionic/ non-ionic of the surfactant. HLB, i.e., the Hydrophilic Lipophilic Balance is the measure of degree to which the liquid is hydrophilic or lipophilic.

A block diagram of the process involved in the preparation of the emulsion is presented in Figure 3.15.

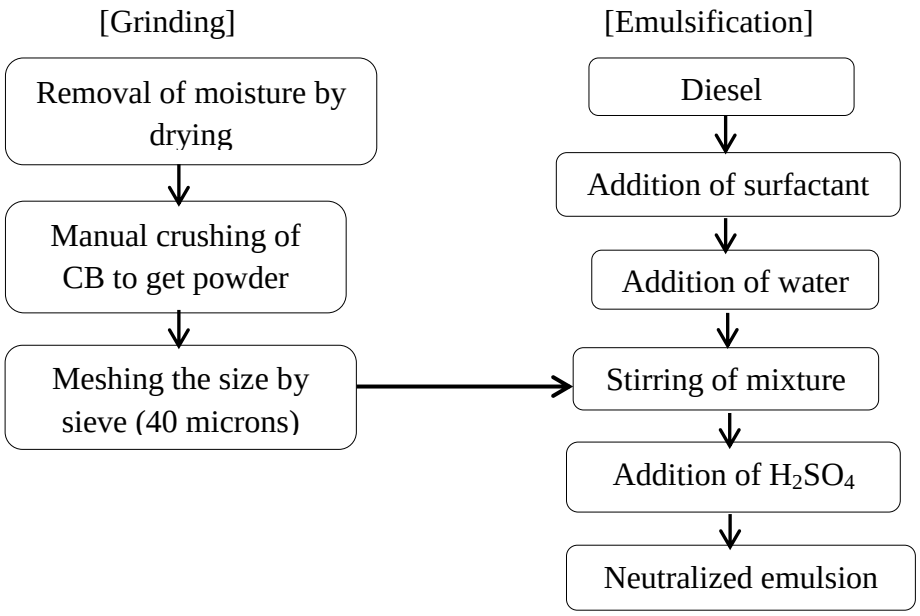

Figure 3.16 Emulsification process [91]

Figure 3.17 and Figure 3.18 portray the photographic views of used with water and surfactant, and emulsion respectively.

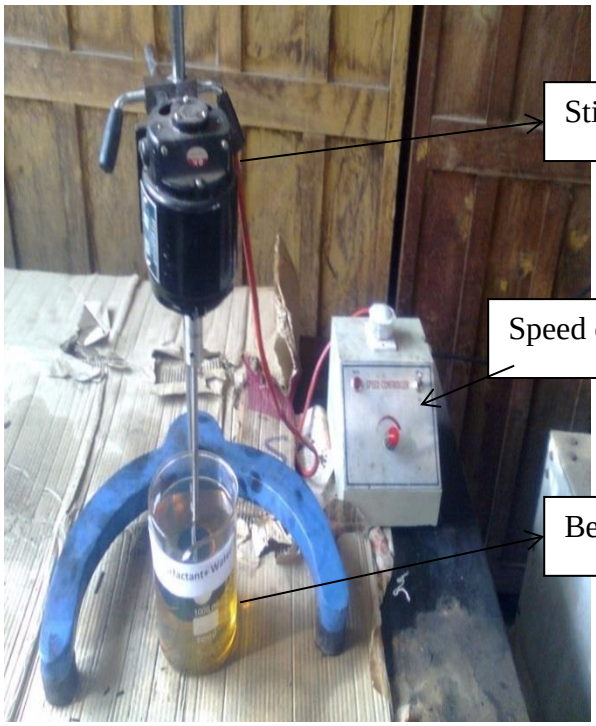

Figure 3.17 Diesel with water and surfactant

Figure 3.18 Emulsion

Similar to the preparation of Carbodiesel, the CB was first dried in direct sunlight for one day, to remove the mositure in it. The CB was then crushed manually by hammering to get it in the form of powder. Then, the powder was further classified by a sieve to get a fine powder size of 40 µ. This was done because, the nozzle size of the fuel injecter of a diesel engine considered in this investigation was 40 µ. The CB was taken at different proportions from 5% to 20%. Initially, diesel was mixed with the water proportionally with the help of a surfactant Tween-20 (polyoxyethylene (20) sorbitan monolaurate). The purpose of additing water with the CB is to increase fluidity and surface tension. The properties of the surfactant used for preparation of emulsion are given in Table 3.7.

Table 3.7 Properties of Surfactant (Tween-20) [91]

Properties	Value/Formula
Surfactant type	Non-ionic
HLB	16
Cloud point	> 70 °C
Physical form at 25°C	Liquid
Density	1.1 g/mL
Molecular formula	C58H114O26

Further, the CB powder was mixed with diesel at room temprature and continuously stirred for 15 minutes to get the emulsion. Some of the residues were removed after filteration. The emulsion was kept in an observation for 30 days and found that there was no seperation of CB from the emulsion. Since the mixture was acidic is nature and has pH>7, each sample was added with a few drops of H_2SO_4 and checked for a pH value by the pH meter. The electricty consumption of the mechanical stirrer used for stirring the mixture, was about 0.15kWh. The composition of the different emulsions used in the study are given in Table 3.8.

Table 3.8 Compositions of CBWD5, CBWD10, CBWD15 and CBWD20 [91]

Diesel %	Water %	Surfactant %	Carbon black %	Name of Fuel
90	3	2	5	CBWD5
85	3	2	10	CBWD10
80	3	2	15	CBWD15
75	3	2	20	CBWD20

3.7.2.4 FT-IR analysis

The functional groups of diesel and all the emulsions used in this study were determined by the FT-IR analysis. The FT-IR test was carried out in the same Perkin Elmer Spectrum one instrument, which was used for analysing the Carbodiesel. The results of the FT-IR analysis for all the emulsions tested in this study in comparison with diesel are depicted in Figure 3.19. The variation of the percentage transmittance with wave number gives the information about the position of various bond vibrations, distinguished by several modes such as stretching, distortion, bending etc. The spectra of the emulsion samples were analysed in terms of the fixed mix of functional groups [91]. The functional groups present in diesel and the CBWD emulsions are given in Table 3.9.

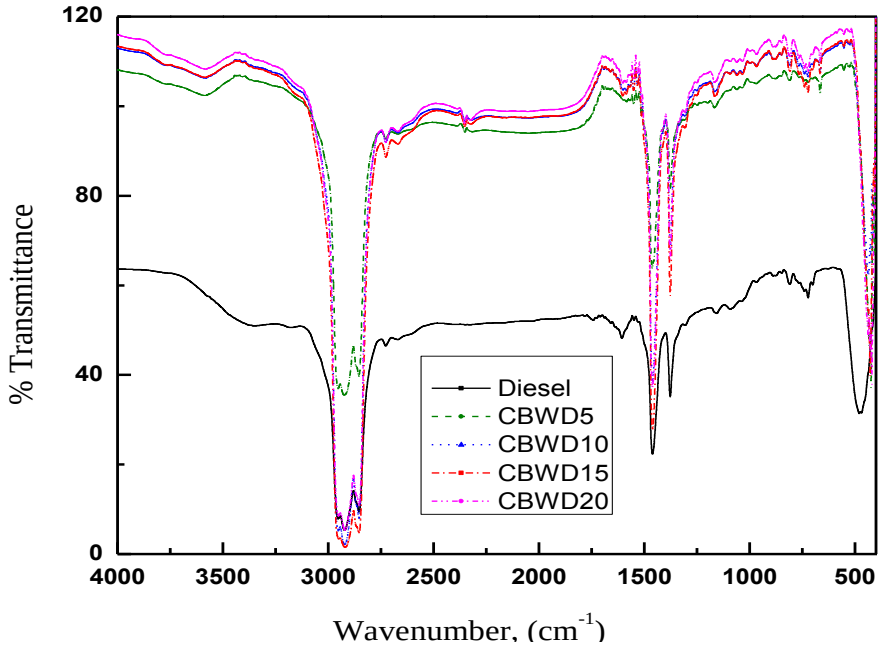

Figure 3.19 FT-IR analysis

Table 3.9 Various bonds present in emulsion and diesel [91]

Wave number cm^{-1}	**Wavelength µm**	**Bond**	**Fuels in which bond is present**
3580.88	2.7 – 3.2	OH and NH stretching	All emulsion
2901.12	3.0 – 3.7	C-H aliphatic	All emulsion and diesel
2853.12	3.5 – 4.1	C-H aliphatic	All emulsion and diesel
1551.21	4.2 – 5.6	C=O	All emulsion and diesel
1460.52	5.9 - 6.3	C-H	All emulsion and diesel
1742.56	5.4 – 6.1	C=O, C-O	Diesel, CBWD10, CBWD15
1155.92	7.4 – 10	C-F	Diesel
808.91	11.9– 12.3	Nitrate	Diesel
480.17	17 – 21	C-I	Diesel

From Table 3.9, it can be observed that the emulsions have strong bonds of carbon with the hydrogen, oxygen, aliphatic etc. The stretching vibrations exist in the functional groups leading to an increase or decrease in bond length [91].

3.7.2.5 Fuel properties of emulsion

The comparison of various physical properties of CBWD5, CBWD10, CBWD15 and CBWD20 with diesel is given in Table 3.10.

Table 3.10 Properties of emulsions [91]

Properties	**CBWD5**	**CBWD10**	**CBWD15**	**CBWD20**	**Diesel**
Density, kg/m^3	831.4	831.9	832.1	833.3	831
Viscosity, cSt	2.64	2.74	2.80	3.19	2.4
Ash content,%	0.004	0.007	0.008	0.008	0.001
Flash point,^{o}C	54	56	58	61	52
Pour point, ^{o}C	< -12	< -12	< -12	< -12	< -12
C.V., MJ/kg	41.77	41.23	40.40	40.10	43.40

3.8 Spray characteristics

Droplet size of a fuel plays an important role in the mixture formation and combustion process. The Sauter mean diameter (SMD) of the fuel was determined by using the MgO coating technique, at an injection pressure of 200 bar and a room temperature of 27^{o}C. Figure 3.20 shows the nozzle injector tester used to produce fuel droplets, on a glass plate.

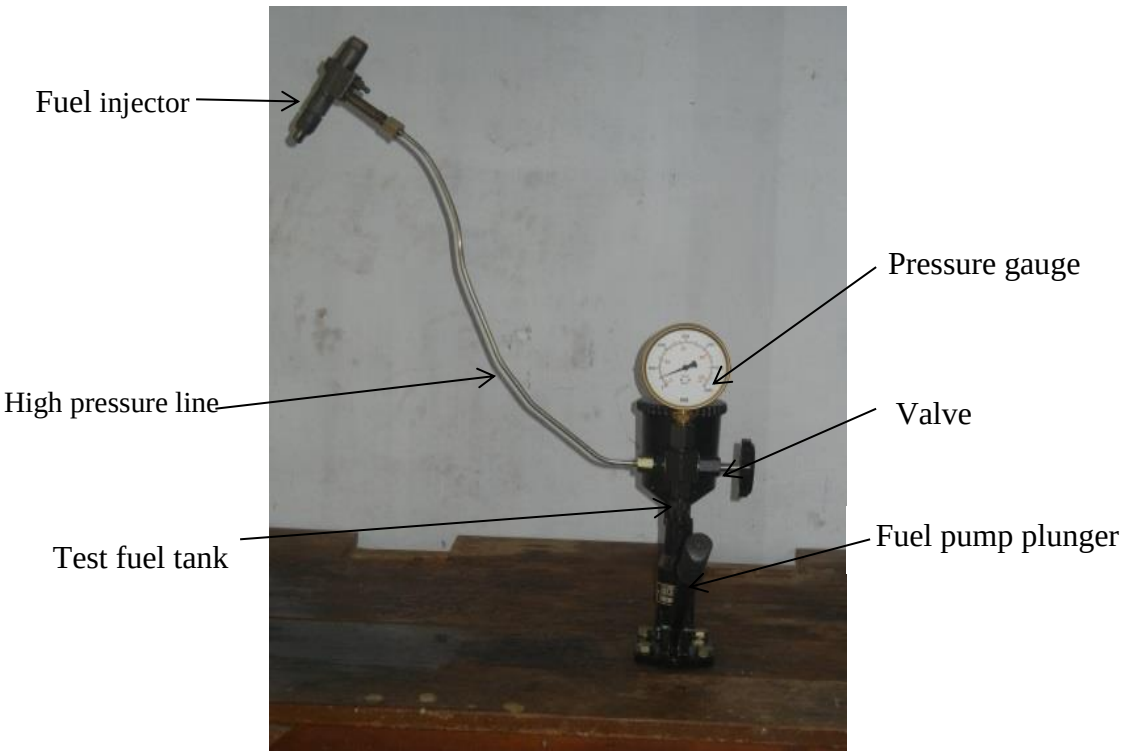

Figure 3.20 Nozzle injector tester [91]

The glass plate was fixed at 762 mm from the nozzle injector. An inverted microscope shown in Figure 3.21 was used for the study of droplet size diameter of different fuels. The impressions of the droplets formed on a glass plate were seen through a 10x microscope and snaps were taken with the help of a camera attached to it. The images were saved in a

computer. The number of droplets was counted manually using NI vision software. It gave the number of droplets at different ranges of diameter of the four emulsions and diesel.

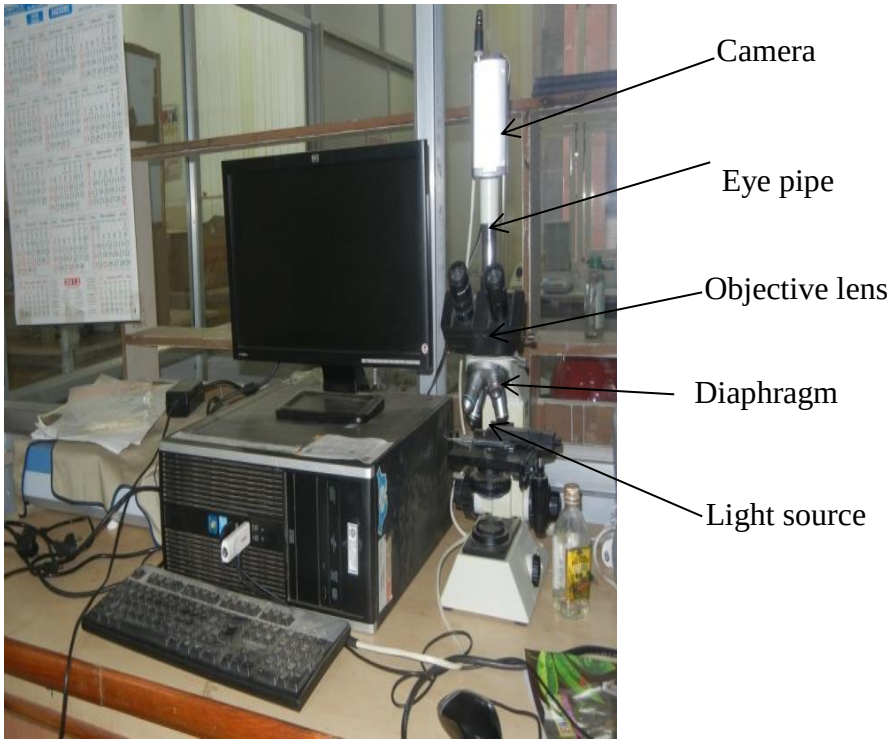

Figure 3.21 An inverted microscope and a computer [91]

The SMD is determined by using the following empirical equation [102].

$$(SMD)_{MgO} = \frac{4\pi/3[N_1\left(\frac{D_1}{2}\right)^3 + N_2\left(\frac{D_2}{2}\right)^3 + N_3\left(\frac{D_3}{2}\right)^3 + \ldots\ldots\ldots]}{4\pi[N_1\left(\frac{D_1}{2}\right)^2 + N_1\left(\frac{D_1}{2}\right)^2 + N_1\left(\frac{D_1}{2}\right)^2 + \ldots\ldots\ldots\ldots]} \quad (3.2)$$

Where, N_1, N_2, N_3 ……..are the numbers of droplets collected on coated glass plate.
D_1, D_2, D_3……are respective diameters of those droplets.

The SMD value was further converted into equivalent value of Malvern particle laser beam analyzer by using the following equation:

$$(SMD)_{laser} = 37\text{-}0.1739(SMD)_{MgO} \quad (3.3)$$

Figure 3.22 shows the images of the droplets of CBWD5, CBWD10, CBWD15, CBWD20 and diesel. A more number of larger droplets of all the emulsions are formed than that of diesel due to high viscosity. It is clearly seen that the maximum number of droplets fall within the range of less than 15 µ and minimum in 60-70 µ [91].

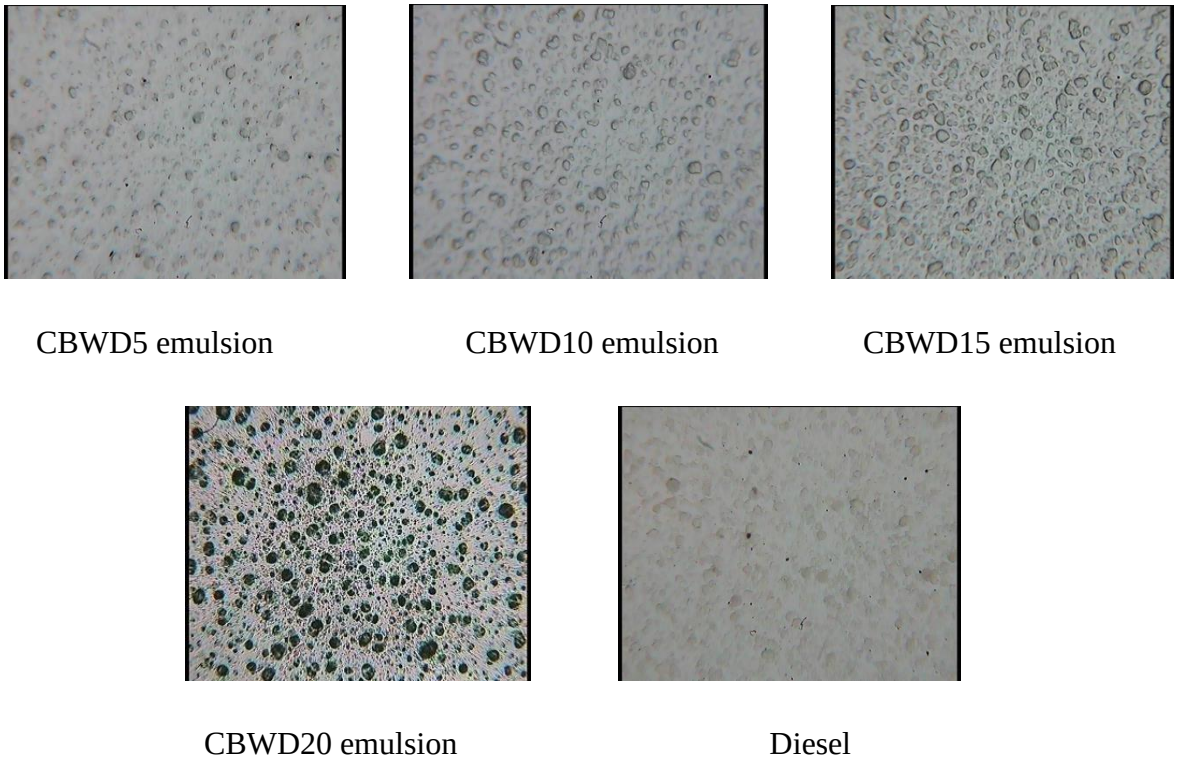

Figure 3.22 Droplet images of CBWD5, CBWD10, CBWD15 CBWD20 emulsion, and Diesel [91]

3.9 Zeta potential of CBWD10 emulsion

Zeta potential, a scientific term used for electro kinetic potential in colloidal dispersions, is a measure of the magnitude of the electrostatic or charge of repulsion or attraction between particles. It can also be stated as a parameter characterizing the electrochemical equilibrium on interfaces, which depends on the properties of the liquid as well as on the properties of the surface of the particles, thereby describing the nature of the electrostatic potential near the surface of a particle [103]. A Zeta potential analysis can be done using a Zeta potential analyser instrument during the dynamic light scattering analysis.

3.9.1 Principle of the Zeta potential analyser (**Laser Doppler Electrophoresis)**

Many colloidal particles have a surface charge when they are under suspension. When an electric field is applied, the particles move due to the interaction between the charged particle and the applied field. The direction and velocity of the motion is a function of particle charge, the suspending medium, and the electric field strength. The particle velocity is then measured by observing the Doppler shift in the scattered light. The particle velocity is proportional to the electrical potential of the particle at the shear plane which is zeta potential. Thus, this

optical measurement of the particle motion under an applied field can be used to determine the zeta potential. The particle motion under an applied electric field is known as electrophoresis. The method used is known as laser Doppler electrophoresis. Sample particles are suspended in a solvent of known refractibe index n, velocity η and dielectric constant ε. The sample is irradiated with the laser light of wavelength λ. An electric field with strength E is applied. Due to the electric field, the particles move. Since the particles are moving, the scattered light at angle θ is measured and the particle velocity V is determined from the frequency shift. Mobility is then readily obtained as the ratio of velocity to electric field strength V/E. The zeta potential is then determined using a model, the most common of which is the Smulochowski model [103]. Figure 3.23 illustrates the principle followed for the zeta potential analysis.

$$U = \frac{\lambda . vd}{2 * E * \eta * Sin\left(\frac{\theta}{2}\right)} \tag{3.4}$$

$$\zeta = \frac{Un}{\varepsilon\, f(ka)} \tag{3.5}$$

where ζ - Zeta potential, U - Electrical mobility, E - Electric field strength, ε - Solvent dielectric constant, n - Solvent refraction index, η - Solvent viscosity, f(ka) - Henry coefficient

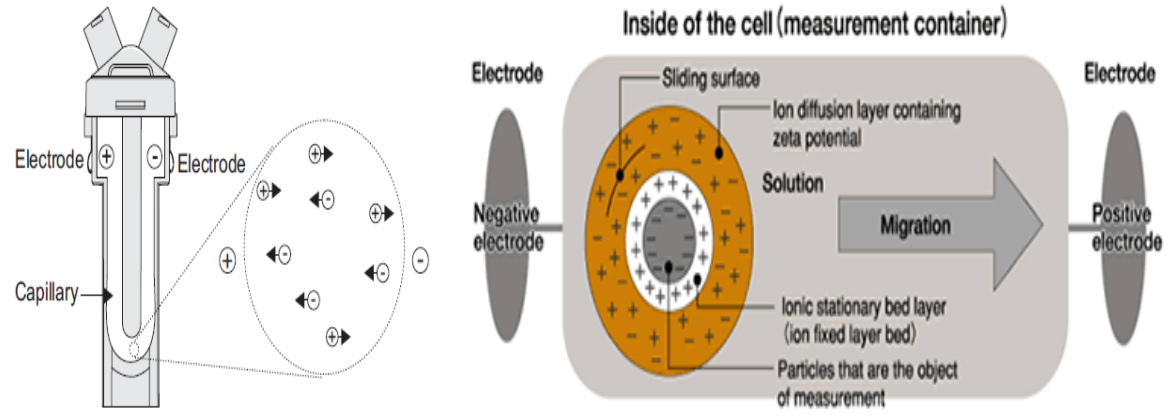

Figure 3.23 Principle followed for the Zeta potential analysis [104]

Figure 3.24 shows the Zeta potential analyser available in the Chemical department laboratory at NIT, Rourkela. Its technical specifications are given in Annexure 6.

Figure 3.24 Zeta potential analyser

The stability of the CBWD10 emulsion was calculated from the electrophoretic mobility obtained from electrophoretic light scattering measurements, by measuring the mean zeta potential (ζ) of sample. Figure 3.25 presents the zeta potentials of the carbon black sample. The data clearly indicates the stability of particles. The zeta potential of the sample measured id -44.4 mV. The high zeta of the sample indicates the higher stability of the sample due to high surface charge on the particle, which exhibits stability due to surface charge repulsion. Thus, sufficient electrostatic repulsion of particles prevents the particles from agglomeration. The high stability of sample proves that the sample can be used in practical applications.

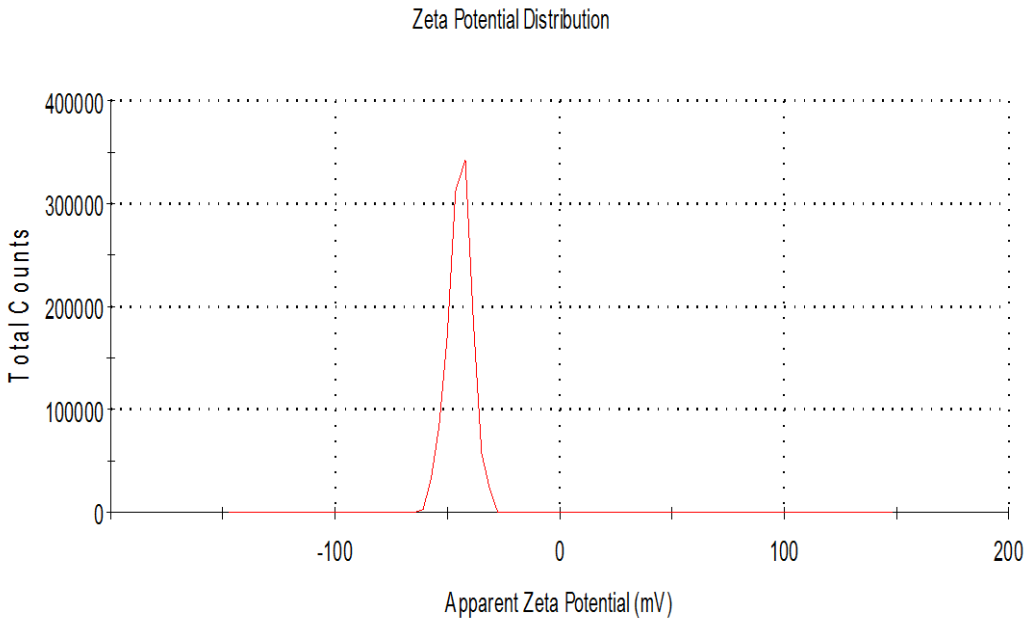

Figure 3.25 Zeta potential distribution of carbon black

3.10 Rheological measurements

Rheological studies of the CBWD10 emulsion were carried out in a rotational cone and plate BOHLIN VISCO-88 viscometer. The angle of the conical section was 5.4^{o}C and diameter 30 mm. A gap of 0.15mm was maintained between the cone and plate for every measurement. A cover was used with a wetted layer of sponge inside to decrease the moisture loss from the emulsion during measurement. The CBWD10 emulsion was carried out at a constant temperature 100^{o}C of the analyser. The data acquired by the computer were used to get the shear rate, shear stress and viscosity plots. The highly concentrated CBWD10 emulsion suspensions generally show a non-Newtonian character in a shear flow. The photograph of BHOLIN VISCO-88 is shown in Figure 3.25, and its technical specifications are given in Annexure 7.

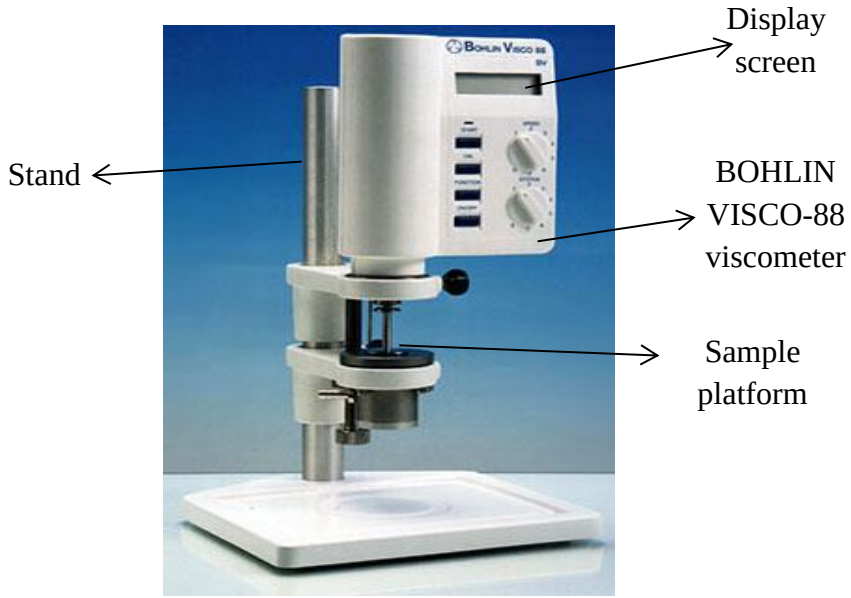

Figure 3.26 BHOLIN VISCO-88 viscometer

The BHOLIN VISCO-88 includes software "Viscosoft" for the calculation. Figure 3.27 shows the BHOLIN VISCO-88 viscometer used in this study available in the Chemical department at NIT, Rourkela.

- torque [mNm]
- shear rate [1/S]
- shear stress [Pa]
- viscosity [Pas]
- temperature [^{o}C]
- rotational speed [Hz]

Figure 3.27 BHOLIN VISCO-88 viscometer analyser with PC at NIT, Rourkela

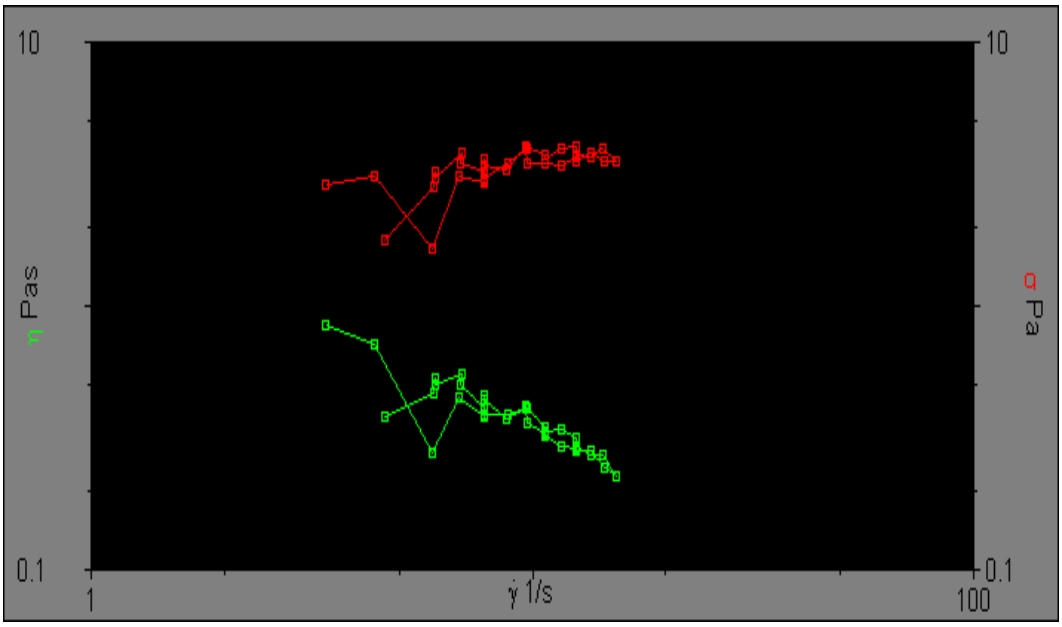

Figure 3.28 Rheological properties of CBWD slurry

Figure 3.28 shows the rheological characteristics of the CBWD10 emulsion, which is a plot drawn between viscosity and shear rate, and between shear stress and shear rate. It is apparent from the figure that, the viscosity and shear stress of the emulsion change with respect to the shear rate. The figure reveals that all the suspensions show shear-thinning behaviour, i.e., the apparent viscosity decreases with an increase in the shear rate of up to 100 S^{-1}.This behaviour of the CBWD emulsion is attributed to the breaking of agglomerates at a higher shear rate [105]. In all the cases, yield stress increases at higher CB concentration, i.e., the wall shear stress has a finite value at zero shear rate, implying that this residual stress must be overcome

before the flow can commence. The variation in the rheological behaviour due to the changes in colloid interactions among the CB particles is clearly seen in Figure 3.29. It is also evident from the results that, the apparent viscosity of the CBWD10 emulsion increases with respect to the shear rate. The experimental results also reveal that, there is a sharp increase in the apparent viscosity of the CBWD10 emulsion with the concentration of CB. This increase may be attributed to the frictional forces between the particles becoming significant, and the accompanying reflected is respected in the increase in viscosity [106]. This increase in viscosity may be due to occlusion of water in the solid structure. Similar results were reported by Ting and Luebbers [107], reported when they carried out an investigation with CWS. An examination of the experimental data also shows that no appreciable settling occurred during the tests. Therefore, the shear stress–shear rate plot gives a clear picture of the rheological behaviour of the CBWD10 emulsion under consideration.

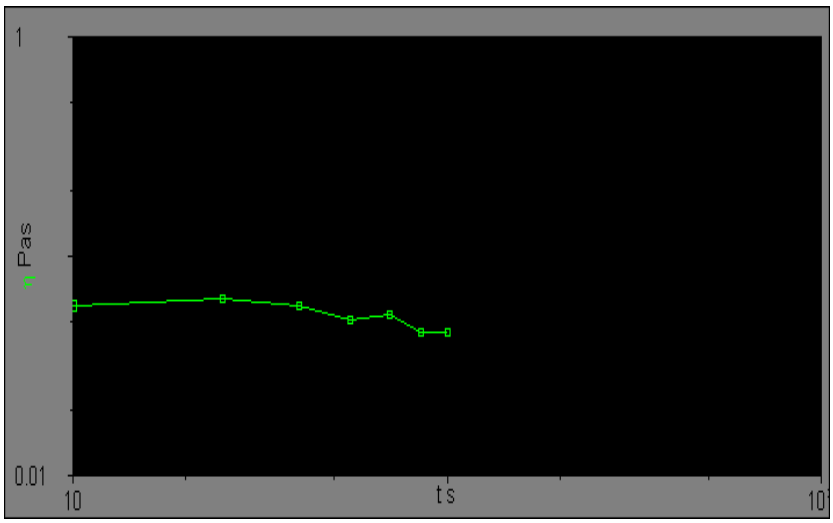

Figure 3.29 Viscosity vs. time at a constant shear rate

Figure 3.29 shows the variation of viscosity with time at a constant shear rate at 53.23 S^{-1} of 30 rpm; the emulsion exhibits a thixotropic behaviour at 30 rpm [108]. The CBWD emulsion after 8s than the viscosity of the CBWD10 emulsion remained unchanged over time.

CHAPTER 4
EXPERIMENTAL SETUP AND METHODOLOGY

4.1 General

In any experimental study, instrumentation plays an important role, as it provides the required data for analysis. Before starting an experimental investigation, it is essential to acquire the basic knowledge about the instruments required for experimentation and details about their working principles, range, accuracy etc. In this chapter, different instruments used for the experimental investigation are described with the necessary illustrations. This also includes the working principle of analysers that were used to measure the exhaust gas emissions and smoke opacity. In addition, information on the accuracies and uncertainty analysis of the instrumentation used, i.e. data acquisition system (DAS), piezo electric transducer and crank angle encoder are presented in this chapter. Also, the methodologies adopted in each and every module of the research study are neatly explained.

4.2 Engine experimental setup

The engine used in this study is a Kirloskar TAF1 model, single cylinder, four stroke, air cooled, DI diesel engine with a developing rated power of 4.4 kW, running at a constant speed of 1500 rpm. The block diagram of the experimental setup is illustrated in Figure 4.1 and a photographic view of the experimental setup is portrayed in Figure 4.2. Annexure 8 provides the technical specifications of the test engine. The engine was coupled to an electrical dynamometer and a load cell. The desired load was provided to the engine with the help of the dynamometer. The load on the engine was varied with the help of a digital controller provided with the dynamometer.

Diesel and an alternative fuel were stored in two different fuel tanks. A valve was located in the fuel line between the diesel and the alternative fuel tanks to allow fuel from anyone of these two tanks. The fuel measuring system consisted of a burette fitted with two optical sensors, one at a higher level and the other at a lower level. As the fuel passed through the higher level optical sensor, the sensor gave a signal to the data acquisition system (DAS) to start the counter time. Once the fuel reached the lower level sensor, the sensor gave a signal to the DAS to stop the counter time and refill the burette. From this, the time taken for the consumption of fuel for a fixed volume was calculated. Diesel or the alternative fuel was

injected by the existing injector of the system. An air box was used to damp out the pulsations produced by the engine, for ensuring a steady flow of air through the intake manifold. Air consumption was measured by a differential pressure sensor fitted in the air box. A K-type thermocouple fitted in the exhaust pipe measured the exhaust gas temperature.

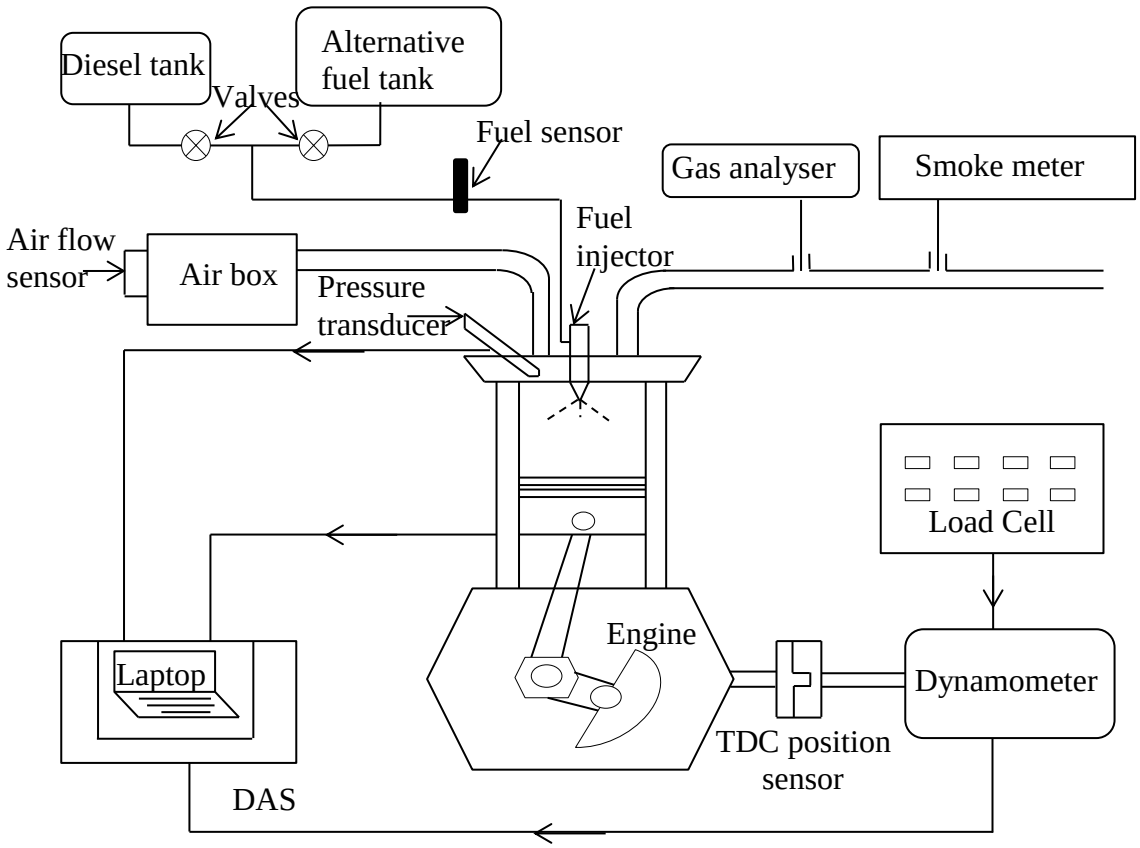

Figure 4.1 Experimental setup

Initially, the engine was operated with diesel fuel for obtaining the reference data. A Kistler piezoelectric pressure transducer model: 5395A, in combination with a charge amplifier, and a TDC position sensor were also connected to the data acquisition system. The cylinder pressure of the engine was obtained by means of the pressure transducer, which was flush mounted on the cylinder head, and the TDC position sensor was fixed on the output shaft of the engine. A non-contact type sensor was connected near the flywheel of the engine to measure the speed. The data collected by the data acquisition system from all the sensors for the corresponding loads were displayed on the monitor of the computer.

Figure 4.2 Photographic view of experimental setup

There are two reasons for using a single cylinder diesel engine instead of a multi cylinder engine for this investigation;

(i) An investigation of this kind on the utilisation of a CB based fuel for a CI engine is at early stage. The fuel cannot be spent lavishly, as fuel structure and condition may be modified for further investigation.

(ii) Fuel consumption will be more than a single cylinder. Also, when the investigation is carried out to study the effect of engine modification, for example, a change of injection timing, then the injection timings of all the cylinders have to carried out, which will consume more time.

An exhaust gas analyser was used to measure the carbon monoxide (CO), unburnt hydrocarbon (HC), and nitric oxide (NO) emissions in the engine exhaust. The probe of the analyser was inserted in the exhaust, whenever the measurement was taken. A diesel smoke meter was used to measure the smoke in the engine exhaust.

Initially, the combustion, performance and emission parameters of the diesel engine were studied with diesel at a compression ratio of 17.5 and nozzle opening pressure of 200 bar, which were prescribed by the manufacturer, by maintaining a rated speed of 1500 rpm to get the diesel data. Then, the engine was run on alternative fuel without and with engine modifications. The data collected for the fuel operation were stored, compared with those of

diesel operation for analysis. The description of each instrument is given in the following subsections.

4.3 Performance parameters

4.3.1 Brake thermal efficiency

Brake thermal efficiency (BTE) is the ratio of the brake power to the input fuel energy.

$$\text{Brake thermal efficiency } (\eta_{bth}) = \frac{brake\ power}{\text{Mass of fuel/s} \times \text{calorific value of fuel}} \quad (4.1)$$

or

$$\text{Brake thermal efficiency } (\eta_{bth}) = \frac{brake\ power \times\ 3600 \times 100}{Volumetric\ fuel\ flow\ rate\ per\ hour \times fuel\ density \times calorific\ value\ of\ fuel} \quad (4.2)$$

4.3.2 Brake specific fuel consumption

Brake specific fuel consumption (BSFC) is the ratio of fuel consumption in kg/hr to the brake power (kW). So, its units are kg/(hr-kW). It is an indication of how much fuel is consumed in producing a power of 1kW for 1 hour.

$$BSFC = \frac{\text{fuel consumption in kg/hr}}{\text{brake power kW}} \quad (4.3)$$

The BTE and BSFC were displayed in the form of excel sheet generated by the data acquisition system software (Engine test express) using the above mentioned expressions.

4.3.3 Brake specific energy consumption

Brake specific energy consumption (BSEC) is calculated as the product of brake specific fuel consumption and calorific value of the fuel. BSEC is a more reliable parameter than brake specific fuel consumption, when two different fuels are used, since the calorific value and density of the two fuels are different [45]. BSFC is the measure of the fuel efficiency of any type of fuel burnt and which produces power.

$$\text{BSEC} = \text{BSFC} \times \text{Calorific value of the fuel} \quad (4.4)$$

4.4 Combustion parameters

4.4.1 Instrumentation

Instrumentation is the use of a variety of measuring instruments to record, monitor and control a process. In a DI diesel engine, the important combustion parameters, such as ignition delay, heat release rate, rate of pressure rise, combustion duration etc., can be calculated from two main inputs: pressure and crank angle. The necessary instruments required to measure these two parameters are the pressure transducer, crank angle encoder (TDC marker) and data acquisition system.

4.4.1.1 Pressure transducer

The cylinder gas pressure was measured using a Kistler piezo-electric transducer (model 5395A) in conjunction with a Kistler charge amplifier, which has the advantage of a good frequency response and linear operating range. Figure 4.3 shows the photographic view of the Kistler pressure transducer. The complete specification of the Kistler make piezo quartz pressure sensor is given in Annexure 9.

Figure 4.3 Photographic view of Kistler pressure transducer

The quartz sensors used in the piezo electric pressure transducers can withstand very high pressures ranging from 0 to 250 bar and have high natural frequency. The stainless steel diaphragm was hermetically sealed to the body. The quartz elements were mounted in a highly sensitive transversal effect arrangement. The connector was welded to the body, but the Teflon insulator was not completely tightened. The pressure sensor was placed in a hole of diameter 5 mm and an internal thread pitch of 1 mm that was drilled on a dummy plug. The sensor was checked properly for its sealing so as to avoid change in the compression ratio of the cylinder. The sensor senses pressure and acts through a diaphragm on the quartz crystal measuring elements, which transform the pressure into an electrostatic charge. Figure

4.4 shows a photographic view of the location at which the pressure transducer is mounted on the cylinder head.

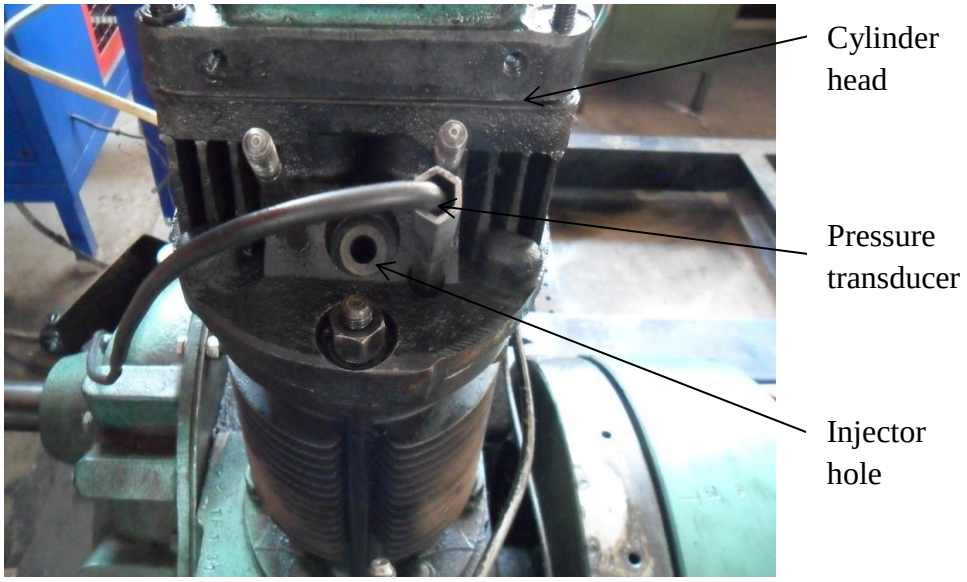

Figure 4.4 Pressure transducer on engine cylinder head

A continuous circulation of air was maintained to cool the transducer and the fins provided larger surface areas for quick heat transfer to the environment. The cylinder pressure data were acquired for 50 consecutive cycles and their average was taken in order to eliminate the effect of cycle-to-cycle variations. The computer (PC), through an analog to digital converter (ADC), reads the output of the charge amplifier. A small drift in the voltage was measured (~2 mV/s) due to charge leakage in the pressure transducer. Since the signal from a piezoelectric transducer indicated only relative pressures, it was necessary to have a means of determining the absolute pressure at some point in the cycle. Hence, the differential pressure had to be compared with a reference.

4.4.1.2 Crank angle encoder

The crank angle encoder was used for obtaining data regarding the instantaneous crank angle positions and related measurements in IC engines. The crank angle encoder comprised of an angle encoder, a signal conditioner and a line terminator. The encoder generated square pulse signals that include a signal with adjustable resolution, a trigger signal and a signal with fixed resolution. These were essential to adjust specific details in the engine management system or engine speed.

The TDC marker (Kistler model 5015A1000) was mounted near the engine flywheel which gave an advantage of an accurate frequency response. At the TDC position, a small metallic

deflector was fitted. The photographic view of the TDC marker and metallic deflector is shown in Figure 4.5. The sensor gave an output in the form of a square wave, exactly when the piston is at the TDC.

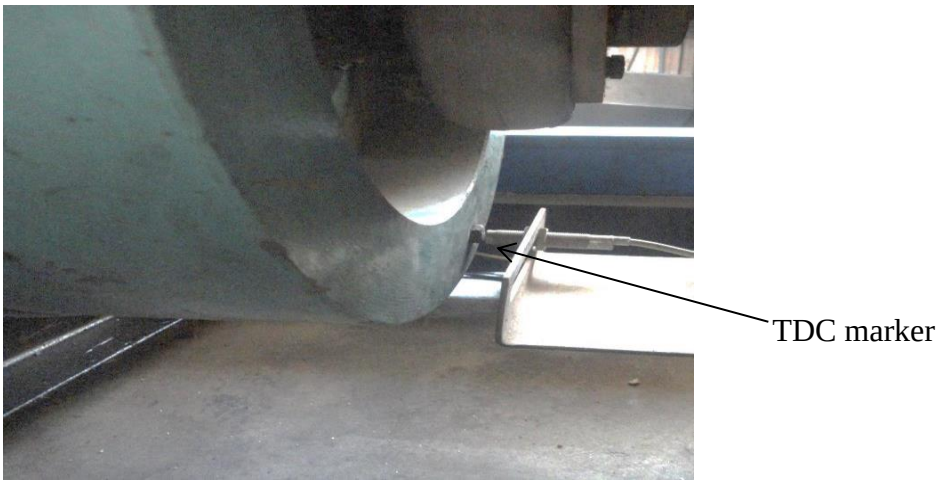

Figure 4.5 Photographic view of TDC marker and deflector

At the Top Dead Center (TDC), a hole was drilled and a voltage pulse was provided exactly when the TDC position was reached. This helped in indicating the position of TDC. The sensor was made up of a matched pair of infrared diode and photo transistor in order to receive the infrared signal from the diode, unless interrupted. A continuous disc was installed that had a small cut at the TDC position with respect to sensor point in order to get the signal when it reached the TDC. The output voltage from photo transistor rose to 5 V at the TDC position and was zero at all other positions. These voltage signals were fed to the 12 bit ADC and then to the DAS along with pressure signals. All data was stored on a computer in the excel worksheet files through the DAS.

4.4.1.3 Data acquisition and processing

Data acquisition can be described as the process of sampling signals that measure real world physical conditions, like data signals sent from the sensors of an experimental setup; and then converting the resulting samples into digital numeric values that can be manipulated by an attached computing source based on the relations fed into it or as pre-programmed by the manufacturer [109]. Data acquisition systems (DAS) typically convert analog waveforms into digital values for processing. DAS products centrally connect all the components together, such as sensors that indicate temperature, flow, performance, combustion parameters etc. The average data of the pressure and crank angle values, occurrence of the peak pressure,

maximum rate of pressure rise, and heat release rate were recorded by the DAS and stored in the computer as excel worksheet files.

The instantaneous experimental data was collected for several cycles. For averaging, pressure data of approximately 50 thermodynamic cycles were chosen by the system. The first voltage signal sent by the TDC indicator was taken as the TDC position. The clock frequency of the data acquisition card was 100 kHz, approximately 370-380 pressure voltage readings were acquired by the PC for each rotation of the crank shaft. By interpolation, the pressure-voltage readings were arranged at a spacing of 1^{o}CA. The values obtained through interpolation were more accurate if spline fitting or regression models were used for the interpolation. Since the engine is a four stroke type, 720 (180 for each stroke) interpolated data points correspond to one complete thermodynamic cycle (intake, compression, combustion and exhaust) of the engine. The data was corrected for the transducer drift by a linearly increasing voltage (≈2 mV/s). These pressure data were required to be referenced using a particular known pressure; i.e, the pressure at inlet BDC was taken as the intake manifold pressure. After the pressure and crank angle data were obtained for every crank angle at every load, other combustion parameters such as ignition delay, heat release rate and combustion duration were calculated using the necessary formulae or empirical relations. The methods of calculation are described below in the subsequent paragraphs.

4.4.2 Determination of the combustion parameters

4.4.2.1 Ignition delay

In a CI engine, after fuel is injected into the cylinder, it does not ignite immediately upon injection into the combustion chamber. There is a short duration of inactivity between the time when the first droplet of the fuel hits the hot air in the combustion chamber, and the time it starts through the actual burning phase. This time difference in the degree crank angle is known as ignition delay [36, 45, 110].

The ignition delay period is divided into two parts (i) physical delay and (ii) chemical delay.

(i) Physical delay: It is the time between the beginning of injection and the attainment of the chemical reaction process. During this process the following reactions take place: atomization of the liquid fuel jet, evaporation of the fuel droplets and mixing of the fuel vapour with air, and raising it to its self-ignition temperature [36, 110].

(ii) Chemical delay: In this process, reactions start slowly and then accelerate until inflammation or ignition takes place [36, 110].

Generally, the chemical delay is larger than the physical delay. These processes are affected by engine design, operating variables, fuel characteristics and the temperature of the surroundings.

Static injection timing is the number of degrees advanced for fuel injection in the engine set by the manufacturer for best performance. Usually the timing for starting a cold engine is not optimal; thus it is possible to advance the timing further for better starting, and then to drop back to the regular timing once the running engine was throttled. Dynamic injection timing is the crank angle point at which the fuel actually enters the combustion chamber [111, 112]. In this study, the static injection timing of the engine has been considered.

From the heat release rate curve, the start of combustion is determined as the point at which the heat release curve changes from a negative axis to a positive one [36].

4.4.2.2 Rate of heat release rate

The rate of heat release at each crank angle was determined by the following formula derived from the first law of thermodynamics

$$\frac{du}{dt} = \dot{Q} - \dot{W} \tag{4.5}$$

$$m\,C_v\,\frac{dT}{dt} = \dot{Q} - P\,\frac{dv}{dt} \tag{4.6}$$

where, $\dot{Q}$ = the combination of the heat release rate and the heat transfer rate across the cylinder wall

$\dot{W}$ = the rate of work done by the system due to the system boundary displacement
U = Internal energy

To simplify equation (4.6) the ideal gas assumption can be used

$$PV = mRT \tag{4.7}$$

where, P = Cylinder pressure in bar
V= Volume of the cylinder (m^3)
m = mass of gas (kg)
T = Absolute temperature

Equation (4.7) can be differentiated (assuming constant mass)

$$\frac{dT}{dt} = \frac{1}{mR}\left[P\,\frac{dV}{dt} + V\frac{dP}{dt}\right] \tag{4.8}$$

After combining equation (4.6) and (4.8), the heat release equation becomes

$$\dot{Q} = \left[\frac{Cv}{R} + 1\right] P\,\frac{dV}{dt} + \frac{C_v}{R}\,V\,\frac{dP}{dt} \tag{4.9}$$

After replacing time (t) with the crank angle (θ), the equation becomes

$$\dot{Q} = \frac{\lambda}{\lambda - 1}\,P\frac{dV}{d\theta} + \frac{1}{\lambda - 1}\,V\,\frac{dP}{d\theta} + Q_w \tag{4.10}$$

where, λ is the ratio of the specific heats ($\frac{C_p}{C_v}$), P is the cylinder gas pressure, V is the instantaneous volume of the cylinder and Q_w is the heat transfer rate across the cylinder wall. The instantaneous cylinder volume can be obtained from the engine geometry and crank angle values.

4.4.2.3 Combustion duration

Combustion duration is the time difference in the degree crank angle measured between the start of combustion and the end of combustion. From the heat release rate curve, the crank angle at which there is a sudden rise in the heat release is taken as the start of combustion. The end of combustion is determined from the cumulative heat release rate curve [110].

4.4.2.4 Rate of pressure rise (ROPR)

The rate of pressure rise defines the load that is imposed by the combustion process on the cylinder head and block, and to a large extent, determines the structural design. It is an indication of the noisy operation of the engine. The rate of pressure rise with respect to the crank angle is derived from the following equation [113].

$$Rate\ of\ pressure\ rise = \frac{dp}{d\theta} \tag{4.11}$$

4.5 Exhaust emission measurement methods

Exhaust emissions are combustible gases that are released to the atmosphere when the exhaust port or valve of the engine is opened during an exhaust stroke. If combustion is complete and the mixture is stoichiometric, the products of combustion will consist only of carbon dioxide (CO_2) and water vapour. However, if there is no complete combustion of fuel air mixture, and hence, the exhaust gas consists of a variety of components, the most

important of them are carbon monoxide (CO), unburned hydrocarbons (UBHC) and oxides of nitrogen (NOx) [114]. Some oxygen and other inert gases would also be present in the exhaust gas. Over the last decade numerous devices have been developed for measuring these various exhaust components. The working principle of some of the more commonly used instruments is given below.

4.5.1 NDIR principle

Non-Dispersive Infra-Red (NDIR) detectors are used to measure the concentration of gases such as HC, CO and CO_2. Each constituent gas in a sample will absorb some infrared at a particular frequency or wavelength. The gas will absorb the infracted energy of this wavelength and transmit the infrared energy of other wavelengths. For example, the absorption band for CO is between 4.5 and 5 microns. So, the energy absorbed at this wavelength is an indication of the concentration of CO in the exhaust gas [115].

Figure 4.6 shows the schematic diagram of the NDIR. It consists of two infrared sources, interrupted simultaneously by an optical chopper. Radiation from these sources passes in parallel paths through a reference cell and a sample cell to the opposite side of a common detector. The sample cell contains the compounds to be analysed, whereas this compound is not present in the reference cell. The latter is usually filled with an inert gas, usually nitrogen, which does not absorb the infrared energy at the wavelength corresponding to the compound being measured. A closed container filled only with the compound to be measured, works as a detector [115].

The detector is divided into two equal volumes by a thin metallic diaphragm. When the chopper blocks the radiation, the pressure in both parts of the detector is the same and the diagram remains in the neutral position. As the chopper blocks and unblocks the radiation, the radiant energy from one source passes through the reference cell unchanged, whereas the sample cell absorbs the infrared energy at the wavelength of the compound in the cell. The absorption is proportional to the concentration of the compound to be measured in the sample cell. Thus unequal amounts of energy are transmitted to the two volumes of the detector, and the pressure differential so generated causes the movement of the diaphragm and the fixed probe, thereby generating an A.C., displayed on a meter. The signal is a function of the concentration of the compound to be measured.

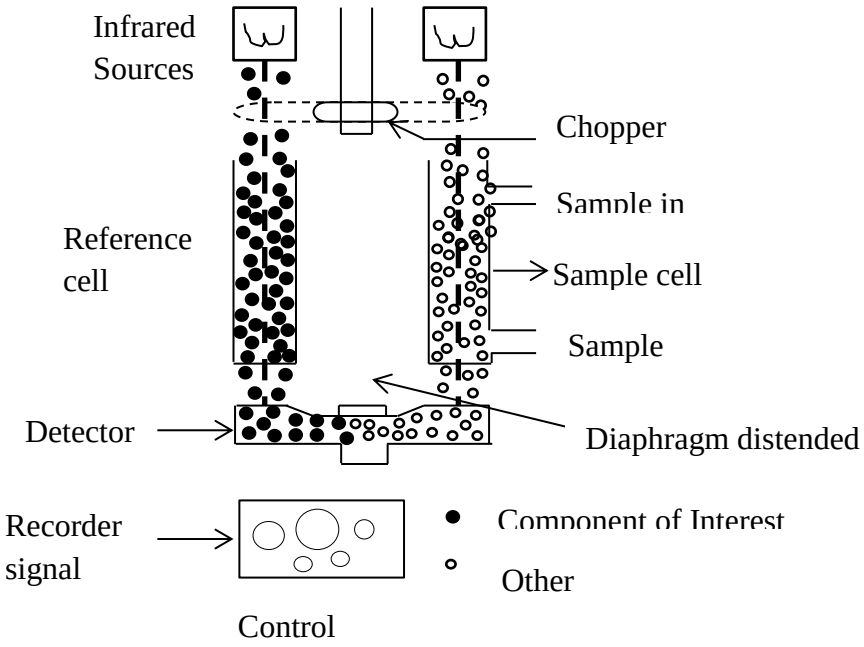

Figure 4.6 Schematic of Non-dispersive Infra-red analyser (NDIR) [111]

The NDIR can accurately measure CO, CO_2 and those hydrocarbons which have clear infrared absorption peaks. However, usually the exhaust sample to be analysed contains other species which also absorb infrared energy at the same frequency. For example, an NDIR analyser sensitized to n-hexane for the detection of HC responds equally well to other paraffin HC but not to olefins, acetylenes or aromatics. Therefore, the reading given by such an analyser is multiplied by 1.8 to correct it to the total unburnt hydrocarbon (UBHC) as measured by an FID analyser in the same exhaust stream [115].

4.5.2 Electrochemical principle for the NO measurement

Nitric oxide (NO) reacts with ozone to convert nitrogen dioxide, the basis of the chemiluminescence measure of NO; it can be oxidised in an electrochemical cell [116]. Electrochemical cells are sensitive to other compounds which are present in the measured gas, instead of the reaction generating light which can be detected in the form of a small electric current. The magnitude of the current is proportional to the mass flow-rate of nitric oxide into the reaction chamber, and can be measured with a high sensitivity using relatively standard electronics. In brief, the NO diffuses across a gas-permeable membrane, and a thin film of electrolyte covering the probe. The NO species are oxidized on the sensor which

consists of a working electrode. The electrochemical cell requires an electrolyte that could be a liquid or, ideally, a solid [116].

4.5.3 AVL Digas 444 analyser

The photographic view of the AVL Digas 444 analyser is illustrated in Figure 4.7 and the details of technical specifications are given in Annexure 10.

The analyser is manufactured by the AVL India Company, and is certified by the ARAI/TA (4G-RV)/AVL/DI gas 444/O910-12. The analyser works on the NDIR principle to measure CO, CO_2 and HC emissions, and on the electrochemical principle to measure the NO emission and O_2 exhaust gases. When the engine was run, CO, CO_2 and O_2 were measured in the form of a volume percentage, and the unburned hydrocarbon (UBHC) emissions were measured in ppm. Similarly, the NO emission is measured in ppm.

Figure 4.7 Photographic view of the AVL Digas 444 analyser

By using the analyser, the exhaust gas emissions were recorded over a span of 120s in consecutive intervals of 20s, which was greater than the instrument response time of 15s, for each case during the engine's running operation. The exhaust gases were tapped from a T joint fitted between the exhaust gas outlet and the smoke meter tapping point. A fine filter was used to remove the particulates and a condensate trap was incorporated, after the main exhaust gas cooled, so that the exhaust inlet temperature to the analyzer was maintained around 40^{o}C, as per the instruction manual. Stray condensates, if any, were tackled by the

condensate separator inbuilt in the analyser, which was flushed before every data recording. Leak check, HC residue test, zero adjustment and condensate purging of the analyser, were also carried out before each observation.

The calibration of the gas analyzer was carried out periodically in order to ensure the accuracy of measurement. The gas analyzer's electronics, optics and its response to environmental factors were checked through calibration. The calibration procedure involved injection of calibration gases of known concentration and validating the response. The compositions of CO, CO_2 and HC gases were; 3.5% volume of CO, 14% volume of CO_2, 2000 ppm volume of propane and the remainder nitrogen, whereas the calibration gas for the NO component is 2200 to 3000 ppm volume of the NO and the remainder N_2. The instrument outputs were then adjusted to the known inputs to correct the variations in the electronic response due to temperature effects, drift or other interferences. Thus, the accuracy of the analyser was assured and an accurate response to the sampled gas was achieved after calibration.

4.5.4 Measurement of exhaust smoke

Smoke meters, namely, Bosch and Hartridge, are basically soot density (g/m^3) measuring devices, whose readings are a function of the mass of carbon in a given volume of exhaust gas [115]. The AVL 437C analyser works on the Hartridge smoke meter and its basic principle is that a fixed quantity of exhaust gas is passed through a fixed filter paper, and the density of the smoke stains on the paper are evaluated optically to determine the soot density. In a recent modification, these types of smoke meter units are used for measuring the intensity of smoke stain on filter paper. The photographic view of the AVL 437C smoke meter is portrayed in Figure 4.8 and details of the technical specifications are given in Annexure 11.

This measuring instrument consists of a sampling probe that sucks a specific quantity of exhaust sample through a white filter paper fitted in the smoke meter. The reflectivity of the filter paper was measured by the smoke meter. This consisted of a light source and an annular photo detector that illuminate the fitter paper to measure the reflected light. Before every sample, it was ensured that the exhaust from the previous measurement was completely driven off from the tube and pump [117].

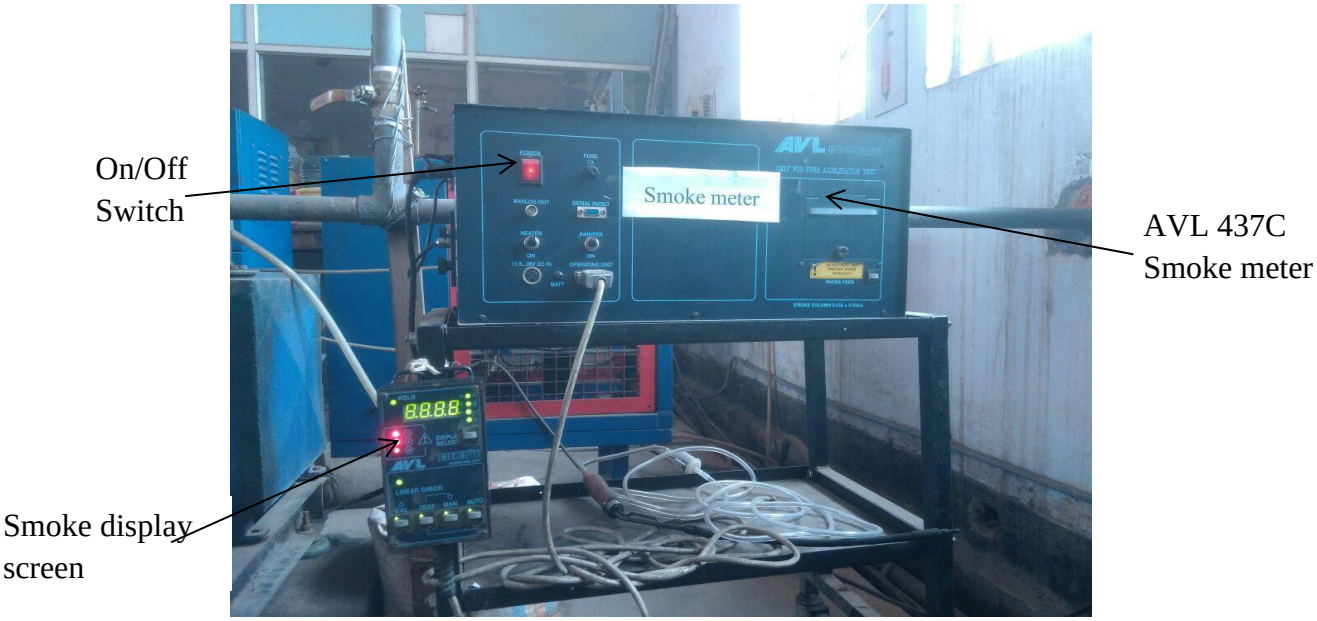

Figure 4.8 Photographic view of the AVL 437C smoke meter

The calibration of the smoke meter was done periodically. The calibration was done by warming the heating elements up to 70^{o}C. The heating was designed to prevent the temperature falling below dew point, and thus to avoid measurement error. Fresh air was allowed to enter the measurement chamber which was drawn through the fitter paper, then it underwent measurement and the zero point was set for calibration. The halogen bulb current irradiates the column of fresh air volume, and the signal from the detector was measured by the microprocessor and the reference value was set for 0% opacity. The linearity can be checked by gently pushing the linearity check knob down/up to its dead position. The calibration plate was thus measured in front of the detector, and the measured opacity value was indicated and printed on the protocol print out. The probe of the exhaust gas analyzer was inserted at the end of the exhaust pipe during the measurement of emissions. Once the engine reached stable operation, the probe was inserted into the exhaust pipe and the measurements were taken.

4.5.5 Conversion of emission values into g/kWh

It is a general practice to express the emission data on a “brake specific” basis, except for the smoke opacity. The brake specific emissions are the mass flow rates of the individual pollutant divided by the engine power. The formulae used to convert the emissions from ppm and % vol into g/kWh are given below:

HC emission in g/kWh is calculated as;

HC (g/kWh) = [{(mf+ma)/(29×1000)} ×(HC (in ppm)×13)/(BP)] (4.12)

CO emission in g/kWh is calculated as;

CO (g/kWh) = [{(mf+ma)/(29×10)} × (CO (in % vol)×28)/(BP)] (4.13)

NO emission in g/kWh is calculated as;

NO (g/kWh) = [{(mf+ma)/(29×1000)} × (NO (in ppm)×32.4)/(BP)] (4.14)

4.6 Calculations and uncertainty analysis

An uncertainty or error analysis is necessary to establish the bounds on the accuracy of the estimated parameters. The evaluations of some unknown uncertainties from the known physical quantities were obtained using the following general equation [118].

$$\frac{U_Y}{Y} = \left[\sum_{i=1}^{n} \left(\frac{1}{Y} \frac{\partial Y}{Y \partial X_i} U_{X_i} \right)^2 \right]^{\frac{1}{2}} \quad (4.15)$$

In the equation cited, Y is the physical parameter that is dependent on the parameters, xi. The symbol UY denotes the uncertainty in Y. As a result, the maximum uncertainty of the experiment obtained was ±2.2%. Table 4.1 lists the instruments used in the present study and their uncertainties. The percentage uncertainties of various parameters like total fuel consumption (TFC), brake power (BP), specific fuel consumption (BFC) and brake thermal efficiency (BTE) were calculated using the percentage uncertainties, and the total percentage of uncertainty of this experiment is [118]

$$= \sqrt{\{(TFC_{UC})^2 + (Brake\ power_{UC})^2 + (BSEC_{UC})^2 + (B.Th_{UC})^2 + (CO_{UC})^2 + (HC_{UC})^2 + (NO_{UC})^2 + (Smoke_{UC})^2 + (EGT_{indicator\ UC})^2 + (Pressure\ pickup_{UC})^2\}}$$

$$= \sqrt{\{(1)^2 + (0.2)^2 + (1)^2 + (1)^2 + (0.2)^2 + (0.2)^2 + (0.2)^2 + (1)^2 + (0.15)^2 + (1)^2\}}$$

= ± 2.2% (4.16)

Table 4.1 Range, accuracy and uncertainty of the instruments

S.No.	Instrument	Range	Accuracy	Uncertainty
1.	Load indicator, kg	250-6000	±10	0.2
2.	Temperature indicator, ^{o}C	0-900	±1^{o}C	0.1
3.	Burette, cc	1-30	±0.2	1.0
4.	Speed sensor, rpm	0-10000	±10	0.1
5.	Exhaust gas analyser NO, ppm HC, ppm CO,%	 0-5000 0-20000 0-10	 ±50 ±10 0.03	 1 0.05 1
6.	Smoke meter, %	0-100	±1	1
7.	Pressure transducer, bar	0-110	±0.1	0.15
8.	Crank angle encoder	0-720	±1	0.3298

4.7 Experimental methodology

The details of various methodologies adopted, and the modifications involved in the engine for the investigation are discussed in this section. Initially, for collecting the reference data of the engine parameters such as combustion, performance and emission, the engine was run on diesel at different engine loads, viz., 25%, 50%, 75% and 100%. Further, engine modification techniques such as different injection timing, nozzle opening pressure, compression ratio and internal jet piston were adopted. The data related to the combustion, performance and emission parameters of the engine run on Carbodiesel/CBWD emulsions were collected for further analysis and comparison.

4.7.1 Experimental investigation on the carbon based slurry (Carbodiesel)

4.7.1.1 Different Carbodiesels

After conducting experiments with diesel to get the relevant data for the combustion, performance and emission parameters, the engine was run on different CB based slurries (Carbodiesel). A mixture containing 5% CB was denoted as Carbodiesel5. Similarly, 10%, 15% and 20% CB in Carbodiesel were denoted as Carbodiesel10, Carbodiesel15 and Carbodiesel20 respectively. The preparation of all four Carbodiesels has already been described in Chapter 3. Table 4.2 gives the composition of the different Carbodiesels as a Carbodiesel5, Carbodiesel10, Carbodiesel15 and Carbodiesel20 with Diesel used in this study.

Table 4.2 Composition of different Carbodiesels

Fuel type	**CB%**	**Diesel%**
Carbodiesel5	5	95
Carbodiesel10	10	90
Carbodiesel15	15	85
Carbodiesel20	20	80

The engine was run on different Carbodiesels at a given compression ratio of 17.5 and nozzle opening pressure of 200 bar which is set by the manufacturer by maintaining a rated speed of 1500 rpm. The data obtained for them were compared with those of diesel operation at all loads. Finally, the engine was allowed to run on diesel to remove traces of the Carbodiesel in the fuel line and fuel filter. The exhaust gas analyser and the diesel smoke meter were switched on before the start of the experiments, in order to stabilize them before starting the measurements. All the instruments were periodically calibrated before testing.

4.7.1.2 Optimisation of injection timing of Carbodiesel

Diesel engines are designed to particularly operate with diesel fuel only. When an alternative fuel is proposed as a CI engine fuel and used, it may not produce better performance and lower emissions, if the fuel has higher density. Hence, optimisation of engine parameters such as injection timing, nozzle opening pressure, compression ratio etc. is necessary. More importantly optimising injection timing will help to further optimise other engine parameters [119-121]. In this experimental module, the effects of fuel injection timing on the combustion, performance and emission characteristics of the engine run on Carbodiesel were investigated. For this purpose, the fuel pump was dismantled to change the injection timing. The static injection timing was changed, by adjusting the number of shims under the mounting flange of the fuel injection pump. The fuel injection timing was changed by adding or removing the number of shims fitted in the fuel injection pump. The standard fuel injection timing of the engine is 23^{o}CAbTDC which was set by the manufacturer, and there were three shims. The thickness of every shim is 0.3 mm. The shim with 0.3 mm thickness was added to get the retarded injection timing, while the shim was removed to get an advanced injection timing. Each shim can either give 1.5^{o}CA advancement or retardation, according to the addition or removal of the shim in the pump. Figure 4.9 (a) and (b) show the photographic view of the shim and the shim with the fuel pump.

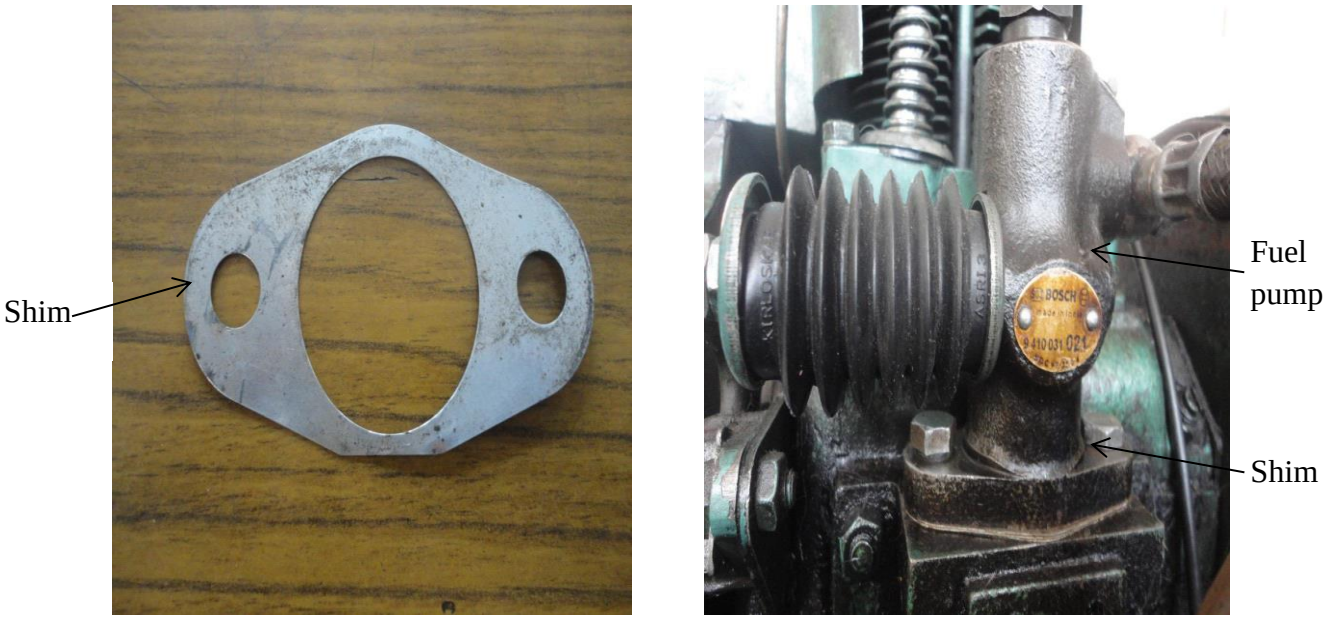

Figure 4.9 Photographic view of the (a) shim (b) shim fitted with the engine

In order to optimise the injection timing of the engine run on Carbodiesel10, experiments were conducted on the diesel engine with two different advanced injection timings and retarded injection timings from 20^{o}CAbTDC to 26^{o}CAbTDC at regular intervals of 1.5^{o}CA. The combustion, performance and emissions were studied in the diesel engine at two advance injection timings (24.5^{o}CAbTDC, 26^{o}CAbTDC) and two retardation injection timings (20^{o}CAbTDC, 21.5^{o}CAbTDC) with the original injection timing (23^{o}CAbTDC). After finishing each set of experiments, the injection timing was restored to the original timing, and the next injection timing was set. The optimum injection timing was determined by analysing the results of Carbodiesel10, and comparing them with the diesel data.

4.7.2 Experimental investigation of CBWD emulsions

4.7.2.1 Different CBWD emulsions

Further, the diesel engine was run on four different emulsions of CB, water and diesel emulsions (CBWDs). An emulsion containing 5% CB was denoted as CBWD5. Similarly, 10%, 15% and 20% CB in emulsion were denoted as CBWD10, CBWD15 and CBWD20 respectively. Table 4.3 gives the composition of different CBWD emulsions as a CBWD5, CBWD10, CBWD15 and CBWD20 with diesel, wate and surfactant used in this study.

Table 4.3 Composition of different CBWD emulsions

Fuel type	CB%	Diesel%	Water%	Surfactant%
CBWD5	5	90	3	2
CBWD10	10	85	3	2
CBWD15	15	80	3	2
CBWD20	20	75	3	2

The preparation of all four emulsions has already been described in Chapter 3. The engine was run on the four different emulsions at standard engine parameters, which were set by the manufacturer. The combustion, performance and emission characteristics of the diesel engine fuelled with the four different emulsions were compared with those of diesel operation of the same engine.

4.7.2.2 Description of mathematical modelling

In research and development, mathematical modelling is a useful method with a low computational cost that may assist the scientists and engineers in their efforts towards the development of more efficient and clean engines [122]. Computer simulation [123] serves as a tool for a better understanding of the effect of the engine operating variables involved, on the engine performance, combustion and emission characteristics, thereby reducing the cost and time.

In recent years, the experimental results were validated with the help of mathematical models and simulations [123], and they have been proven to be fruitful.

The simulation model by MATLAB program for a numerical solution was used to analyze the engine parameters of a single cylinder 3.5 kW rated power diesel engine fuelled with diesel, Palm Oil Methyl Ester and POME-diesel blends [124]. The results reported that, the simulated results of the brake thermal efficiency and in-cylinder pressure were closer by about 2-3 % to the experimental results. A single-zone thermodynamic model was developed for a diesel engine fuelled with biodiesel from waste [125]. The single zone model coupled with a triple-Wiebe function was designed to simulate the heat release and cylinder pressure. It was reported that, the heat release rate and cylinder pressure predicted by the used model were 2.5% and 2.2% closer to the experimental results of the engine. A two dimensional

multi-zone model was developed for a DI diesel engine run with an ethanol–diesel blend fuel [126] and vegetable oil, bio-diesel and diesel [127]. The simulation model was supported by Fortran V language, and solved numerically by a solution matching technique with a computational step size of 1^{o} crank angle. The mass, energy and state equations were used in each zone to provide local temperatures and cylinder pressure. The model followed each zone with its own time history as the spray penetrates into the swirling air environment of the combustion chamber before and after wall impingement. It was also reported that, the high equivalence ratio areas of fuel spray were limited when bio-diesel or vegetable oil fuels were used instead of diesel fuel. The diesel engine run under motoring conditions, with the heat transfer formulations for the used computational fluid dynamics (CFD) codes [128] was evaluated and compared with the experimental data. The model predicted more accurately the heat transfer during the compression stroke for motored operation, and at the same time, the predicted peak heat flux was closer to the experimental results. The computational time required was not affected in the multi-dimensional modelling. The combustion model for a diesel engine was developed, using Computational Fluid Dynamics (CFD) software-AVL Fire, and the performance, and emission characteristics for second generation biodiesel were analysed [129]. The simulated results reported that, biodiesel provided better performance and efficiency, and significantly reduced engine emissions. The quasi-dimensional multi-zone (QDMZ) models [130, 131] were formulated by the quasi steady equations, which described the individual processes that occur in the engine cylinder such as fuel atomization, fuel injection, air entertainment, air-fuel mixing, combustion and heat transfer. A combustion model [132] was developed for the theoretical DI diesel engine and performance parameters. It was reported that the developed model could be adapted to an alternative fuel in a diesel engine, and the performance and cylinder pressure results brought closer to the theoretical ones.

As the researcher is familiar with MATLAB program, the experimental results obtained from running the engine on the carbon black diesel water emulsion (CBWD10) were validated using a two zone mathematical modelling, which was carried out with the help of a MATLAB program. The comparison between the mathematical modelling and the experimental results are discussed.

4.7.2.3 Description of the model

A mathematical model was developed for the above-mentioned engine which had a hemispherical bowl shaped piston head. In principle, the fuel is injected using a pintle nozzle having 3 holes that are symmetrically placed about the nozzle tip of the fuel injector. Fuel injection occurs at 23^o CA bTDC and at a pressure of 200 bar. The model incorporates the processes occurring inside the engine between the IVC and EVO events when the valves are closed.

The model structure is divided into various important parts that interact with each other. Those parts are: Engine geometry; the integration of 1^{st} law and gas state equations that describe the mass flow rate between the two zones. The combustion models includes the ignition delay, fuel combustion and heat transfer to the walls; and the emissions models, including emissions of NO, soot and other exhaust gases.

The calculations were done by taking step size $\Delta\theta = 1^o$ CA. (4.17)

For the heat release rate and cylinder pressure each and every crank angle

4.7.2.4 Engine geometry

The instantaneous piston position as a function of CA is modelled by the equation derived from the basic geometry of the engine as a slider-crank mechanism:

$$X = a + \ell + \sqrt{(\ell^2 - a^2.\sin^2\theta)} - a.\cos\theta \quad (4.18)$$

where θ denotes the crank angle.

So, the instantaneous volume of the cylinder as a function of CA is found out by adding up the clearance volume and the instantaneous swept volume and is given the equation:

$$V_{inst} = Vc + (\pi D^2/4).X$$
$$= Vc + (\pi D^2/4).[\, a + \ell + \sqrt{(\ell^2 - a^2.\sin^2\theta)} - a.\cos\theta \,] \quad (4.19)$$

where Vc is the clearance volume and D is the bore diameter. 'a' and 'ℓ' are the crank radius and length of connecting rod respectively.

4.7.2.5 First law and ideal gas state equations

After the IVC (inlet valve closing) event, the dynamics inside the engine are taken into consideration till the EVO (exhaust valve opening) event of the same cycle. So, the calculations are done corresponding to this time interval, which can technically be considered

as a closed cycle. The ideal gas equation and the equation of 1st law of thermodynamics for a closed system are applied to the system.

$$dQ = dE + pdV \quad (4.20)$$

$p.V = n.R_{mol}.T$ where n = no. of moles of air = m_a/M

where M = molecular mass of charge

Initially, during the compression stroke, only air exists in the cylinder. Hence, only the air zone exists. After the ignition of the fuel, the two zone formation starts. A corresponding burning zone is created apart from the current non-burning zone or air zone. Air is transferred from the non-burning zone to the burning zone along with a change in enthalpy caused due to the fuel. So, the thermodynamic equations are written as follows:

For the burning zone

$$dQ = dE + dW - h_a m_a - h_f m_f \quad (4.21)$$

For the existing air zone, due to the transfer of air to the burning zone, the thermodynamic state equations for the non-burning zone are written as:

$$dQ = dE + dW + h_a m_a \quad (4.22)$$

4.7.2.6 Ignition delay

Ignition delay is defined as the time lapse between the start of injection of fuel and the start of ignition. It is generally denoted as τ_{id} and $\tau_{id} = \int_0^t \tau . dt$. After the fuel has been injected, the fuel droplets vapourize and mix with the air present. In addition, the heavier hydrocarbons in the fuel break down into lighter and comparatively simpler ones during the process. This accounts for the ignition delay. The end of ignition delay is characterized as the state where very fast rate of exothermic reaction occurs emitting visible light from the fuel spray surface.

$$\tau_{id} = a.\ p_m^{-c}.\exp(E_a/R_m T_m) \quad [133] \quad (4.23)$$

where T_m and p_m are the mean temperature and pressure of the two zones.

4.7.2.7 Heat transfer

Heat transfer between the cylinder trapped mass and the surrounding walls is calculated. Heat released from the combustion of the fuel air mixture is transferred to the walls of the cylinder

by both convection and radiation. A comparatively larger surface area of the combustion chamber is exposed to the gases during the period of combustion. In this model, Hohenberg's correlation is considered for the instantaneous rate of heat transfer to the walls.

Thus, the heat loss from the gas chamber to the cylinder walls is given as a function of time as:

$$\dot{Q}_t = h_c.A_s.(T_{cyl} - T_w) + c.(T_{cyl}^4 - T_w^4) \quad (4.24)$$

where h_c is the heat transfer coefficient, A_s is the surface area available at the instant, T_{cyl} is the instantaneous bulk temperature of the gases in the cylinder, T_w is the temperature of the walls and c is the radiative heat transfer constant. The heat transfer coefficient is given as:

$$h_c = [130 \times P_{cyl} \times (u_p + 1.4)^{0.8}]/[V_{inst}^{0.06} \times T_{cyl}^{0.04}] \quad [134] \quad (4.25)$$

where P_{cyl} is the instantaneous cylinder pressure, u_p is the piston velocity and V_{inst} is the instantaneous cylinder volume. Further, the average heat transferred to the walls per degree crank angle in one cycle can be calculated as:

$$\dot{Q}_\theta = \dot{Q}_t \times 60/(2\pi n) \quad (4.26)$$

where n is the piston speed in rpm.

4.7.2.8 Fuel spray

The model follows each zone, with its own time history, as the spray penetrates into the swirling air environment of the combustion chamber, before and after wall impingement. The fuel spray is achieved by direct injection of the CBWD10 emulsion into the combustion chamber at 23^o bTDC at 200 bar using an injector with a pintle nozzle. The nozzle has 3 holes present symmetrically in the nozzle. The fuel spray is characterized by conical jets fired into the combustion chamber assuming no wall impingement. The fuel breaks up into fine globules, vapourizes and mixes with the entrained air from the non-burning zone.

The mean fuel injection rate is given by:

$$m_{fi} = m_{ft}/(3 \times \Delta\theta_{inj}) \quad (4.27)$$

The mean spray velocity is given by:

$$u_i = m_{fi} \times [6N/(\rho_l \times F)] \quad (4.28)$$

where $F = d_n^2/4$ (d_n = diameter of nozzle hole).

The pressure drop in the nozzle is given by:

$\Delta p = 0.5 \times \rho_l \times (v_{inj}/C_d)^2$ (4.29)

where C_d is the discharge coefficient.

4.7.2.9 Combustion sub-model

After the mixture has been prepared physically and chemically, ignition takes place. The mass of evaporated fuel as calculated is available for combustion. The rate of burning is assumed to be controlled by an Arrhenius type equation, which also includes the influence of the available amount of evaporated fuel or unburned air.

For calculating the amount of fuel burnt and the combustion rate, Wiebe's function is used. The Wiebe function is given by: $W(\theta) = 1 - \exp(- a(\frac{\theta - \theta inj}{\Delta\theta})^n)$ (4.30)

where $W(\theta)$ gives the mass fraction of fuel burnt per ^oCA [135]. The equation has two constants a and n, which are to be found out by using curve fitting methods to find a close approximation to the actual values obtained from the experimental observations.

4.7.2.10 Emissions sub-model

The emissions for the system constitute of the following chemical species: CO_2, CO, H_2O, N_2, NO, OH, H_2, H, O, OH and unburnt hydrocarbons. For modelling the emission characteristics, the chemical equilibrium scheme proposed by Way [135] is used for this chemical system. The concentration of each of the mentioned species is calculated by using the scheme that involves solving a set of 11 equations based on the chemical equilibrium. The equilibrium equations are as follows:

$N_2 + O_2 \rightleftharpoons 2NO$ $2H_2O + O_2 \rightleftharpoons 4OH$ $2CO + O_2 \rightleftharpoons 2CO_2$ $2H_2 + O_2 \rightleftharpoons 4OH$

$N_2 \rightleftharpoons 2N$ $H_2 \rightleftharpoons 2H$ $O_2 \rightleftharpoons 2O$

Similarly, the equilibrium constants are found out using the chemical equilibrium equations and are used in the model to find out the concentration of the individual species.

4.7.2.11 NOx formation

For computing the amount of NOx emissions, the kinetics formation scheme of Lavoie et al. [136] is used. This scheme constitutes the following equations. The respective reaction rate constants are mentioned by each reaction.

$N + NO \rightleftharpoons N_2 + O$ $k_{1f} = 3.1 \times 10^{10} \exp(-160/T)$

$N + O_2 \rightleftharpoons NO + O$ $\quad k_{2f} = 6.4 \times 10^6 \exp(-3125/T)$

$N + OH \rightleftharpoons NO + H$ $\quad k_{3f} = 4.2 \times 10^{10}$

Equilibrium constant = $\alpha = NO/NO_e$

The change of NO concentration is computed by solving the equilibrium equations and using chemical kinetics.

4.7.2.12 Soot formation

For calculating the soot formation rate, the model proposed by Hiroyasu et al. [137] is used. The net soot formation rate is given as $\dot{m}_s = \dot{m}_f - \dot{m}_d$, where the variable $\dot{m}$ denoted mass rate and the subscripts s, f and d denote the net soot formation rate, soot formation rate and soot oxidation rate respectively.

$$\dot{m}_f = A_f \times m_f^{0.8} \times p^{0.5} \exp(-E_f/R_{mol}T) \quad (4.31)$$

$$\dot{m}_d = A_d \times m_d \times (p_{O2}/p) \times p^n \exp(-E_d/R_{mol}T) \quad (4.32)$$

The values of n, constants A_f, A_d and the activation energies E_f and E_d are evaluated by mathematical models or found out by using curve-fitting techniques on the experimental data.

4.7.2.13 Numerical solution procedure

The model was computed using the mentioned formulae and equations. The codes and iterations were computed in Matlab® software by Mathworks Inc. For the calculations, a step size of 1^o CA was taken. The iterations were started from the IVC event and end at the EVO event. The data about the engine geometry, physical quantities, physical and chemical properties of the fuel, etc. were provided at the start of the calculations from the data acquisition system. Then the states and properties were modelled accordingly.

At the IVC event, the pressure, temperature and crank angle were introduced. The instantaneous volume of the cylinder for step 1 was calculated using the formula mentioned in Eq. (4.18) in section 4.7.2.4. The trapped amount of air (in moles) n_{at} was calculated using the ideal gas equation. The initial internal energy E_1, at state 1 was calculated using the fourth order polynomial equation dependent on T_1.

The crank angle for the second time step was given as $\theta_2 = \theta_1 + \Delta\theta$, where $\Delta\theta = 1$. The instantaneous volume V_2 for the second step was calculated using Eq. (4.18). Considering

isentropic change in the compression cycle (which is pure air zone) the pressure, temperature for the next step were calculated as shown. Υ is the ratio of specific heats i.e. C_p/C_v.

$$T_2 = T_1(V_1/V_2)^{\Upsilon-1} \text{ and } p_2 = (V_1/V_2)(T_2/T_1)p_1 \quad (4.33)$$

The internal energy corresponding to T_2 was calculated. The work done for the time step was calculated as:

$$dW = 0.5(p_2 + p_1)(V_2 - V_1) \quad (4.34)$$

The amount of heat transfer and the heat release rate were calculated using the formula mentioned in Eq. (4.24-4.28) in section 4.7.2. The error equation $f(T) = E_2 - E_1 + dW - dQ$ was solved using Newton-Raphson method to find an approximate value of T_2. This value of T_2 was further used to find the new value of pressure p_2 using the ideal gas law equation. This process was continued until the crank angle reaches 23^o CA bTDC, the value at the start of fuel injection.

4.7.2.14 After expansion phase:

The two-zone system was connected with the previous single-zone (expansion phase). The temperatures of both the non-burning zone and the burning zones were denoted and initialized as: $T_{2a} = T_2$, $T_{2b} = T_2$ and the volumes of the respective zones were initialized as $V_{2a} = V_2$, $V_{2b} = 0$.

The conditions for the next time step were set as as $\theta_2 = \theta_1 + \Delta\theta$ as has been done before. Similarly, V_2 was calculated from the engine geometry equation. The fuel injection rate, cumulative injected fuel and amount of entrained air were calculated. Pressure was estimated considering isentropic process: $p_2 = p_1(V_1/V_2)^{\Upsilon}$.

4.7.2.15 Calculations carried out in the air zone:

Internal energy E_1 and enthalpy h_1 were calculated as a function of T_{1a}. The instantaneous volume of the air zone V_{1a} was calculated as: $V_{1a} = n_{1a}\times R_{mol}\times T_{1a}/p_1$. The amount of the various constituents (in kmol) present in the air zone (specifically oxygen and nitrogen) was computed. So, the total amount of air zone is given by: $n_{2a} = n_{at} - (m_a/M_a)\times 3$ kmol. The air loss due to entrainment to the burning zone is given by: $n_{loss} = n_{1a} - n_{2a}$. Then the volume of the air zone after air loss was calculated as: $V_{2a} = n_{2a}\times R_{mol}\times T_{2a}/p_2$. And the work done in this process is given by: $dW = 0.5(p_1+p_2)(V_{2a}-V_{1a})$. The 1^{st} law for an open system was used and a better estimate of T_{2a} was computed.

4.7.2.16 Calculations carried out in the burning zone:

Internal energy of the burning zone after mixing was calculated using the temperature of mixing, T_{mix}. Further, temperature after combustion of fuel for the current time step is estimated, considering it to be an isentropic process, i.e.

$$T_{2b} = T_{mix}(p_2/p_1)^{\frac{y-1}{y}} - \frac{dmf \times QL \times (y-1)}{nmix \times Rmol} \quad (4.35)$$

The volume of the burning zone was calculated using the gas equation, $V_{2b} = n_{mix} \times R_{mol} \times T_{2b}/p_2$.

The instantaneous mixture compositions of the constituents in the burning zone were calculated in kmol. This was solved using a system of higher order equations and matrices derived from the equilibrium equations of the individual reactions during the combustion process.

Now, the internal energy was calculated as a function of T_{2b} and volume after the combustion in the current time step was over was calculated as:

$$V_{2b} = (n_{2b} \times R_{mol} \times T_{2b})/p_2 \quad (4.36)$$

The work done in this process is given as:

$$dW = 0.5(p_1+p_2)(V_{2b}-V_{mix}) \quad (4.37)$$

The first law was applied for this process considering a closed system and the equation obtained was solved to find a better estimate value of T_{2b}. The total work done for the process of mixing and combustion is given as:

$$dW = 0.5(p_1+p_2)(V_{2b}-V_{1b}) \quad (4.38)$$

The above steps were repeated until it's assumed that fuel still exists.

Then the mean state variables for the model were computed assuming the interactions between the zones are isenthalpic. The mean temperature was calculated as : the equation $H - H_{2a} - H_{2b} = 0$ was solved using Newton-Raphson method iterated to a sufficient index so as to find a better estimate value of T_2, which is the mean temperature of the two zones. Here, H, H_{2a} and H_{2b} are enthalpies for the mean temperature, temperature in air zone and that in burning zone respectively.

4.7.2.17 Validation

Following the computations of the two-zone model, the obtained results were validated against the values of experiment results for diesel and the CBWD10 emulsion. To satisfy the empirical relations used in this model, certain values were to be evaluated against the constants occurring in those equations. To arrive at a suitable model, the equations were simulated using various curve-fitting techniques in Matlab® 2014a that include a few regression models and least squares method, to obtain the best fit between the experimental curves and the simulated curves. The combustion characteristics were represented in the form of four characteristic graphs showing variations of pressure, bulk temperature, mass fraction of fuel burnt and heat release rate with the crank angle for an average cycle.

4.7.3 CBWD10 emulsion at different injection timings

Based on the performance and emission results, CBWD10 was chosen as an optimum emulsion among the four emulsions studied initially. Similar to the study mentioned in section 4.7.1.2, experiments were conducted at different injection timings with the CBWD10 emulsion. The data pertaining to the combustion, performance and emission parameters were collected for the analysis. After every set of experiments, the engine was operated in standard conditions with diesel to ensure a steady state.

4.7.4 Combined effects of injection timing, nozzle opening pressure and compression ratio on CBWD10 fuelled engine behaviour

After analysing the results obtained from the experimental study of Carbodiesel10 and CBWD10 emulsions on running at different injection timings, it was found that the advanced injection timing of 26^{o} CA bTDC was the optimum, based on the performance and emission parameters. Comparing both the fuels, the CBWD10 emulsion proved to be a better fuel at the mentioned optimum injection timing.

Furthermore, the combined effects of injection timing, nozzle opening pressure and compression ratio on the engine behaviour were studied, when it was run on the CBWD10 emulsion. The reason behind further engine modification and the step by step procedure involved for varying the nozzle opening pressure and compression ratio, are discussed in the subsequent subsections;

4.7.4.1 Methods of varying nozzle opening pressures

Studies reported that, operating the engine with higher nozzle opening pressures might yield a better fuel atomization at the nozzle outlet and improve the fuel-air mixing and thus, can gave better performance and lower emissions [138, 139]. Figure 4.10 and Figure 4.11 portray a photographic view of the nozzle tester and view of the fuel injector.

Initially, the nozzle opening pressure of the engine was set as 200 bar (as set by the manufacturer), and the injection timing of the engine was 23^{o}bTDC. After an analysis of the results, an optimum injection timing (26^{o}bTDC) was chosen. At this injection timing, the nozzle opening pressure was varied from 200 bar to 240 bar at regular intervals of 10 bar, and the nozzle opening pressure was varied by tightening or loosening the screw of the injector. The nozzle opening pressure was checked by a fuel injector pressure tester. The performance, emissions and combustion characteristics were recorded from no load to full load, at a constant speed of 1500 rpm for the CBWD10 emulsion.

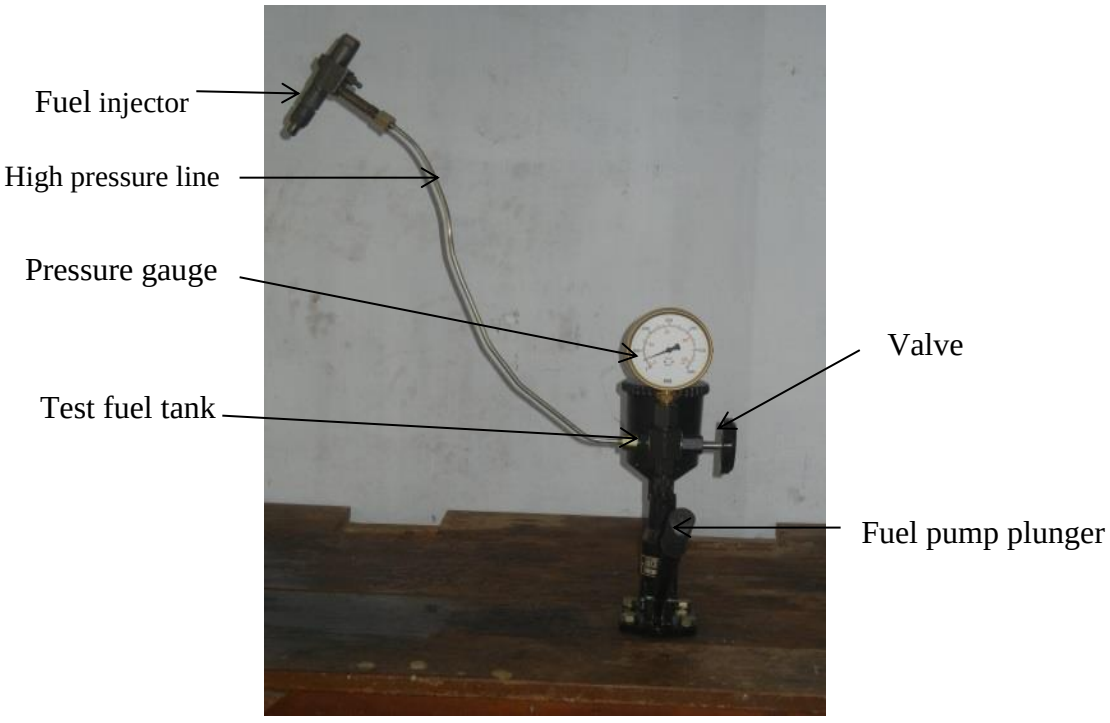

Figure 4.10 Photograph of nozzle pressure tester

Figure 4.11 Photograph of fuel injector

4.7.4.2 Method of varying compression ratios

The method of varying the compression ratio is discussed in this section. There are different methods to change the compression ratio in CI engines, such as variation of the volume of the combustion chamber; moving the cylinder head; variation of the piston skirt height; connecting rod geometry modification; variation of the effective stroke length, moving the crankshaft axis etc. [140-1142].

In the present investigation, the compression ratio was changed by changing the clearance volume by inserting gaskets of different thicknesses between the cylinder and the cylinder head. Figures 4.12 and 4.13 (a), (b) show the photographic views of the cylinder head gasket and changing the head gasket.

The following steps are involved in the calculation of the compression ratio:

$$\text{Compression ratio (CR)} = \frac{\text{Maximum cylinder volume (Vs + Vc)}}{\text{Clearance volume (Vc)}} \tag{4.39}$$

where, Vs = Stroke volume

Vc = Clearance volume

$Vs = \frac{\pi d^2}{4} \times$ L (where d = bore = 8.75 cm, L = stroke = 11 cm)

$CR = 17.5 = \frac{Vs + Vc}{Vc}$

$17.5 = \frac{Vs}{Vc} + 1$

$16.5 = \frac{Vs}{Vc}$

$Vc = \frac{Vs}{16.5} = \frac{661.45}{16.5} = 40.08\ cm^3$

Gasket Volume 7.21 cm^3 (d = 8.75 cm, t = 0.12 cm)

For CR = 18.5, $Vc = \frac{Vs}{17.5} = \frac{661.45}{17.5} = 37.79\ cm^3$

Clearance volume excluding gssket volume + Gasket volume

= 37.79 cm^3

32.87 + Gasket volume = 37.79 cm^3

18.5 CR for required gasket volume = 4.92 cm^3

Gasket thickness required = 0.08

Figure 4.12 Photographic view of cylinder head gasket

In the same manner, the gasket volume and thickness required for the compression ratio = 16.5 were calculated. The calculated gasket volume and thickness corresponding to different compression ratios are given below in Table 4.4.

(a) (b)

Figure 4.13 Photographic view of dismantled engine head (a) without head gasket and (b) with head gasket

Table 4.4 Gasket volume and thickness required for different compression ratios

Compression ratio	Gasket thickness (cm)	Gasket volume (cm^3)
16.5	0.16	9.8
17.5	0.12	7.21
18.5	0.08	4.92

4.7.4.3 Design of experiments

In order to study the combined effects of injection timing, nozzle opening pressure and compression ratio, a design of experiments was prepared. Table 4.5 shows 27 models of experiments conducted by varying compression ratios with different injection timings and nozzle opening pressures.

When the CBWD10 emulsion was tested in the same diesel engine with minor modifications of the injection timing, nozzle opening pressure and compression ratio, the results revealed that the BTE of the engine fuelled with the CBWD10 emulsion was increased by about of 4% at an advanced injection timing of 26^{o}bTDC, 220 bar nozzle opening pressure and compression ratio of 18.5. This is due to the fine fuel spray and optimised droplet size of

CBWD10 achieved at 220 bar fuel nozzle opening pressure. But, the efficiency was a bit lower than that of diesel operation, while the smoke was a bit higher than that of diesel operation.

Table 4.5 Model of experiment [Diesel-A, CBWD10-B]

CR Ratio	Injection timing ^{o}CA, bTDC	Injection pressure, bar	Fuel tested
16.5	23	200	B
16.5	24.5	200	B
16.5	26	200	B
16.5	23	220	B
16.5	24.5	220	B
16.5	26	220	B
16.5	23	240	B
16.5	24.5	240	B
16.5	26	240	B
17.5	23	200	A and B
17.5	24.5	200	B
17.5	26	200	B
17.5	23	220	B
17.5	24.5	220	B
17.5	26	220	B
17.5	23	240	B
17.5	24.5	240	B
17.5	26	240	B
18.5	23	200	B
18.5	24.5	200	B
18.5	26	200	B
18.5	23	220	B
18.5	24.5	220	B
18.5	26	220	B
18.5	23	240	B
18.5	24.5	240	B
18.5	26	240	B

4.7.5 Experimental investigations with the CBWD10 emulsion at internal jet piston

The air motion inside the cylinder greatly influences the performance of diesel engines. The shape of the bowl in the piston, such as piston cavity and the variation of intake system etc., lead to a change in the air-fuel mixing flow inside the DI diesel engine.

In recent years many researchers have reported that the in-cylinder air motions in direct injection (DI) diesel engines were altered through different arrangements, such as shaping the piston cavity [143-145] to study the engine behaviour in terms of the combustion,

performance and emissions. The direct methods of generating turbulence were found to be more flexible in terms of managing its timing and intensity, than those obtained from swirl and swish motions. This turbulence arrangement generally pushes air into the air cell during the compression stroke and injects compressed air into the combustion chamber. The effect of turbulence is induced late in the combustion period by burnt gas from an auxiliary chamber installed in the cylinder head [146]. The brake thermal efficiency of the diesel engine was improved with an improvement in the air entrainment and increased swirl in the combustion chamber [147]. The use of an air cell is the usual approach for controlling soot through well-timed turbulence which enhanced mixing in the combustion chamber. A considerable reduction in the smoke level was reported and it was attributed to the kinetic energy of the gas jet [148]. It was reported that the shortening of the combustion duration at high loads improved the thermal efficiency. The limits of the gas jet mixing on in-cylinder turbulence and observed that a properly timed gas mixing will have beneficial effects only at higher loads [149]. It was also reported that, the ending part of the combustion period increase in the turbulence helps to reduce soot without adversely influencing the NOx emission level. The effect of the geometry of the combustion chamber on fuel spray behaviour was studied, and it was found that a re-entrant type combustion chamber and fuel distribution was better than a simple cylindrical combustion chamber [150, 151]. An internal jet piston was used to improve the turbulence inside the combustion chamber, and it tested to achieve complete combustion, and hence, the overall performance of the engine is increased.

Hence, an attempt was made to improve the engine performance by inducing more turbulence in the combustion chamber, when the engine was run on the CBWD10 emulsion. For this, the combustion chamber of the engine was modified by making two small micro holes in the piston, which were used to create effective air motion in the combustion chamber. After assembling the piston into the engine, the CBWD10 emulsion was tested in the engine with the modified piston for determining the combustion, performance and emissions of the engine at different load conditions. Figure 4.14 portrays the block diagram, and Figure 4.15 shows photographic view of the base piston and turbulence induced (internal jet) piston.

Figure 4.16 portrays the photographic view of the internal jet piston assembled in the diesel engine. Two holes on the piston crown were provided for the turbulence to be induced in the cylinder. The holes of 3.0 mm diameter width and 7.0 mm depth were drilled diametrically opposite in the plane of the piston crown, parallel to the piston pin axis. The holes were

drilled from the centre of the piston's flat surface such that the jets enter near the bottom of the cavity in the direction of the swirl. The angle of the holes drilled from the centre of the piston's flat surface towards the base of the bowl is 40° to the vertical axis of the piston [141]. The combustion, performance and emission parameters were measured and compared with those of the base engine piston results.

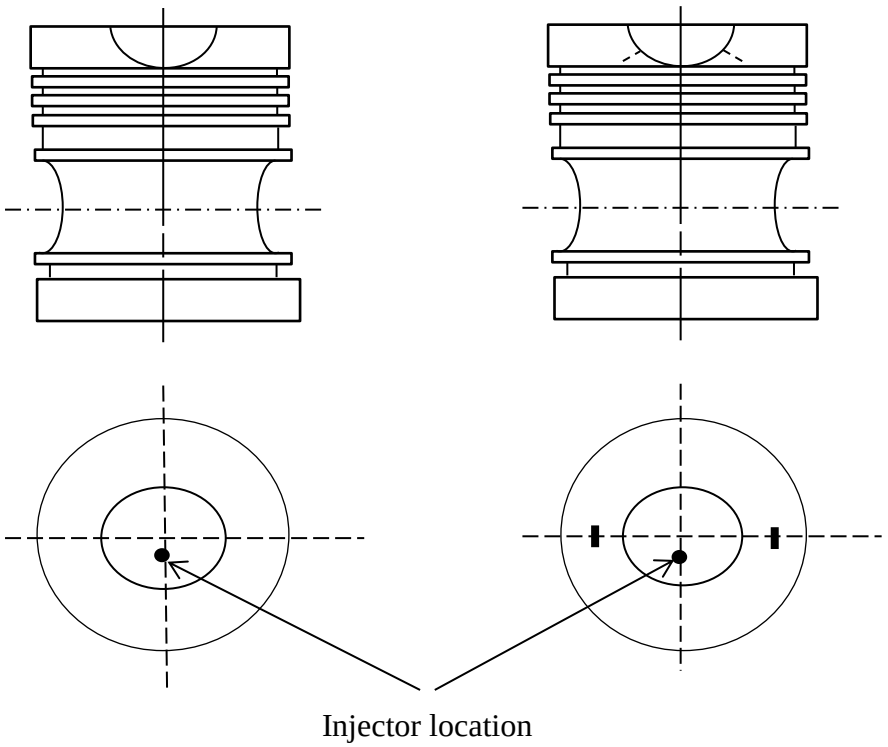

(a) Original engine piston (b) Internal jet piston

Figure 4.14 Block diagram of the piston without and with an internal jet piston

Figure 4.15 Photographic view of the piston without and with an internal jet piston

Figure 4.16 Photographic view of an internal jet piston assembled in a diesel engine

CHAPTER 5
RESULTS AND DISCUSSION

5.1 Preliminary studies on the combustion, performance and emissions with Carbodiesels

5.1.1 General

This chapter presents a detailed discussion on the results obtained for the combustion, performance and emission characterisation of a 4.4 kW single cylinder, four stroke, air-cooled, DI diesel engine, run on two different categories of fuels that were derived from CB; a solid organic waste obtained from pyrolysis of waste automobile tyres. In the first category, CB at different percentages was mixed with diesel to form slurries, and the slurries were designated as Carbodiesels. In this section, the results of the combustion, performance and emission parameters of the engine fuelled with different Carbodiesels are analysed, compared with those of diesel operation of the same engine and presented. The numerical value after Carbodiesel refers to the percentage of CB in the slurries. For example, Carbodiesel10, is composed of 10% CB and 90% diesel.

5.1.2 Combustion analysis

5.1.2.1 Cylinder pressure with crank angle

The cylinder peak pressure of a CI engine mainly depends on the amount of fuel accumulated in the delay period and the combustion rate in the initial stages of premixed combustion [152]. It is also affected by the fuel air mixture preparation during the delay period. The variation of the cylinder pressure with crank angle at full load for different Carbodiesels and diesel is portrayed in Figure 5.1. All the tested Carbodiesels follow a cylinder pressure pattern similar to that of diesel at full load condition. The cylinder pressure of Carbodiesels obtained at full load is found to be lower than that of diesel at full load. This may be lower cetane number, poor volatility and lower heating value. It can be observed that, the cylinder pressure of diesel is found to be 79.4 bar at full load. It can also be observed that, the maximum cylinder pressure for Carbodiesel5, Carbodiesel10, Carbodiesel15 and Carbodiesel20 are found to be about 78.2 bar, 76.4 bar, 73.8 bar and 71.7 bar respectively at full load. The occurrence of ignition at full load is the earliest for diesel, which is about 0.33^{o}CA, while the delay is found to be approximately 0.34^{o}CA 0.35^{o}CA, and 0.61^{o}CA for Carbodiesel5, Carbodiesel10, Carbodiesel15 and Carbodiesel20. The commencement of

ignition for Carbodiesel is later due to their lower cetane numbers and higher densities than that of diesel. Similar reasons were stated by Balamurugan et al., [153] for the results they have obtained in a DI diesel engine. The occurrence of ignition for Carbodiesel20 is the farthest among all Carbodiesels as a result of slow ignition.

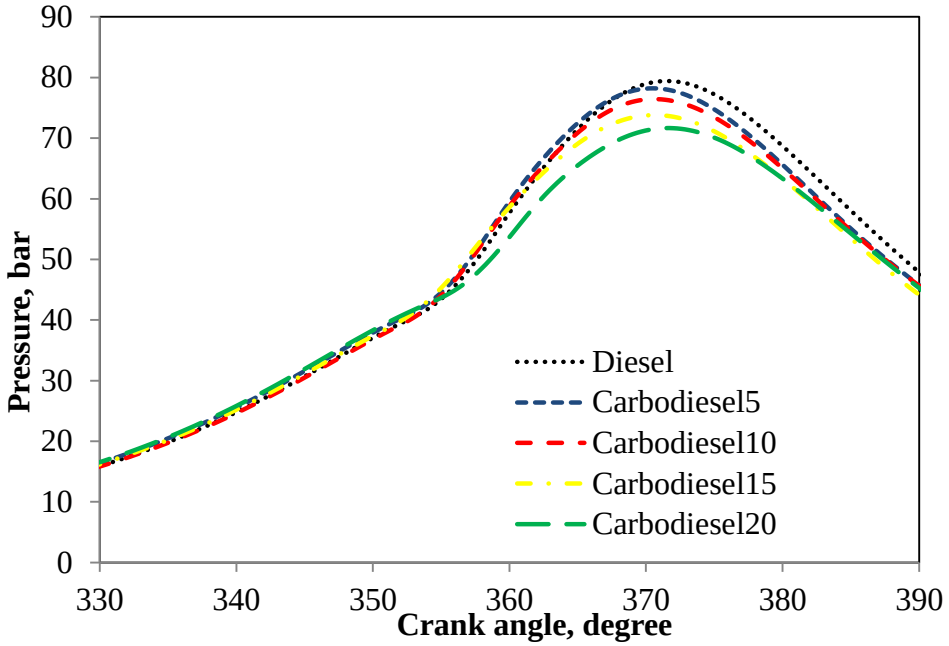

Figure 5.1 Variation of pressure with crank angle at full load

5.1.2.2 Ignition delay

The physical properties of a fuel such as viscosity, cetane number and flash point affect the ignition delay. Viscosity affects atomisation and vapourisation of fuel affects the mixing of fuel with air [154]. Figure 5.2 illustrates the variation of the ignition delay with brake power for diesel and all Carbodiesels. It can be observed that, the ignition delay decreases with an increase in the brake power. This is because of as the load increases the heat prevailing inside the cylinder increases, and helps the fuel air mixture to ignite sooner. This trend is generally reported in almost all the cases [155, 156]. At full load, the effect of Carbodiesels on the cylinder gas temperature is more as a result of longer ignition delay than that of diesel fuel in the entire engine operation. This may be due to their higher viscosity fuel affects atomisation and vapourisation which is affects the mixing of fuel with air, and poor spray formation for all Carbodiesels than that of diesel, which increase the ignition delay. The ignition delay for diesel, Carbodiesel5, Carbodiesel10, Carbodiesel15 and Carbodiesel20 at full load is by about 9.31^{o}CA, 10.3^{o}CA, 10.4^{o}CA, 10.5^{o}CA and 10.6^{o}CA respectively, because all the Carbodiesels have a lower cetane number and higher viscosity in comparison with diesel.

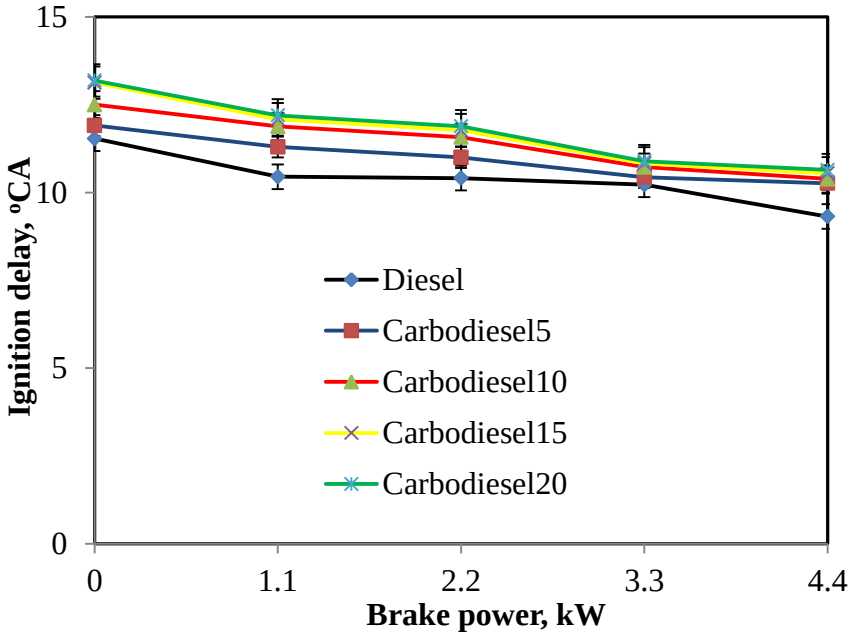

Figure 5.2 Variation of ignition delay with brake power

5.1.2.3 Heat release rate with crank angle

Figure 5.3 depicts the variation of the heat release rate with the crank angle for different Carbodiesels and diesel at full load. The heat release rate depends on the start of combustion, ignition delay and the fuel burned in the premixed mode, and differences in the combustion rates of fuels [45]. The fuel doses not ignite immediately upon injection into the combustion chamber. First droplet of fuel hits the hot air in the combustion chamber and the time starts through the actual burning phase. Fuel is taken heat by the hot air due to this reason heat release rate showing negative. It can be observed from the figure, that the maximum heat release rate is found to be lower for all the Carbodiesels compared to that of diesel at full load. The higher maximum heat release rate for diesel is attributed to its better mixture formation and higher heating value. This reason is in good agreement with Mani et al., [157] for the results they reported by conducting investiations in a DI diesel engine run on waste plastic oil. The reason for the lower maximum heat release for Carbodiesels is attributed to a longer ignition delay and high density. Similar reasons were reported by Elango and Senthil for the Jatropha blends that were used as fuels in a unmodified DI diesel engine [158]. It can also be noticed that the maximum heat release that occurs for diesel is at 54.3 J/^{o}CA. The occurrences of the maximum heat release rate for Carbodiesel5, Carbodiesel10, Carbodiesel15 and Carbodiesel20 are found at about 50.6, 49.6, 49.2 and 48.7 J/^{o}CA respectively, at full load. At full load, the maximum heat release rate is lower by about 0.7 J/^{o}CA, 1.7 J/^{o}CA, 2.2 J/^{o}CA and 2.7 J/^{o}CA for the Carbodiesel5, Carbodiesel10,

Carbodiesel15 and Carbodiesel20 than that of diesel. The CB blends are having lower heating value, higher density and lower cetane number due to this reason shows lower heat release rate.

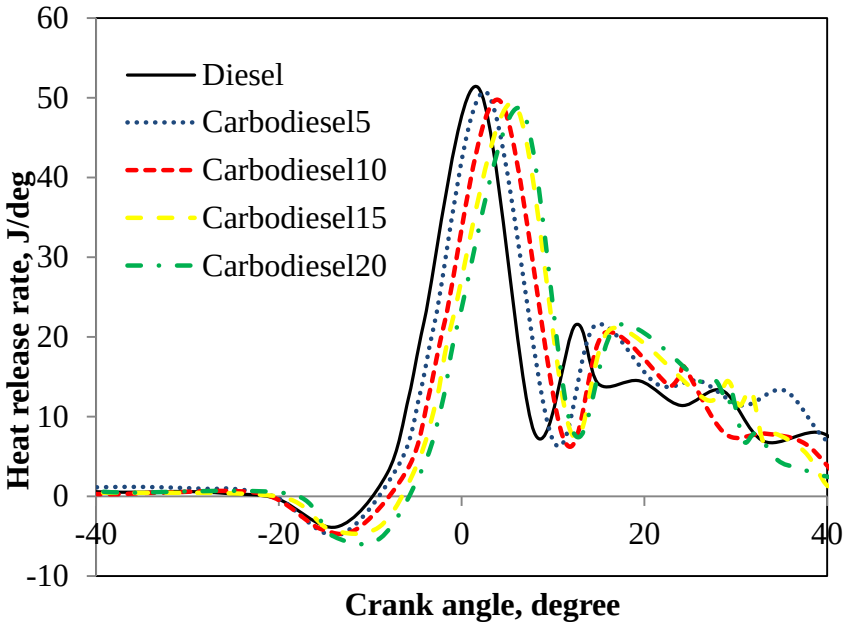

Figure 5.3 Variation of the heat release rate with crank angle at full load

5.1.2.4 Combustion duration

Figure 5.4 depicts the variation of the combustion duration with respect to different brake power of the engine. Combustion duration is the time between start of combustion to end of combustion.

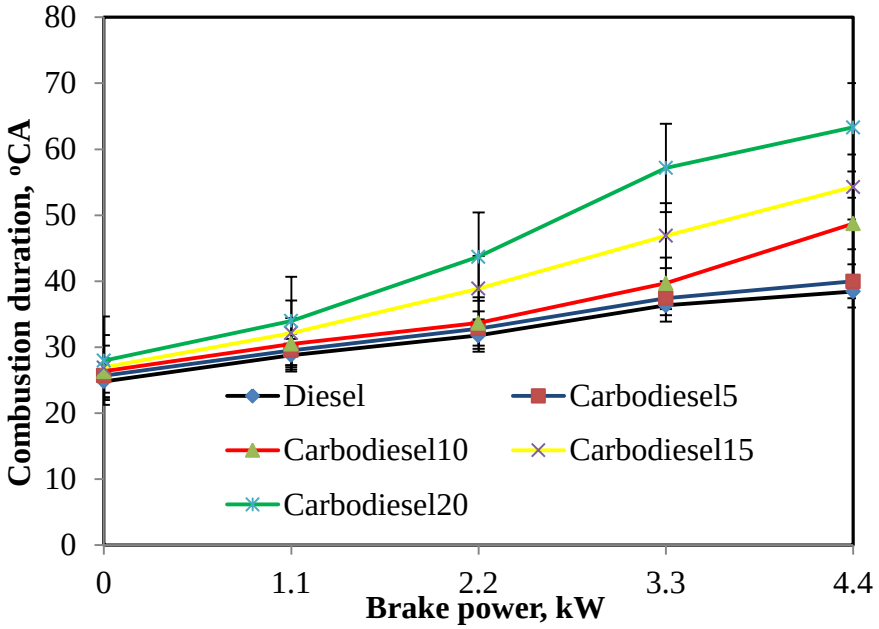

Figure 5.4 Variation of the combustion duration with brake power

From the heat release rate curve, the crank angle at which there is sudden rise in the heat release was taken as the start of combustion. End of combustion was determined from the cumulative heat release rate curve [45]. It can be observed from the figure, that the combustion duration increases with an increase in the brake power for all the Carbodiesels and diesel, which may be due to increase in the quantity of fuel injected. The values of the combustion duration of diesel, Carbodiesel5, Carbodiesel10, Carbodiesel15 and Carbodiesel20 are found to be about 38.4^{o}CA, 39.9^{o}CA, 48.7^{o}CA, 54.2^{o}CA and 63.3^{o}CA respectively at full load. Increasing the CB percentage in Carbodiesels, results in a longer combustion duration. Because, CB is a solid fuel which will take more time for the combustion. This may be due to slow combustion as a result of longer combustion duration. Similar reason was corroborated by Subramanian [159], when they conducted experiments in a single cylinder, four stroke, DI diesel engine. This is also evident from the exhaust gas temperature data, which will be discussed in Section 5.1.3.3.

5.1.2.5 Combustion efficiency

The variation of the combustion efficiency with brake power for diesel and different carbodiesels is portrayed in Figure 5.5. The combustion efficiencies are determined on the basis of energy left through unburned combustible products. These combustible products left in the exhaust gas i.e., CO, unburned hydrocarbon and particulate. The higher amounts of these products reflect combustion efficiency. The combustion efficiency (η_c) can be calculated using equation given below [160].

$$\eta_c = \left(1 - \frac{\sum X_i Q_{cvi}}{\left[\frac{m_f}{m_a + m_f} \right] Q_{cvf}} \right) \times 100 \qquad (5.1)$$

Where: η_c = Combustion efficiency, X_i = mass fractions of CO,
Q_{cvi} = lower heating values of CO
m_a and m_f = mass of air and mass of fuel, Q_{cvf} = lower heating values of fuel

It can be observed that, the combustion efficiency increases with the increase in the brake power. The combustion efficiency of diesel is the highest which is due to the better air fuel mixing and higher calorific value. The combustion efficiency for diesel is more than 99% because the diesel fuel gives more completes combustion in the combustion chamber. The

combustion efficiency for the Carbodiesel5, Carbodiesel10, Carbodiesel15 and Carbodiesel20 at maximum brake power is found by about 93%, 90.5%, 90% and 86.6% respectively, which is due to the inferior combustion and presence of CB particle in these fuels.

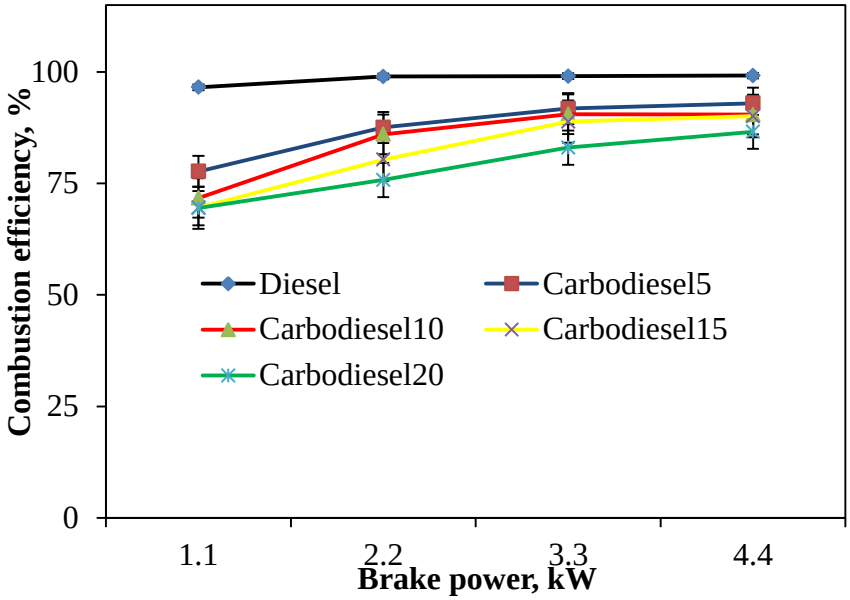

Figure 5.5 Variation of the combustion efficiency with brake power

5.1.2.6 Mass fraction burned

Mass fraction burned in each individual engine cycle is a normalized quantity with a scale of 0 to 1, describing the process of chemical energy release as a function of crank angle [161]. Figure 5.6 portrays the variation of mass fraction burned with the crank angle for diesel and Carbodiesels at full load. The mass fraction burned of Carbodiesel5, Carbodiesel10, Carbodiesel15 and Carbodiesel20 exhibit similar trend of diesel. It can also be observed from the figure, that the 10% mass fraction burned for all the Carbodiesels fuel seems to be earlier than that of diesel at full load. The 10% and 50% mass fraction burned vary with a minimum difference of 1.5^{o}CA to a maximum of 3^{o}CA for all Carbodiesels from that of diesel. The crank angles at which the 90% mass fraction burned vary with a minimum difference of 1^{o}CA to a maximum of 2^{o}CA, than that of diesel at full load. For the same crank angle values, the mass fraction burned of Carbodiesel5, Carbodiesel10, Carbodiesel15 and Carbodiesel20 fuels, are marginally higher than that of diesel at full load. This may be due presence of CB particles in all Carbodiesel fuel. Based on the experimental results and diesel replacement with CB, the optimum blend is found to be CB-10. This CB-10 blend combustion efficiency little bit lower compared to CB-5. But, on the basis on fuel replacement I have choosen CB-10 blend is further used as fuel throughout the investigations.

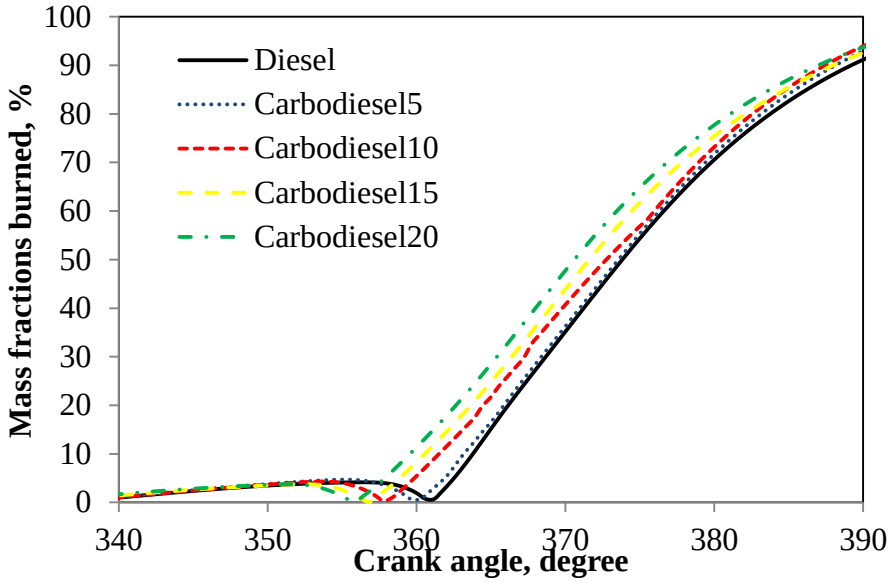

Figure 5.6 Variation of mass fractions burned with crank angle

5.1.2.7 Maximum heat release rate

In a CI engine the maximum heat release rate depends on the fuel burning rate during the premixed burning phase, which in turn leads to better combustion and heat release rate [45]. The variation of the maximum heat release rate with brake power for diesel and tested Carbodiesels is portrayed in Figure 5.7.

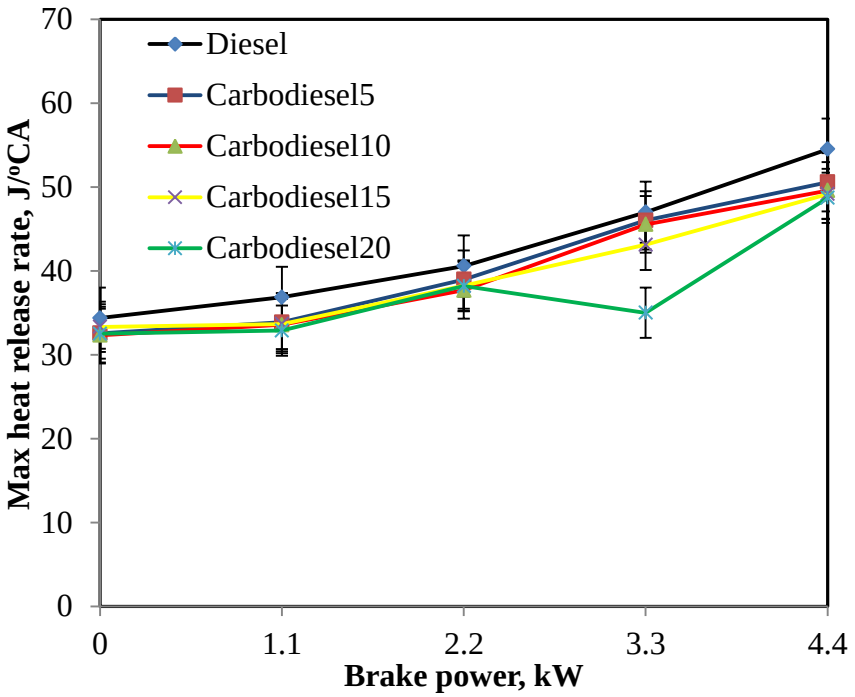

Figure 5.7 Variation of maximum heat release rate with brake power

It can be observed from the figure, that the maximum heat release rate increases with increase in the load of the engine. The maximum heat release rate for diesel is found to be 54.5 J/deg.

at the full load. Similarly, the maximum heat release rates are found to be about 50.6, 49.6, 49.2 and 48.7 J/deg. for Carbodiesel5, Carbodiesel10, Carbodiesel15 and Carbodiesel20 respectively, at the full load. The maximum heat release rate of all the Carbodiesels are marginally lower than that diesel at full load. This may be due the higher density and viscosity of the Carbodiesels that results in poor combustion in the combustion process compared to that of diesel operation. This may also be due to the high specific gravity and relatively poor mixing, which leads to a longer ignition delay and hence, a lower heat release rate. Similar results were projected by Prabhakar for Pongamia methyl ester fuelled in DI diesel engine [162].

5.1.2.8 Maximum rate of pressure rise

The engine noise increases linearly with an increase in the amount of premixed combustion and the maximum rate of pressure rise, regardless of the kind of fuel. Therefore, the maximum rate pressure rise and the amount of premixed combustion are considered to be critical factors for controlling the engine noise [163].

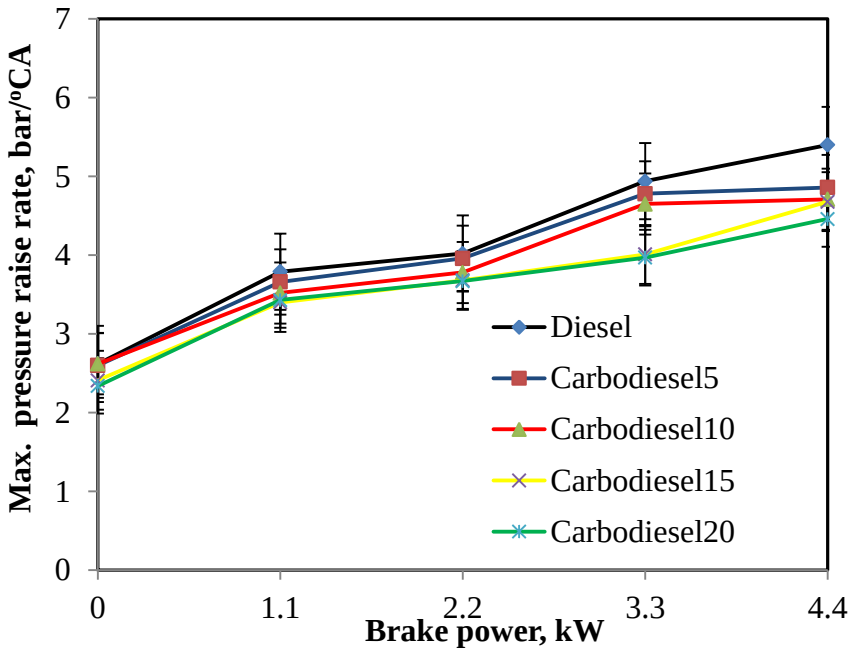

Figure 5.8 Variation of maximum rate of pressure rise with brake power

Figure 5.8 depicts the variation of the maximum rate of pressure rise with the engine brake power for diesel and different Carbodiesels. It can be observed from the figure, that the maximum rate of pressure rise increases with increases the brake power. The rate of pressure rise is the first derivative of cylinder pressure that relates to the smoothness of the engine operation. The maximum rate of pressure rise for diesel is found to be 5.34 bar/ ^{o}CA at full

load. The maximum rate of pressure rise for Carbodiesel5, Carbodiesel10, Carbodiesel15 and Carbodiesel20 are found to be 4.9, 4.7, 4.68 and 4.5 bar/ ^{o}CA respectively, at the full load. The maximum rate of pressure rise for diesel is the highest compared to those of all the Carbodiesel fuel, because better combustion of diesel in combustion chamber. The rate of pressure rise for all Carbodiesels are found to be within the limits (ie.7 bar/ ^{o}CA) which is prescribed for the rate of pressure rise for a single cylinder, four stroke DI diesel engine [164].

5.1.3 Performance analysis

5.1.3.1 Brake thermal efficiency

The variation of the brake thermal efficiency with brake power for the all Carbodiesels and diesel is illustrated in Fig. 5.9.

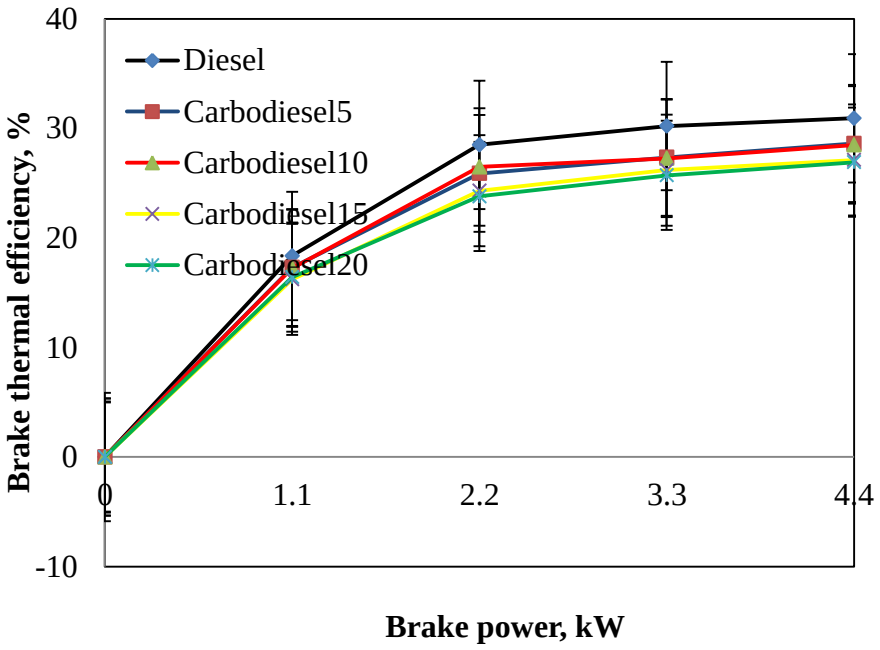

Figure 5.9 Variation of the brake thermal efficiency with brake power

It can be observed from the figure, that the brake thermal efficiency of all the tested fuel increases with increase in brake power. The brake thermal efficiency for diesel is found to be highest in this study. Because diesel has a higher calorific value and proper air-fuel mixing that results in more complete combustion. It can be also observed from the figure, that Carbodiesel5 and Carbodiesel10 exhibit higher brake thermal efficiencies at full load, compared to that of Carbodiesel15 and Carbodiesel20. This is because of the additional lubricity offered by the fuel, as a result of marginally higher viscosity and sulphur present in them. For Carbodiesel15 and Carbodiesel20, the thermal efficiency is found to be lower than

that of Carbodiesel5 and Carbodiesel10, because of the higher density, lower calorific compared to that of diesel, at full load. Similar reasons were documented by Nazzal [165] for vegetable oil when it was tested as an alternative fuel in a DI diesel engine. The value of the brake thermal efficiency for diesel is found to be about 30.9% at the full load respectively. Similarly, the values of the brake thermal efficiency for Carbodiesel5, Carbodiesel10, Carbodiesel15, and Carbodiesel20 are recorded as 28.6%, 28.5%, 27.1%, and 26.9% respectively, at full load.

5.1.3.2 Brake specific energy consumption (BSEC)

The variation of the BSEC with the brake power is portrayed in Figure 5.10. It can be observed from the figure the BSEC same trend is followed for diesel and all Carbodiesel tested fuel. The BSEC of Carbodiesel5, Carbodiesel10, Carbodiesel15 and Carbodiesel20 are found to be higher than that of diesel at all loads. The higher density and lower calorific value are the reasons for the higher BSEC. Similar results are reported by Altun et al., [166] for the results they obtained with sesame oil-diesel mixture fuelled in DI diesel engine. The BSEC of diesel is found to be the lowest, which is about 10.8 MJ/kWh. Similarly, the values of brake specific energy consumption for Carbodiesl5, Carbodiesl10, Carbodiesel15 and Carbodiesel20 are found to be about 11.3, 11.7, 13.5, 14.0 and 14.3 MJ/kWh, respectively, at full load.

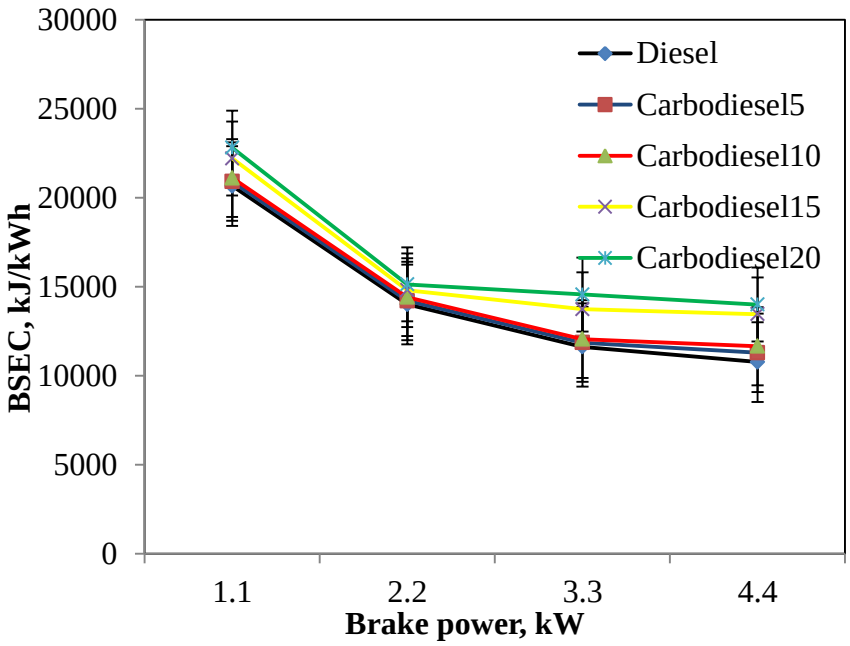

Figure 5.10 Variation of the BSEC with brake power

5.1.3.3 Exhaust gas temperature

Figure 5.11 illustrates the variation of the exhaust gas temperature for all Carbodiesels and diesel, with respect to the brake power. The exhaust gas temperature gives an indication about the amount of heat kept with the exhaust gases [167]. It can be observed from the figure that with the increase in the brake power, the exhaust gas temperature increases for diesel. It is a common reason stated by most of the researchers for example [168-170]. All the tested Carbodiesel fuels follow similar trend. The exhaust gas temperature value for diesel at full load is found to be 327^{o}C. It can also be observed that, the values of exhaust gas temperature are found to be about 341^{o}C, 366^{o}C, 401^{o}C, and 410^{o}C for Carbodiesel5, Carbodiesel10, Carbodiesel15 and Carbodiesel20 respectively at full load. The exhaust gas temperatures for all Carbodiesels are found to be higher than that of diesel in the entire engine operation. This may be due to the increased combustion duration as a results of slow combustion of all Carbodiesels.

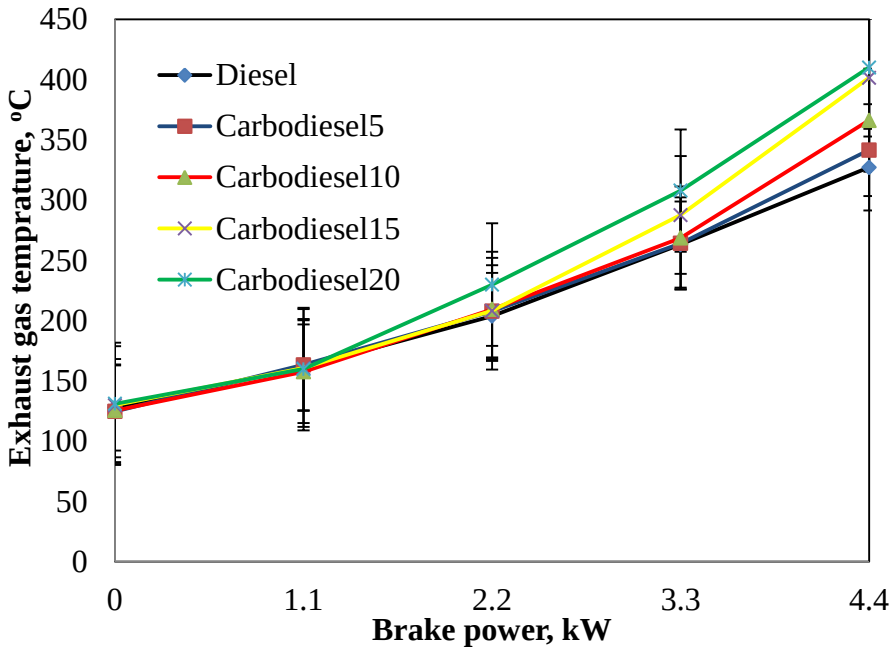

Figure 5.11 Variation of exhaust gas temperature with brake power

5.1.4 Emission analysis

5.1.4.1 Carbon monoxide (CO) emission

The CO emission is due to the incomplete combustion of fuel air mixture in the combustion chamber because of insufficient amount of air in the air-fuel mixture or insufficient time in the cycle for the completion of combustion. Generally, the compression ignition engines give low CO emissions as they operate with a lean mixture. The CO emission in a CI engine is

quite negligible compared to that of SI engines, as the former is operated with excess air [171]. The variation of the CO emission with brake power for all Carbodiesels and diesel is depicted in Figure 5.12. It can be observed from the figure that, the CO emission is found to be the highest for Carbodiesel20, compared to that of Carbodiesel5, Carbodiesel10, Carbodiesel15 and diesel, respectively at full load. This may be due to lack of oxygen. Similar, reason was indicated by Xue et al., [172] in their study when they conducted experiments with biodiesel in a single cylinder, four stroke, air cooled, DI diesel engine run at a constant speed. The CO emissions of CB blends are more compared to diesel, but CO emissions depend on the complete combustion and availability of oxygen for the combustion process. Due to poor mixture formation and incomplete combustion CB blends given more CO emission compared to diesel. They do not have time to undergo combustion, and have higher CO emissions than that of diesel at full load. For the given power output, the concentration of the CO emission is found to be about 0.006 g/kWh for Carbodiesel5, 0.0081 g/kWh for Carbodiesel10, 0.0094 g/kWh for Carbodiesel15 and 0.011 g/kWh for Carbodiesel20 at full load, whereas it is 0.006 g/ kWh for diesel, at full load.

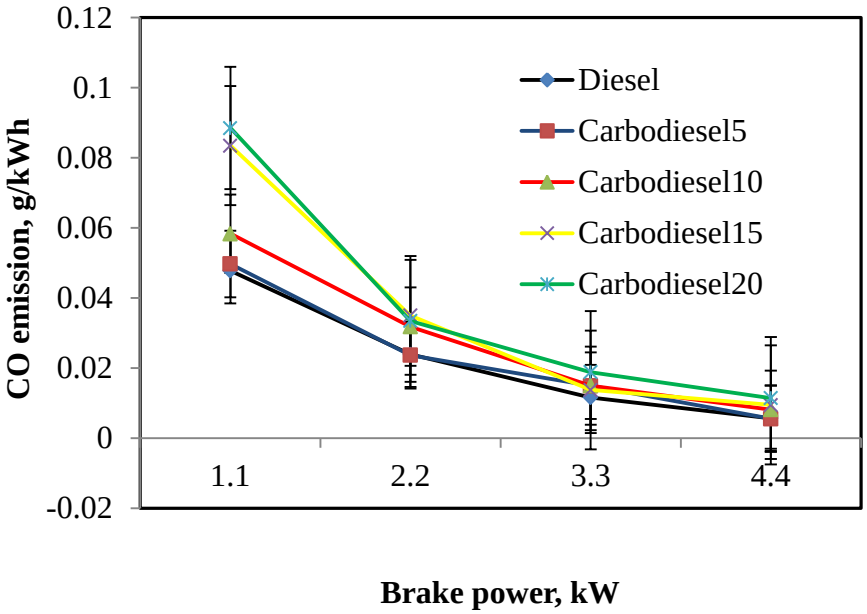

Figure 5.12 Variation of the CO emission with brake power

5.1.4.2 Hydrocarbon (HC) emission

The unburnt hydrocarbon emission is the direct result of incomplete combustion, due to the incomplete mixing of the air and fuel [106]. The variation of the hydrocarbon (HC) emission for the Carbodiesels and diesel are portrayed in Figure 5.13. It can be observed from the

figure that the HC emission for Carbodiesel20 is found to be the highest followed by Carbodiesel15, Carbodiesel10, Carbodiesel5 and diesel at full load. The higher the HC emission is due to the poor atomisation of high density fuel that results in incomplete combustion. The HC emission for Carbodiesel5 is lower than that of the other Carbodiesels, but marginally higher than that of diesel at full load. For diesel fuel, the HC emission is found to be about 0.026 g/kWh at full load. The values of HC emission for Carbodiesel5, Carbodiesel10, Carbodiesel15 and Carbodiesel20 are found to be 0.031 g/kWh, 0.032 g/kWh, 0.034 g/kWh and 0.037 g/kWh at respectively full load.

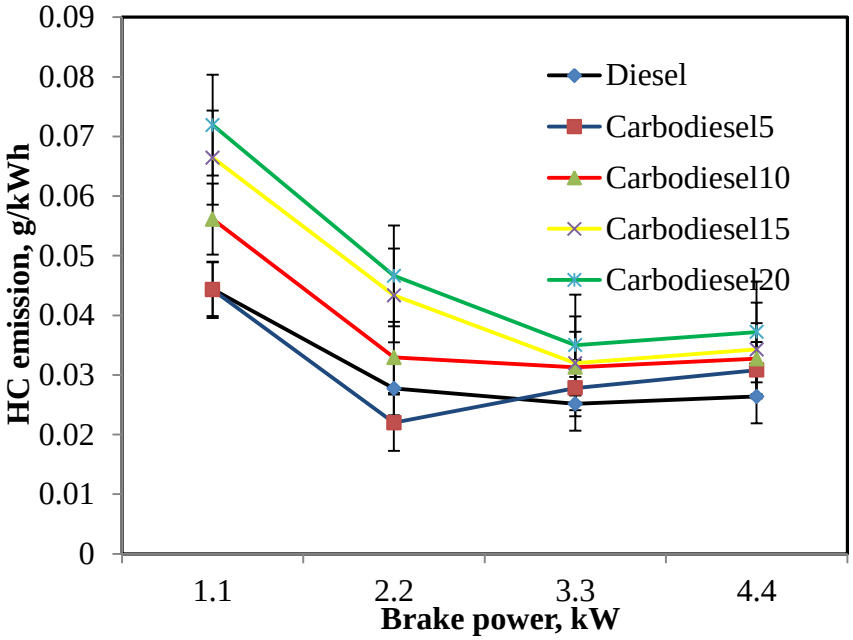

Figure 5.13 Variation of the HC emission with brake power

5.1.4.3 Nitric oxide (NO) emission

Two important parameters predominantly affect the formation of the NO emission in a CI engine. One is stoichiometry and the other one is in-cylinder temperature. The in-cylinder temperature has a strong effect on the formation of the NO emission. If the combustion temperature is higher, then higher NO emission is formed [36, 45]. Figure 5.14 portrays the variation of nitric oxide (NO) emission with respect to brake power for the Carbodiesels and diesel. It can be observed from the figure that, as the brake power increases the NO emission decreases for a given output power for all fuels, as expected. It can also be observed that all Carbodiesel shows lower value than that of diesel at a full load. This is probably due to the lower heat released as a result of poor combustion. This is also evidenced from the heat release rate graph. The value of the NO emission is found to be about 4.2g/kWh at full load for diesel. It can also be observed that the value for Carbodiesel5 is found to be about 4.1

g/kWh at full load, while it is 3.9 g/kWh for Carbodiesel10, 3.8 g/kWh for Carbodiesel15 and 3.70 g/kWh for Carbodiesel20 respectively, at full load. The in-cylinder temperature has a strong effect on the formation of the NO emission. If the combustion temperature is higher, then higher NO emission is formed [36, 45]. Due to lower heat release rate and lower in-cylinder temperature CB blends show lower NO emission compared to Diesel.

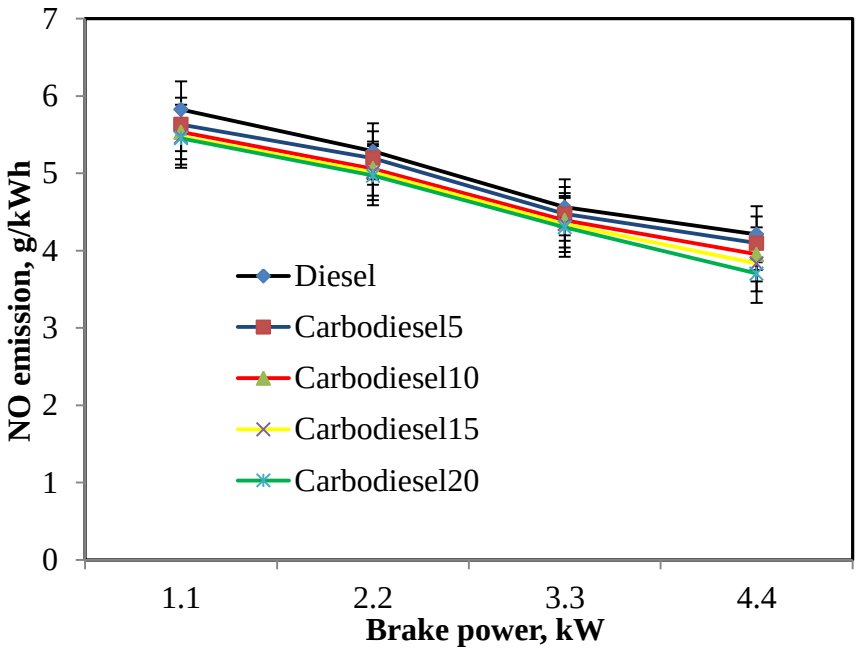

Figure 5.14 Variation of the NO emission with brake power

5.1.4.4 Smoke emission

The variation of the smoke emission with brake power for Carbodiesels and diesel is shown in Figure 5.15. Smoke is nothing but solid soot particles suspended in the exhaust gas [45]. It can be observed from the figure that, the smoke emission increases with increase in the blend percentage of Carbodiesel. The smoke emission is found to be the lowest for diesel, as a result of better air-fuel mixing and combustion. Among all the Carbodiesel fuels, Carbodiesel20 shows the highest smoke value, followed by Carbodiesel15, Carbodiesel10 and Carbodiesel5, at full load. The smoke emission for diesel at full load is found to be 61% respectively, at full load. Similarly, the smoke emission value of Carbodiesel5 at full load is found to be 66.5%, Carbodiesel10 shows about 68% at full load, while Carbodiesel15 shows the value as 70% at full load. The value of Carbodiesel20 at full load is noticed as 73%. Higher smoke values may be attributed to the unburned and partially reacted hydrocarbons as well as higher density carbon black particles present in all the Carbodiesels used as a fuel in this study. The higher carbon-to-hydrogen ratio of Carbodiesel may also be the reason for the higher smoke emission compared to that of diesel. Similar reasons were reported by

Banapurmath et al., when they carried out an investigation with honge, jatropha and sesame oil methyl esters as alternative fuel in a CI engine [173].

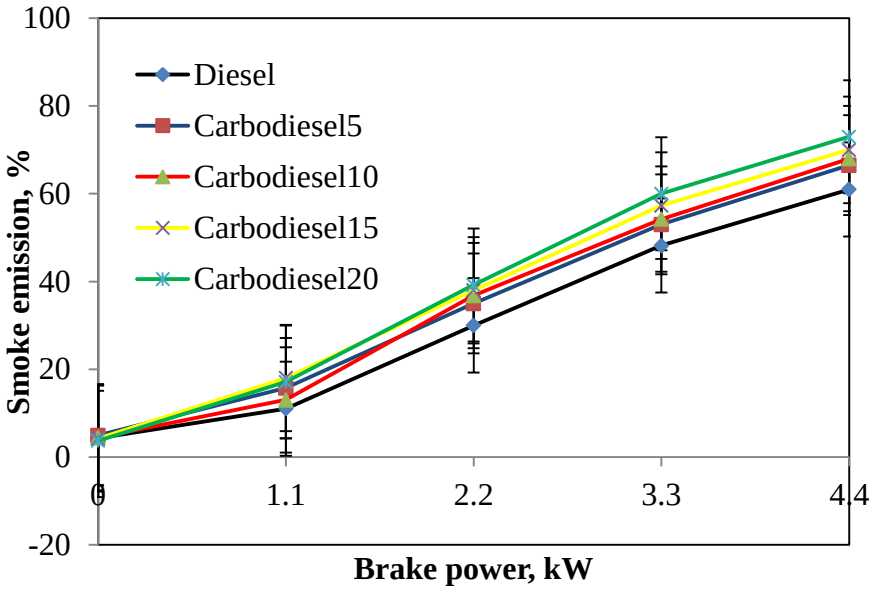

Figure 5.15 Variation of the smoke emission with brake power

5.1.5 Summary

From the results of the investigation, it is summarised that the engine can run Carbodiesels successfully without any engine modification. The engine was able to run with a maximum blend ratio of 20% of CB in Carbodiesel. The use of different percentage of Carbodiesels in a diesel engine has shown that, the engine can perform with marginally lower brake thermal efficiency than that of diesel, because of the higher density and lower calorific value. From the analysis of the combustion, performance and emission of the engine run on four Carbodiesels viz., Carbodiesel5, Carbodiesel10, Carbodiesel15 and Carbodiesel20 among of Carbodiesel10 gave a better performance and lower emissions than those of other Carbodiesels. A maximum 10% of diesel can be replaced by Carbodiesel10, when it is used as a fuel in the diesel engine. Table 5.1.1 provides the values of important engine parameters obtained for different Carbodiesels and diesel at full load.

Table 5.1.1 Values on combustion, performance and emission parameters at full load for different Carbodiesls

S.No.	Parameters	Diesel	Carbodiesel5	Carbodiesel10	Carbodiesel15	Carbodiesel20
Combustion parameters						
1	Maximum cylinder pressure, (bar)	79.4	78.2	76.4	73.8	71.7
2	Ignition delay, (^{o}CA)	9.31	10.26	10.38	10.54	10.64
3	Max. heat release rate, (J/^{o}CA)	54.52	50.6	49.6	49.18	48.73
4	Combustion duration, (^{o}CA)	38.46	39.98	48.73	54.29	63.3
5	Combustion efficiency, (%)	99	93	90.5	90	86.6
6	Maximum rate of pressure rise, (bar/^{o}CA)	5.4	4.86	4.71	4.61	4.46
7	90% Mass fraction burned, (^{o}CA)	389.47	388.36	387.69	387.2	386.42
Performance parameters						
1	Brake thermal efficiency, (%)	30.92	28.6	28.46	27.1	26.9
2	Brake specific energy consumption, (kJ/kWh)	10772.3	11294.79	11658.11	13460.36	13997.74
3	Exhaust gas temperature, (^{o}C)	327.19	341.5	366.28	401.63	410.08
Emission Parameters						
1	CO emission, (g/kWh)	0.006	0.006	0.0081	0.0094	0.011
2	HC emission, (g/kWh)	0.026	0.031	0.033	0.034	0.037
3	NO emission, (g/kWh)	4.21	4.09	3.95	3.83	3.70
4	Smoke emission, (%)	61	66.5	68	70	73

5.2 Optimisation of injection timing of Carbodiesel10

5.2.1 General

From the previous study, it is understood that the engine was able to run with the Carbodiesels. Carbodiese10 gave better results in terms of the combustion, performance and emissions compared to those of other Carbodiesels and 10% fuel replacement. Therefore, considering Carbodiesel10 as optimum slurry, further investigations were carried out to study the effect of varying the injection timing of the engine, when the engine was run with Carbodiesel10. The results of the combustion, performance and emission parameters of engine fuelled with the Carbodiesel10 at different injection timings are analysed, compared with those of diesel fuel and presented in this section. The standard injection timing of the engine is 23^{o}CA bTDC. The injection timing of the engine was set at two advance crank angles 26^{o}CA bTDC and 24.5^{o}CA bTDC and two retarded injection timings 21.5^{o}CA bTDC and 20 ^{o}CA bTDC.

5.2.2 Combustion parameters

5.2.2.1 Cylinder pressure with crank angle

The cylinder pressure data is the most effective tool to predict engine combustion behaviour [174]. Figure 5.16 depicts the variation of cylinder pressure with the crank angle for Carbodiesel10 at different injection timings and diesel. Carbodiesel10 at original injection timing indicates a lower maximum cylinder pressure as a result of higher density and poor volatility in comparison with diesel at full load. The peak cylinder pressure increases for the advanced injection timing and decreases for the retarded injection timing at a given full load. With the advanced injection timing, more fuel is accumulated in the combustion chamber and hence a higher maximum pressure is attained, than that of original injection timing. Similar trend is reported by Agarwal et al., when they operated the engine with diesel fuel at different injection timings [123]. With the advanced injection timings of 26°CA bTDC and 24.5°CA bTDC, the Carbodiesel10 operation exhibits a higher cylinder pressure of 85.4 bar at 368.6°CA, and 80.6 bar at 368.9°CA respectively, which are earlier than that of the original injection timing 23°CA bTDC. It can also be observed that, the cylinder pressure of diesel is higher than that of Carbodiesel10 for the original injection timing of 23°CA bTDC, and retarded injection timings of 21.5°CA and 20°CA bTDC. The value of the cylinder pressure for diesel is found to be about 80 bar at 369.5°CA and the Carbodiesel10 for the original injection timing of 23°CA bTDC, and for retarded injection timings of 21.5°CA and 20°CA

bTDC are found to be about 78.2 bar, and 68.5 bar, 65.0 bar respectively at full load, which occur at 370.5°CA and 374.1°CA, 373.1°CA respectively, at full load.

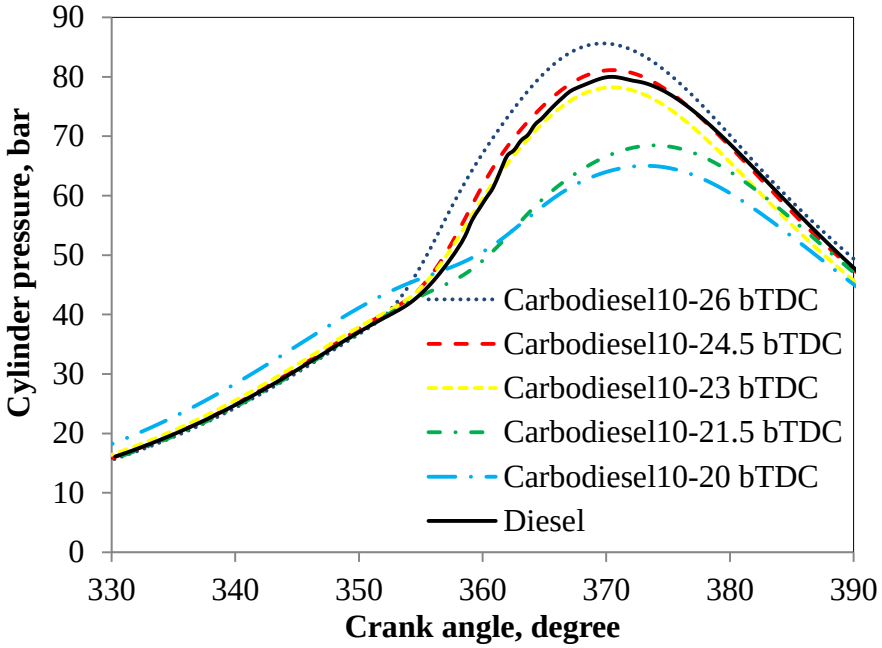

Figure 5.16 Variation of pressure with crank angle at full load

When injection timing is retarded for Carbodiesel10, amount of fuel accumulated is lesser the delay period and hence results in lower cylinder peak pressure. Similar results were reported by Mani and Nagarajan for the results obtained from the waste plastic oil fuelled in single cylinder, four stroke, DI diesel engine operated with different injection timings [121].

5.2.2.2 Ignition delay

Figure 5.17 illustrates the variation of the ignition delays with brake power for diesel and Carbodiesel10 at different timings. It is apparent from the figure that, the ignition delay decreases with the increase in the brake power for Carbodiesel10 at original, advanced and retarded injection timings and diesel. It can also be observed that at full load the ignition delay is reduced, and combustion is dominated by the cylinder temperature. At full load, the value of ignition delay for diesel is approximately 10°CA at original injection timing. The delay for diesel is shorter than that of the original injection timing of Carbodiesel10 which is due to its higher cetane number. At low loads with longer delay periods, more fuel is accumulated in the premixed combustion. The ignition delay for Carbodiesel10 at the original injection timing, at full load is found to be about 10.4°CA and for the advanced injection timings of 26°CA bTDC and 24.5°CA bTDC the delays are found to be about 9.9°CA and 10.4°CA respectively. Similarly, for the retarded injection timings of, 21.5°CA bTDC and

20°CA bTDC the delays are found to be about 12.5°CA and 12.9°CA respectively, at full load. At advanced injection timings shorter ignition delay period this may be due to combustion is dominated by the cylinder pressure.

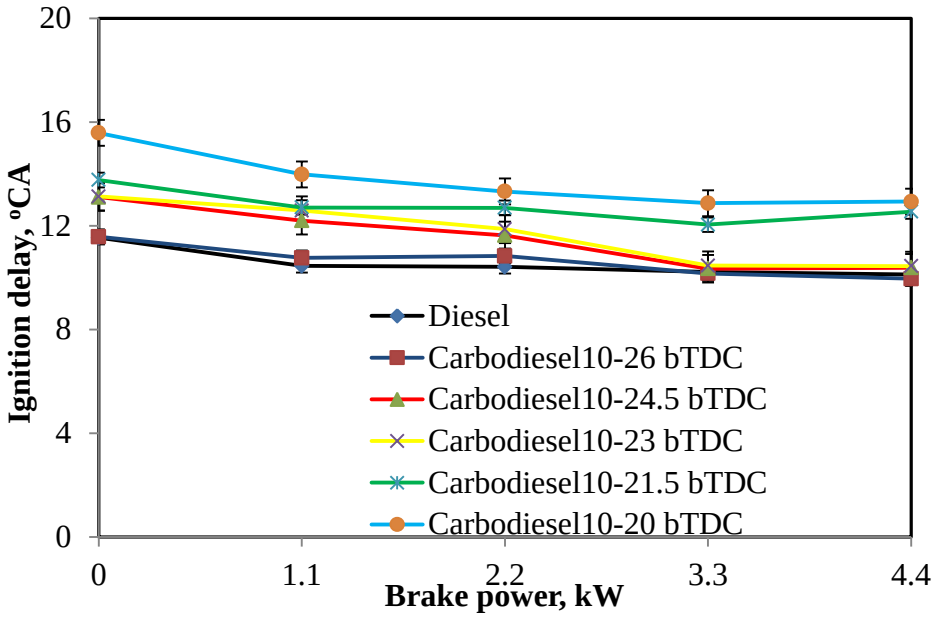

Figure 5.17 Variation of ignition delay with brake power

5.2.2.3 Heat release rate with crank angle

The trends of heat release rate with the crank angle for diesel and the Carbodiesel10 at the original injection timing, advanced injection timings, and retarded injection timings at full load, are portrayed in Figure 5.18. The heat release rate in a CI engine predominantly affected by ignition delay, density, adiabatic flame temperature and bulk modulus characteristics [175-177].

The rates of heat release at advanced injection timing for Carbodiesel10 are higher than those of the original and retarded injection timings and also from that of the diesel operation. The maximum heat release rate in the premixed combustion phase for the advance injection timing is higher than those of the original and retarded injection timings, which is due to more accumulation of fuel air mixture in the delay period. The heat release rate decreases, while retarding the injection timing. The maximum heat release rate occurs for diesel is higher than that of the Carbodiesel10 at original injection timing due to proper air fuel mixing. It can also be noticed that, the maximum heat release that with the original injection timing occurs at about 56.4 J/°CA at 363.6°CA. The maximum heat release rates for the advanced injection timings of 26°CA bTDC and 24.5°CA bTDC are found to be 56.9 J/°CA

at 360.9°CA, 56.0 J/°CA at 361.6°CA respectively. For the retarded injection timings of 21.5°CA bTDC and 20°CA bTDC, the values are found to be 55.6 J/°CA at 365.5°CA and 55.4 J/°CA at 366.1°CA respectively, at full load. Heat release rate between -10^0 CA to -25^0 CA are shown as lower in negative because fuel is taken heat through the hot air from the combustion chamber.

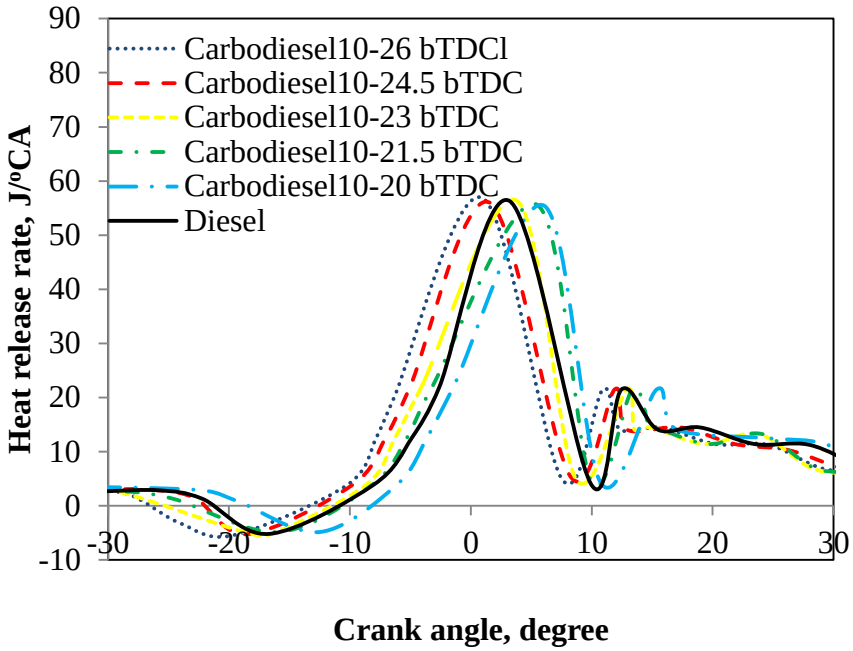

Figure 5.18 Variation of heat release rate with crank angle at full load

5.2.2.4 Combustion duration

Figure 5.19 portrays the variation of the combustion duration with the different brake power conditions of the engine run with Carbodiesel10 at different injection timings and diesel. Advancing and retarding injection timing from the original injection timing results in early and late combustion respectively. It can be observed from the figure, that the combustion duration increases with increase in the brake power for diesel and the Carbodiesel10 at all injection timings, which may be due to the increase in the quantity of fuel injected. The maximum heat release rate for Carbodiesel10 at advanced injection timing is higher compared to that of diesel and others injection timing. This may be due to early fuel injected and more fuel accumulated in the combustion chamber. The values of the combustion duration of carbodiesel10 at advanced injection timing at full load are found to be about 48.1°CA for 26°CAbTDC and 47.0°CA for 24.5°CAbTDC. Similarly, the combustion duration value at 23°CAbTDC, 21.5°CA bTDC and 20°CAbTDC are found to be about 46.2°CA, 45.7°CA and 43.4°CA respectively, at the full load.

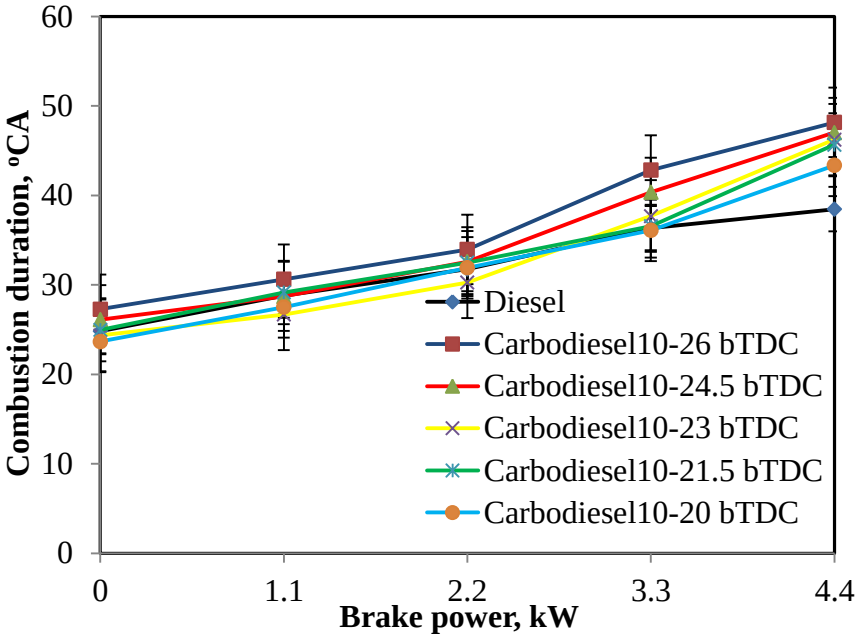

Figure 5.19 Variation of combustion duration with brake power

5.2.2.5 Maximum heat release rate

The variation of the maximum heat release rate with brake power for the diesel and different injection timing of Carbodiesel10 is presented in Figure 5.20.

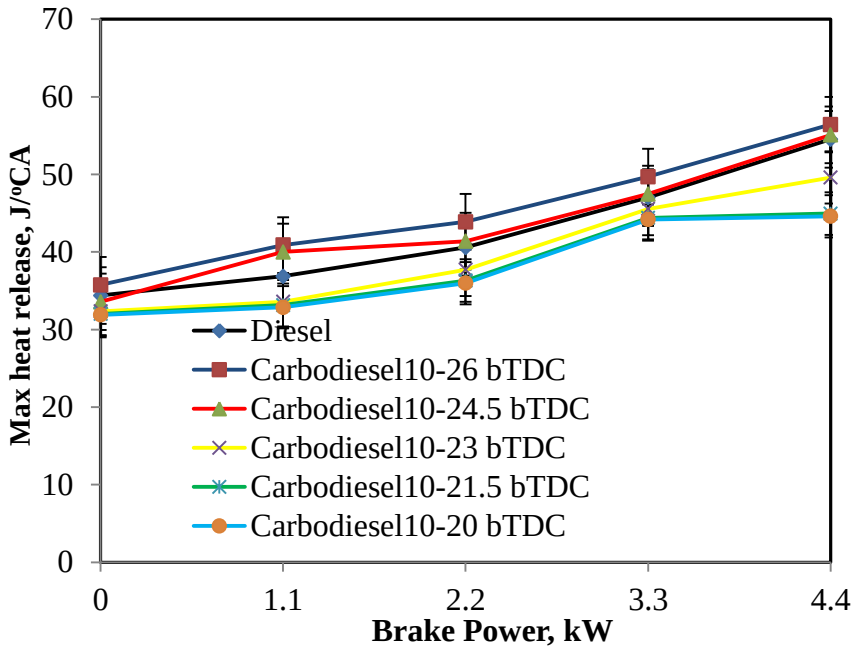

Figure 5.20 Variation of maximum heat release rate with brake power

It is apparent from the figure the maximum heat release rate increases with increase in the brake power. The maximum heat release rate for diesel is found to be 54.5 J/deg. at the full load. Similarly, the maximum heat release rates for Carbodiesel10 with different injection

timings at 26°CA bTDC, 24.5°CA bTDC, 23°CA bTDC, 21.5°CA bTDC and 20°CA bTDC are found to be 56.4 J/deg, 55.1 J/deg, 49.2 J/deg, 44.9 J/deg and 44.6 J/deg. The maximum heat release rate is higher at the advance injection timing compared to those of diesel and original injection timing of Carbodiesel10.

5.2.2.6 Maximum pressure rise rate

Figure 5.21 portrays the variation of the maximum rate of pressure rise with brake power for Carbodiesel10 with different injection timings and diesel. It can be observed from the figure, that the maximum rate of pressure rise increases with the increase in the brake power for the entire variable injection timings of Carbodiesel10. The maximum rate of pressure rise for diesel is found to be 5.4 bar/ °CA at the full load. It can also be observed the maximum rate of pressure rise for the Carbodiesel10 with the advance injection timing is higher than that of diesel. This may be due to, larger amount of fuel injected, thus higher pressure occurred before TDC. For the Carbodiesel10, the maximum rate of pressure rise at advance injection timing 26 °CAbTDC and 24.5°CAbTDC are found to be 5.8 bar/°CA and 5.46 bar/°CA and 23°CAbTDC original injection timing is 4.71 bar/°CA. For the retarded injection timing at 21.5 bTDC and 20 bTDC for the maximum rate of pressure rise are 3.51 bar/°CA and 3.3 bar/°CA. Retarded injection timing exhibits a lower rate of pressure rise due to may be poor air fuel mixing in combustion chamber [178] compared to that of original injection timing of Carbodiesel10.

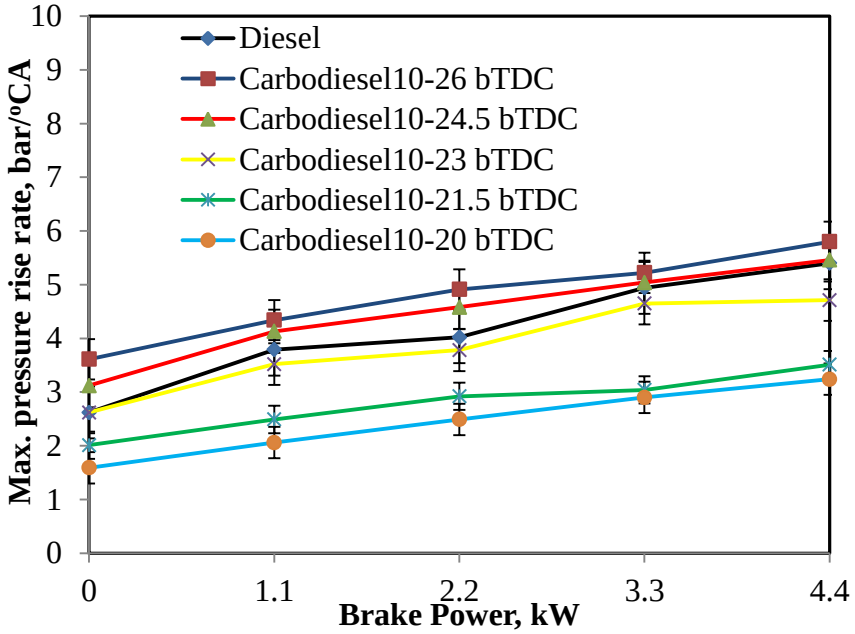

Figure 5.21 Variation of maximum pressure rise rate with brake power

5.2.3 Performance parameters

5.2.3.1 Brake thermal efficiency

The variation of the brake thermal efficiency with the brake power for Carbodiesel10 at different injection timings and diesel is shown in Figure 5.22.

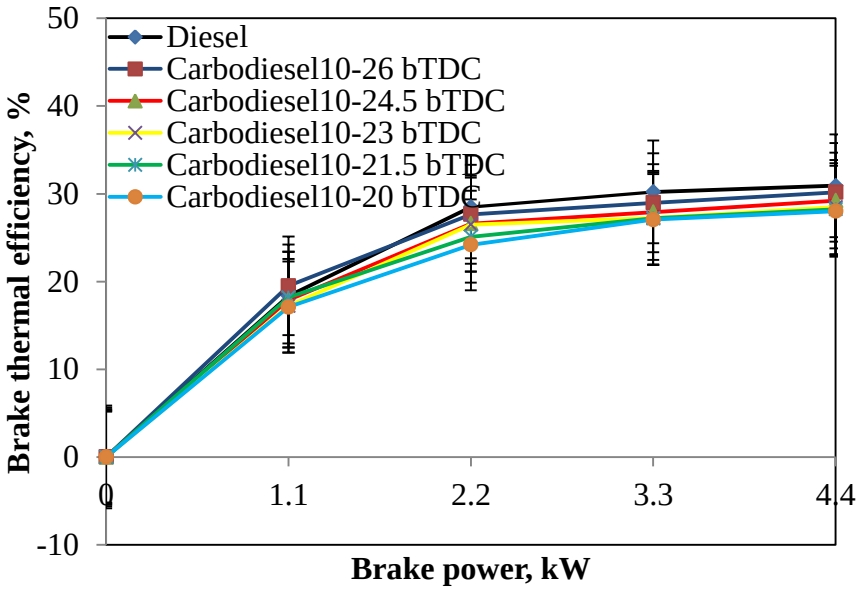

Figure 5.22 Variation of brake thermal efficiency with brake power

The brake thermal efficiency increases with the increase in the brake power for diesel and Carbodiesel10. The efficiency of Carbodiesel10 is lower by about 2.3% than that of diesel at original injection timing. This may be due to poor volatility and lower calorific value of Carbodiesel10. The increase in the brake thermal efficiency of Carbodiesel10 at the advanced injection timings is due to the high heat release rate in the premixed combustion phase. At this time, the peak pressure reaches closer to the TDC, which results in higher effective pressure to do more work. Also the earlier start of combustion in advanced injection timing reduces the time of vaporization of fuel. This is found to be in good agreement with the results documented by Kannan and Anand [179]. When the fuel injection is retarded to 21.5°CA bTDC and 20°CA bTDC, fuel injection starts later. As a result, less fuel takes part in effective combustion to produce power. Similar results were reported by Sathish and Mahalingam when they carried out an investigation with dual bio fuels with retarded injection timings [180]. The values of the brake thermal efficiency for diesel and Carbodiesel10 at 23°CA bTDC original injection timing are found to be about 30.9% and 28.4% respectively, at full load. Similarly, for the Carbodiesel10 at advanced injection timings of 26°CA bTDC and 24.5°CA bTDC the brake thermal efficiencies are found to be

about 30.1%, 29.2% and for the retarded injection timings 21.5°CA bTDC and 20°CA bTDC they are recorded as 28.2%, 28.0% respectively, at full load.

5.2.3.2 Brake specific energy consumption (BSEC)

Figure 5.23 portrays the variation of BSEC with brake power for diesel and Carbodiesel10 at different injection timings. It can be observed from the figure, that the BSEC decreases, as the brake power increases for all injection timings for Carbodiesel10 and diesel.

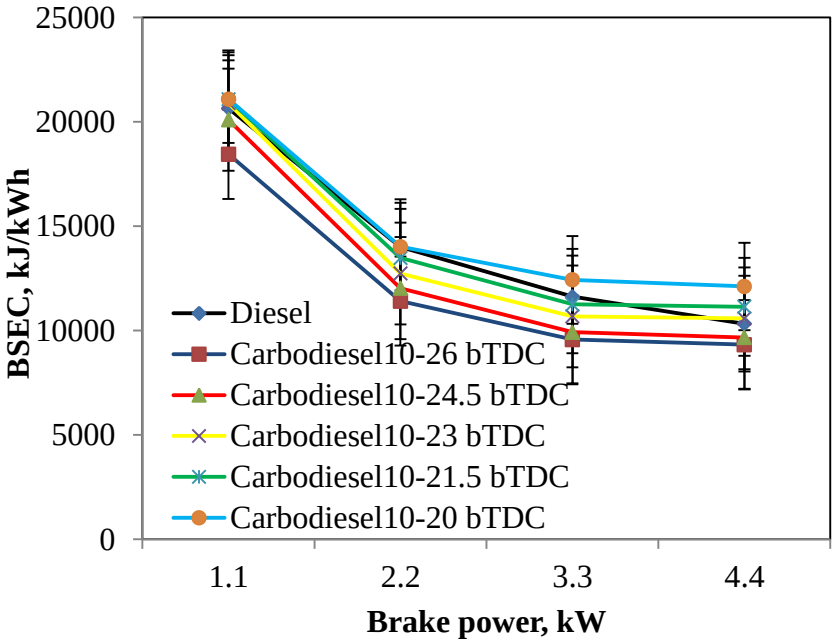

Figure 5.23 Variation of BSEC with brake power

At original injection timing the BSEC for Carbodiesel10 is increased by about 2.4% than that of diesel at the full load because due to its lower calorific value and higher density of Carbodiesel10. The BSEC is lower by about 11.9% and 9.5% at advancing injection timing of 26°CA bTDC and 24.5°CA bTDC respectively, while it is higher by about 9.7% and 12.6% with the retarded injection timing of 21.5°CA bTDC and 20 °CA bTDC respectively, compared to that of original injection timing at full load. When advancing the injection timing from 23^{o} bTDC to 26°CA bTDC and 24.5°CA bTDC, high heat release rates are prominently seen, that result in lesser BSEC. With the advanced injection timing, the ignition delay is shorter due to early commencement of ignition. As a result, minimum BSEC was obtained at advanced injection timings for Carbodiesel10. While retarding the injection timing combustion is incomplete that result in higher BSEC at a full load, than that of the original injection timing and diesel. Retarded injection timing means later combustion, and therefore the pressure rises only when the cylinder volume expands rapidly away from the

TDC, and results in a reduced effective pressure to do work. Similar reasons were explained by Bari et al., [138] when they carried out investigations with different injection timing in a DI diesel engine fuelled with waste cooking oil as an alternative fuel.

5.2.3.3 Exhaust gas temperature (EGT)

Figure 5.24 shows the variation of exhaust gas temperature with brake power for diesel and Carbodiesel10 at different injection timings. It can be observed from the figure that, the exhaust gas for diesel increases with the increase in the brake power. Same pattern is observed for the Carbodiesel10 at the original, advanced and retarded injection timing. It can also be observed, the exhaust gas temperature is higher for Carbodiesel10 at all the injection timing than that of diesel. The higher values of exhaust gas temperature may be due to slow combustion of Carbodiesel10 during the diffusion combustion stage.

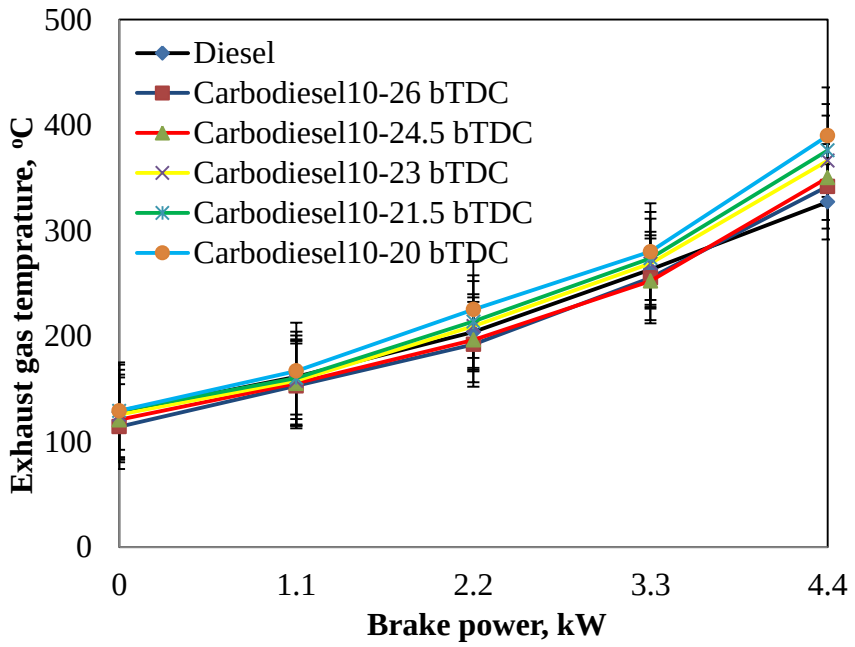

Figure 5.24 Variation of exhaust gas temperature with brake power

The exhaust gas temperature is found to be lower at advancing injection timing which is due to the occurrence of combustion earlier, and the burnt gas had more time to interact with cooling medium before exiting through exhaust valve. With the retarding the injection timing of Carbodiesel10, the exhaust gas temperature is found to increase as a result of partial burning of fuel mixture during the exhaust stroke [181]. The value of exhaust gas temperature for diesel is found to be about 327.2^{o}C at the full load. Similarly, the values of exhaust gas temperature for Carbodiesel10 are found to be about 342^{o}C, 350.3^{o}C, 366.2^{o}C, 376^{o}C and

390°C for 26°CA bTDC, 24.5°CA bTDC, 23°CA bTDC, 21.5°CA bTDC and 20°CA bTDC injection timing respectively, at the full load.

5.2.4 Emission parameters

5.2.4.1 CO emission

Figure 5.25 illustrates analysis of the CO emission of the test engine with brake power for diesel and Carbodiesel10 at different injection timings. The CO emission relates to the available fuel-air ratio, and it is a measure of the combustion efficiency [45]. The CO emission for diesel and Carbodiesel10 at all injection timings decreases with the increase in the brake power.

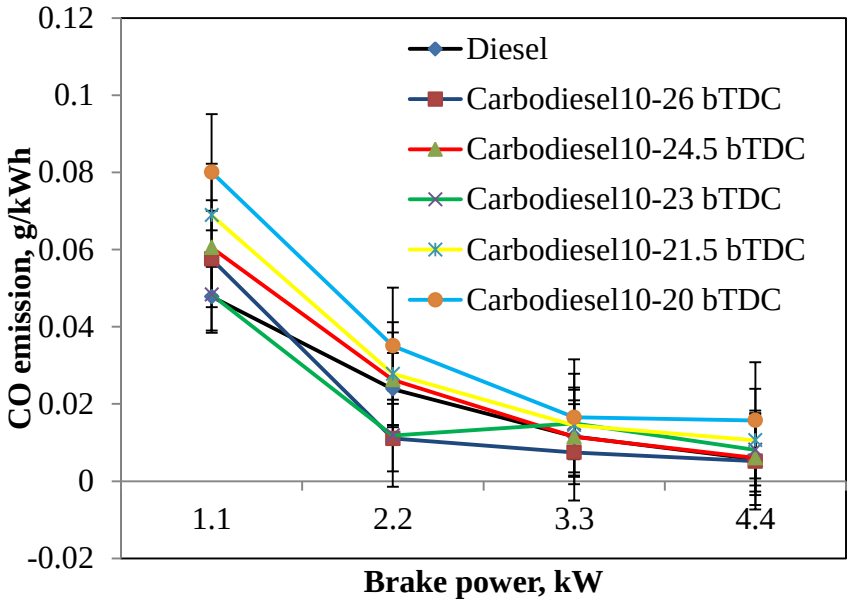

Figure 5.25 Variation of CO emission with brake power

As seen in Figure 5.25, at the original injection timing, the CO emission of Carbodiesel10 is higher by about 22% than that of diesel at full load. This is due to the longer ignition delay and poor mixture formation. It can also be observed that, the retarded injection timings give a higher CO emission than those of the original and advanced injection timings at full load. With the advanced injection timings, the CO emission is less, due to a higher cylinder temperature and increased oxidation between the carbon and oxygen molecules, and the conversion into carbon dioxide [45]. The CO emission found to be about 0.006 g/kWh for diesel which is closer to advance injection timing of Carbodiesel10. For the given power output, the concentration of the CO emission for Carbodiesel10 is found to be about 0.0051 g/kWh for 26°CA bTDC, and 0.0061 g/kWh for 24.5°CA bTDC respectively. The values of

the CO emission are approximately 0.010 g/kWh for 21.5°CA bTDC and 0.015 g/kWh for 20°CA bTDC respectively at full load, whereas it is 0.008 g/kWh for 23°CA bTDC at full load.

5.2.4.2 HC emission

The variation of the HC emission with the brake power for the Carbodiesel10 blends at different injection timings, compared to the original injection timing and diesel are shown in Figure 5.26.

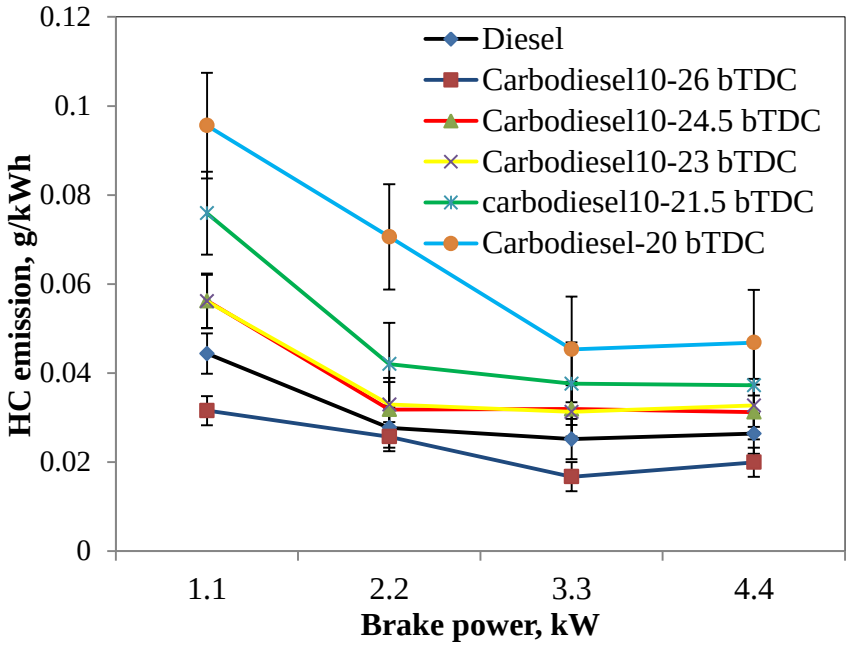

Figure 5.26 Variation of HC emission with brake power

The HC emission decreases with the increase in the brake power for diesel and Carbodiesel10 due to more complete combustion. The HC emission at no load is higher due to under mixing of the fuel. It is seen that, Carbodiesel10 gives a lower hydrocarbon emission for the advanced injection timings at full load. Advancing the injection timing causes an earlier start of combustion relative to the TDC. Because of this, the cylinder charge being compressed as the piston moves to the TDC that results in relatively higher temperatures, and thus reduces the HC emissions. Same reason was supported by Pandian et al., [182] when they investigated the HC emissions in a single cylinder, DI diesel engine run on bio-diesel blend at different injection timings. With the retarded injection timings, the HC emission is found to be higher throughout the engine operation. It can also be observed from figure, that the HC emission value for the diesel is found to be about 0.026 g/kWh at the full load. The HC emission at full load for the original injection timing 23°CA bTDC is found to be about 0.032

g/kWh, and at full load for the retarded injection timings of 21.5°CA bTDC and 20°CA bTDC they are about 0.037 g/kWh and 0.046 g/kWh respectively. Similarly, for the advanced injection timings of 26°CA bTDC and 24.5°CA bTDC they are found to be 0.019 g/kWh and 0.032 g/kWh at full load respectively.

5.2.4.3 NO emission

Figure 5.27 shows the variation of the NO emission with the brake power for the original, advanced and retarded injection timings of an engine fuelled with Carbodiesel10, and diesel at the original injection timing.

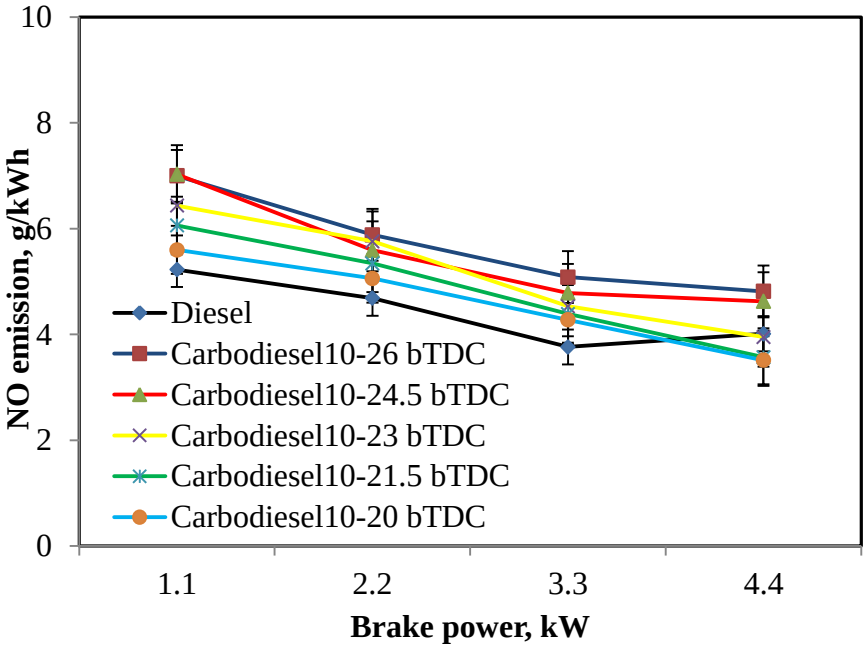

Figure 5.27 Variation of NO emission with brake power

The formation of NO emission is highly dependent on the in-cylinder temperature, oxygen concentration and residence time for the reaction to take place. The cylinder gas temperature is influenced by the combustion and heat release rate. The availability of oxygen depends on the air fuel ratio and the nature of the fuel [183]. The NO emission decreases with the increase in the brake power. The NO emission for Carbodiesel10 is higher about 23% than that of diesel at full load. This is because of higher combustion temperature. The NO emission at the advanced injection timings are significantly higher at all loads compared to those of diesel and Carbodiesel10 at original injection timing. Advancing the injection timing caused an earlier start of combustion relative to the TDC and the higher combustion temperature [184]. The NO emission is found to be about 4.0 g/kWh and 3.9 g/kWh at full load for diesel and original injection timing of 23°CA bTDC, whereas for the retarded

injection timings of 21.5°CA bTDC and at 20°CA bTDC it is found to be about 3.6 g/kWh and 3.5 g/kWh respectively at full load. Similarly, the NO emission for the advanced injection timing of 26°CA bTDC is found to be about 4.8 g/kWh and at 24.5°CA bTDC it is found to be about 4.6 g/kWh respectively at full load. The NO emission at the retarded injection timings is significantly lower at all loads, because more fuel burns after the TDC.

5.2.4.4 Smoke emission

The variation of smoke emission with respect to the brake power for Carbodiesels10 at different injection timings and diesel is portrayed in Figure 5.28. The smoke emission increases with the increase in brake power for diesel and Carbodiesel10 at all injection timings. As the load increases, more fuel is injected, and this increases the formation of smoke. Similar reasons were reported by Sayin when they correlated the results obtained from running a DI diesel engine on diesel methanol blends [185]. The smoke emission value of diesel is found to be about 59% at original injection timing at the full load.

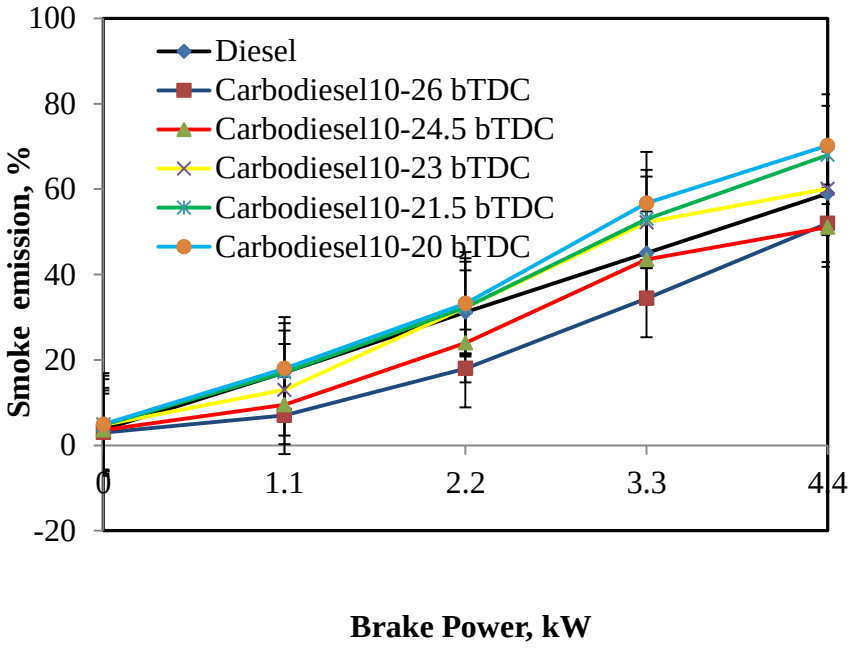

Figure 5.28 Variation of smoke emission with brake power

The smoke emission of Carbodiesel10 is higher by about 1.9% compared to that of diesel at full load. This may be due to attributed to the unburned and partially reacted hydrocarbons as well as higher density carbon black particles present in it. The smoke level of Carbodiesel10 is lower with the advanced injection timings and higher with retarded injection timings. Higher smoke values at retarded injection timings with the entire operation may be due to unburned and partially reacted hydrocarbons. The smoke emission for the Carbodiesel10 at

full load at the original injection timing is found to be 60.1%. The smoke emission values of Carbodiesel10 at the advanced injection timings of 26°CA bTDC and 24.5°CA bTDC at full load are found to be about 52% and 55.1% respectvely, and at the retarded injection timings of 21.5°CA bTDC and 20°CA bTDC, they are found to be about 68% and 72% respectively.

5.2.5 Summary

From the above discussion, it is summarised that the engine could operate with the Carbodiesel10 at original, advanced and retarded injection timing. Based on the combustion, performance and emission parameters results of Carbodiesel10 are found that the advance injection timing 26^{o}CAbTDC gave the better results compared to results obtained for other injection timings. Carbodiesel10 gave higher brake thermal efficiencies of about 5.9% and 2.5% at 26^{o}CA bTDC and 24.5^{o}CA bTDC respectively, compared to those of that of the original injection timing. Table 5.2.1 provides the values of important engine parameters obtained for Carbodiesel10 operated at different injections timings and diesel at full load.

Table 5.2.1 Values on combustion, performance and emission parameters at full load for different injection timings of Carbodiesels10

S.No.	Parameters	26°CA bTDC Advanced injection	24.5°CA bTDC Advanced injection	23°CAbTDC Original injection	21.5 °CAbTDC Retarded injection	20°CAbTDC Retarded injection
Combustion parameters						
1	Maximum cylinder pressure, (bar)	85.4	80.6	80	78.2	65
2	Ignition delay, (°CA)	9.9	10.38	10.44	12.54	12.93
3	Max. heat release rate, (J/°CA)	56.42	55.09	49.6	44.95	44.6
4	Combustion duration, (°CA)	48.14	47.02	46.23	45.66	43.35
6	Maximum rate of pressure rise, (bar/°CA)	5.8	5.46	4.71	3.51	3.24
Performance parameters						
1	Brake thermal efficiency, (%)	30.16	29.22	28.48	28.23	28.02
2	Brake specific energy consumption, (kJ/kWh)	9327.65	9668.27	10583.74	11140.38	12113
3	Exhaust gas temperature, (°C)	341.97	350.3	366.28	376.0	389.99
Emission Parameters						
1	CO emission, (g/kWh)	0.005	0.006	0.008	0.01	0.015
2	HC emission, (g/kWh)	0.019	0.031	0.033	0.037	0.026
3	NO emission, (g/kWh)	4.81	4.62	3.95	3.57	3.51
4	Smoke emission, (%)	52	55.1	60.1	68	72

5.3 Different carbon black-water-diesel emulsions (CBWDs)

5.3.1 General

In the previous section, the experimental results obtained for the combustion, performance and emissions of the engine run on Carbodiesel10 at different injection timings were discussed. However, there were a few problems noticed with the utilisation of Carbodiesel, such as long-time stability problem, poor spray formation and higher NO emission. Research works indicated that a solid fuel can be used with water in the form of emulsion, and can improve spray formation and reduce NO emission when it is used as fuel in CI engine. The preparation and characterisation of different CBWD emulsions have already been described in Chapter 4. This section presents a detailed discussion on the results obtained for the combustion, performance and emission of a single cylinder, four stroke, air cooled, DI diesel engine, fuelled with different CBWD emulsions. The numerical value after the CBWD emulsion refers to the percentage of CB in the emulsion. For example, CBWD10, is composed of 10% CB and the remaining are water, surfactant and diesel. The respective results are discussed in comparison with those of diesel, in this chapter.

5.3.2 Combustion analysis

5.3.2.1 Cylinder pressure with crank angle

The variation of the cylinder pressure with crank angle at full load for diesel and all the tested CBWD emulsions in this study is portrayed in Figure 5.29. In a CI engine, the cylinder pressure depends on the burned fuel fraction during the premixed burning phase, and the early or later occurrences of the ignition are attributed to the increased or decreased cylinder gas temperatures respectively [186]. All the CBWD emulsions tested in this study follow a cylinder pressure pattern similar to that of diesel at full load condition**.** It can be observed from the figure that, the combustion starts later by about 2.9^{o}CA, 2.3^{o}CA, 2.8^{o}CA and 2.4^{o}CA for the CBWD5, CBWD10, CBWD15 and CBWD20 emulsions respectively, compared to that of diesel at full load. As a result of the presence of water in the emulsions, the mixture of fuel and air takes more time to ignite, resulting in the postponement of ignition. Similar results were reported by Chiosa et al., when a diesel-water emulsion was tested in a single cylinder, four stroke, DI diesel engine [187]. The peak cylinder pressure of all emulsions are found to be lower than that of diesel at full load, as a result of the higher density of the emulsions than that of diesel. It can be observed from the figure that, the cylinder pressure of diesel is found to be about 79.4 bar at 371.0^{o}CA at full load. Similarly, the peak cylinder pressures of CBWD5, CBWD10, CBWD15 and CBWD20 are found to be

about 76.3 bar at 372.1°CA, 75.2 bar at 372.2°CA, 76.1 bar at 372.2°CA and 75.9 bar at 372.1°CA respectively, at full load.

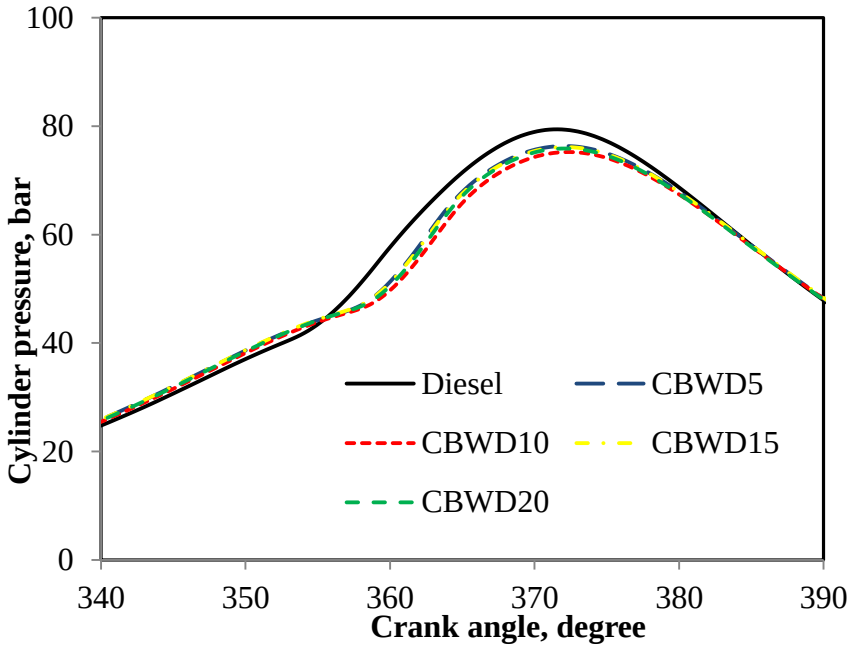

Figure 5.29 Variation of cylinder pressure with crank angle at full load

5.3.2.2 Ignition delay

Figure 5.30 illustrates the variation of the ignition delay with respect to brake power for diesel, and different emulsions tested in this study. It can be observed from the figure, that the ignition delay decreases with an increase in the brake power of all the tested fuels in this study. This trend is genuine, because as the load increases the heat prevailing inside the cylinder increases, and helps the fuel air mixture to ignite sooner [188]. It can also be observed that, all the emulsions exhibit a longer ignition delay than that of diesel. This may be due to the lower cetane number of the emulsions, poor mixture formation and the presence of water in the emulsion. Salmani et al., documented the same reasons in their study of the ignition characteristics of coconut oil emulsion obtained from a diesel engine [189]. The ignition delay for diesel at full load is found to be about 9.3°CA. Similarly, the ignition delays for the CBWD5, CBWD10, CBWD15 and CBWD20 emulsions are found to be about 12.3°CA, 12.7°CA, 13.1°CA and 13.3°CA at full load respectively. The ignition delay for the CBWD5, CBWD10, CBWD15 and CBWD20 emulsions are longer by about 1.6°CA, 2°CA, 2.4°CA and 2.6°CA than that of diesel respectively, at full load.

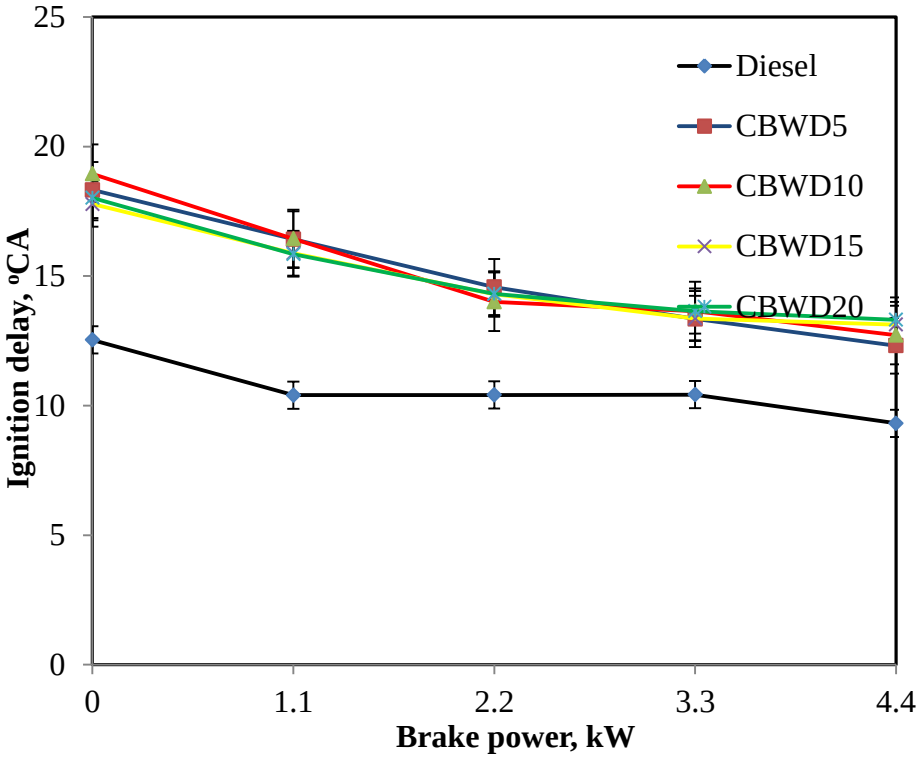

Figure 5.30 Variation of ignition delay with brake power

5.3.2.3 Heat release rate with crank angle

Figure 5.31 depicts the variation of the heat release rate with crank angle for the CBWD5, CBWD10, CBWD15 and CBWD20 emulsions and diesel respectively, at full load. It can be observed form the figure that, the intensity of the premixed combustion is found to be higher for the CBWD5 emulsion than those of other emulsions, but lower than that of diesel at full load. The higher maximum heat release for the CBWD5 is due to more accumulation of fuel than other emulsions. It can also be observed from the figure that, the maximum heat release rate is found to be lower for all the emulsions as a result of poor mixture formation and lower heating value, compared to that of diesel at full load. Another reason may be that, the latent heat of emulsion increases due to the presence of water. As a result, more energy is absorbed by the emulsion for vaporisation, and hence lowers the maximum heat release rate. The reason indicated here is in good agreement with the results obtained by Kannan and Anand [190]. The maximum heat release that occurred for diesel is at about 54.5 J/^{o}CA at 366.5^{o}CA. The maximum heat release rates for CBWD5, CBWD10, CBWD15 and CBWD 20 are found to be about 53.1 J/ ^{o}CA at 366.9^{o}CA, 53.4 J/ ^{o}CA at 367.5 ^{o}CA, 53.1 J/ ^{o}CA at 367.9^{o}CA and 52.9 J/ ^{o}CA at 8.2 ^{o}CA, respectively, at full load.

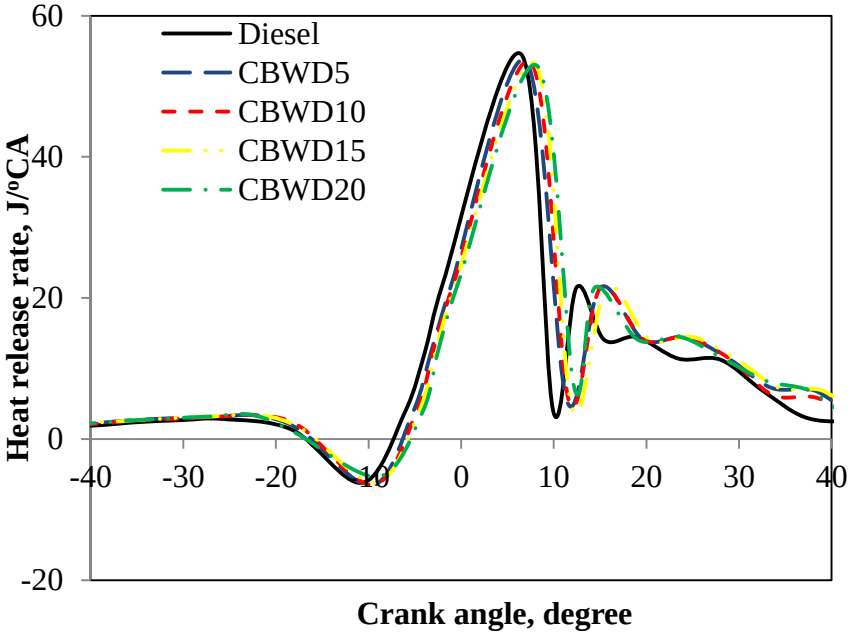

Figure 5.31 Variation of heat release rate with crank angle at full load

5.3.2.4 Combustion duration

Figure 5.32 portrays the variation of the combustion duration with the brake power of the engine for all the tested emulsions and diesel respectively.

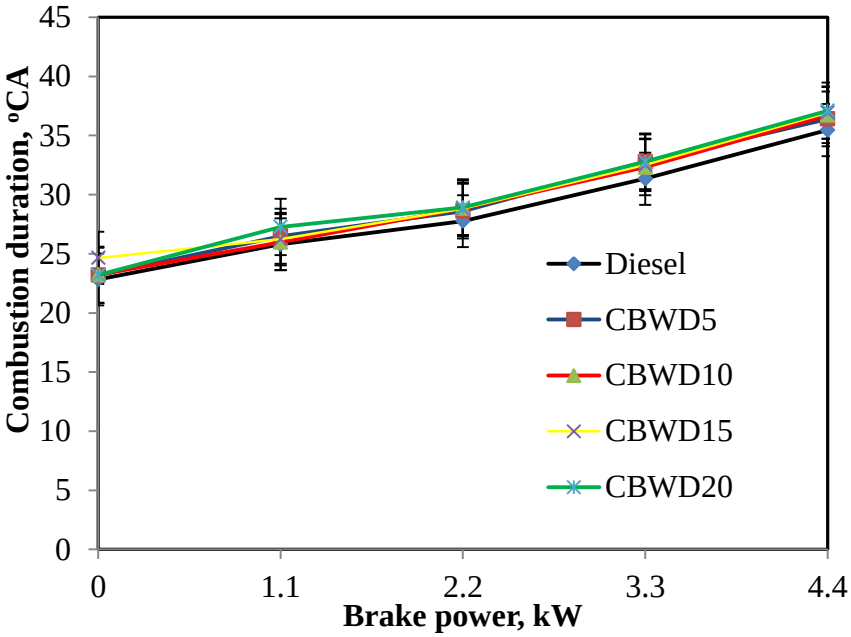

Figure 5.32 Variation of combustion duration with brake power

The combustion duration increases with the increase in the brake power owing to the increase in the fuel quantity. The increase in the CB percentage in the emulsion as a take time for the

combustion results in slow combustion, and hence the combustion duration is longer for the emulsions than for diesel throughout the load. Subramanian and Ramesh reported a similar reason when they investigated water-diesel emulsion with oxygen- enriched air [159]. This is also evident from the diffusion combustion for CBWD5, CBWD10, CBWD15 and CBWD20 compared to that of diesel operation. The values of the combustion duration at full load are found to be about 35.5^{o}CA, 36.4^{o}CA, 36.7^{o}CA, 36.9^{o}CA and 37.1^{o}CA for diesel, and CBWD5, CBWD10, CBWD15 and CBWD20 emulsions respectively, at full load.

5.3.2.5 Mass fraction burned

Figure 5.33 portrays the variation of the mass fraction burned with respect to the crank angle for diesel and all the CBWD emulsions at full load. The CBWD5, CBWD10, CBWD15 and CBWD20 emulsion results follow a trend similar to that of diesel. Mass fraction burned between 350^{0} CA to 360^{0} CA shown was almost zero because of start of the combustion**.** It can be observed from the figure that the 10% and 50% mass fraction burned for all the emulsions, seems to be sooner than that of diesel at full load. The 10% and 50% mass fraction burned varies with a minimum difference of 2^{o}CA to a maximum of 3.5^{o}CA for the emulsions from that of diesel. The crank angles at which the 90% mass fraction burned varies with a minimum difference of 1.5^{o}CA to a maximum of 4^{o}CA, from that of diesel at full load. For the same crank angle values, the mass fraction burned of the CBWD5, CBWD10, CBWD15 and CBWD20 emulsions, is marginally higher than that of diesel at full load. Mass fraction burned for CBWD20 looks higher than CBWD10 due to exces of CB particles.

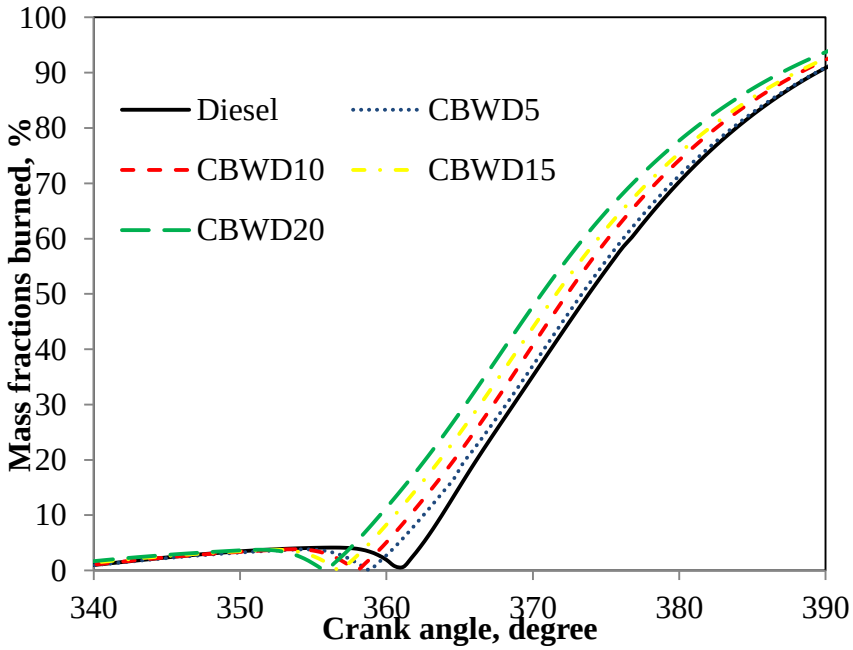

Figure 5.33 Variation of mass fractions burned with crank angle

5.3.2.6 Maximum heat release rate

Figure 5.34 depicts the variation of the maximum heat release rates with brake power for the CBWD5, CBWD10, CBWD15 and CBWD20 emulsions and diesel. It can be observed from the figure that, the maximum heat release rate increases with brake power. The maximum heat release rate for diesel is found to be about 54.5 J/deg. at the full load. Similarly, the maximum heat release rates are found to be about 53.2, 53.4, 53.15 and 52.9 J/deg. for the CBWD5, CBWD10, CBWD15 and CBWD20 emulsions respectively, at full load. The maximum heat release rates of all the CBWD emulsions are marginally lower than that diesel at full load. This may be due to the higher density and viscosity and lower heating value of the CBWD emulsion compared to that of diesel [191].

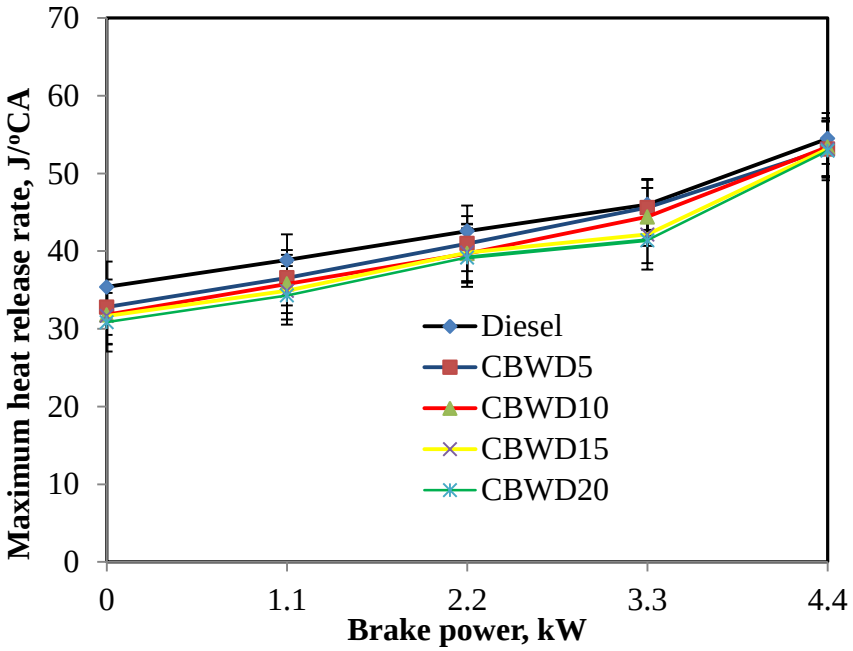

Figure 5.34 Variation of maximum heat release rate with brake power

5.3.2.7 Maximum rate of pressure rise

The variation of the maximum rate of pressure rise with respect to the engine brake power for all the CBWD emulsion, in comparison with diesel is shown in Figure 5.35. The maximum rate of pressure rise defines the rate at which the pressure imposed at every crank angle during the combustion process on the cylinder head and other components. The rate of pressure rise depends on the amount of heat released in the initial stages of combustion and the fuel quality [45]. The higher the maximum rate of pressure rise, the higher the brake power on the piston and other components, which may lead to severe damage of the parts

[192]. The maximum rate of pressure rise increases with an increase in the brake power. It can be observed from the figure that, the maximum rate of pressure rise for diesel is found to be about 5.34 bar/ ^{o}CA at full load. Similarly, it can also be observed that the maximum rate of pressure rise for the CBWD5, CBWD10, CBWD15 and CBWD20 emulsions are found to be about 5.2, 5.1, 4.9 and 4.7 bar/ ^{o}CA respectively, at the maximum brake power. The maximum rate of pressure rise for diesel is the highest compared to those of all the CBWD emulsions. As the rates of pressure rise for all the CBWD emulsions are lower than that of diesel, the engine piston will not be affected by the pressure imposed in it.

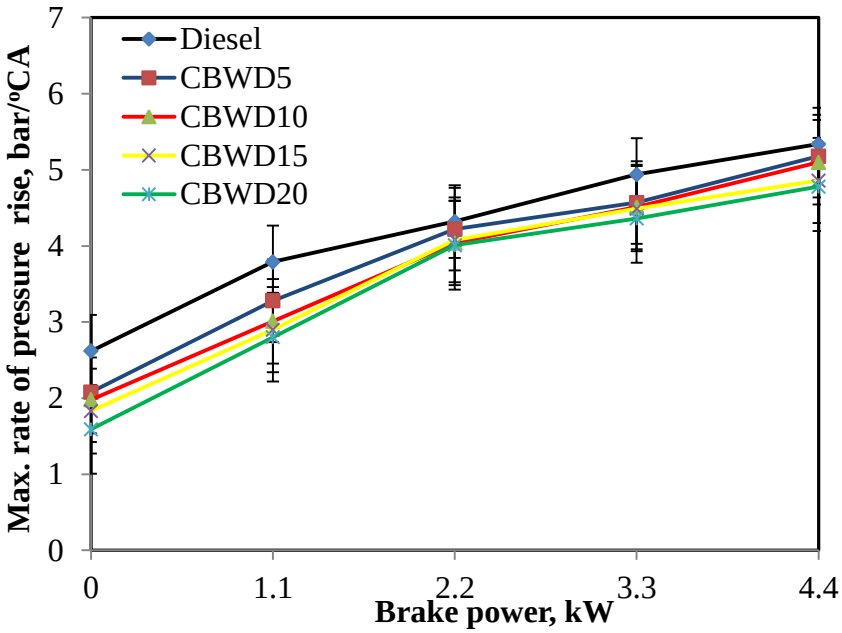

Figure 5.35 Variation of maximum rate of pressure rise with brake power

5.3.3 Performance analysis

5.3.3.1 Brake thermal efficiency

Figure 5.36 shows the variation of brake thermal efficiency with respect to brake power for diesel and all the tested emulsions in this study. It can be observed from the figure that the brake thermal efficiency increases with increases in the brake power for diesel and all the emulsions. The values of the brake thermal efficiencies at full load are 30.9%, 29.7%, 28.8%, 28.5% and 28.2% for diesel, and the CBWD5, CBWD10, CBWD15 and CBWD20 emulsions respectively. It is seen that the thermal efficiencies of CBWD5 and CBWD10 emulsions are lower than that of diesel by about 3.8% and 6.7% respectively, at full load. This may be due to their lower heating value and higher density compared to that of diesel. Also the slower

combustion processes of all the tested emulsions result in lower brake thermal efficiency. Similar results were reported by Sadhik Basha and Anand [193] when they carried out an experimental investigation on the utilisation of nanoparticle blended water–biodiesel emulsion fuel in a single cylinder, four stroke, DI diesel engine.

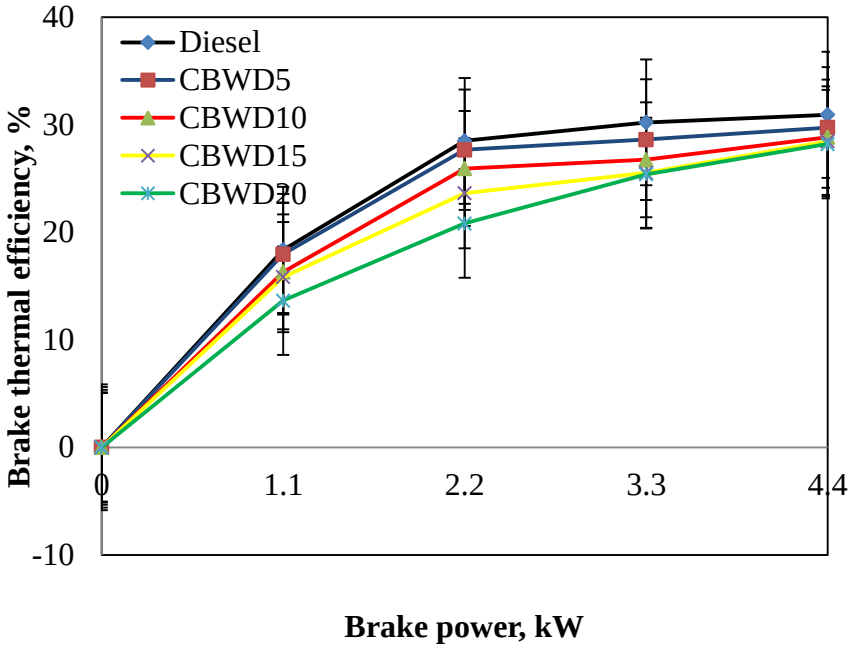

Figure 5.36 Variation of brake thermal efficiency with brake power

5.3.3.2 Brake specific energy consumption

Figure 5.37 depicts the trend of BSEC with brake power for diesel and the four different emulsions. The BSECs of CBWD5, CBWD10, CBWD15 and CBWD20 show higher values than those of diesel at all loads. Their higher density and lower calorific value are the reasons for the higher BSEC of CBWD5, CBWD10, CBWD15 and CBWD20. Also, because of the presence of water in the emulsion, the heating value decreases, and results in higher BSEC. The absorption of energy for the vaporization of the water in the emulsion also causes a higher BSEC than that of diesel. The BSEC of diesel is found to be the lowest, which is about 10.77 MJ/kWh. The values of BSEC for diesel, CBWD5, CBWD10, CBWD15, and CBWD20 are found to be about 10.8, 11.9, 12.3, 13.3 and 14.3 MJ/kWh respectively, at full load. Similar results were reported by Alahmer et al., [194] when they carried out an experimental investigation on the utilisation of diesel-water emulsified fuel in a single cylinder, four stroke, DI diesel engine.

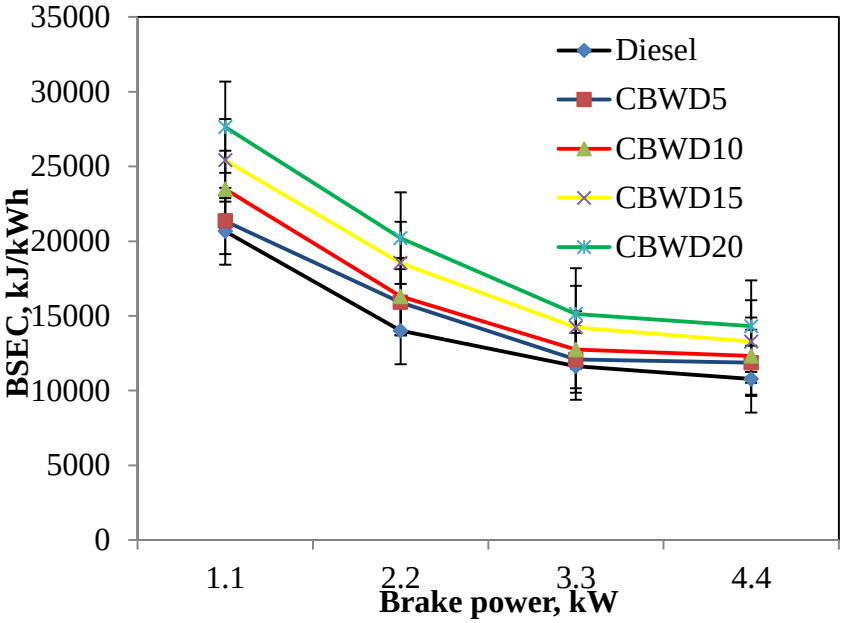

Figure 5.37 Variation of BSEC with brake power

5.3.3.3 Exhaust gas temperature

The variation of exhaust gas temperature with brake power is illustrated in Figure 5.38. The exhaust gas temperature increases with the increase in the engine load for all the emulsions and diesel.

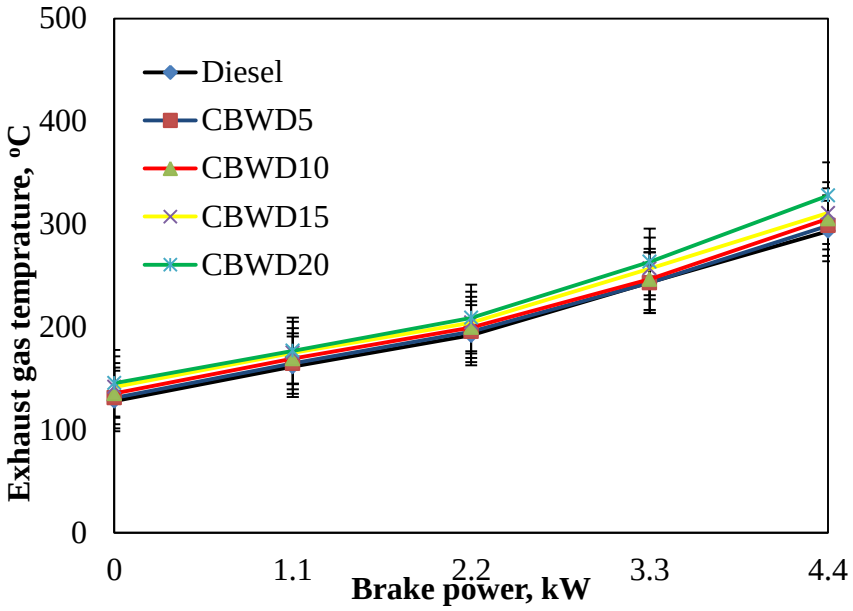

Figure 5.38 Variation of the exhaust gas temperature with brake power

The exhaust gas temperature for CBWD5, CBWD10, CBWD15, and CBWD20 is found to be higher than that of diesel, in the entire engine operation. The poor atomization of the

emulsion is, because of the higher viscosity and density in the emulsion, and hence the cylinder temperature is high for all the emulsions. The combustion of diesel appears to have a lower exhaust gas temperature, primarily because of its higher heating value and proper combustion without water content than those of the four emulsions. The exhaust gas temperature value for diesel at full load is found to be about 293.2^{o}C. It can also be observed that the values of the exhaust gas temperature are found to be about 298.5^{o}C, 305.2^{o}C, 310.8^{o}C, and 327.2^{o}C for CBWD5, CBWD10, CBWD15 and CBWD20 respectively at full load.

5.3.4 Emission analysis

5.3.4.1 CO emission

Figure 5.39 depicts the variation of the carbon monoxide (CO) emission with respect to brake power for diesel and all the CBWD emulsions.

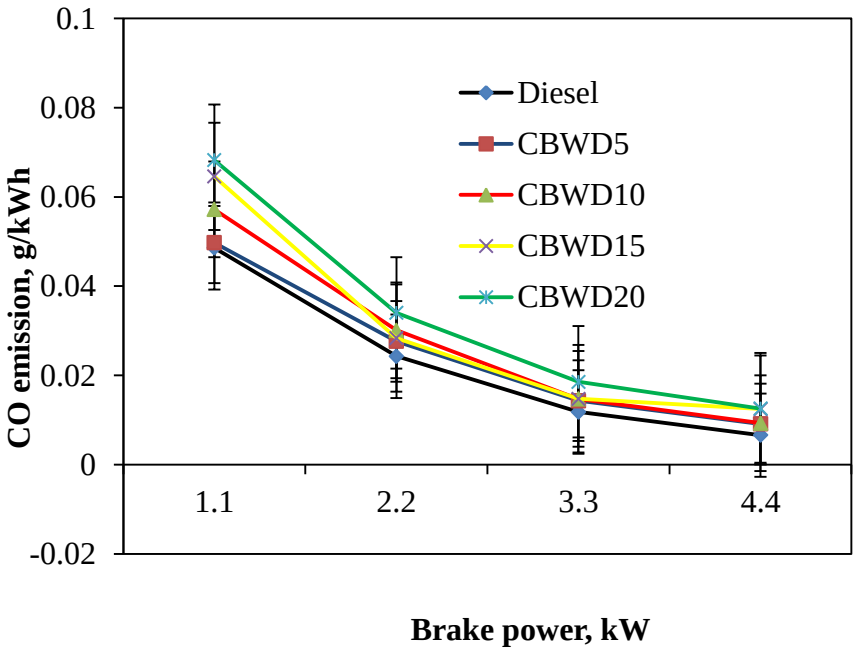

Figure 5.39 Variation of CO emissions with brake power

The CO emission for the emulsions is higher than that of diesel throughout the load, due to incomplete combustion, as a result of the longer ignition delay. It can be observed from **t**he figure that, the CO emission for all the emulsions is found to be higher than that of diesel. It can also be observed from the figure that, the CO emission is found to be the highest for CBWD20 compared to CBWD15, CBWD10, CBWD5 and diesel, at full load. As the percentage of CB increases in the emulsion, the CO emission increases as a result of poor

mixture formation and poor air entrainment. However, the values of the CO emission for all the emulsions are found to be lesser than 0.1%, which is with-in the acceptable limit [45]. The concentration of CO emission is found to be about 0.009 g/kWh for CBWD5, 0.009 g/kWh for CBWD10, 0.01 g/kWh for CBWD15, and 0.013 g/kWh for CBWD20 at full load, whereas it is 0.006 g/ kWh for diesel, at full load.

5.3.4.2 HC emission

The variation of the HC emission with brake power for diesel and all the tested CBWD emulsions is portrayed in Figure 5.40.

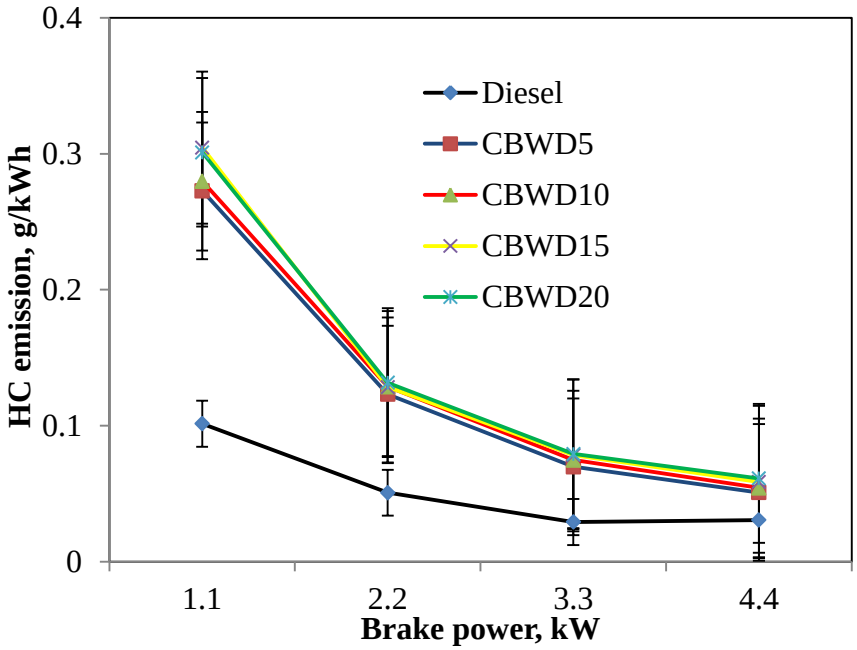

Figure 5.40 Variation of the HC emission with brake power

The concentration of hydrocarbon decreases with the increase in the engine brake power [195] for the given output. As similar, trend is also observed for all the CBWD emulsions. It can be observed that CBWD5, CBWD10, CBWD15 and CBWD20 exhibited higher HC emissions than diesel that of in the entire engine operation. This is due to the poor atomization of the high density fuel that results in a more incomplete combustion. Matsuo Odaka et al. observed similar results for the increasing trend of CO and HC emissions with water injection [196]. The HC emission for diesel is found to be about 0.03g/kWh at full load, while, the HC emissions for the CBWD5, CBWD10, CBWD15 and CBWD20 emulsions are found to be about, 0.05g/kWh, 0.05g/kWh, 0.06g/kWh and 0.06g/kWh at full load, respectively. The HC emissions for the CBWD5 and CBWD10 emulsions are 40%

higher than that of diesel, and for the CBWD15 and CBWD20 emulsions 50% higher compared to that of diesel at full load.

5.3.4.3 NO emission

Figure 5.41 depicts the NO emission corresponding to different values of brake power for all the CBWD emulsions, and diesel. For the given output, the trend of NO emissions is found to be similar from no load to full load for all the fuels tested in this study. The measured NO emissions are found to be lower for the emulsions in comparison with diesel, due to the lower combustion temperature caused by the lower heat release rate in the premixed combustion. This is also evident from the heat release curves. A similar trend has also been reported by Nadeem et al. [197] when they investigated a water-diesel emulsified fuel in a diesel engine. It is found that CBWD20 shows the lowest value among diesel and the other emulsions due to its higher density and increased latent heat of vaporization. The value of NO emission is found to be about 4.0 g/kWh at full load for diesel. It can also be observed that the value for CBWD5 is found to be 3.5 g/kWh at full load, while it is 3.2 g/kWh for CBWD10, 3.1 g/kWh for CBWD15 and 2.8 g/kWh for CBWD20 respectively, at full load.

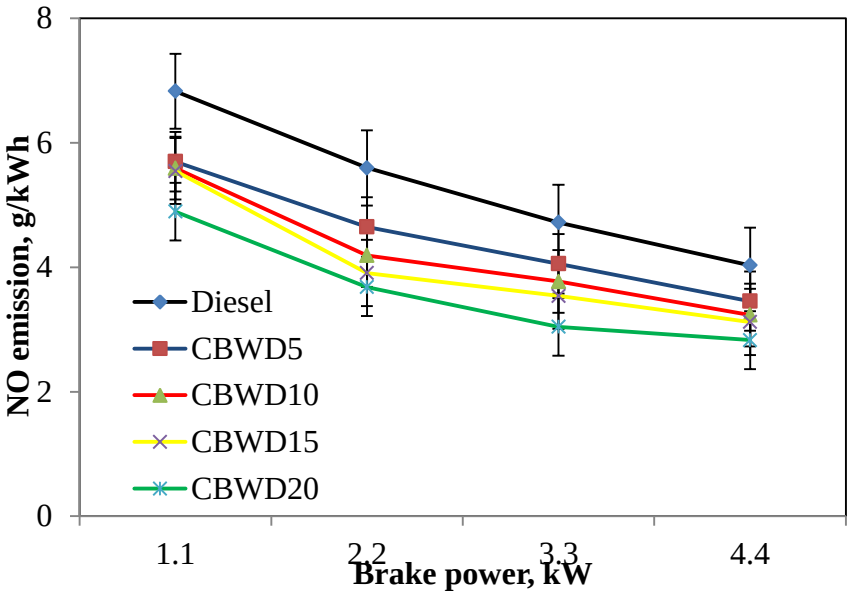

Figure 5.41 Variation of NO emission with brake power

5.3.4.4 Smoke emission

Figure 5.42 shows the variation of smoke emission with respect to brake power for diesel, and the CBWD5, CBWD10, CBWD15 and CBWD20 emulsions. It can be observed from the figure that, as the load increases, more fuel is injected and hence this increases the formation of smoke. For all the emulsions, the smoke values are found to be higher than that

of diesel in the entire engine operation. This may be due to the higher C/H ratio of the emulsions than that of diesel. It may also be due to slow combustion as a result of poor mixture formation of the emulsion. Higher smoke values at full load or entire operation may also be due to unburned hydrocarbon and longer ignition delay. The carbon percentage is high due to the carbon black particles emitted from the combustion chamber, which are dispersed with the fluctuation of the exhaust gas [198]. The smoke emission for diesel at full load is found to be about 45%. The smoke emission values of CBWD5, CBWD10, CBWD15 and CBWD20 at full load are found to be about 51%, 56.8%, 60.3% and 64% respectively.

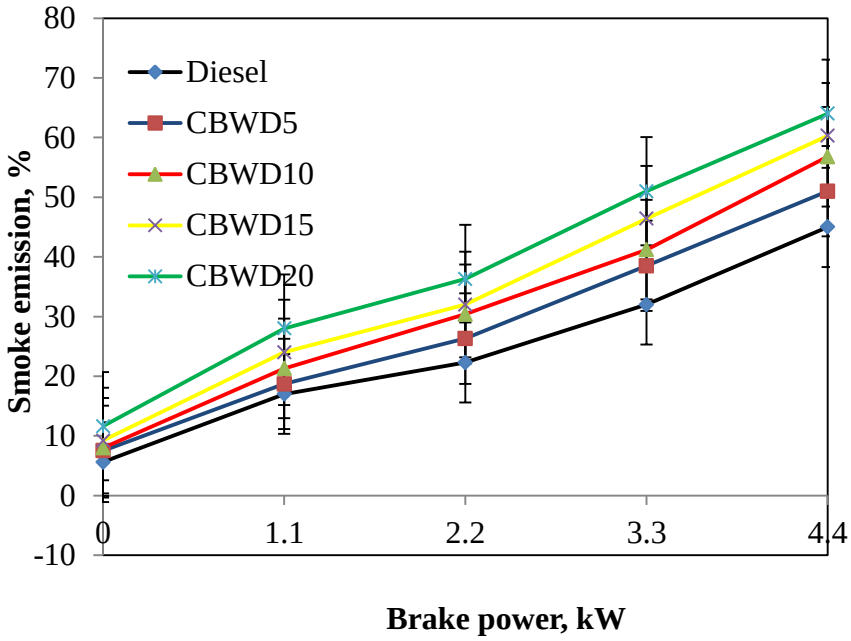

Figure 5.42 Variation of the smoke emission with brake power

5.3.5 Summary

It is concluded that, a stationary diesel engine was able to successfully run on different CBWD emulsions. There was no abnormal noise noticed during the entire engine operation run on the emulsions. The results have shown that, the engine could perform with a higher BSEC of about 0.79–25% than that of diesel, because of the higher density and lower calorific value, and the water percentage present in it. The carbon monoxide (CO) emission was found to be higher for all the emulsions, overall by about 29% to 51% than that of diesel at full load. The NO emission level was found to be lower by about 16% to 42% for all the emulsions, respectively, compared to that of diesel at full load. Table 5.3.1 provides the values of the important engine parameters obtained for the different CBWD emulsions and diesel at full load.

Table 5.3.1 Values on combustion, performance and emission parameters at full load for different CBWD emulsions

S.No.	Parameters	Diesel	CBWD5	CBWD10	CBWD15	CBWD20
Combustion parameters						
1	Maximum cylinder pressure, (bar)	79.4	76.3	75.2	76.1	75.9
2	Ignition delay, (^{o}CA)	9.31	12.31	12.7	13.12	13.3
3	Heat release rate, (J/^{o}CA)	54.5	53.1	53.4	53.1	52.9
4	Combustion duration, (^{o}CA)	38.46	36.4	36.52	36.63	36.4
5	90% Mass fraction burned, (^{o}CA)	388.56	389.47	389.1	388.24	387.24
6	Maximum rate of pressure rise, (bar/^{o}CA)	5.34	5.18	5.1	4.86	4.78
Performance parameters						
1	Brake thermal efficiency, (%)	30.92	29.7	28.83	28.45	28.2
2	Brake specific energy consumption, (kJ/kWh)	10772.3	12668.7	13932.9	15713.6	15922.5
3	Exhaust gas temperature, (^{o}C)	327.2	298.5	305.2	310.8	327.7
Emission Parameters						
1	CO emission, (g/kWh)	0.006	0.0091	0.0093	0.0124	0.0125
2	HC emission, (g/kWh)	0.030	0.050	0.054	0.0586	0.061
3	NO emission, (g/kWh)	4.03	3.46	3.77	3.12	3.04
4	Smoke emission, (%)	45	51	56.8	60.3	64

5.4 Analysis of the Two-zone modelling of combustion, performance and emission formation in DI diesel engine operating on CBWD10 emulsion

5.4.1 General

This section discusses the development of a mathematical model to validate the experimental results that were obtained from a single cylinder, four stroke, DI diesel engine fuelled with the CBWD10 emulsion. A two zone model, using a MATLAB software program was used for validation. One zone consisted of pure air called the non-burning zone, and the other zone consists of fuel and combustion products called burning zone. The first law of thermodynamics and equations of state were applied in each of the two zones, to get the cylinder temperatures and cylinder pressure histories. Using the two zone combustion model, the combustion parameters and the chemical equilibrium composition were determined theoretically. The extended Zeldovich mechanism was used to predict the NO emission, while the soot density was determined using a semi-empirical model. The comparison between mathematical modelling and experimental results are discussed in this section.

5.4.2 Combustion characteristics

1. The pressure vs crank angle graph diesel and CBWD10 emulsion is depicted in Figure 5.43(a). It can be observed that the simulated curve of cylinder pressure is closer to the curve representing the experimental values of cylinder pressure measured by the pressure transducer fixed inside the combustion chamber. A maxima is observed at a point just after the combustion of fuel has been initiated. And the pressure gradually decreses as the fuel gets consumed. It can be mentioned that the model clearly defines the variation of mean pressure inside the cylinder per degree crank angle. It can observed from the figure for the experiment and simulation analysis of CBWD10 emulsion, the peak cylinder pressure of CBWD10 emulsions are found to be lower than that of diesel, as a result of the higher density of the emulsions than that of diesel and presence of water in the emulsions, the mixture of fuel and air takes more time to ignite, resulting in the postponement of ignition.

2. The curve as shown in Figure 5.43 (b) is obtained by the simulation of the model at each crank step to find out the bulk temperature of the gases inside the cylinder. The temperature of the non-burning zone increases at a lower rate in the compression phase until the ignition of the fuel air mixture, where the temperature increases up to a maximum value around the same crank angle as that of the maximum pressure, i.e. a few degrees after the start of combustion. The high temperatures of the burning zone are responsible for the formation of

NO and soot [199]. The temperature then gradually decreases as the amount of fuel-air mixture reduces till the combustion comes to an end. However, the temperature of the air zone does not show any such huge increase, rather it increases slightly and gradually decreses as the combustion process comes to an end.

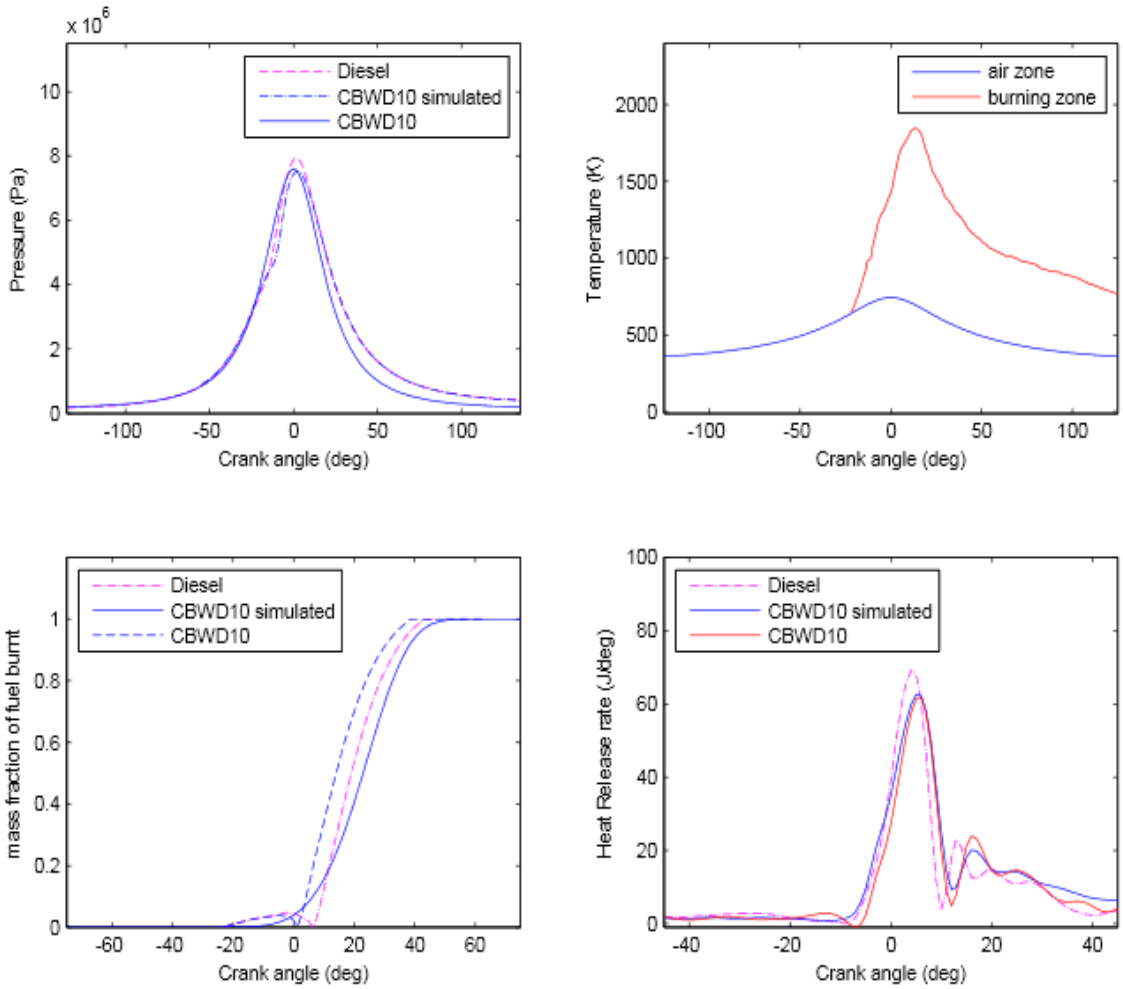

Figure 5.43 Variations of (a)pressure, (b) temperature, (c) mass fraction of fuel burnt and (d) heat release rate per degree crank angle

3. Using the Wiebe model for determining the mass fraction of fuel burnt, it can be seen from Figure 5.43 (c), that the simulated curve based on the calcualtions in the model is closer to the curve representing the experimental values of the mass fraction of fuel burnt. The constants in the empirical relations are found out using the curve fitting techniques and the simulated curve obtained gives the best fit for the same. The curves vary exponentially based on the Eq.(4.30) in section 4.7.2.9 This equation also corresponds to the original curve obtained from the experimental values when the constants in the empirical realtion of

Eq.(4.30), a=5 and n=3. Mass fraction burnt rate are higher for CBWD-exp and CBWD-sim. than that of diesel this may be due to percentage of CB presence in CBWD emulsion.

4. Figure 5.43 (d) depicts the variation of heat release rate with the crank angle based on the simulation of the model proposed in this paper and also the values obtained from experimentation. The heat release computed according to the given model closely approximates the curve representing the experimental values of the same. The values of constants found out from the curve fitting methods can be considered the best estimate due to the close approximation to the real values. It can also be observed from the figure that, the maximum heat release rate of CBWD10 emulsion of experiment and simulation is found to be lower compared to the diesel as a result of poor mixture formation and lower heating value.

5.4.3 Emission characteristics

5.4.3.1 NO emission

Two important parameters predominantly affect the formation of the NO emission in a CI engine. One is stoichiometry and the other one is in-cylinder temperature. The in-cylinder temperature has a strong effect on the formation of the NO emission.

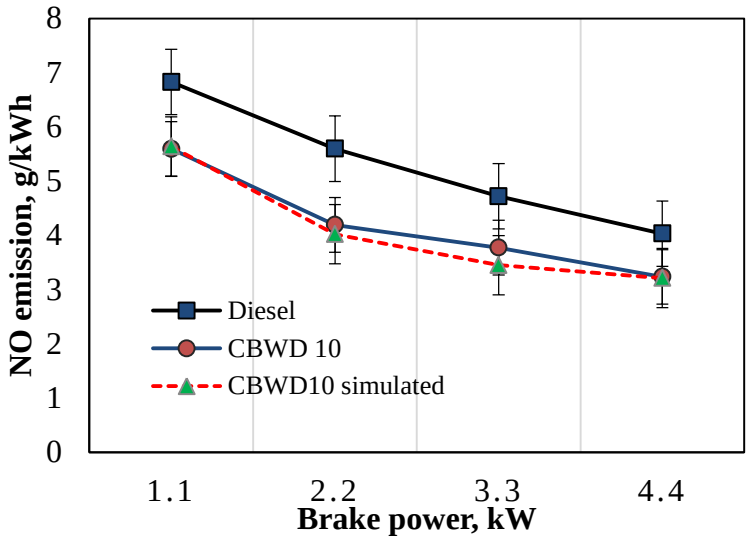

Figure 5.44 Variation of NO emission with brake power

The variation of nitric oxide (NO) emission with different brake power for the simulated and experimental results for diesel and the CBWD10 emulsion is depicted in Figure 5.44. It can be observed from the experimental results that CBWD10 follows similar trend simulated results trend as a diesel. The parameters that affect the NO formation in the CI engine are

basically the stoichiometry and the in-cylinder temperature. The measured NO emissions are found to be lower for the CBWD10 emulsion in comparison with diesel, due to the lower combustion temperature caused by the lower heat release rate in the premixed combustion. This is also evident from the heat release curves. Similar trend has also been reported by Nadeem et al. [197] when they investigated with an emulsified fuel.

5.4.3.2 CO emission

Figure 5.45 represents the variation of carbon monoxide (CO) emissions at with brake power for the simulated and experimental results for diesel and the CBWD10 emulsion. The CO emission for the emulsions is higher than that of diesel throughout the load, due to incomplete combustion, as a result of the longer ignition delay. It can be observed from the figure that, the CO emissions for the experimental and simulated results of the CBWD10 emulsion found to be higher and also than that of diesel at the full load respectively.

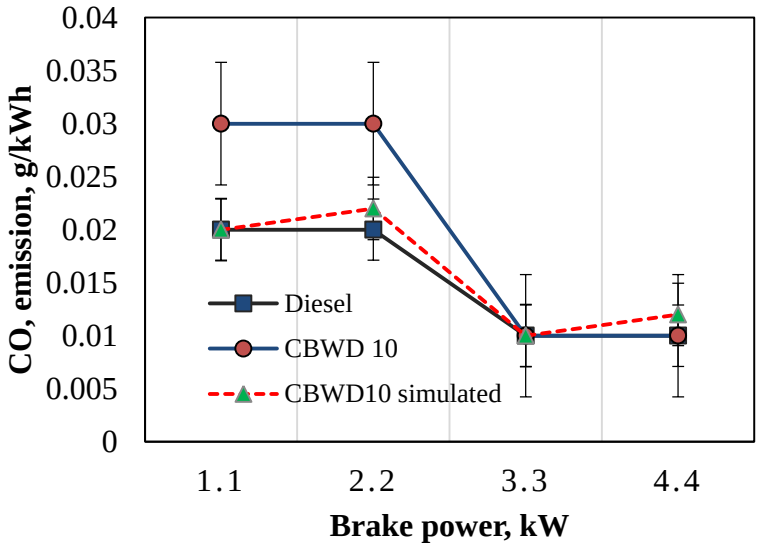

Figure 5.45 Variation of CO emission with brake power

5.4.3.3 HC emission

Figure 5.46 depicts the variation in unburnt hydrocarbon (HC) emissions with brake power for the CBWD10 emulsion and diesel. The concentration of HC emission decreases with the increase in the engine load [196] for the given output. It can be observed that the CBWD10 of experiment and simulasion results of HC emissions are than that of diesel in the entire engine operation. This is due to the poor atomization of high density fuel that results in a more incomplete combustion. Matsuo Odaka et al. observed similar results for the increasing trend of CO and HC emissions with emulsion injection [197].

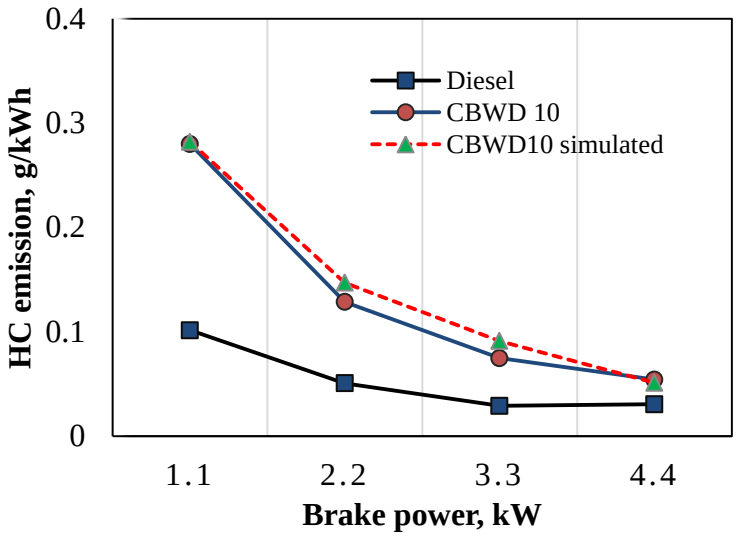

Figure 5.46 Variation of HC emission with brake power

5.4.3.4 Smoke emission

Figure 5.47 depicts the variation of smoke emission for experimental and simulated results obtained at different loads for the CBWD10 emulsion and diesel. It can be observed from the figure, that as the load increases, more fuel is injected and hence this increases the formation of smoke. For the emulsion, the smoke values are found to be higher than that of diesel during the entire engine operation. This may be due to higher C/H ratio of emulsion than that of diesel. It may also be due to slow combustion as a result of poor mixture formation of emulsion. Higher smoke values at full load or entire operation may be due to unburned hydrocarbon and longer ignition delay, and also the carbon percentage is high due to the fact that CB particles are emitted from the combustion chamber and are dispersed with the fluctuation of the exhaust gas [198].

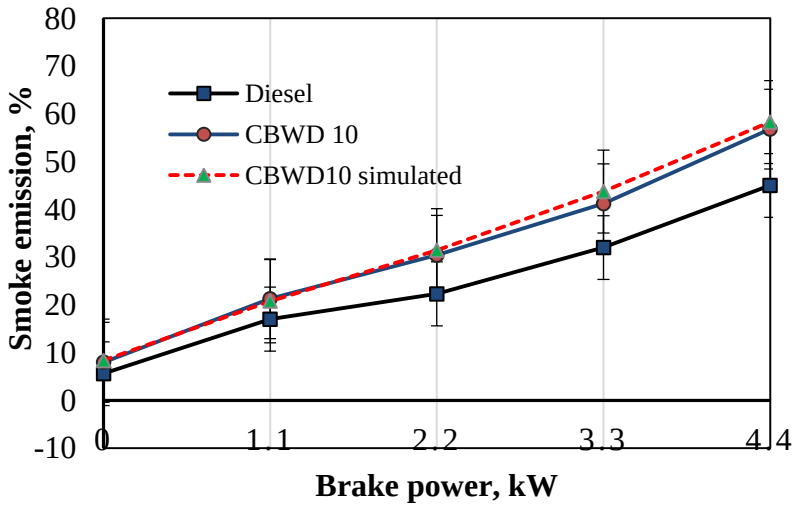

Figure 5.47 Variation of smoke emission with brake power

5.4.5 Summary

In the present work, a comprehensive, one dimensional, two-zone model was developed for a DI diesel engines running on the CBWD10 emulsion and diesel. The experiment results are used to validate a numerical model. The proposed two-zone model proves to be very effective in predicting the engine performance, combustion and exhaust emissions. Specifically, the effect of the major operating parameter of load on NO emissions and soot concentration is well verified for a wide spectrum of variation of these parameters. It is important to note, that the same values of the set of calibration constants of the various sub-models are used here for all conditions examined performance and emission wise, following a judicious multi-parametric analysis for their optimum choice.

By comparing the experimental and simulation results obtained for diesel and the CBWD10 emulsion, the combustion and emission parameters as calculated from the model showed deviation from the experimental results. The pressure values showed deviation of around 8.3%, heat release rate 2.3% and mass fraction of fuel burnt showed an average deviation of 13.24%. The NO, CO, HC and smoke emissions showed mean deviations of 3.4%, 21.5%, 3.8 and 3.8% respectively.

Table 5.4.1 Values on combustion and emission parameters at full load for Diesel, CBWD10-exp and CBWD10-simulation emulsions at full load

S.No.	Parameters	Diesel	CBWD10-experiment	CBWD10-Simulated
Combustion parameters				
1	Maximum cylinder pressure, (bar)	79.4	75.2	74.9
2	Heat release rate, (J/^{o}CA)	54.5	53.4	53.8
3	90% Mass fraction burned, (^{o}CA)	388.56	389.1	387.2
Emission parameters				
1	CO emission, (g/kWh)	0.006	0.0093	0.012
2	HC emission, (g/kWh)	0.030	0.054	0.51
3	NO emission, (g/kWh)	4.03	3.77	3.21
4	Smoke emission, (%)	45	56.8	58.2

5.5 Optimisation of injection timing of CBWD10 emulsion

5.5.1 General

The trial runs of a diesel engine fuelled with different CBWD emulsions at different loads were successful. The CBWD10 emulsion was chosen as the optimum one, as it gave better results in terms of the combustion, performance and emissions than the other emulsions. Further investigations were carried out to study the effect of varying the injection timing of the engine fuelled with the optimum CBWD10 emulsion. The results of the combustion, performance and emission parameters of the engine fuelled with the CBWD10 emulsion at different injection timings are analysed, compared with those of diesel fuel operation and presented in this section. The standard injection timing of the engine is 23^{o}CA bTDC. The injection timing of the engine was set at two advanced crank angles of 26^{o}CA bTDC and 24.5^{o}CA bTDC and two retarded injection timings of 21.5^{o}CA bTDC and 20^{o}CA bTDC.

5.5.2 Combustion analysis

5.5.2.1 Cylinder pressure crank angle

Figure 5.48 shows the cylinder pressure patterns of the CBWD10 emulsion with different injection timings at full load condition. It can be observed that, as the injection timing is advanced, the peak cylinder pressure increases, and as the injection timing is retarded the peak pressure decreases for the CBWD10 emulsion, at a given brake power. With the advanced injection timing, more fuel is accumulated; a higher peak pressure is attained, than that of the original injection timing [45]. By advancing the injection timing from 23^{o}bTDC to 26^{o}bTDC, the maximum peak cylinder pressure of the CBWD10 emulsion increases, and it occurs at an earlier crank angle, because the combustion starts earlier due to the advancement in the fuel injection timing. With the advanced injection timings of 26°bTDC and 24.5°bTDC, the CBWD10 emulsion operation exhibits higher cylinder peak pressure values of 78.2 bar at 371.0°CA bTDC, and 73 bar at 372.2°CA bTDC respectively, which is earlier than that of the original injection timing of 23°CA bTDC at full load. It can also be observed that, the peak cylinder pressure of the CBWD10 emulsion for the original injection timing of 23°bTDC, and retarded injection timings of 21.5°bTDC and 20°bTDC are found to be about 75.2 bar, and 72.4 bar, and 71.1 bar respectively, at the maximum brake power, which occurs at 372.2°CAbTDC and 372.0°CAbTDC, and 373.1°CA bTDC respectively.

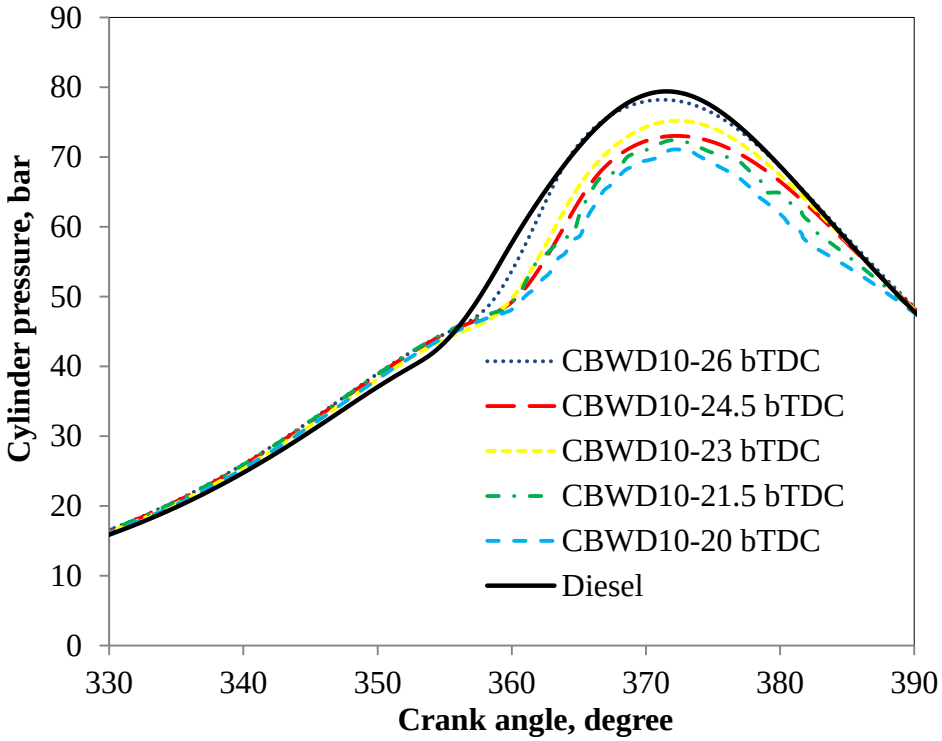

Figure 5.48 Variation of pressure with crank angle at full load

5.5.2.2 Ignition delay

Figure 5.49 portrays the variation of ignition delay for the CBWD10 emulsion (at different injection timings) and diesel with brake power. The ignition delay period depends on the Cetane number, density and viscosity of the fuel. The ignition delay period decreases with the increase in the brake power. This may be attributed to the higher combustion temperature and exhaust gas dilution at higher loads. For the advanced injection timing of the CBWD10 emulsion, the ignition delays are shorter than that of diesel in the entire operation. Similar results were presented by Nwafor et al., for a rapeseed oil fuelled diesel engine run at an advanced injection timing [111]. The ignition delay at the original injection timing of the CBWD10 emulsion is longer by about 1^{o}CA than that of diesel at full load, because of its lower cetane number. The delay is shortened by about 2 – 3^{o}CA when the injection timing is advanced. In the case of retardation, the delay is increased by about 1 – 2^{o}CA at the maximum brake power. The ignition delays observed for the CBWD10 emulsion at 26^{o}CA bTDC, 24.5^{o}CA bTDC, 23^{o}CA bTDC, 21.5^{o}CA bTDC and 20^{o}CA bTDC are found to be 9.1^{o}CA, 9.3^{o}CA, 10.1^{o}CA, 11.9^{o}CA and 12.8^{o}CA respectively, at full load.

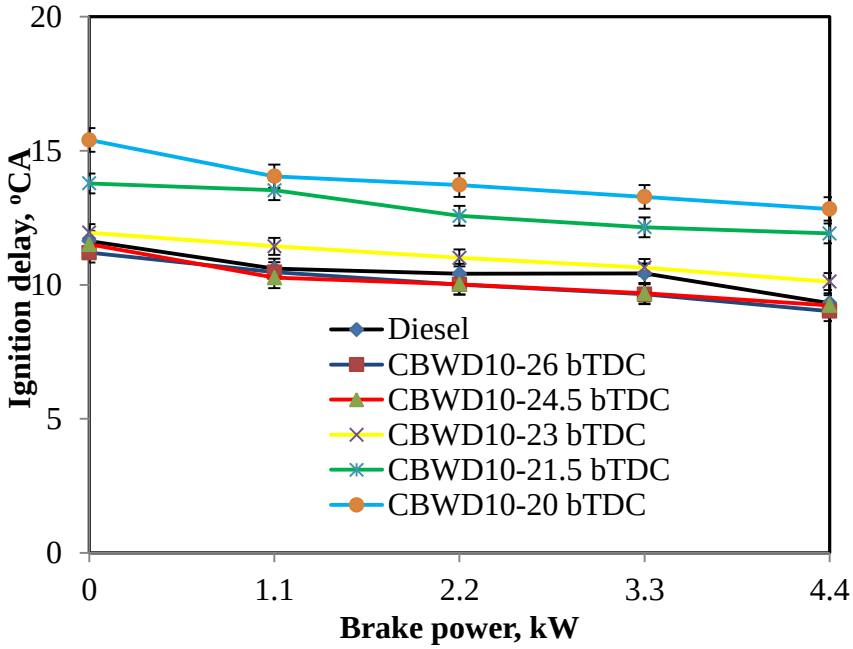

Figure 5.49 Variation of ignition delay with brake power

5.5.2.3 Rate of heat release rate

The variation of the heat release rate with crank angle for the CBWD10 emulsion and diesel at full load for different injection timings is presented in Figure 5.50. It can be observed from the figure that, the maximum heat release rate of the CBWD10 emulsion at the original injection timing is lower than that of diesel because the calorific value and cetane number are lower, and the density of the CBWD10 emulsion is higher. The maximum heat release rates at the maximum brake power for diesel and the CBWD10 emulsion with the original injection timing are found to be about 54.6 J/°CA at 365.5°CA and 53.4 J/°CA at 365.8°CA respectively. The maximum heat release rates for the advanced injection timings of 26°CA bTDC and 24.5°CA bTDC are found to be about 56.1 J/°CA at 362.4°CA, 55.3 J/°CA at 364.1°CA respectively, and for the retarded injection timings of 21.5°CA bTDC and 20°CA bTDC, the values are found to be approximately 52.6 J/°CA at 368.2°CA and 52.1J/°CA at 369.3°CA respectively, at the maximum brake power. From the results, it is understood that the advanced injection timing exhibits higher maximum heat release rate in comparison with the original and retarded injection timings, because the combustion starts earlier due to the advancement in the fuel injection timing. The retarded injection timing increases the ignition delay period, and the poor combustion reduces the heat release rate. With the advanced injection timing of 26^{o} bTDC, the maximum heat release of the CBWD10 emulsion occurs at an earlier crank angle and its magnitude increases. A similar reason was documented by

Uzkan and Horton when coal water slurry was used as fuel in a DI diesel engine run at different injection timings [38].

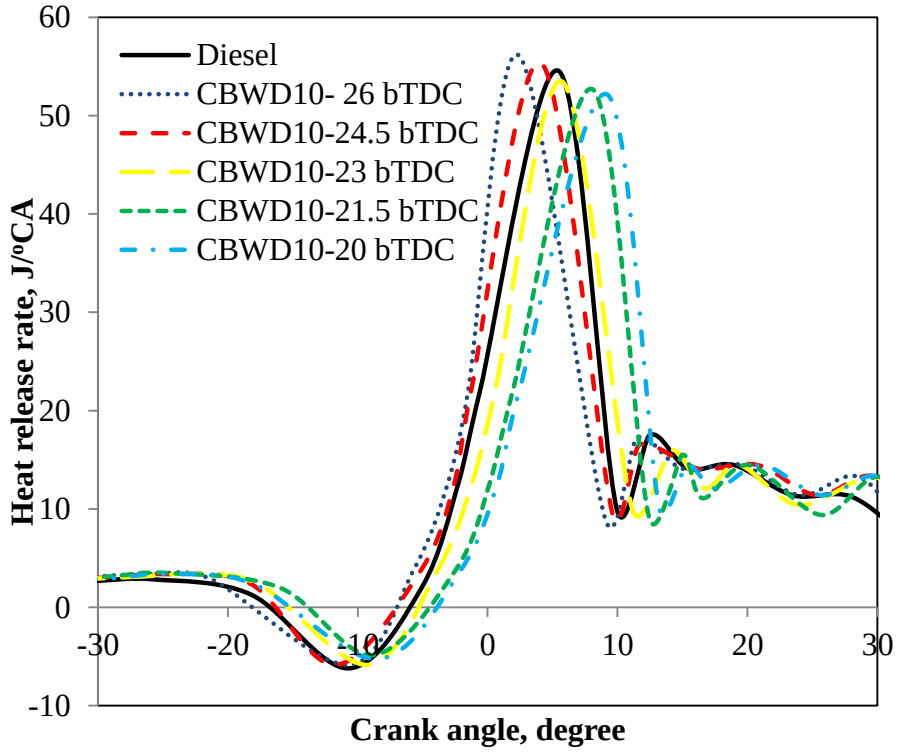

Figure 5.50 Variation of heat release rate with crank angle at full load

5.5.2.4 Combustion duration

Figure 5.51 portrays the variation of the combustion duration at various loads of the engine run on the CBWD10 emulsion at different injection timings respectively. Combustion duration is the time between start of combustion to end of combustion. From the heat release rate curve, the crank angle at which there is sudden rise in the heat release was taken as the start of combustion. It can be observed from the figure that, the combustion duration increases with the increase in the brake power for the CBWD10 emulsion, at all injection timings, which may be due to the increase in the quantity of the emulsified fuel and diesel. The combustion durations for the CBWD10 emulsion at different injection timings of 26, 24.5, 23, 21.5 and 20^{o}CA bTDC are found to be about 37.4, 38.1, 38.5, 39.4 and 40.5^{o}CA respectively, at full load. The combustion duration of the CBWD10 emulsion, at the original injection timing is about 1% ^{o}CA which is longer than that of diesel at full load. Similarly, it is lower by about 1–3% ^{o}CA for the advanced injection timing, and higher by about 2–

5.2%^{o}CA compared to that of the original injection timing of the CBWD10 emulsion at full load, respectively.

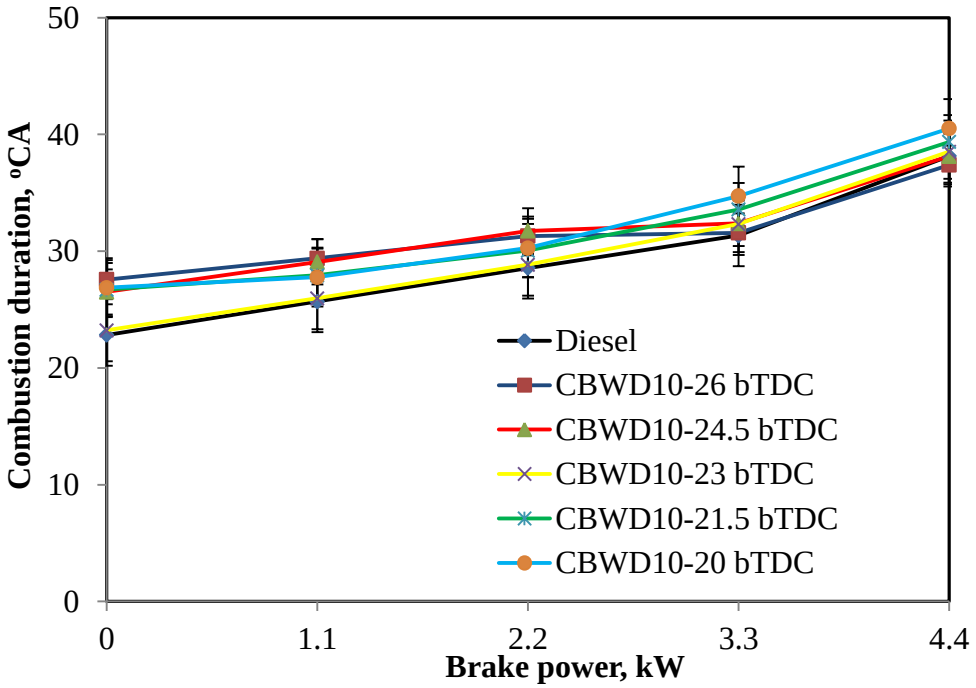

Figure 5.51 Variation of the combustion duration with brake power

5.5.2.5 Mass fraction burned

Figure 5.52 portrays the variation of the mass fraction burned with respect to the crank angle for the CBWD10 emulsions at the two advanced injection timings and two retarded injection timings with the original injection timing and diesel at full load. At the all injection timings, the CBWD10 emulsion results follow a trend similar to that of diesel. It can be observed from the figure that, the 10% mass fraction burned is earlier by about 0.3^{o}CA for 24.5^{o}CA bTDC advanced injection timing, and later by about 1^{o}CA for 26^{o}CA bTDC advanced injection timing compared to than that of diesel at full load. It can also be observed that, the 50% mass fraction burned varies with a minimum difference of 1.5^{o}CA to a maximum of 4^{o}CA for the retarded injection timing and mass fraction earlier from that of diesel. For the advanced injection timings the 50% mass fraction burned are later by about 1 and 2^{o}CA than that of diesel at the full load respectively. The 90 % mass fraction burned for the retarded injection timing is by 1 to 2^{o}CA earlier and for the advanced injection timing is later by about 0.5 to 1.5^{o}CA compared to that of diesel at full load.

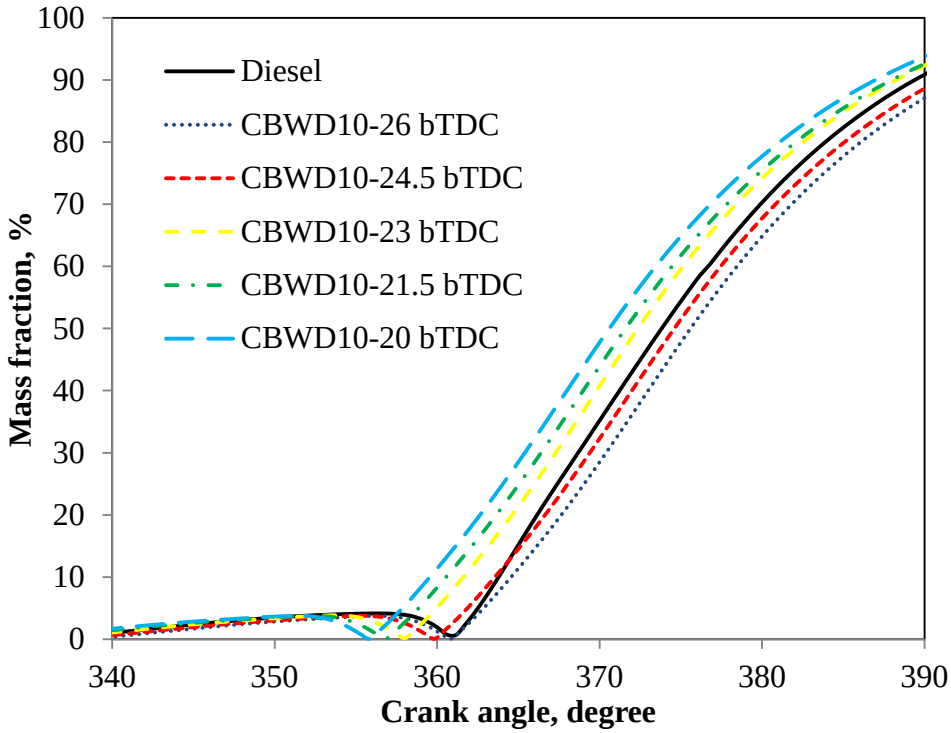

Figure 5.52 Variation of mass fractions burned with crank angle

5.5.2.6 Maximum heat release rate

Figure 5.53 depicts the variation of the maximum heat release rate with brake power for the CBWD10 emulsion with the two advanced and retarded injection timings, and for diesel. In a CI engine the maximum heat release rate depends on the fuel burning rate during the premixed burning phase, which in turn leads to better combustion and heat release rate [45]. It can be observed from the figure that, the maximum heat release rate increases with an increase in the brake power in the entire engine operation. The maximum heat release rate for the CBWD10 emulsion at the standard injection timing of 23^{o}CA bTDC is found to be 53.4 J/deg at full load. Similarly, the maximum heat release rates for the CBWD10 emulsion at advanced injection timings of 26^{o}CA bTDC and 24.5^{o}CA bTDC are found to be 56.2 J/deg and 55.3 J/deg, and at the two retarded injection timings of 21.5^{o}CA bTDC and 20^{o}CA bTDC are recorded to be 52.6 J/deg and 52.2 J/deg respectively, at full load. It can also be observed from the figure that, the maximum heat release rate at the advanced injection timing is higher than that of diesel due to more fuel accumulated at advanced injection timing in the entire engine load range. Similar results were documented by Ganapathy et al., [200] when they obtained results in DI diesel engine run on Jatropha biodiesel at different injection timings.

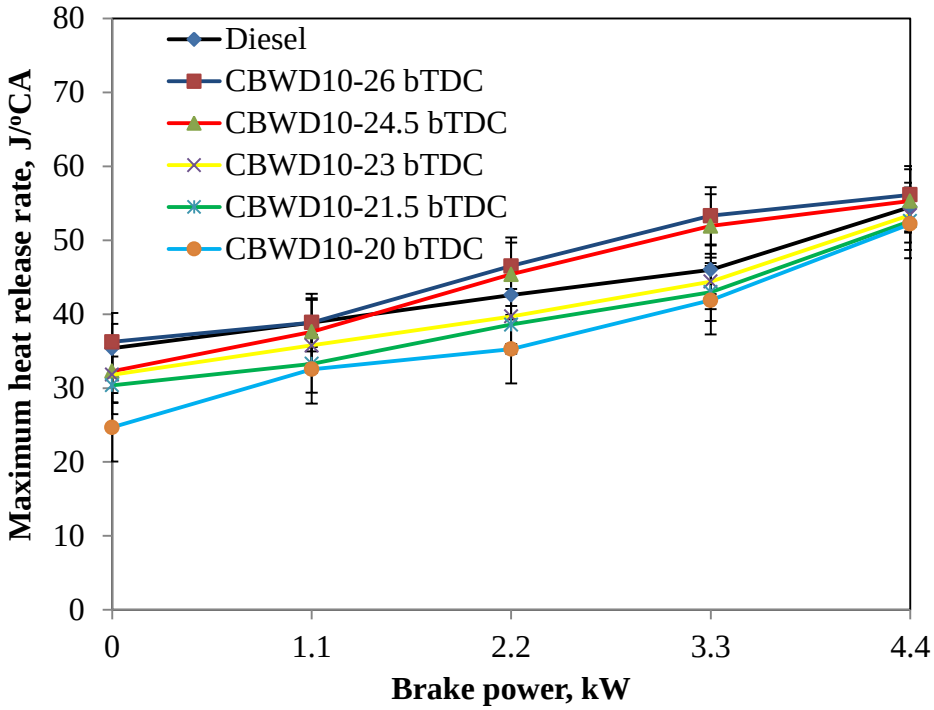

Figure 5.53 Variation of maximum heat release rate with brake power

5.5.2.7 Maximum rate of pressure rise

The variation of the maximum rate of pressure rise with brake power for different injection timings of CBWD10 emulsion and diesel is illustrated in Figure 5.54. It is apparent that the maximum rate of pressure rise of diesel and the CBWD10 emulsion at different injection timings increases with an increase in the brake power for the entire engine operation. The maximum rate of pressure rise for diesel is found to be about 5.4 bar/ ^{o}CA at full load. The maximum rate of pressure rise for the CBWD10 emulsion for the advanced injection timings of 26 and 24.5^{o}CA bTDC is higher than that of diesel. This may be due to the larger amount of fuel injected; thus higher pressure occurred before the top dead centre (TDC). The maximum rates of pressure rise for the CBWD10 emulsion at 26^{o}CA bTDC, 24.5^{o}CA bTDC, 23^{o}CA bTDC, 21.5^{o}CA bTDC and 20^{o}CA bTDC are found to be approximately, 5.6 bar/^{o}CA, 5.5 bar/^{o}CA, 5.1 bar/^{o}CA, 3.7 bar/^{o}CA and 3.3 bar/^{o}CA respectively, at full load. Retarded injection timing exhibits a lower rate of pressure rise which is due to the increase in the ignition delay compared to that of the original injection timing of the CBWD10 emulsion.

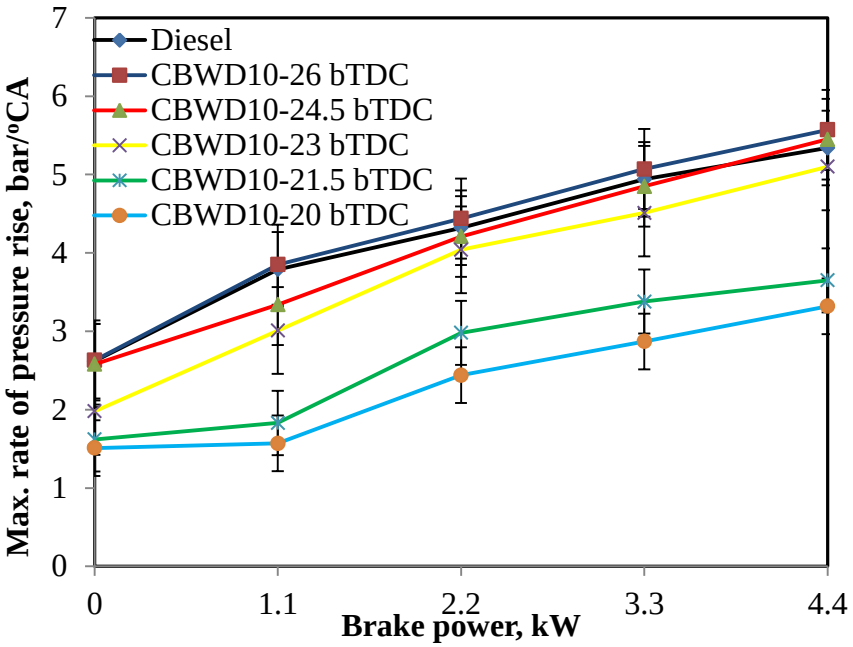

Figure 5.54 Variation of maximum rate of pressure rise with brake power

5.5.3 Performance analysis

5.5.3.1 Brake thermal efficiency (BTE)

Figure 5.55 depicts the variation of BTE with brake power for diesel and the CBWD10 emulsion at two different advanced and two retarded injection timings. The brake thermal efficiency of diesel, and the CBWD10 emulsion for all the injection timings increases with the increase in the brake power. The BTE is lower for the CBWD10 emulsion at the original injection timing than that of diesel at full load, which is due to the lower calorific value and poor air-fuel mixing. The same reason was reported by Scarpete when a diesel-water emulsion fuel was utilised in a single cylinder, four stroke, DI diesel engine [201]. But, the increase in the BTE of the CBWD10 emulsion at the advanced injection timings is due to the high heat release rate. With the advanced injection timings, the peak pressure is reached closer to the TDC, which results in higher effective pressure to do work, which leads to the maximum BTE, than that of the original injection timing. Similar results were presented by Raheman and Ghadge [202] for a biodiesel fuelled DI diesel engine. The CBWD10 emulsion shows a higher brake thermal efficiency at 26°CA bTDC and 24.5°CA bTDC with the advanced injection timings, because of the maximum heat release rate which is followed by the original injection timing, and at the retarded injection timings of 21.5°CA bTDC and 20°CA bTDC at the maximum brake power. Fuel injection starts early, when the fuel injection was advanced to 26°CA bTDC and 24.5°CA bTDC. The value of the BTE at full

load for diesel is found to be about 30.9% and for the CBWD10 emulsion at the original injection timing of 23°CA bTDC, it is about 30.4%. Similarly, for the advanced injection timings of 26°CA bTDC, and 24.5°CA bTDC the efficiencies are found to be about 31.2%, and 30.7%, and for the retarded injection timings of 21.5°CA bTDC, and 20°CA bTDC they are recorded as 30.1%, and 29.9% respectively, at full load.

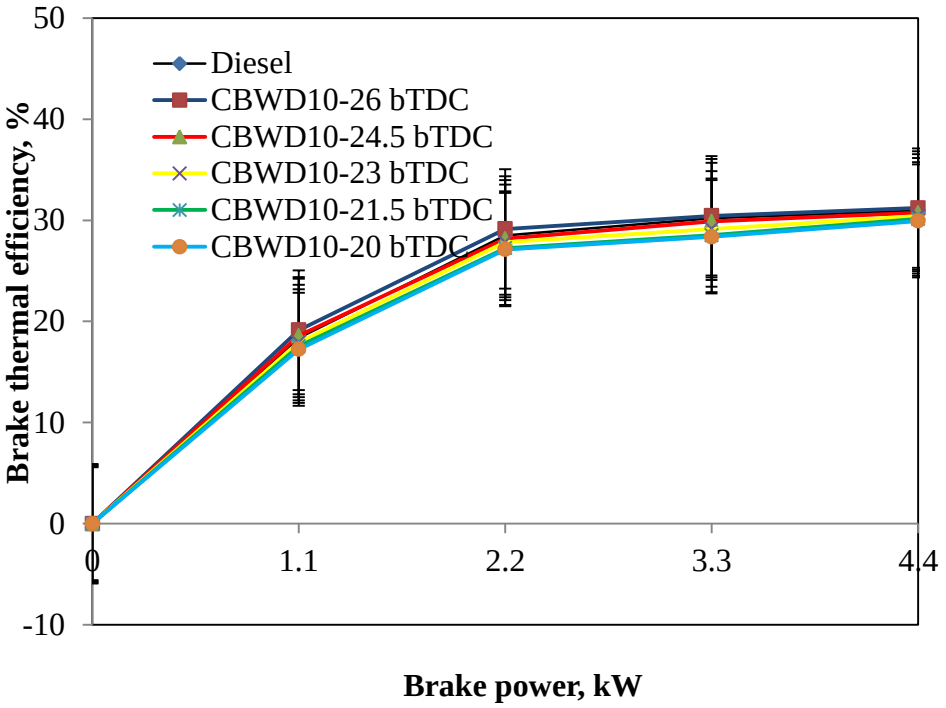

Figure 5.55 Variation of brake thermal efficiency with brake power

5.5.3.2 Brake specific energy consumption (BSEC)

Figure 5.56 portrays the variation of BSEC with brake power for the CBWD10 emulsion at different injection timings and for diesel. The BSEC of diesel decreases with an increase in the brake power. A similar trend is followed by the CBWD10 emulsion for both the advanced injection and retarded injection timings. Generally, the BSEC of the CBWD10 emulsion at the original injection timing is higher than that of diesel at full load. This may be due to the higher density and lower calorific value of the CBWD10 emulsion. Also, because of the presence of water in the emulsion, the heating value decreases, and results in a higher BSEC. Similar results were documented by Alahmer when he tested a single cylinder, four stroke DI diesel engine with a water-diesel emulsified fuel [203]. The value of BSEC for diesel is found to be 10.7 MJ/kWh at full load. The BSEC recoded for the CBWD10 emulsion at different injection timings of 26^{o}CA bTDC, 24.5^{o}CA bTDC, 23^{o}CA bTDC, 21.5^{o}CA bTDC and

20°CA bTDC are found to be about 9.7 MJ/kWh, 10.7 MJ/kWh, 12.3 MJ/kWh, 12.6 MJ/kWh and 13.4 MJ/kWh respectively, at full load.

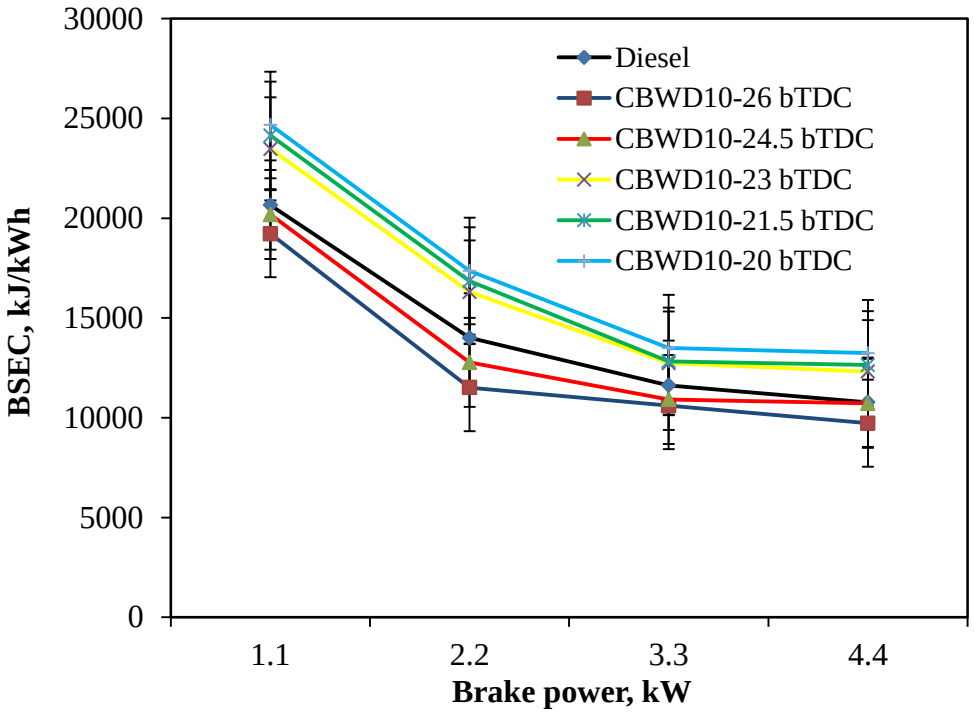

Figure 5.56 Variation of BSEC with brake power

5.5.3.3 Exhaust gas temperature

The variation of the exhaust gas temperature with brake power for different injection timings of the CBWD10 emulsion is illustrated in Figure 5.57. The exhaust gas temperature increases with engine brake power for all the injection timings for the CBWD10 emulsion tested fuel, because of the increased quantity of fuel injected. It is seen that the exhaust gas temperature of the CBWD10 emulsion is higher at the retarded injection timing, than that of the original and advanced injection timings. The exhaust gas temperatures recorded for the CBWD10 emulsion at different injection timings of 26°CA bTDC, 24.5 °CA bTDC, 23°CA bTDC, 21.5°CA bTDC and 20°CA bTDC are found to be about 303°C, 306.3°C, 309.2°C, 314.3°C and 323.9°C respectively, at full load. The exhaust gas temperature is found to be lower for the advanced injection timing, due to the main heat release occurring closer to the TDC in the expansion stroke, which might provide enough time for the hot gases to expand and cool down before the exhaust valves are opened. Similar results were reported by Agarwal et al. [139]. This would cause superior heat utilization and more cooling of the combustion products, and hence, reduced exhaust gas temperature.

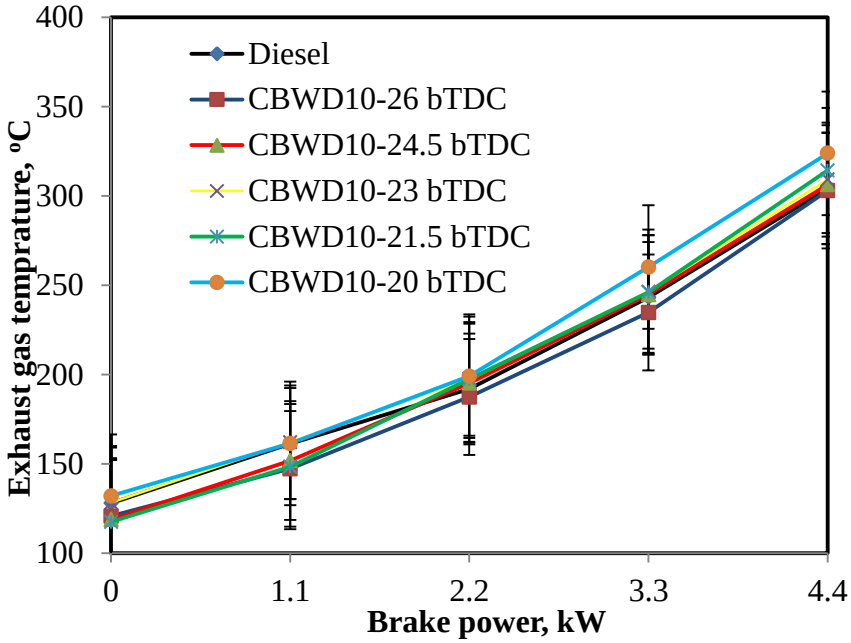

Figure 5.57 Variation of the exhaust gas temperature with brake power

5.5.4 Emission analysis

5.5.4.1 CO emission

In the ideal combustion process, carbon (C) and oxygen (O_2) combine to produce CO_2, while incomplete combustion of carbon leads to the CO formation. The variation of CO emissions at different loads for CBWD10 at different injection timings, and for diesel is depicted in Figure 5.58. The formation of CO generally takes place, when the oxygen present during combustion is insufficient to form CO_2. The CO emission reduces steadily when the engine brake power is increased. When the brake power increases, the combustion temperature increases, due to higher cylinder gas temperatures at the maximum brake power, which leads to more efficient combustion of fuel at higher temperature, producing lower quantities of these emissions and proper fuel–air mixing in the combustion chamber [204]. At the original injection timing, the CO emission is 0.006 g/kWh at the maximum brake power. When the injection timing is advanced, the level of CO emission decreased. By advancing the injection timing, the CO emissions reduce by about 16 – 18 % for the CBWD10 emulsion at full load, compared to that of the original injection timing at full load. The advanced injection timing exhibits a higher cylinder temperature and increased oxidation process between the carbon and oxygen molecules. This causes a reduction in the CO emissions [45]. However, retarding the injection timing increases the CO emission; for the given power output, the concentration of the CO emission for the CBWD10 emulsion is found to be about 0.0052 g/kWh for 26°CA

bTDC, and 0.0054 g/kWh for 24.5°CA bTDC respectively. The values of the CO emission are approximately 0.010 g/kWh for 21.5°CA bTDC and 0.013 g/kWh for 20°CA bTDC respectively, at full load, whereas it is 0.005 g/kWh for diesel, at full load. All the CO values for the CBWD10 emulsion are higher than those of diesel operation, due to the presence of the carbon black particles.

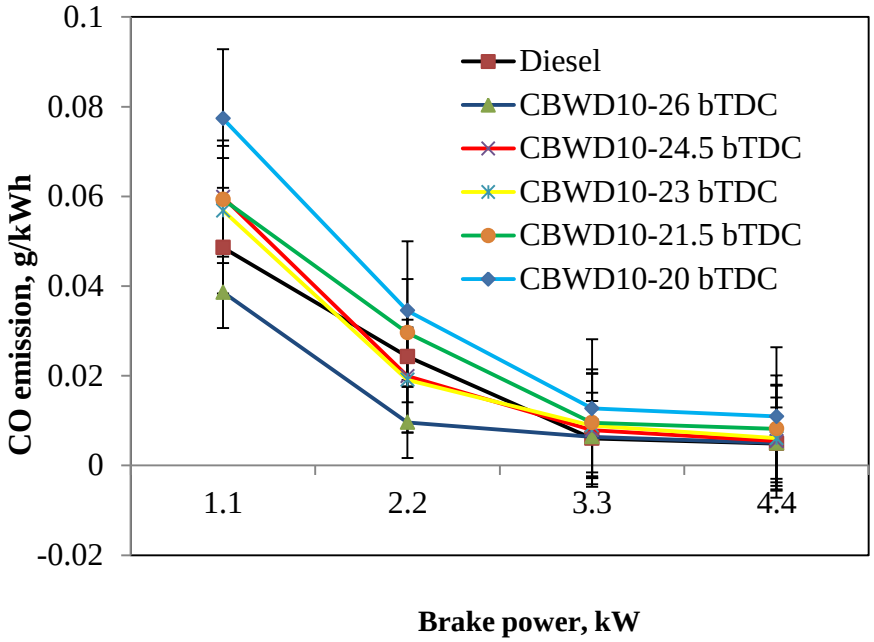

Figure 5.58 Variation of CO emissions with brake power

5.5.4.2 HC emission

Figure 5.59 shows the variation of the HC emission for the CBWD10 emulsion at different injection timings, compared to those of the original injection timing and diesel. The HC emission for the CBWD10 emulsion at all injection timings is higher than that of diesel operation due to incomplete combustion, because some carbon black particles do not combust properly in the combustion chamber. The increase in the HC emission of the CBWD10 emulsion compared to that of diesel is due to the presence of water in the CBWD10 emulsion fuel, because the water particles reduce the auto ignition characteristics of the CBWD10 emulsion, and increase the cooling effect in the lean fuel air mixture zone of the engine cylinder. Similar results and reasons were reported by Kannan et al., when they fuelled diestrol oil at varying injection pressures and injection timings in a single cylinder, four stroke CI engine [205]. It is seen that the CBWD10 emulsion gave a lower HC emission for the advanced injection timing (26°CA bTDC and 24.5°CA bTDC) at full load compared to those of the other injection timings, but higher than that of diesel. Advancing the injection

timing causes an earlier start of combustion relative to the TDC. Because of this, the cylinder charge, being compressed as the piston moves to the TDC, had relatively higher temperatures, and thus lowered the HC emissions [206]. With the retarded injection timings, the HC emission is found to be higher throughout the engine operation. The HC emission at the maximum brake power for the diesel operation at 23°CA bTDC is found to be about 0.020 g/kWh, and for CBWD10 emulsion at the original injection timing of 23°CA bTDC is found to be about 0.028 g/kWh, and at the maximum brake power for the retarded injection timings of 21.5°CA bTDC and 20°CA bTDC, it is 0.032 g/kWh and 0.038 g/kWh respectively. Similarly, for the advanced injection timings of 26°CA bTDC and 24.5°CA bTDC, the values are approximately 0.021 g/kWh and 0.025 g/kWh at the maximum brake power, respectively.

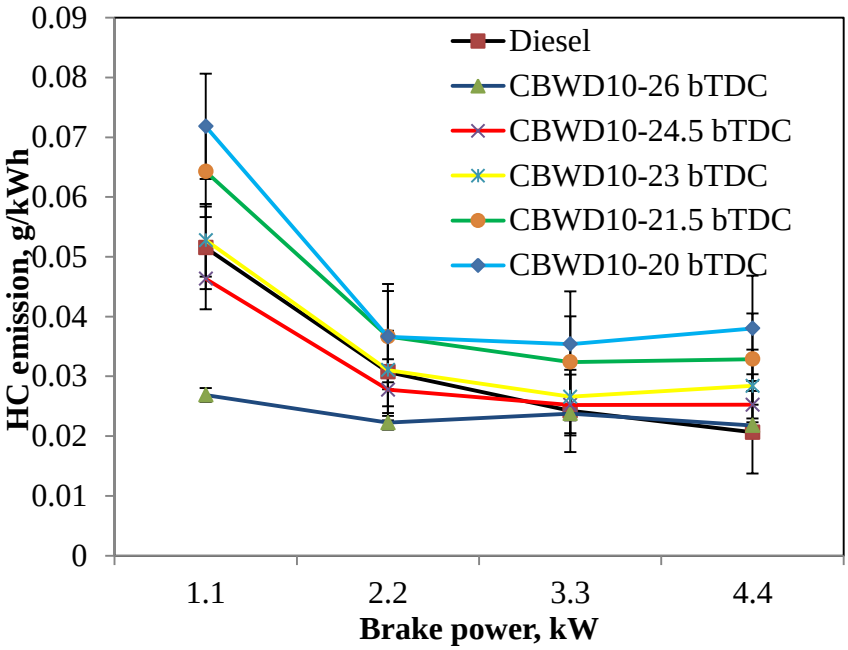

Figure 5.59 Variation of HC emission with brake power

5.5.4.3 NO emission

This is the most important emission parameter of the diesel engine. It is the most harmful gaseous emission from engines, and its reduction is always the target for engine researchers and manufacturers. Thermal NO refers to the NO formed through the high temperature oxidation of nitrogen (N_2) in the combustion chamber [205, 207]. The variation of the NO emission with brake power for the original, advanced and retarded injection timings of the engine fuelled with the CBWD10 emulsion and diesel is shown in Figure 5.60.

The NO emission for the CBWD10 emulsion is found to be lower than that of diesel operation, due to the presence of water in the emulsion and the lower incylinder temperature [80]. The NO emission at the advanced injection timings of 26°CA bTDC and 24.5°CA bTDC are significantly higher at all values of brake power; this is because of faster combustion and higher cylinder gas temperatures [205]. The NO emission is found to be about 2.8 g/kWh at full load for the original injection timing of 23°CA bTDC, whereas for the retarded injection timing of 21.5°CA bTDC it is found to be about 2.7 g/kWh, and at 20°CA bTDC it is found to be about 2.6 g/kWh at full load. Similarly, the NO emission for the advanced injection timing of 26°CA bTDC is found to be about 3.0 g/kWh and at 24.5°CA bTDC it is found to be about 2.8 g/kWh at full load. The NO emissions at the retarded injection timings are significantly lower at all loads, because more fuel burns after the TDC. Because of this, the cylinder charge being compressed as the piston moves to the TDC, had relatively higher temperatures, and thus, increased the NO emissions at the maximum brake power than that of the original injection timing. This statement is in good agreement with the results of Prasad et al., who investigated the effect of injection timing on the performance and emissions of a palm methyl ester blend fuelled DI diesel engine operated at different loads [208].

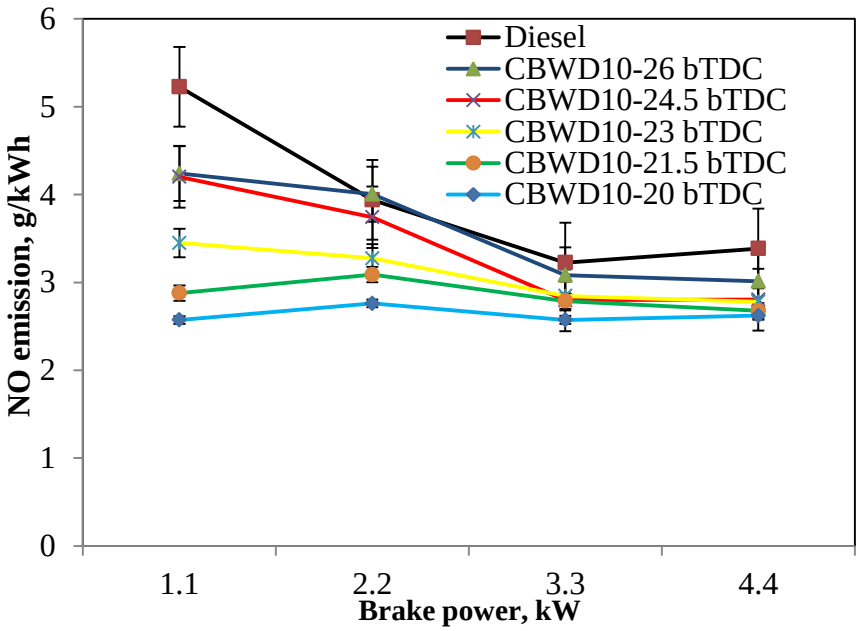

Figure 5.60 Variation of NO emission with brake power

5.5.4.4 Smoke emission

The formation of smoke primarily results from the incomplete burning of the hydrocarbon fuel and the partially reacted carbon content in the liquid fuel. The results of smoke opacity with brake power are depicted in Figure 5.61 for the CBWD10 emulsion at different injection timings and for diesel respectively. The smoke emission increases with the increase in the engine brake power. As the load increases, more fuel is injected, and this increases the smoke formation [209]. The CBWD10 emulsion at all injection timings gave higher smoke emission than that of diesel due to incomplete combustion. This may be due to the higher C/H ratio of the CBWD10 emulsion than that of diesel. It may also be due to slow combustion as a result of the poor mixture formation of the emulsion. Similar results were documented by Armas [210] when a light duty DI diesel engine was operated with a water-diesel emulsion fuel. The higher smoke values at the maximum brake power are due to the longer combustion duration and higher carbon percentage. The smoke values for the CBWD10 emulsion at 26, 24.5, 23, 21.5 and 20 ^{o}CA bTDC are measured as 40.6%, 41.4%, 45.8%, 51.2% and 54.4% respectively.

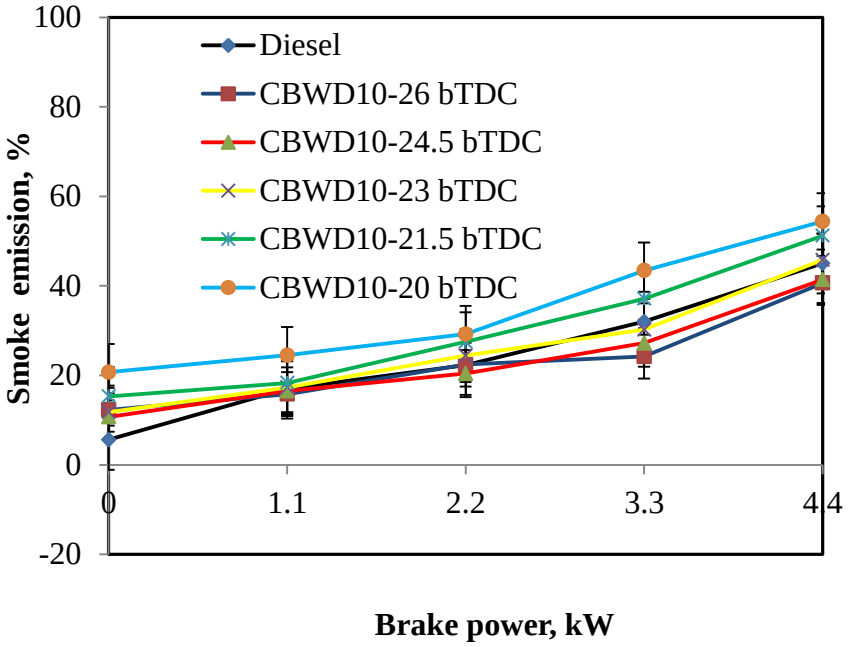

Figure 5.61 Variation of smoke emission with brake power

5.5.5 Summary

From the results and discussion, it is concluded that the engine could successfully run with the CBWD10 emulsion at the original (23 ^{o}CAbTDC), two advanced and two retarded

injection timings. Based on the results of the combustion, performance and emission parameters, the advanced injection timing of 26^{o}CAbTDC gave better results compared to those obtained for other injection timings. The brake thermal efficiency at full load for the CBWD10 emulsion operated at 26^{o}CAbTDC is higher by about 1.3% and 2.3% than that of diesel, and the CBWD10 emulsion at the original injection timing respectively. The NO emission is found to be lower by about 21% compared to that of diesel. Table 5.5.1 provides the values of the important engine parameters obtained for the CBWD10 emulsion operated at different injection timings and for diesel at full load.

Table 5.5.1 Values of the combustion, performance and emission parameters at full load for different injection timings of CBWD10 emulsion

S.No.	Parameters	26°CA bTDC	24.5°CA bTDC	23°CAbTDC	21.5 °CAbTDC	20°CAbTDC
Combustion parameters						
1	Maximum cylinder pressure, (bar)	78.2	73.0	75.2	72.4	71.1
2	Ignition delay, (°CA)	8.3	9.3	10.1	11.9	12.8
3	Max. heat release rate, (J/°CA)	56.14	55.31	53.4	52.6	52.21
4	Combustion duration, (°CA)	37.38	38.13	38.52	39.36	40.5
5	Maximum rate of pressure rise, (bar/°CA)	5.57	5.45	5.1	3.65	3.32
6	90% Mass fraction burned, (°CA)	392.2	391.1	389.1	388.2	287.1
Performance parameters						
1	Brake thermal efficiency, (%)	31.2	30.7	30.4	30.1	29.9
2	Brake specific energy consumption, (kJ/kWh)	9726.9	10719	12316.9	12643.6	13240.8
3	Exhaust gas temperature, (°C)	303.04	306.3	309.1	314	323.9
Emission Parameters						
1	CO emission, (g/kWh)	0.0049	0.0050	0.0054	0.0060	0.010
2	HC emission, (g/kWh)	0.020	0.0218	0.0252	0.0284	0.0380
3	NO emission, (g/kWh)	3.01	2.8	2.78	2.67	2.6
4	Smoke emission, (%)	40.6	41.4	45.8	51.2	54.4

5.6 Combined effects of Compression ratios, nozzle opening pressures and injection timings

5.6.1 General

In this work the combined effects of compression ratio, nozzle opening pressure and injection timing were studied further. The results of the combustion, performance and emission of the engine fuelled with the CBWD10 emulsion by varying injection timing, nozzle opening pressure and compression ratio simultaneously were compared with the diesel data, obtained for the original compression ratio, injection timing and nozzle opening pressure of the engine, analysed and presented in this section.

5.6.2 Combustion analysis

5.6.2.1 Cylinder pressure with crank angle

Figure 5.62 depicts the variation of the cylinder pressure with the crank angle for the engine running on the CBWD10 emulsion at different compression ratios with different nozzle opening pressures and injection timings, and diesel at full load. It can be observed from the figure that, the cylinder pressure is higher at the compression ratio of 18.5 compared to that of standard and lower compression ratios. This may be due to higher combustion temperature and increased air temperature helps in better atomization of fuel, proper air-fuel mixing which contributes to complete combustion [45]. The peak cylinder occurs for diesel is 79.4 bar at full load. It can also be observed from the figure, that the combustion starts earlier in the range between 1 and 4^{o}CA for the CBWD10 emulsion, with the different compression ratios and at all three nozzle opening pressures, injection timings, compared to that of diesel at full load. At the lower compression ratio of 16.5, the peak cylinder pressure is found to be lower in the range of 65.0 to 76.7 bar compared to that of diesel operation at full load. Similar reason was mentioned by Kannan and Anand [179] in their investigation which was carried out in a diesel engine, fuelled with biodiesel obtained from waste cooking oil. At 17.5 compression ratio the cylinder pressure for the CBWD10 emulsion is lower by about 5.28% at standard nozzle opening pressure and injection timing than that of diesel, which is 1.2^{o}CA the combustion starts earlier compared to that of diesel at full load. But, at advanced injection timing of 26^{o}CA bTDC and 220 bar nozzle opening pressure, the cylinder peak pressure is increases by about 2 to 7.5% than that of other injection timings and nozzle opening pressures at full load condition. The peak cylinder pressure for the CBWD10 emulsion is found to be in the range of 73.0 to 78.5 bar at full load, respectively.

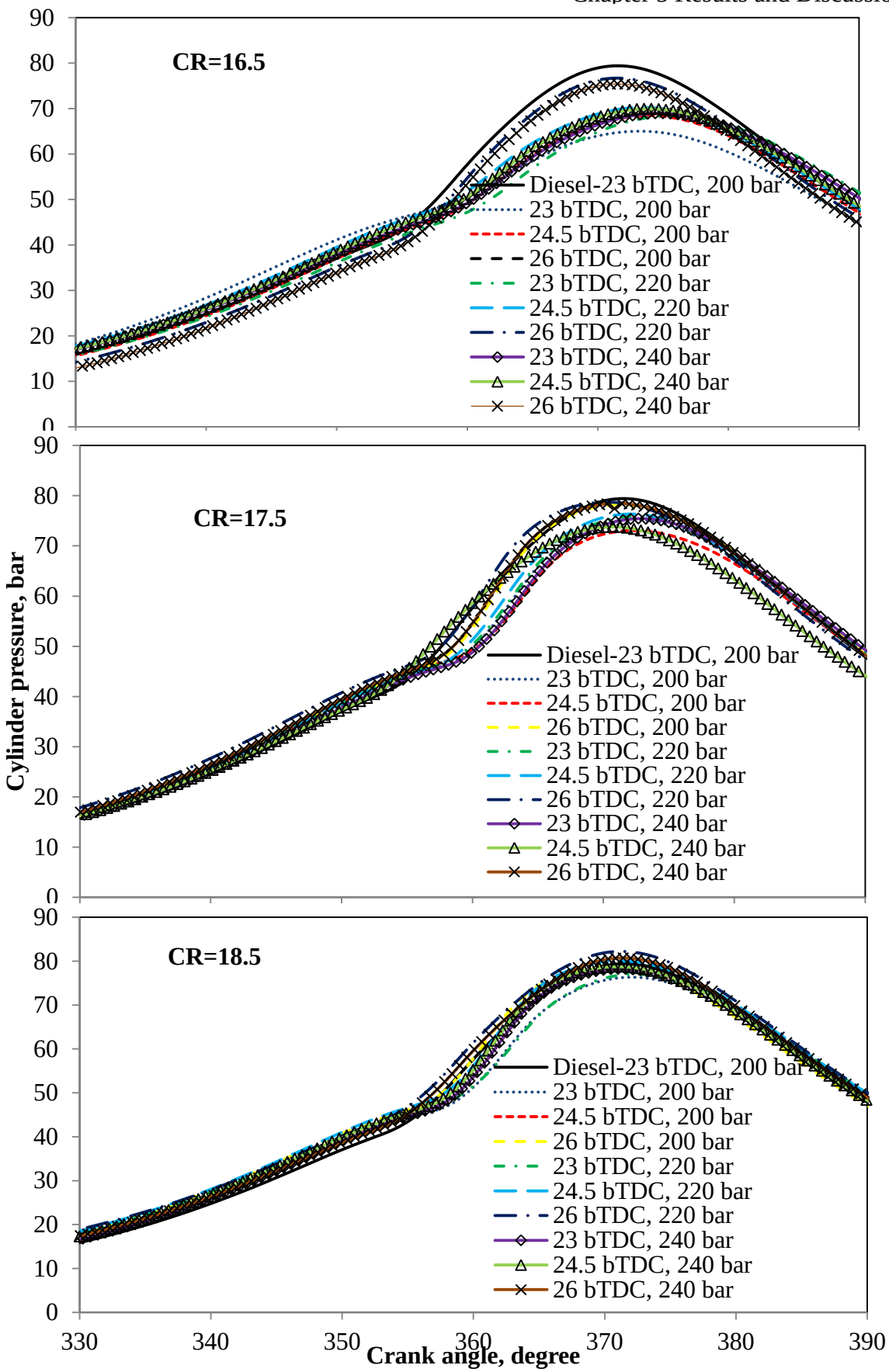

Figure 5.62 Pressure crank angle diagram at different compression ratios, nozzle opening pressures and injection timings

At 18.5 compression ratio, the peak cylinder pressure for the CBWD10 emulsion is higher by about 1.7 % than that diesel at full load. The peak cylinder pressure for the CBWD10 emulsion is found to be in the range of 78.2 to 80.7 bar at full load, respectively. It is seen from the figure, that among all the tested compression ratios and at 26^{o}CA bTDC advanced injection timings and 220 bar nozzle opening pressure, with the compression ratio of 18.5 operation produced the highest cylinder pressure, which is earlier by 2.9 and 1^{o}CA than those of diesel. It can also be observed that, the peak cylinder pressure for the CBWD10 emulsion is about 80.4 bar higher at 220 bar nozzle opening pressure. This may be due to the improved spray pattern of the CBWD10 emulsion. Beyond 220 bar nozzle opening pressure, the peak cylinder pressure decreases for 240 bar nozzle opening pressure, due to a lesser heat release rate during combustion, owing to a lesser spray penetration inside the combustion chamber.

5.6.2.2 Ignition delay

Figure 5.63 portrays the variation of ignition delay with brake power at different compression ratios with different nozzle opening pressures and injection timings for the CBWD10 emulsion and diesel. The ignition delay of diesel decreases with the increase in brake power and the CBWD10 emulsion follow the same trend for different compression ratio, nozzle opening pressures and injection timings. The ignition delay is found to be lower with the increase in the brake power, compression ratio and advancement in the injection timing. The reduction in the ignition delay in these conditions might be the result of a higher combustion chamber wall temperature at the time of injection and the reduced exhaust gas dilution [211, 212]. The ignition delay can be observed from the figure for diesel is 9.31^{o}CA at the full load, respectively.

At the lower compression ratio of 16.5, the ignition delay for the CBWD10 emulsion is found to be longer by about 0.91 to 2.31^{o}CA than that diesel at full load. This may be due to the lower cylinder temperature. It is apparent from the figure that, at full load condition, the ignition delay of the CBWD10 emulsion is found to be lower at advanced injection timings and 220 nozzle opening pressure due to better atomization and proper mixing of the fuel droplets with air. At the original compression ratio of 17.5, the ignition delay is lower compared to that of lower compression ratio and higher compared to that of higher compression ratio. The ignition delay for the CBWD10 emulsion is found to be shorter 0.3 to 0.34^{o}CA at advanced injection timings with 220 nozzle opening pressure and is found to be longer in the range of 0.5 to 1.0^{o}CA other injection timings and nozzle opening pressures than that of diesel at full load, respectively.

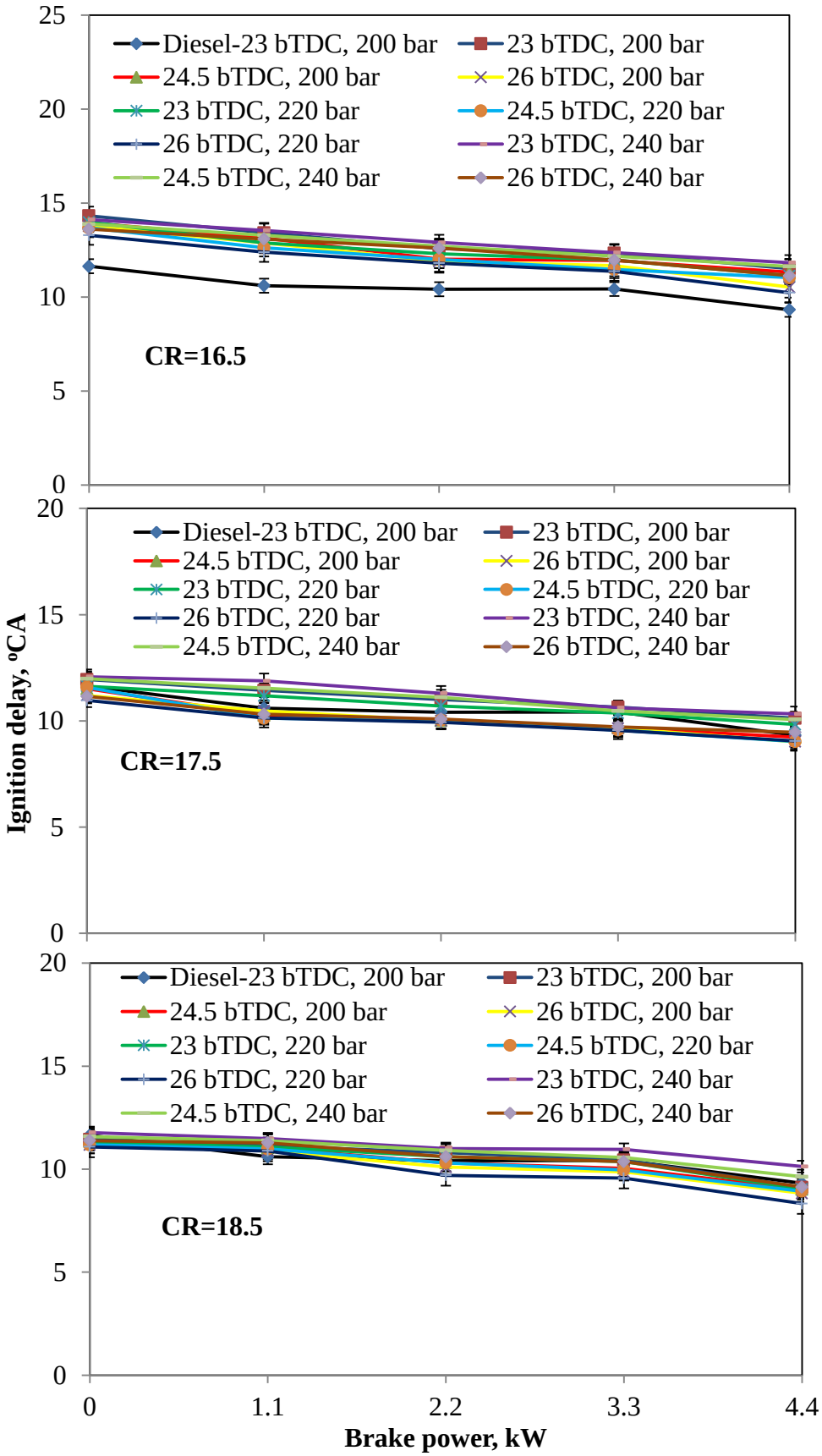

Figure 5.63 Ignition delay with brake power at different compression ratios, nozzle opening pressures and injection timings

At the higher compression ratio of 18.5, the ignition delay for the CBWD10 emulsion is shorter compared to that of diesel and other compression ratio. The ignition delay for the CBWD10 emulsion at compression ratio of 18.5 is found to be shorter in the range of 0.1 to 1.1^{o}CA at full load, respectively. Among all the tested compression ratios, nozzle opening pressures and injection timings, the minimum ignition delay period of 8.3^{o}CA is observed for the CBWD10 emulsion, with the compression ratio of 18.5, 220 bar pressure and injection timing of 26^{o}CA bTDC. The reduction in the ignition delay period is mainly due to the increased cylinder gas temperature, at a higher compression ratio and a higher cetane number of the CBWD10 emulsion, compared to that of diesel.

5.6.2.3 Heat release rate with crank angle

Figure 5.64 depicts the variation of the heat release rate with crake angle for the CBWD10 emulsion at different compression ratios viz; 16.5, 17.5 and 18.5 with different nozzle opening pressures viz; 200, 220 and 240 bar and injection timings of 23, 24.5 and 26°CA bTDC at full load and compared to diesel. Because of the vaporization of the fuel accumulated during the ignition delay period, at the beginning a negative heat release is observed and after combustion, this behaviour becomes positive.

It can also be observed from the figure, that the maximum heat release rate is found to be higher at the higher compression ratio of 18.5 compared to original and lower compression ratio of 16.5 at full load. This may be due to improve the combustion [213]. At the compression ratio of 16.5 the heat release rate for the CBWD10 emulsion is found to be lower by about 1.2% to 7.5% than that of diesel. This may be due to poor combustion. It can also be observed from the figure that the heat release rate at compression ratio of 17.5 with 26^{o}CAbTDC advanced injection timings and 220 nozzle opening pressure has improved compared to other nozzle opening pressures. This could be attributed to the greater accumulation of fuel, because of the ignition delay as the injection of fuel takes place earlier in the compression process, and the maximum heat release rate during the premixed combustion phase owing to the higher nozzle opening pressure. Similar reasons were documented by Sukumar et al., for the results they obtained with linseed oil methyl ester as an alternative fuel in a DI diesel engine with different injection pressures [214]. The heat release rate at the compression ratio of 17.5 is found to be higher by about 1.5% to 6% with advanced injection timing and 220 nozzle opening pressure than that of diesel.

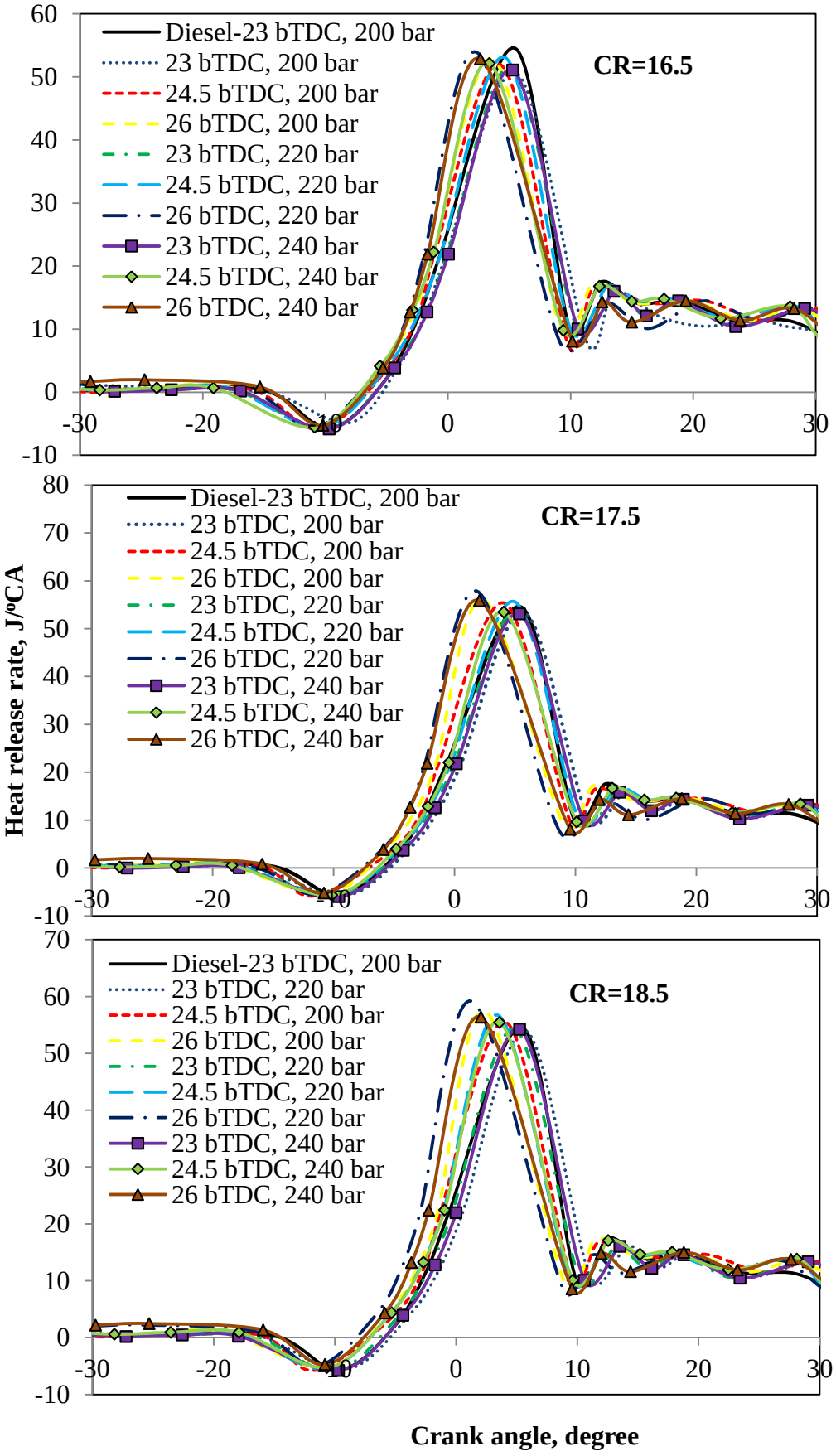

Figure 5.64 Heat release rate with crank angle at different compression ratios, nozzle opening pressures and injection timings

Similarly, at the compression ratio of 17.5, the heat release for the CBWD10 emulsion is found to be lower 1.1% to 2.64% at other injection timings and nozzle opening pressures than that of diesel. At the compression ratio of 18.5, the heat release rate for the CBWD10 emulsion is found to be higher by about 0.4% to 9% than that of diesel at full load, respectively. This may be due to premixed phase of combustion decreases with respect to increase in compression ratio. Also, the compression ratio increases change the duration of combustion. Usually higher compression ratio offers shorter duration of combustion and cause better performance. Similar reasons were presented by Senthil Kumar et al., for the results they obtained for mahua methyl ester fuelled in a DI diesel engine with combined effect of different compression ratios, injection pressures and injection timings [215].

5.6.2.4 Combustion duration

Figure 5.65 portrays the variation of the combustion duration with brake power for the CBWD10 emulsion for the combined effects of varying compression ratios, nozzle opening pressures and injection timings and compared to that of diesel at full load. It can also be observed from the figure that the combustion duration increases with increasing brake power for all the compression ratios, nozzle opening pressures and injection timings of the CBWD10 emulsion as trend diesel results. The combustion duration decreases with increasing the compression ratio. At the compression ratio of 18.5, the combustion duration is lower compared to that of original and lower compression ratio. This may be due to high heat release rate prevailing inside the cylinder [36]. The combustion duration for diesel at standard parameters is 38.16^{o}CA at full load, respectively.

It can be observed from the figure, at the compression ratio of 16.5, the values of combustion duration for the CBWD10 emulsion are found to be longer in the range of 40.64 to 47.4^{o}CA with different nozzle opening pressures and injection timings. The combustion duration at the compression ratio of 16.5 is longer than that of diesel at full load, respectively. As the calorific value of the CBWD10 emulsion is lower than that of diesel, a greater quantity of fuel is consumed to maintain the engine speed constant at various loads. Hence, the higher total fuel consumption is the cause for the longer combustion duration of the CBWD10 emulsion than that of diesel. Similar reasons were correlated by Arulmozhi et al., [216] for the results they have obtained when they ran diesel-biodiesel-ethanol blends fuel in diesel engine.

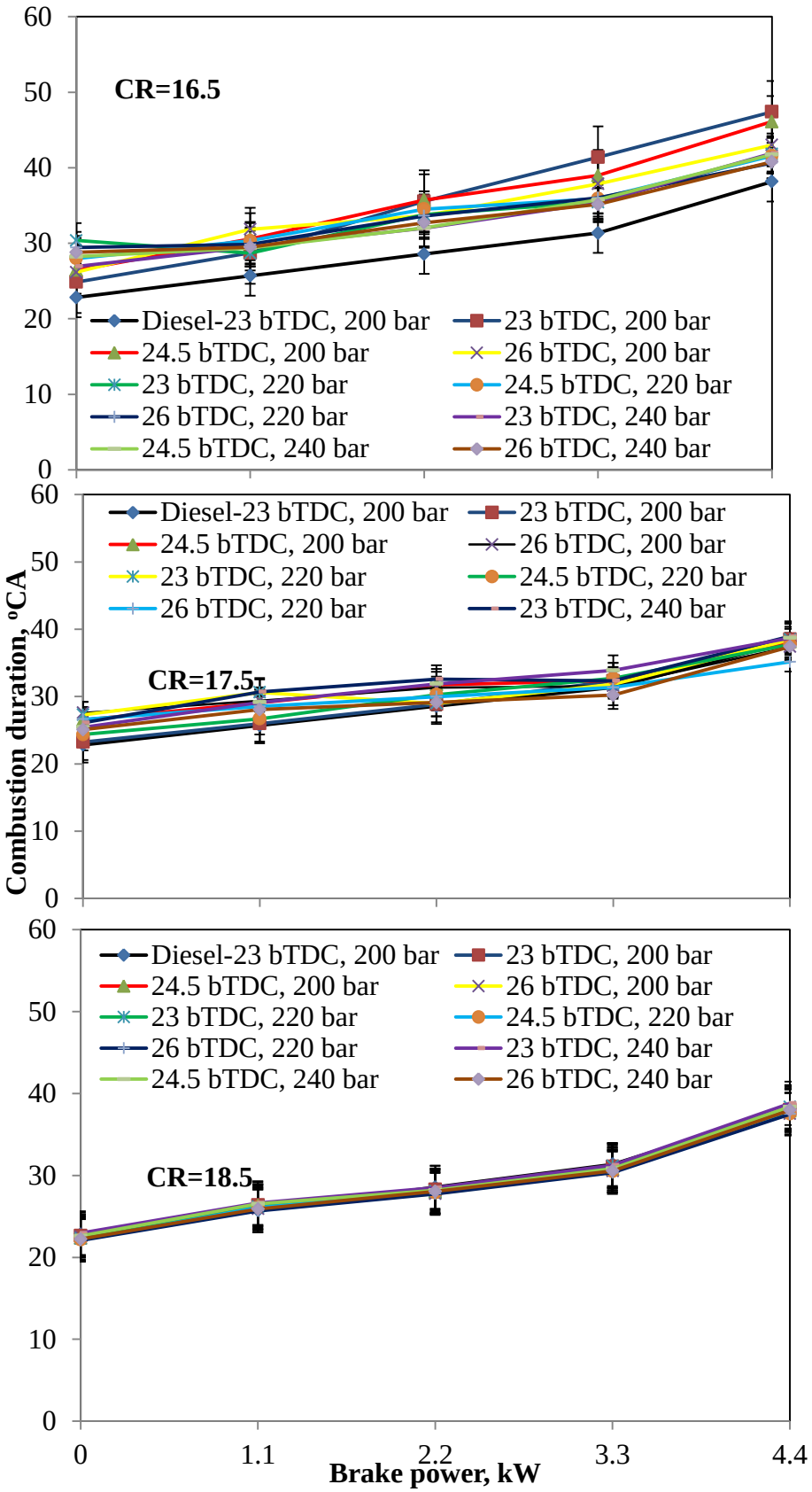

Figure 5.65 Combustion duration with brake power at different compression ratios, nozzle opening pressures and injection timings

At the standard 17.5 compression ratio, the combustion duration is found to be shorter in the range of 35.1 to 37.8^{o}CA than that of diesel at full load with the advanced injection timing of 26^{o}CA and 220 bar nozzle opening pressure, which is attributed to a shorter ignition delay. At 18.5 compression ratio and at full load for the CBWD10 emulsion, the values of combustion duration are found to be lower in the range of 37.4 to 38.1^{o}CA with all injection timings and nozzle opening pressures than that of diesel. It can be observed from the figure that, the higher compression ratio the combustion duration is lower compared to those of standard and lower compression ratios. This may be due to shorter ignition delay and maximum heat release rate. Beyond 220 bar nozzle opening pressure the combustion duration is longer, this may be due to, too high injection pressure may be responsible to higher velocity of droplet which will leave away without mixing air properly with fuel as a results poor combustion. Similar reasons were indicated by Sharma et al., for the results they have obtained in a single cylinder, four stroke, DI diesel engine [217].

5.6.2.5 Maximum heat release rate

The variation of the maximum heat release rate with brake power for the CBWD10 emulsion at different compression ratios viz; 16.5, 17.5 and 18.5 with different nozzle opening pressures viz; 200, 220 and 240 bar and injection timings 23 24.5 and 26^{o}CAbTDC and diesel is depicted in Figure 5.66. It can be observed from the figure that, at all the compression ratios the maximum heat release rate increases with increase in the brake power same trend follows the CBWD10 emulsion and diesel. The maximum heat release rate is found to be approximately 54.5 J/^{o}CA for the diesel at full load, respectively. It can be observed from the figure that at a higher compression ratio, the maximum heat release rate is higher compared to that of standard and lower compression ratio.

At the compression ratio of 16.5, the maximum heat release rate for the CBWD10 emulsion is found to be in the range of 50.6 to 53.8 J/deg, which is lower than that of diesel respectively, at the full load. But, at the advanced injection timing of 26^{o}CAbTDC, with 220 bar nozzle opening pressure, the maximum heat release rate is increased. This may be due to proper mixing of fuel with air as a result a better combustion in the entire combustion chamber.

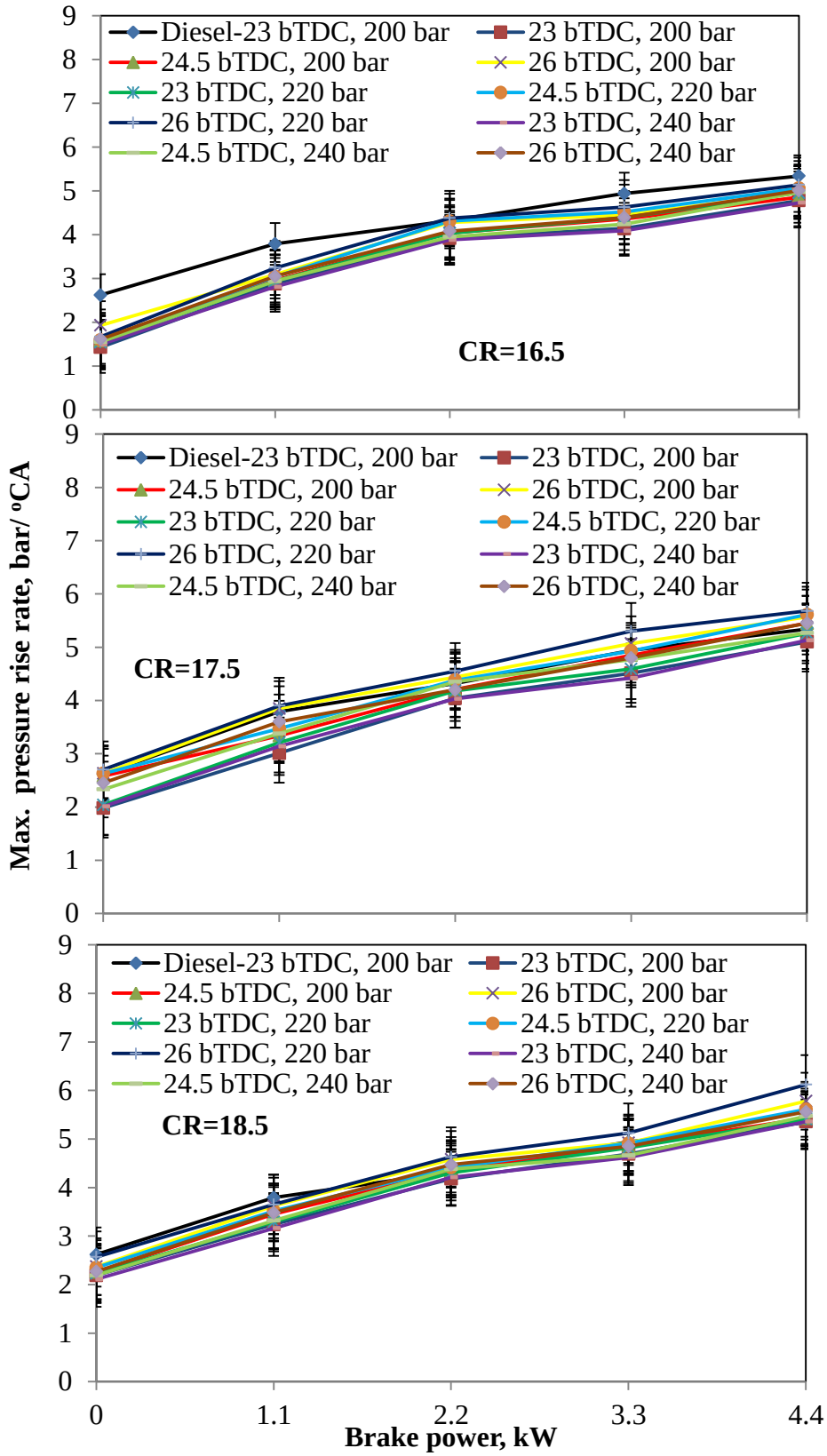

Figure 5.66 Max. heat releases rate with brake power at different compression ratios, nozzle opening pressures and injection timings

For the CBWD10 emulsion, the maximum heat release rate at 17.5 compression ratio with the standard injection timing and nozzle opening pressure is found to be by about 1.8% lower than that of diesel, because of lower heating value and poor combustion. But, compared to lower compression ratio, the maximum heat release rate is improved due to a higher combustion temperature. At the higher compression ratio of 18.5 with different nozzle opening pressures and injection timings, the maximum heat release rate for the CBWD10 emulsion is higher in the rage of 54.4 to 59.1 J/deg than that of diesel at full load, respectively. It can also be observed from that, the figure at a higher compression ratio with the advanced injection timing of 26^{o}CAbTDC and 220 bar nozzle opening pressure, the maximum heat release rate is found to be about 8.6% higher than that of diesel at full load.

5.6.2.6 Maximum rate of pressure rise

Figure 5.67 depicts the variation of the maximum rate of pressure rise with brake power for the CBWD emulsion at different compression ratios with different injection timings and nozzle opening pressure, and diesel. It can be observed from the figure that, the maximum rate of pressure rise for diesel and the CBWD10 emulsion at all compression ratios increases with increase in brake power for the entire engine operation. The maximum rate of pressure rise for diesel is found to be about 5.4 bar/ ^{o}CA at the full load. With the lower compression ratio of 16.5, the peak cylinder pressure for the CBWD10 emulsion are found to be lower compared to that of diesel at all nozzle opening pressures and injection timings, and at higher compression ratios, the trend is the opposite. It can also be observed that, the peak cylinder pressure increases with the increase in injection timing from 23 to 26^{o}CAbTDC. At the advanced injection timing, the CBWD10 emulsion shows a faster premixed combustion, which leads to a higher peak cylinder gas pressure. At the compression ratio of 16.5 and all three injection timings and nozzle opening pressure, the maximum cylinder pressure of the CBWD10 emulsion is found to be lower in the range between 4.7 and 5.1 bar compared to that of diesel operation at full load. At the compression ratios of 17.5, and 18.5, and at standard and advanced injection timings, the maximum cylinder pressure values of the CBWD10 emulsion are higher in the range of 5.4 to 6.1 bar compared to that of diesel operation at full load. This may be due to the reduction in the clearance volume, which increases the density of the cylinder gases during the burning process. This increases the peak cylinder pressure and temperature. Beyond 220 bar nozzle opening pressure, the peak cylinder pressure decreases at all compression ratios. This may be due to very high velocity fine particle improperly mix with the air as a result poor air-fuel mixing.

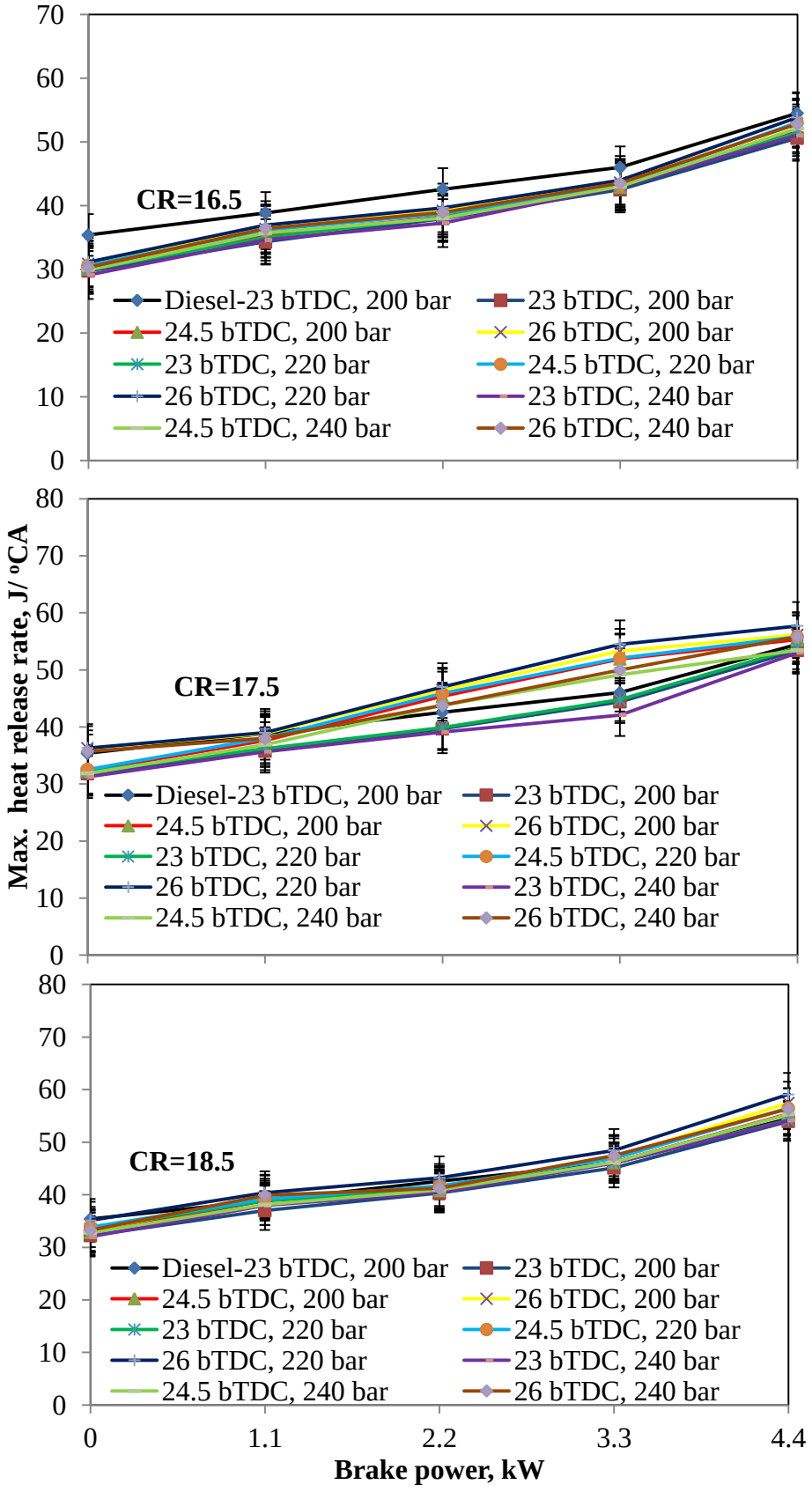

Figure 5.67 Max. pressure rise rate with brake power at different compression ratios, nozzle opening pressures and injection timings

5.6.3 Performance analysis

5.6.3.1 Brake thermal efficiency (BTE)

The variation of brake thermal efficiency with brake power for the CBWD10 emulsion at combined different compression ratios (16.5, 17.5 and 18.5), injection timings and nozzle opening pressure are compared with the diesel data is depicted in Figure 5.68. The brake thermal efficiency increases with the increase in the brake power. The brake thermal efficiency with the original compression ratio, injection timing and nozzle opening pressure at the full load of the CBWD10 emulsion is lower by about 1.1% compared to that of diesel, which may be due to the combined effect of higher viscosity, high density, lower heating value and poor air fuel mixture formation. The effect of variating the compression ratios on brake thermal efficiency indicates that, increasing compression ratio improves the engine efficiency. Similar results were documented by Hirkude and Padalkar [218] for the results obtained for biodiesel fuelled DI diesel engine with different compression ratios. It can also be observed from these figures that the brake thermal efficiency is about 7.8 % to 4.3 % lower than that of diesel for the 16.5 compression ratio for all different injection timings and nozzle opening pressures at the full load. This may be due to poor mixture formation and high specific fuel consumption.

At the original compression ratio of 17.5, the brake thermal efficiency at the advanced injection timing of 26^{o}CA bTDC with 200 bar and 24.5^{o}CA bTDC, 26^{o}CA bTDC with 220 bar nozzle opening pressure is higher by about 1.4%, 0.4% and 3.1% compared to that of diesel due to improved their poor atomization and combustion characteristics. The brake thermal efficiency of the engine fuelled with the CBWD10 emulsion at the compression ratio of 18.5 is higher by about 1.6 % to 5.1% than that of diesel with different injection timings and nozzle opening pressures at the full load. Because, increasing the compression ratio will increase the operating temperature and hence there is an increase in the brake thermal efficiency at higher compression ratios. At a higher compression ratio, improvement the combustion temperature and hence the thermal efficiency is higher. Similar results were indicated by Kassaby [219] in their research article.

Overall, from these figures, it is found that at the compression ratio of 18.5 the brake thermal efficiency is found to be higher about 5.1% at the advanced injection timing of 26^{o}CA bTDC and 220 bar than that of diesel at the full load. This may be due to the fact that at the advanced injection timing, air-fuel takes a shorter duration for proper formation in

combustion process and resulting in improved BTE [215]. At 220 bar, the CBWD10 emulsion might give the better combustion because finer fuel droplets providing more surface area and better mixing of the fuel-air, and improved fuel spray characteristics. The brake thermal efficiency at 18.5 compression ratio is found to be higher by about 1.7% to 5.1% than that of diesel at the full load respectively. It is also seen that increasing the nozzle opening pressure above 220 bar decreases the BTE at the maximum brake power. This may be due to a decrease in the droplet size of the fuel. A smaller fuel droplet will have lesser momentum that will affect the fuel distribution in the air. The decrease in the relative velocity of the fuel corresponding to air, resulted in poor air entrainment leading to incomplete combustion. Similar reason was claimed Jaichandar and Annamalai, when they have fuelled biodiesel in single cylinder, four stroke, DI diesel engine [220].

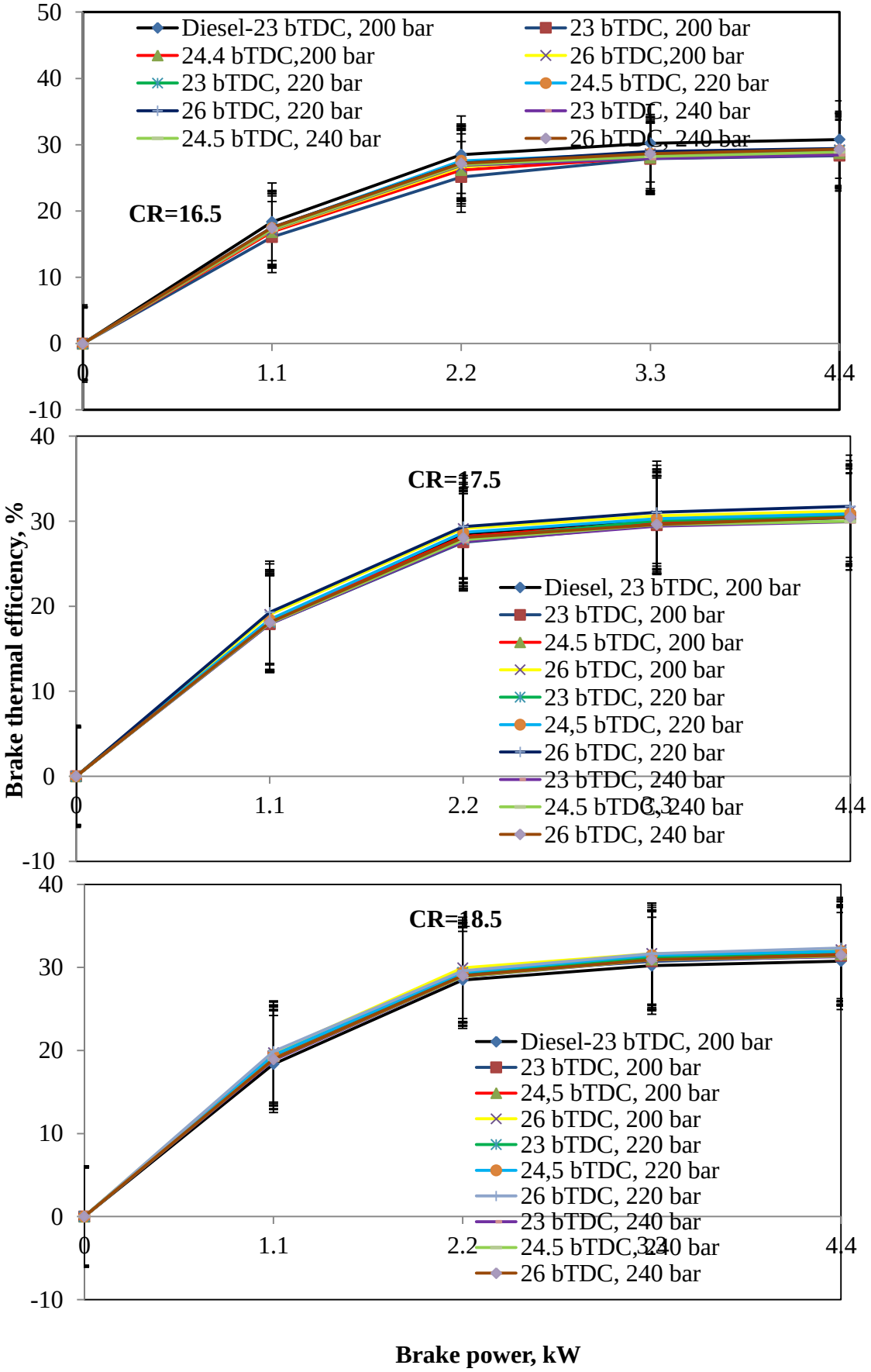

Figure 5.68 Brake thermal efficiency with brake power at different compression ratios, nozzle opening pressures and injection timings

5.6.3.2 Brake specific energy consumption (BSEC)

Figure 5.69 portrays the variation of BSEC with brake power for the CBWD10 emulsion at combined effects of different compression ratios viz; 16.5, 17.5 and 18.5, nozzle opening pressures viz; 200, 210, 220, 230 and 240 bar and injection timings of 23, 24.5 26^{o}CA bTDC and diesel. The BSEC of diesel decreases with the increase in the brake power. Similar trend is followed by the CBWD10 emulsion at all compression ratios, nozzle opening pressures and injection timings. The value of BSEC for diesel is approximately 10.7 MJ/kWh at full load. As illustrated in the figures, the BSEC of the CBWD10 emulsion is higher compared to that of diesel without change in any engine modification due to the lower calorific value and higher density.

At the compression ratio of 16.5 the BSEC of the CBWD10 emulsion at full load is higher by about 5.8% to 19.8% than that of diesel for all the injection timings and nozzle opening pressure due to incomplete combustion. At the original compression ratio of 17.5, the BSEC is lower by about 2% to 3% than that of diesel with the advanced injection timing of 26^{o}CA bTDC at full load, which is due to the better air-fuel formation. The BSEC decreases with the increase in compression ratio. A decrease in BSEC with an increase in compression ratio could be due to the decreased ignition delay and increased thermal efficiencies of the engine resulting in a smoother engine operation at a higher compression ratio. At the compression ratio of 18.5, the BSEC lower by about 1.8% to 9.1% than that of diesel at full load. The decrease in BSEC can be attributed to the more efficient utilization of the fuel at a higher compression ratio, because of better combustion. At 26^{o}CAbTDC advanced injection timing and 220 bar nozzle opening pressure with 18.5 compression ratio, it is found to be by about 9.1% lowest BESC for the CBWD10 than that of diesel, at full load respectively.

It can also be observed from the figure that, the BSEC is lower with 18.5 compression ratio at 26^{o}CAbTDC advanced injection timing and 220 bar nozzle opening pressure compared to that of other injection timings and nozzle opening pressures. This may be due to improved combustion as the atomization and proper air-fuel combustion. This reason is in a good agreement with Subba Reddy et al., [221] for the reason they claimed for the results they have obtained for biodiesels fuelled DI diesel engine run at different injection pressures.

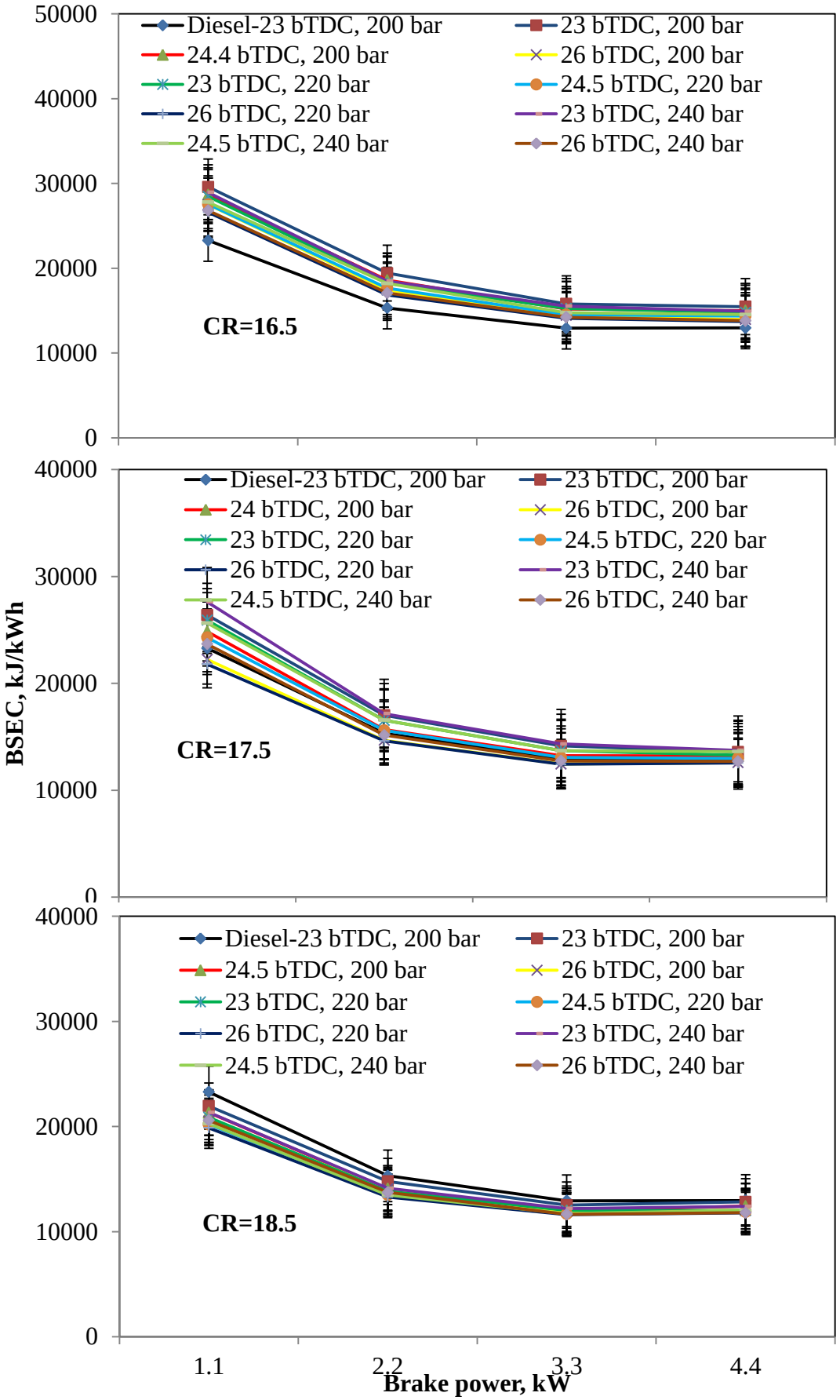

Figure 5.69 BSEC consumption with brake power at different compression ratios, nozzle opening pressures and injection timings

5.6.3.3 Exhaust gas temperature

The variation of exhaust gas temperature (EGT) with brake power of the engine when, fuelled with the CBWD10 emulsion for three compression ratios, different injection timings, and different nozzle opening pressure and diesel is portrayed in Figure 5.70. Generally the EGT increases with increase in the brake power for the CBWD10 emulsion and diesel because more fuel is burnt to meet the power requirement same trend comes with different compression ratios, injection timings and nozzle opening pressures. The EGT for the CBWD10 emulsion is lower at the higher compression ratio which may be due to an increase in burning velocity and the reduced time required for complete combustion. Similar results were presented by Bora et al., [222]. It can also be observed from the results that the EGT for the CBWD10 emulsion at the compression ratio of 18.5 is found to be lower by about 3.3% to 9.8 % compared to than that of diesel at full load respectively. This may be due to the fact that air enters during the suction stroke at a higher compression ratio is compressed, which increases the air temperature. The increased air temperature helps for better atomization of fuel, proper air-fuel mixing which contributes in complete combustion and resulting reduction in the EGT. Similar reasons were indicated by Raheman and Ghadge [202] when they fuelled biodiesel at varying compression ratio and ignition timing in single cylinder, four stroke, DI diesel engine.

The EGT at the compression ratio of 16.5 is higher by about 8.6% to 23.4% compared to that of diesel at full load. This may be due to more amount of heat is released during diffusion phase as a result more heat leaving along with exhaust gas. At the compressions ratio of 17.5 and with the original injection timing, the EGT is found to be by about 4.2% to 9.2% higher at the full load respectively. As a result, the combustion products in the form of gases come out at higher temperature and incomplete combustion. The EGT is found to be lower for the higher compression ratio of 18.5 and 26^{o}CA bTDC advanced injection timing and 220 bar nozzle opening pressure, due to the heat release occurring closer to the TDC in the expansion stroke, which might provide enough time for the hot gases to expand and cool down before the exhaust valves are opened. This reason is well suited with the reasons reported by Agrwal et al., [139] for the results they obtained from biofuel operated single cylinder, four stroke, DI diesel engine. It can also be observed from the figure at 220 bar the nozzle opening pressure decreases the EGT at full load than that of other the nozzle opening pressures. This may be due to finer droplet size distribution, gave a relatively better fuel–air mixing and smoother combustion better atomization, and vaporization of the fuel droplets.

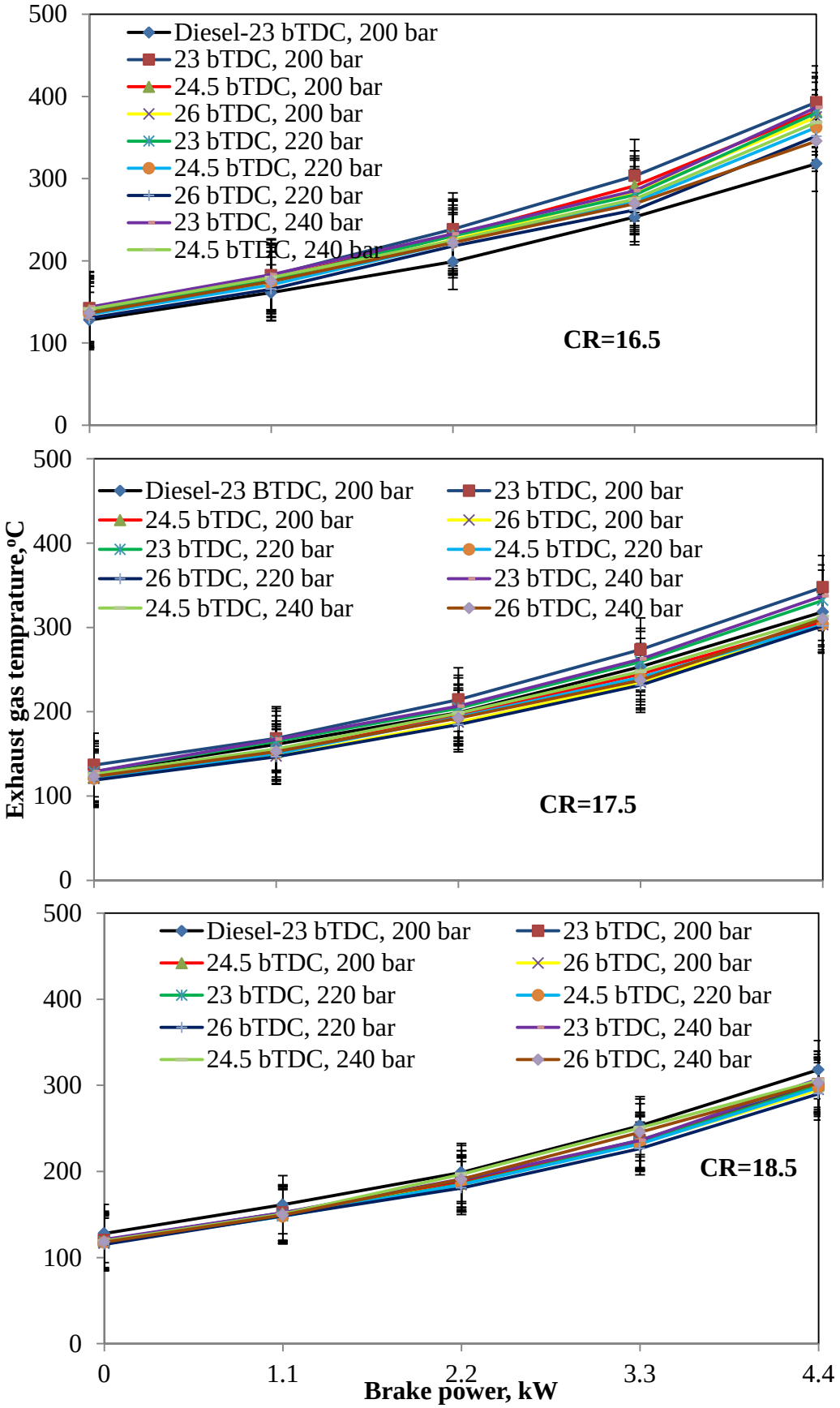

Figure 5.70 EGT with brake power at different compression ratios, nozzle opening pressures and injection timings

5.6.4 Emission analysis

5.6.4.1 CO emission

Figure 5.71 portrays the variation of CO with the brake power when the engine run on the CBWD10 emulsion with the different compression ratios, injection timings and nozzle opening pressures, in comparison with diesel. The CO emission decreases with increase in compression ratio and injection timing for the CBWD10 emulsion compared to that of diesel operation at full load. The improved conditions for the combustion process may result in the reduction of emission levels at higher compression ratio [218]. It can be observed from the results for the CBWD10 emulsion that, the CO emission for the compression ratio of 18.5 is lower compared to that of 16.5 and 17.5 compression ratios at full load. The possible reason for this trend could be that the increased compression ratio actually increases the air temperature inside the cylinder. This may increase better and more complete combustion of the fuel. The higher nozzle opening pressure and advanced injection timing is relatively improved fuel atomizing characteristics in the cylinder chamber. Similar reasons were indicated by Radivoje et al., [223] for the results they have obtained in a single cylinder, four stroke, DI diesel engine run on diesel at different compression ratios.

The CO emission for the CBWD10 emulsion at the compression ratio of 16.5 is found to be 53.5% to 122.2% higher compared to that of diesel at the full load with different injection timings and nozzle opening pressure. At the compression ratio of 17.5 the CO emission is found to be about 35.9% to 32.3% lower than that of diesel at full load with the advanced injection timing of 26^{o}CA bTDC and 220 bar nozzle opening pressure . It can be observed from the figure, that the CO emission is lower at the advanced injection timing and 220 bar nozzle injection pressures. This may be due to better atomization of fuel spray. This causes a reduction in the CO emissions [224] for the same compression ratio, the CO emission is found to be by about 11.1% to 21.3% is higher than that of diesel with other injection timings and nozzle opening pressures. This may be due to poor air-fuel mixture formation. It can also be observed from the figure the CO emission for CBWD10 at the compression ratio of 18.5 is found to be lower by about 7% to 46.2% than that of diesel with various nozzle opening pressures and injection timings at the full load respectively.

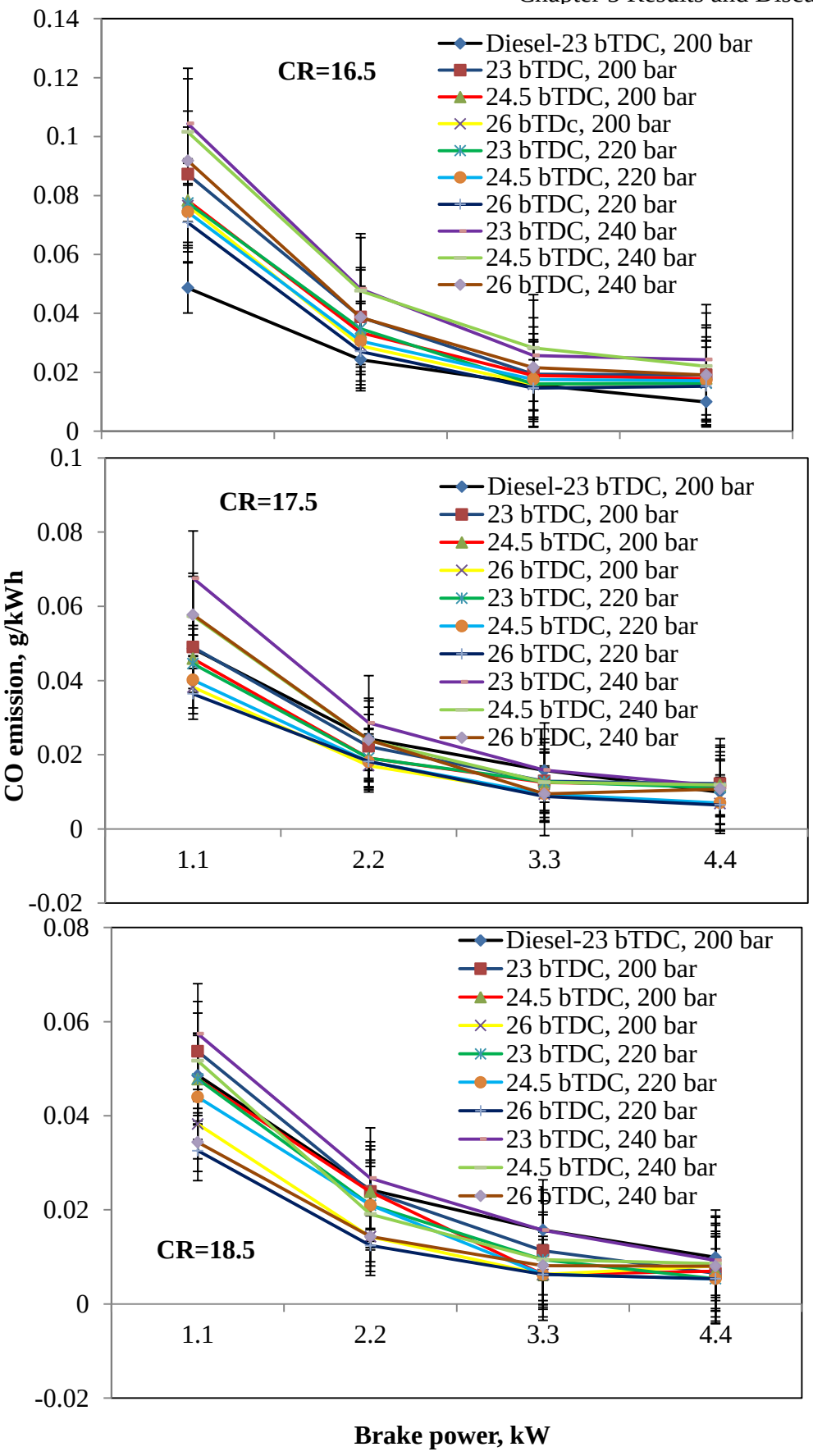

Figure 5.71 CO emission with brake power at different compression ratios, nozzle opening pressures and injection timings

5.6.4.2 HC emission

The variation of HC emission with brake power for the CBWD10 emulsion at different compression ratios viz; 16.5, 17.5, 18.5, nozzle opening pressures viz; 200, 220 and 240 bar, and injection timings viz; 23 ,24.5 and 26^{o}CA bTDC are compared with those of diesel and presented in Figure 5.72. The HC emissions at all the compression ratios for the tested fuels in this study decrease with the increase in the brake power over the entire engine operation, due to the more complete combustion in the cylinder. The HC emission decreases with the increase of compression ratio. This is due to diffused combustion, increased temperature and after burning phenomenon [225]. This is in good agreement with Anbazhagan et al., for the results obtained for Jatropha curcas oil in diesel engine with different compression ratios.

It can also be observed from the figure that at the compression ratio of 16.5 the HC emission is much higher at all the injection timings and nozzle opening pressures, which may be due to incomplete combustion due to the effects of viscosity, fuel spray quality, and lower compression ratio results less temperature during the compression stroke which results in poor combustion [222]. The HC emission at the compression ratio of 16.5 found to be about 34% to 66.6% higher with different injection timings and nozzle opening pressures at full load respectively. The HC emission is higher for the CBWD10 emulsion at original compression ratio, injection timing and nozzle opening pressure compared to that of diesel due to which is poor atomization of high density fuel. At 17.5 compression ratio, the HC emission for the CBWD10 emulsion is found to be by about 3.2% to 33.9% higher than that of diesel at full load respectively. But, the HC emission decrease at the advanced injection timing of 26^{o}CA bTDC with 220 bar nozzle opening pressure, the HC emission is lower by about 5% due to complete combustion and finer droplet of the fuel in the combustion chamber as a result of better air fuel mixing.

The HC emission for the CBWD10 emulsion is lower than that of diesel fuel at 18.5 compression ratio. This is because of better combustion of the CBWD10 inside the combustion chamber due to increase in cylinder temperature during the compression stroke which results in better combustion. Cenk and Gumus [226] have also reported same reasons for the results they have obtained in a biodiesel fuelled biodiesel-blended diesel fuel in single cylinder, four stroke, DI diesel engine at different compression ratios and injection parameters.

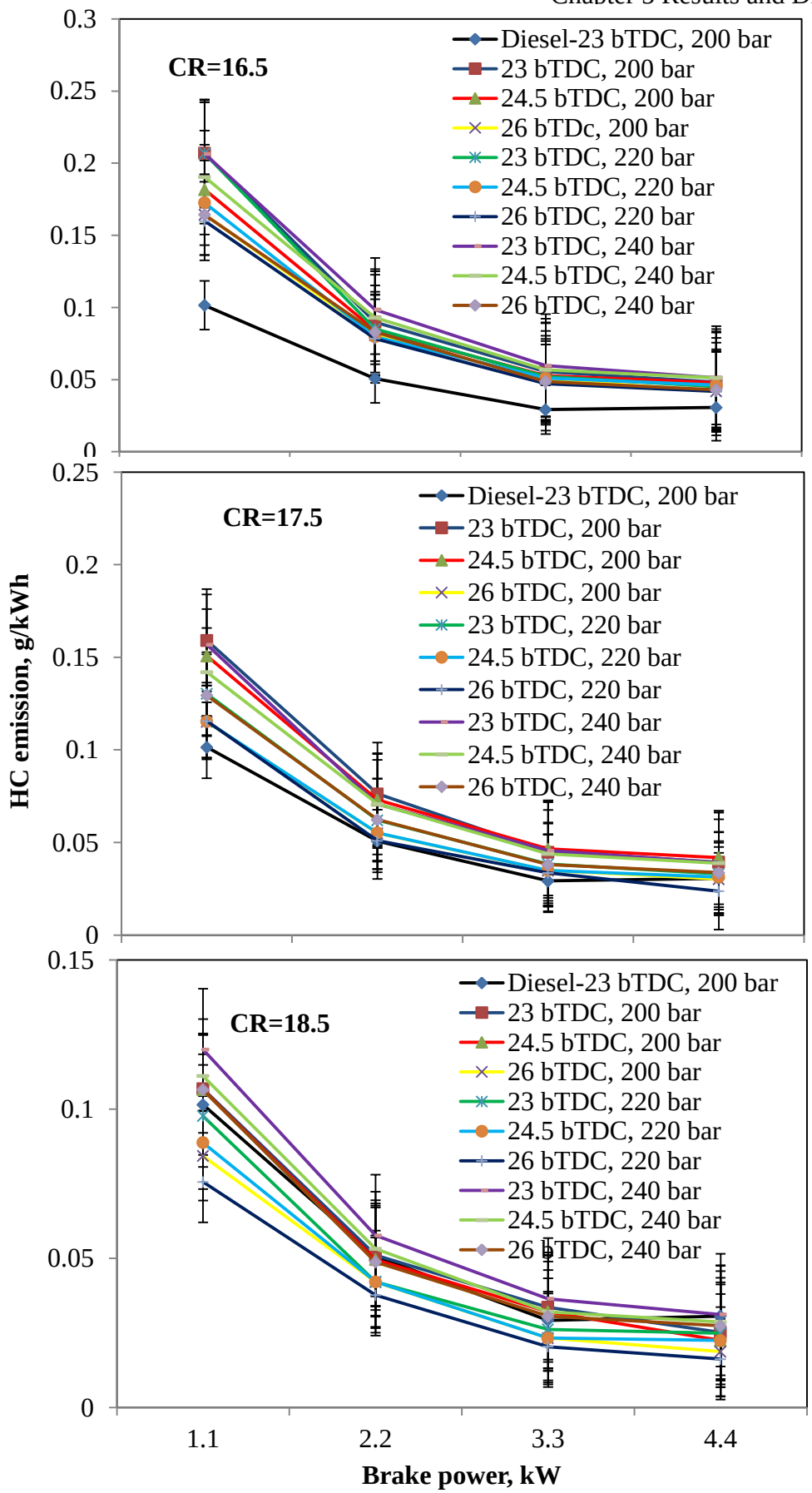

Figure 5.72 HC emission with brake power at different compression ratios, nozzle opening pressures and injection timings

Overall, the HC emission at 26 ^{o}CA bTDC advanced injection timing with 220 bar nozzle opening pressure found to be lower by about 35%. The value of the HC emission at the compression ratio of 18.5 found to be lower in the range about 0% to 35% lower with different injection timings and nozzle opening pressures at full load respectively. It can be observed from the figure that, at all compression ratios, beyond the 220 bar nozzle opening pressure, the HC emission for the CBWD10 emulsion increases with the increase in the nozzle opening pressure at the full load, due to improper air-fuel mixing, because some fuel particles quenched in the combustion chamber walls; they do not burn properly, and give a high hydrocarbon exhaust from the engine [45]. This reason is well suited with the results and discussion documented by Hariharan et al., related to the investigation of Sea lemon oil in a single cylinder, four stroke, DI diesel engine at different injection pressure [227].

5.6.4.3 NO emission

The variation of NO emission with brake power at different compression ratios with the different nozzle opening pressures and injection timings for the CBWD10 emulsion in comparison with diesel is depicted in Figure 5.73. It can be observed from the figure that, at all compression ratios the NO emission decreases with increases in the brake power. It can be also observed at different compression ratios of 16.5, 17.5 and 18.5 with different nozzle opening pressures and injection timings the NO emission for the CBWD10 emulsion is lower compared to than that of diesel at all load because, the emulsion was stabilized by the surfactant and water content. The finely dispersed water droplets of the CBWD10 emulsion might absorb heat for its vaporization there, by lowering the in-cylinder temperature of the burned gases, and thus reduce the production of NO emission. This reason was also supported by Singh for the results he obtained with water-diesel emulsion fuelled in DI diesel engine [191]. At the compression ratio of 16.5, it can be observed from the figure that for the CBWD10 emulsion, the NO emission is reduced by about 20.2% to 31% to than that of diesel and also exhibits lower NO emission compared to the other compression ratios at the full load respectively, with different injection timings and nozzle opening pressures. This may due to the lower combustion temperature resulted from combustion of the CBWD10 emulsion.

The NO emission is lower for the CBWD10 emulsion than that of diesel at the compression ratio of 17.5, nozzle opening pressure and injection timing due to the lower combustion temperature. This is, because water is present in the emulsion the CBWD10. The NO emission value for the compression ratio of 17.5 is reduced by about 19% to 22.4% to than that of diesel at full load respectively

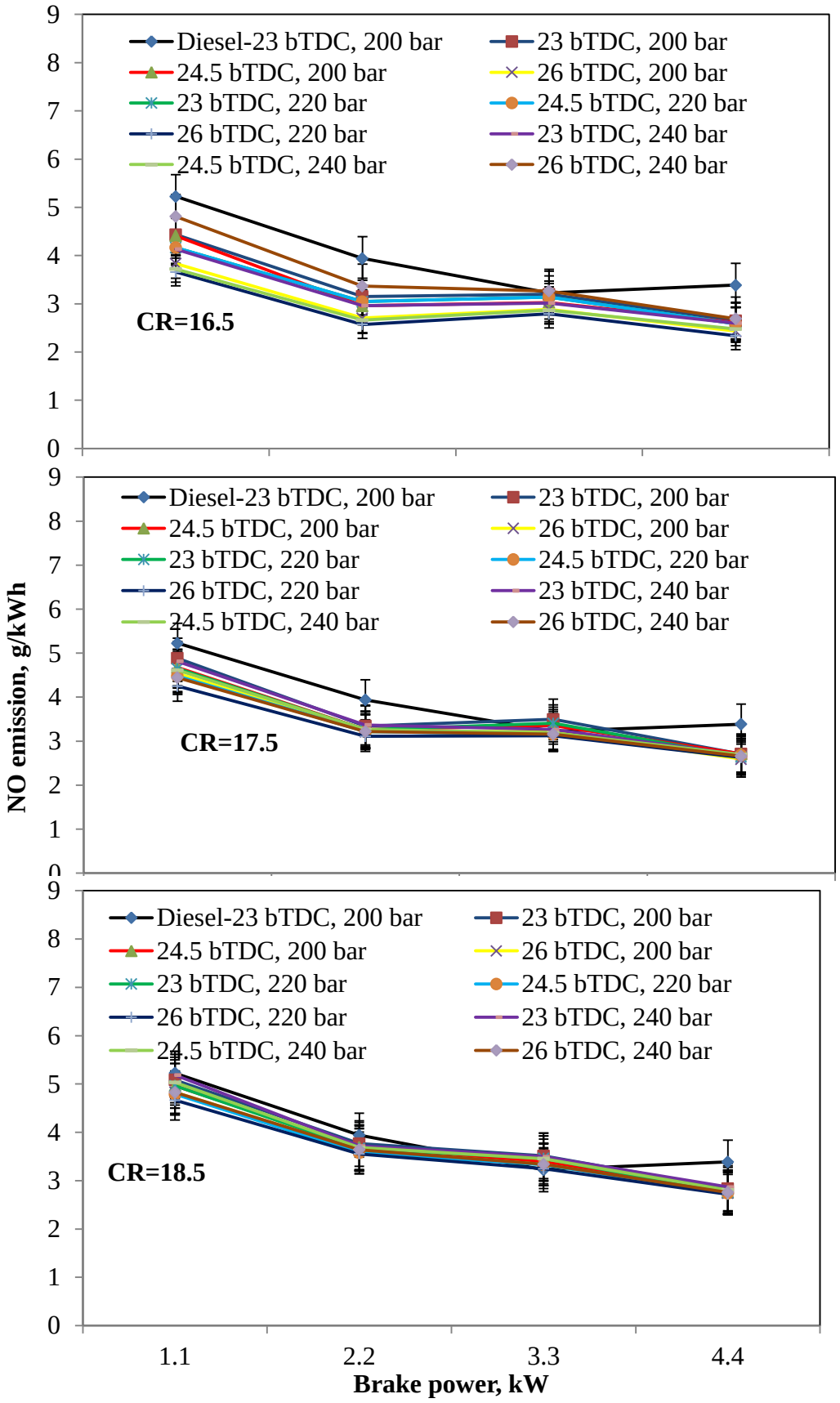

Figure 5.73 NO emission with brake power at different compression ratios, nozzle opening pressures and injection timings

As observed from this figure, at the higher compression ratio of 18.5, the NO emission is higher compared to that of original and lower compression ratios. It is quite obvious that, at the higher compression ratio, the temperature in the combustion chamber is expected to be higher due to improved combustion, results in higher amount of NO formation. The increase in the air intake temperature due to the rise in the compression ratio generates faster combustion rates, resulting in higher burned gas temperatures. The NO emission value for the compression ratio of 18.5 is lower in the range from 12.6 to 17.1% than that of diesel at the full load respectively, but higher compared to other compression ratios.

5.6.4.4 Smoke emission

Figure 5.74 shows the variation of smoke emission of the CBWD10 emulsion with brake power for the lower, original and higher compression ratios at different injection timings and nozzle opening pressures. The formation of smoke primarily results from the incomplete burning of the hydrocarbon fuel and the partially reacted carbon content in the liquid fuel. The smoke emission generally increases with the increase in the brake power for all experiment. For the CBWD10 emulsion at all compression ratios, the smoke values are found to be higher than that of diesel in the entire engine operation. This may be due to higher C/H ratio of emulsion than that of diesel. It may also be due to slow combustion as a result of poor mixture formation of emulsion. As the compression ratio increases, the clearance volume decreases which in turn increases the temperature and pressure of the charge during the end of the compression stroke. The increased combustion temperature results in better combustion of fuel and the smoke emission decreased. It can also be observed from the figure that the smoke emission for the compression ratio of 16.5 is higher compared to that of higher compression ratio. This is may be due to incomplete combustion and lower in-cylinder temperature. The smoke emission values for the CBWD10 at 16.5 is by about 17% to 53% higher than that of diesel with the different injection timings and nozzle opening pressures at the full load respectively. At the compression ratio of 17.5, the smoke value for the CBWD10 emulsion is found to be about 6.7% to 15% higher than that of diesel at the full load, respectively.

At the higher compression ratio, the smoke reduces at full load due to the maximum temperature reached during the combustion process. Similar reasons were supported by Gnanamoorthi and Devaradjane [228].

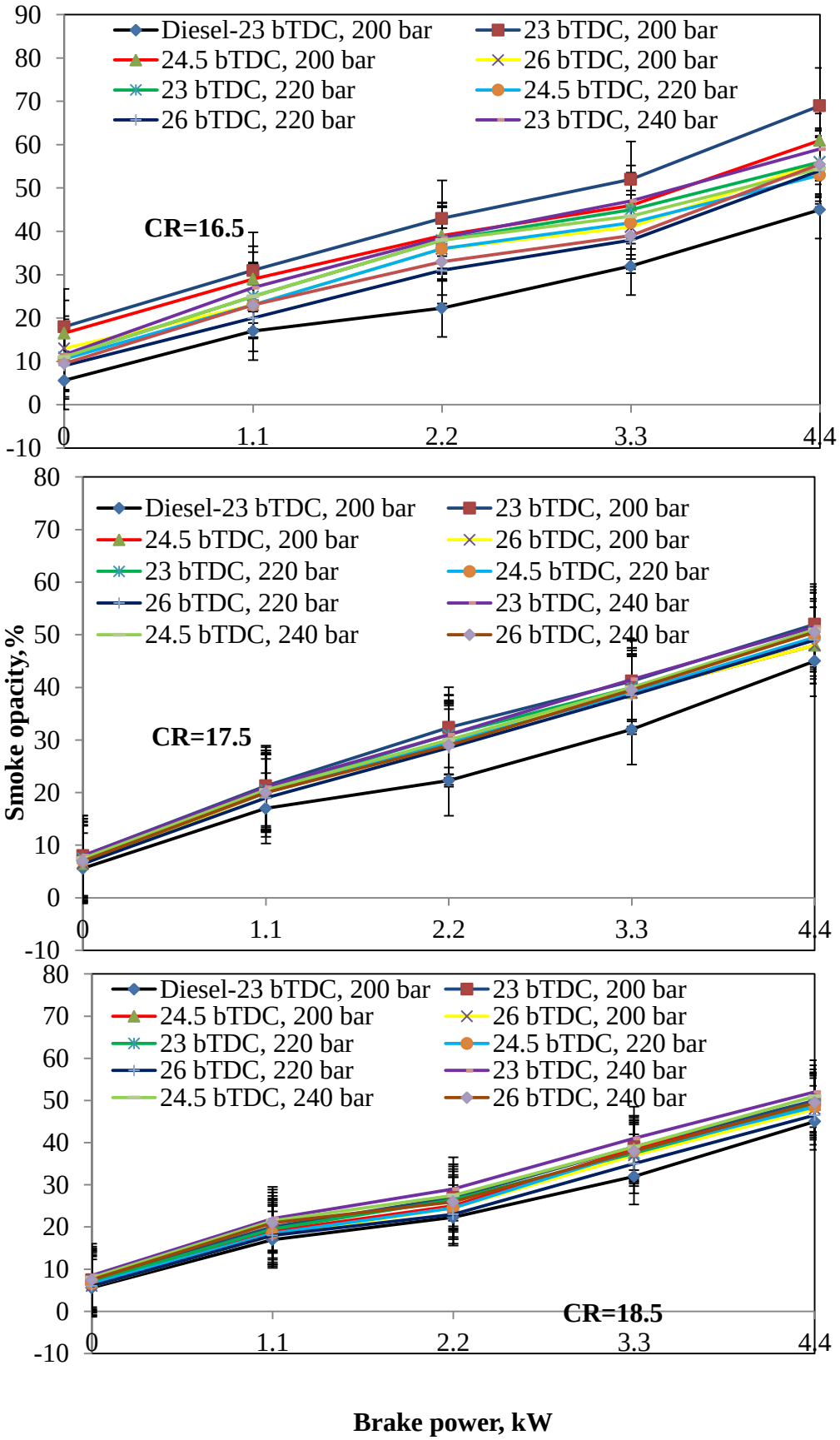

Figure 5.74 Smoke emission with brake power at different compression ratios, nozzle opening pressures and injection timings

It can be observed from the figure that of the CBWD10 emulsion at 18.5 compression ratio gives lower smoke emission compared to the other compression ratios, due to complete combustion and high combustion temperature. But, compared to diesel the smoke value is found to be exhibit higher at the compression ratio of 18.5. The value of smoke emission for the CBWD10 emulsion is higher by about 3% to 14% compared to that of the diesel at full load respectively. It can also be observed that, the smoke level is higher at 240 bar nozzle opening pressure than that of diesel. This may be due to much finer fuel droplets and they do not find air to form a homogeneous mixture. The promotion of fuel air mixing caused by the spray injected with high pressure results in a longer combustion duration, incomplete combustion, and a reduction of the local fuel rich region. Choi and Reitz gave similar reasons for the results; they have obtained in a multiple injection strategies on DI diesel engine [229].

5.6.5 Summary

The summary of the experimental results on the combined effects of varying compression ratio, nozzle opening pressure and injection timing on the combustion, performance and emission parameters obtained in a single cylinder diesel engine fuelled with the CBWD10 emulsion indicates that, the CBWD10 emulsion gives an improved the combustion, performance and lower emissions, when the engine is operated with a higher compression ratio of 18.5 with the advanced injection timing of 26^{o}CA bTDC and 220 bar nozzle opening pressure. At 18.5 compression ratio, the heat release rate is found to be higher by about 0.4% to 9% and the BTE is also found to be higher by about 1.7% to 5.1% than that diesel, at full load. The CO and HC emissions were reduced by about 46.2% and 35 % respectively for CBWD10 emulsion at 18.5 compression ratio with the advanced injection timing of 26^{o}CA bTDC and 220 bar nozzle opening pressure at full load respectively. The smoke opacity of the CBWD10 emulsion with this compression ratio and at the advanced injection timing of 26^{o}CA bTDC and 220 bar nozzle opening pressure is found to be higher by about 3% to 14% compared to that of diesel at full load. Table 5.6.1, 5.6.2 and 5.6.3 provide the values of important engine parameters obtained for the CBWD10 emulsion at 16.5, 17.5 and 18.5 compression ratios with 200, 220 and 240 bar nozzle opening pressures and 23, 24.5 and 26^{o}CA bTDC injection timings.

Table 5.6.1 Values of important engine parameters obtained for the CBWD10 emulsion at 16.5 Compression ratio with different nozzle opening pressures and injection timings at full load.

S.No.	Parameters	23bTDC, 200 bar	24.5bTDC ,200 bar	26bTDC, 200 bar	23bTDC, 220 bar	24.5bTDC ,220 bar	26bTDC, 220 bar	23bTDC, 240 bar	24.5bTDC, 240 bar	26bTDC, 240 bar
Combustion parameters										
1	Maximum cylinder pressure, (bar)	65.02	66.80	69.95	68.45	70.18	76.71	68.94	69.9	75.41
2	Ignition delay, (^{o}CA)	11.5	11.31	10.52	11.12	11.02	10.22	11.82	11.62	11.12
3	Max. heat release rate, (J/^{o}CA)	50.6	51.82	52.85	51.46	53.04	53.83	51.06	52.14	52.83
4	Combustion duration, (^{o}CA)	47.4	46.1	43.01	14.8	41.58	40.64	41.92	41.74	40.78
5	Maximum rate of pressure rise, (bar/^{o}CA)	4.78	4.86	4.96	4.96	5.06	5.14	4.73	4.97	5.01
Performance parameters										
1	Brake thermal efficiency, (%)	28.3	28.7	29.2	29.1	29.2	29.4	28.4	28.9	29.3
2	BSEC, (kJ/kWh)	392.8	14994.1	13956.1	14791.3	14375.1	13721.7	14925.1	14541.5	13819.4
3	Exhaust gas temperature, (^{o}C)	15473.2	381.5	375.1	380.0	362.2	351.4	386.5	368	345.6
Emission parameters										
1	CO emission, (g/kWh)	0.0191	0.0178	0.0163	0.01623	0.0171	0.0152	0.0242	0.0220	0.01906
2	HC emission, (g/kWh)	0.0481	0.0478	0.0418	0.0452	0.0461	0.0418	0.05131	0.0511	0.0429
3	NO emission, (g/kWh)	2.65	2.615	2.43	2.58	2.56	2.33	2.59	2.47	2.69
4	Smoke emission, (%)	69	61	56	56	53	54	59	54.5	55.5

Table 5.6.2 Values of important engine parameters obtained for the CBWD10 emulsion at 17.5 Compression ratio with different nozzle opening pressures and injection timings at full load.

S.No.	Parameters	23bTDC, 200 bar	24.5bTDC ,200 bar	26bTDC, 200 bar	23bTDC, 220 bar	24.5bTDC ,220 bar	26bTDC, 220 bar	23bTDC, 240 bar	24.5bTDC, 240 bar	26bTDC, 240 bar
Combustion parameters										
1	Maximum cylinder pressure, (bar)	75.2	73.04	78.21	75.8	76.34	78.71	75.42	73.79	77.41
2	Ignition delay, (^{o}CA)	10.11	9.23	9.01	9.82	9.02	9.05	10.32	10.06	9.45
3	Max. heat release rate, (J/^{o}CA)	53.4	55.31	56.14	53.9	55.83	57.7	53.01	53.45	55.8
4	Combustion duration, (^{o}CA)	38.52	38.13	37.38	38.44	37.7	35.14	38.92	38.7	37.39
5	Maximum rate of pressure rise, (bar/^{o}CA)	5.1	5.45	5.57	5.26	5.61	5.68	5.13	5.27	5.45
Performance parameters										
1	Brake thermal efficiency, (%)	30.4	30.7	31.20	30.6	30.9	31.7	29.9	29.9	30.5
2	BSEC, (kJ/kWh)	13581.8	13207.6	12583.1	13293.8	12979.9	12555.1	13735.3	13623.9	12703.1
3	Exhaust gas temperature, (^{o}C)	347.53	306.3	303.04	331.97	303.28	301.63	337.30	312.5	309.9
Emission parameters										
1	CO emission, (g/kWh)	0.0121	0.0118	0.0067	0.011	0.007	0.0064	0.0115	0.01186	0.0107
2	HC emission, (g/kWh)	0.0393	.0418	0.030	.033	0.0313	0.023	0.039	0.0387	0.033
3	NO emission, (g/kWh)	2.71	2.71	2.59	2.64	2.68	2.627	2.69	2.69	2.66
4	Smoke emission, (%)	52	51	48	50.5	49.5	47	51.5	51	50.5

Table 5.6.3 Values of important engine parameters obtained for the CBWD10 emulsion at 18.5 Compression ratio with different nozzle opening pressures and injection timings at full load.

S.No.	Parameters	23bTDC, 200 bar	24.5bTDC ,200 bar	26bTDC, 200 bar	23bTDC, 220 bar	24.5bTDC ,220 bar	26bTDC, 220 bar	23bTDC, 240 bar	24.5bTDC, 240 bar	26bTDC, 240 bar
Combustion parameters										
1	Maximum cylinder pressure, (bar)	76.3	78.2	78.7	77.02	80.12	80.67	77.91	78.41	79.7
2	Ignition delay, (^{o}CA)	9.11	9.01	8.82	9.02	8.92	8.32	10.12	9.62	9.12
3	Max. heat release rate, (J/^{o}CA)	53.97	55.41	57.45	54.21	56.45	59.09	54.12	55.32	56.34
4	Combustion duration, (^{o}CA)	38.02	37.87	37.52	38.34	37.53	37.47	38.8	38.36	37.96
5	Maximum rate of pressure rise, (bar/^{o}CA)	5.36	5.43	5.78	5.41	5.61	6.12	5.36	5.47	5.56
Performance parameters										
1	Brake thermal efficiency, (%)	31.39	31.58	32.11	31.88	31.96	32.34	31.28	31.39	31.48
2	BSEC, (kJ/kWh)	12822.04	12420.74	12012.54	12005.69	11853.71	11783.23	12397.62	12041.86	11803.69
3	Exhaust gas temperature, (^{o}C)	301.17	299.76	295.10	299.58	297.67	290.288	307.3	305.65	302.85
Emission parameters										
1	CO emission, (g/kWh)	0.0065	0.0069	0.008	0.0053	0.0053	0.0053	0.0092	0.0085	0.0080
2	HC emission, (g/kWh)	0.025	0.0224	0.0187	0.0248	0.0224	0.0162	0.0311	0.0286	0.0273
3	NO emission, (g/kWh)	2.83	2.76	2.74	2.75	2.73	2.71	2.87	2.81	2.75
4	Smoke emission, (%)	50	49	48	49	48.5	46.5	52	51	49.5

5.7 Diesel and the CBWD10 emulsion run in a diesel engine with and without internal jet piston

5.7.1 General

It is understood from the results and discussion of the previous section that, a single cylinder DI diesel engine can run on the CBWD10 emulsion without and with modification. However, the performance of the engine was inferior than that of diesel operation of the same engine. Therefore, an attempt has been made to improve the engine performance by inducing more turbulence with the help of internal jets provided in the combustion chamber. The results of the combustion, performance and emission of the engine run on the CBWD10 emulsion without and with internal jet piston are compared, with those of diesel operation and presented in this section.

5.7.2 Combustion analysis

5.7.2.1 Cylinder pressure with crank angle

Figure 5.75 depicts the variation of maximum cylinder pressure with crank angle for diesel, and the CBWD10 emulsion without and with the internal jet piston operations. The cylinder pressure increases with the increase in brake power as the engine gains more heat. The peak cylinder pressure of the CBWD10 emulsion is 4-5 bar lower compared to that of diesel for the engine run with original jet piston. This may be due to poor air-fuel mixing and combustion [45]. It can be observed from the figure, that the cylinder pressures are higher for the engine run on diesel and the CBWD10 emulsion with internal jet piston in comparison with the engine without internal jet piston at full load. This may be due to better combustion of the fuel at higher temperature of the combustion chamber by the internal jet piston, and better air fuel mixing through turbulence, resulting in a better combustion of diesel and the CBWD10 emulsion, and hence increases in cylinder pressure. Similar reason was documented by Rajan and Senthil [145] for the results they have obtained for a biodiesel fuelled diesel engine with internal jet piston. It can also be observed that, the peak cylinder pressure of diesel and the CBWD10 emulsion for the engine run without internal jet piston are found to be about 79.2 bar and 75.3 bar, respectively, at full load, which occurs at 372.2°CAbTDC and 373.1°CAbTDC respectively. Similarly, with internal jet piston the peak cylinder pressures are found to be about 80.7 bar at 371.3°CAbTDC and 76.8 bar at 371.6°CAbTDC for diesel and the CBWD10 emulsion at the full load, respectively.

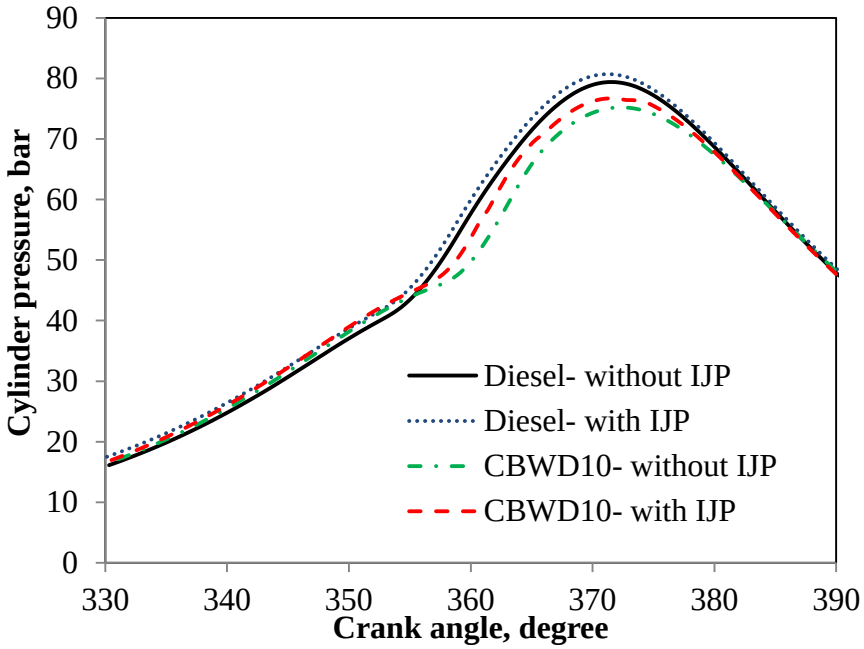

Figure 5.75 Variation of pressure with crank angle at full load

5.7.2.2 Ignition delay

Figure 5.76 portrays the variation of ignition delay with brake power for diesel and the CBWD10 emulsion for the engine without and with internal jet piston. The ignition delay gives a great attention in the combustion analysis in engine as noise, vibrations, mechanical stress, and polluting emissions largely depend on this parameter [45]. It can be observed from the figure, that the ignition delay period decreases with the increase in the brake power for with and without both the internal jet piston operations. The ignition delay period for diesel and the CBWD10 emulsion is approximately 9.3^{o}CA and 10.1^{o}CA without the internal jet piston at full load. The ignition delay of the CBWD10 emulsion is higher in comparison with the diesel operation, because of its lower cetane number and higher viscosity. The ignition delay is lower for diesel and the CBWD10 emulsion with the internal jet piston which is due to faster combustion of the fuel compared to that of the engine run without internal jet piston. This may be due to the higher combustion temperature of the internal jet piston, resulting in a shorter delay period. This reason is in good agreement with Prabhahar [230] which they mentioned for the results they have obtained for Pongamia methyl ester fuelled in a single cylinder, four stroke, DI diesel engine with modified piston. The ignition delay period for diesel and the CBWD10 emulsion is approximately 8.9^{o}CA and 9.7^{o}CA with the internal jet piston at full load, respectively.

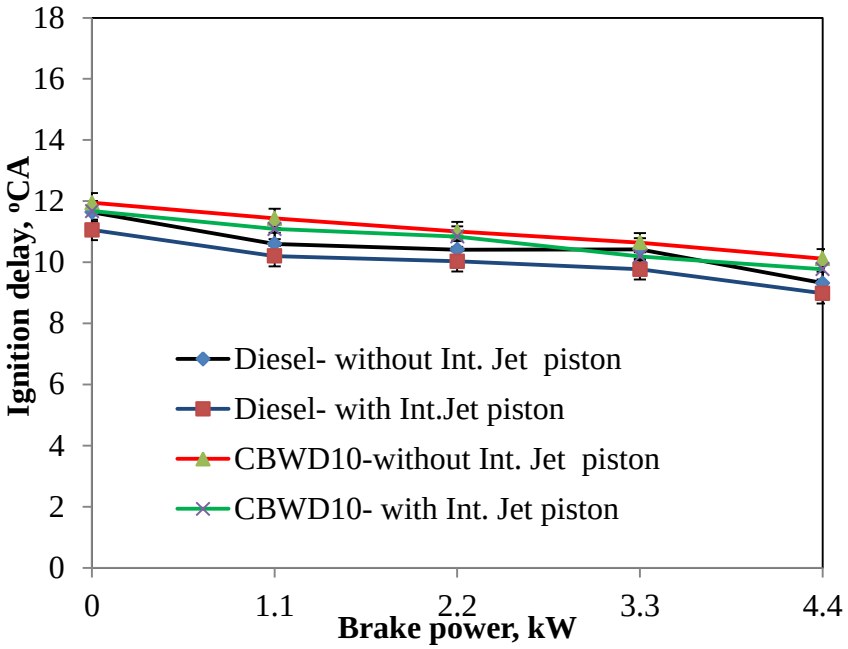

Figure 5.76 Variation of ignition delay with brake power

5.7.2.3 Heat release rate with crank angle

The variation of the maximum heat release rate with crank angle for diesel and the CBWD10 emulsion for the engine run without and with the internal jet piston at full load is portrayed in Figure 5.77. The maximum heat release rate of the CBWD10 emulsion is lower than that of diesel without internal jet piston operation, which is due to poor mixture formation, compared to that of diesel and heat of emulsion decreases due to the presence of water [231]. At full load, the maximum heat release rate for diesel with and without internal jet piston are found to be about 54.5 J/°CA at 365.5°CA, 56.6 J/°CA at 366.1°CA respectively. And also the maximum heat release rate for the CBWD10 emulsion with and without internal jet piston are found to be about 53.1 J/°CA at 367.5°CA and 53.8J/°CA at 367.2°CA respectively, at the full load. It can also be observed from the figure that, the maximum heat release rate for diesel is found to be higher by about 3.8% for the engine run with the internal jet piston compared to that of the engine run without internal jet piston. Similarly, for the CBWD10 emulsion, the maximum heat release rate is found to be about 1.9% higher with internal jet piston than that of base engine piston. The maximum heat release rate is found to be higher for diesel and the CBWD10 emulsion with internal jet piston compared to that of the engine run without the internal jet piston. This may be due to shorter ignition delay and the corresponding decrease in the diffusion combustion phase. Similar reason was supported by

Rajan et al., [232] for the results they have obtained from a single cylinder, four stroke, DI diesel engine with thermal barrier coated internal jet piston.

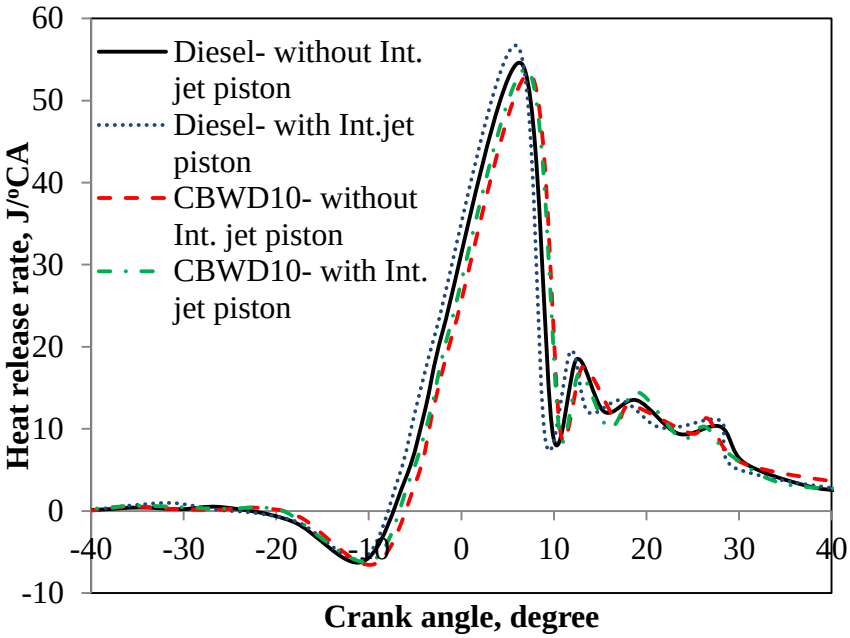

Figure 5.77 Variation of heat release rate with crank angle at full load

5.7.2.4 Combustion duration

Figure 5.78 shows the variation of the combustion duration with different brake power of the engine run on diesel and the CBWD10 emulsion without and with internal jet piston, respectively. It can be observed from the figure, that the combustion duration increases with the increase in the brake power for diesel and the CBWD10 emulsion, for both the piston conditions, which may be due to the increase in the quantity of the fuel injected in the engine [36]. It can also be observed that, the combustion duration is lower for diesel and the CBWD10 emulsion with internal jet piston compared to that of original piston operation. This may be due to the better fuel-air mixing rate and the higher combustion temperature of the internal jet piston, resulting in a shorter combustion duration. The values of the combustion duration without internal jet piston at full load are found to be 38.2^{o}CA and 39.5^{o}CA for diesel and the CBWD10 emulsion. Similarly, for the internal jet piston the values of combustion duration are found to be about 37.3^{o}CA and 38.2^{o}CA for diesel and the CBWD10 emulsion at the full load, respectively. The CBWD10 emulsion exhibits a longer combustion duration compared to that of diesel for the both piston operations. This may be due to slow combustion as a result of poor mixture formation of the CBWD10 emulsion.

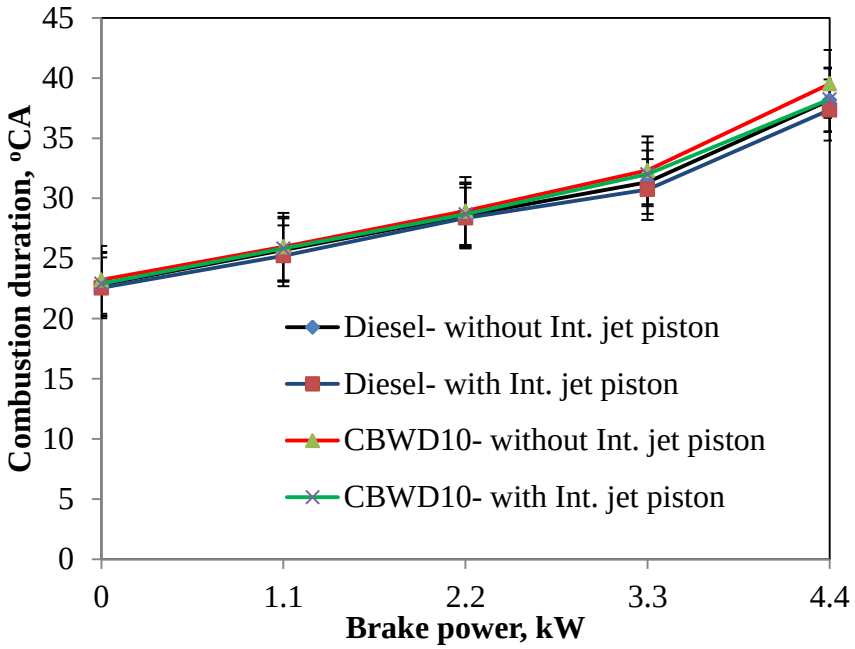

Figure 5.78 Variation of combustion duration with brake power

5.7.2.5 Mass fraction burned

Figure 5.79 portrays the variation of mass fraction burned with respect to the crank angle for diesel and the CBWD10 emulsion with and without internal jet piston at full load.

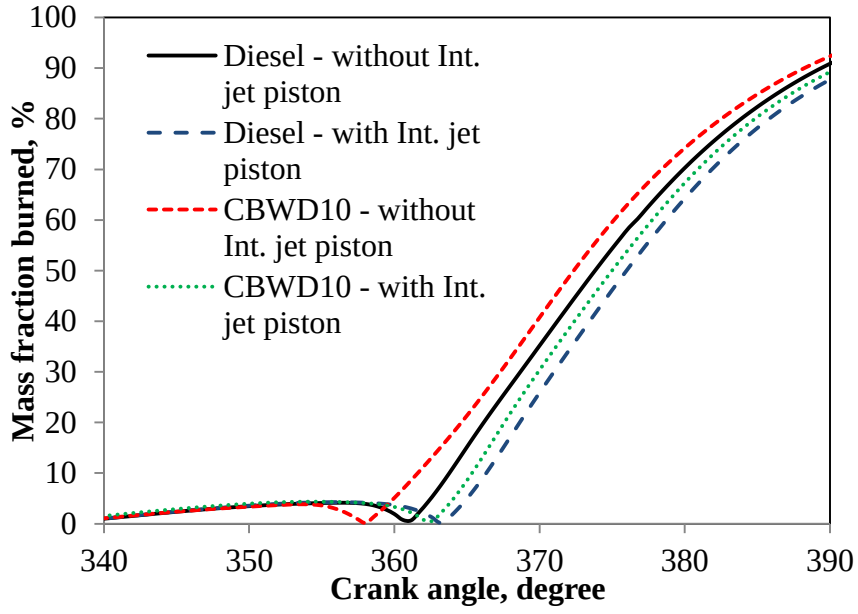

Figure 5.79 Variation of mass fractions burned with crank angle

It is apparent from the figure that the diesel and the CBWD10 emulsion curve follow similar trend for both the piston operations. It can be observed from the figure that the crank angles at which 10% and 50% mass fraction burned for diesel with internal jet piston is later than

that of without internal jet piston operation at full load. The CBWD10 emulsion with the internal jet piston for which 10% and 50% mass fraction burned is later than that of without internal jet piston. The 90% mass fraction burned crank angles are later for diesel and the CBWD10 emulsion with the internal jet piston by about 2 and 4^{o}CA respectively, at full load. For the same crank angle values, the mass fraction burned of diesel and the CBWD10 emulsion without the internal jet piston is marginally higher than that of with internal jet piston operation at full load.

5.7.2.6 Maximum heat release rate

The variation of the maximum heat release rate with brake power for diesel and the CBWD10 emulsion with base piston and internal jet piston is portrayed in Fig. 5.80.

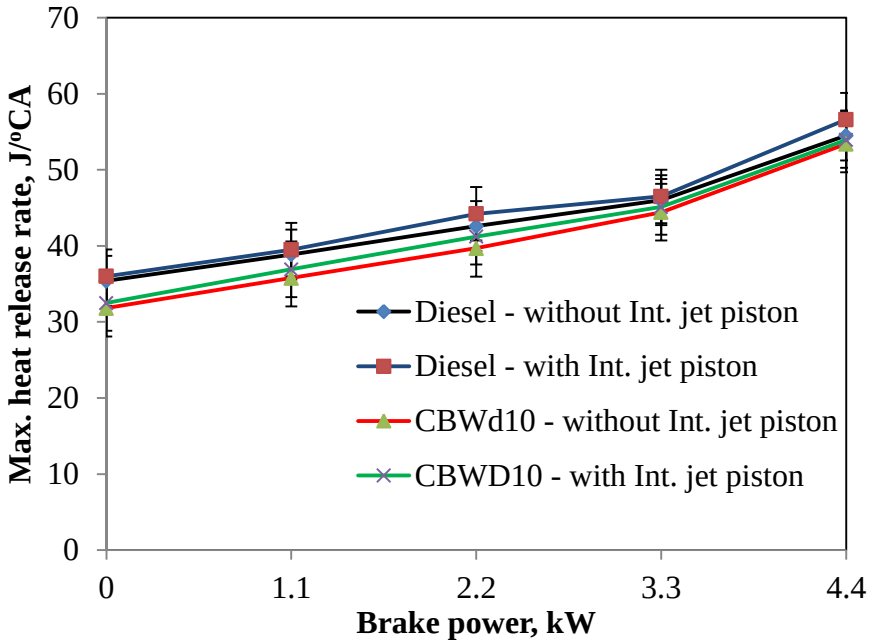

Figure 5.80 Variation of maximum heat release rate with brake power

It can be observed from the figure, that the maximum heat release rate increases with increase in brake power in the entire engine operation for diesel and the CBWD10 emulsion in both the piston arrangements. The maximum heat release rates for diesel and the CBWD10 emulsion without internal jet piston are found to be about 54.5 J/deg and 53.4 J/deg respectively, at full load. It can also be observed from the figure that at full load, the maximum heat release rate with internal jet piston for diesel and the CBWD10 emulsion are found to be about 56.6 J/deg and 54.0 J/deg respectively. Internal jet piston provides better turbulence and proper mixing with air as a result there is a higher the maximum heat release. Jaichandar et al., [233] have stated similar reasons when they correlated the results which

they have obtained in a DI diesel engine run on biodiesel with modified combustion chamber geometries.

5.7.2.7 Maximum rate of pressure rise

Figure 5.81 depicts the variation of the maximum rate of pressure rise with brake power with and without internal jet piston operation for diesel and the CBWD10 emulsion. It can be observed from the figure that the maximum rate of pressure rise of diesel and the CBWD10 emulsion in both the piston operations increases with increases brake power for the entire engine operation. The maximum rate of pressure rise for diesel and the CBWD10 emulsion without internal jet piston are found to be approximately 5.4 bar/ ^{o}CA and 5.1 bar/ ^{o}CA at the full load. It can also be observed the maximum rate of pressure rise with internal jet piston for diesel and the CBWD10 emulsion are approximately 5.6 bar/ ^{o}CA and 5.3 bar/ ^{o}CA respectively, at the full load. The maximum rate of pressure rise for diesel and the CBWD10 emulsion with internal jet piston is higher by about 5.2% and 3.5% than that of without internal jet piston operations. Because of the internal jet piston, the turbulence and combustion efficiency are improved.

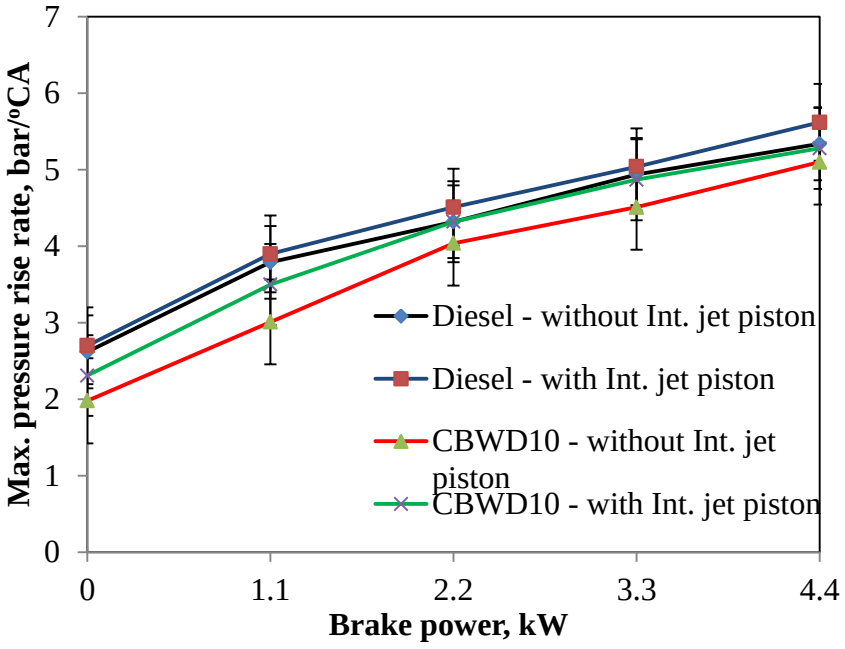

Figure 5.81 Variation of maximum rate of pressure rise with brake power

5.7.3 Performance analysis

5.7.3.1 Brake thermal efficiency (BTE)

Figure 5.82 portrays the variation of the brake thermal efficiency with brake power for the CBWD10 emulsion and diesel, in comparison without and with the internal jet piston results. It can be observed from the figure that, the BTE of diesel and the CBWD10 emulsion fuels increases with the increase in the brake power for the base piston and internal jet piston. It can be also observed, that the BTE of the CBWD10 emulsion is 2.3% lower than that of diesel operation for the engine run with base piston. The BTE increases with the internal jet piston compared to that of the engine run without internal jet piston for the both tested diesel and the CBWD10 emulsion. This may be due to better mixture formation of fuel and air as a result of higher turbulence motion of air in the combustion chamber by the internal jets, which leads to a better combustion of the fuel, and thus increases the BTE. Similar reasons were indicated by Rajan et al., [146] when they ran a single cylinder, four stroke, DI diesel engine by biodiesel with internal jet piston. The values of the BTE obtained for diesel and the CBWD10 emulsion with the internal jet piston are found to be 31.7% and 30.6% respectively, whereas for the base engine it is 30.9% and 30.2% at full load. The BTE for the CBWD10 emulsion is lower than that of diesel with base piston and internal jet piston. This may be due to the higher density, lower calorific value and poor air fuel mixture formation in the combustion chamber compared to that of diesel, this process leads to poor combustion, resulting in a lower BTE for the CBWD10 emulsion.

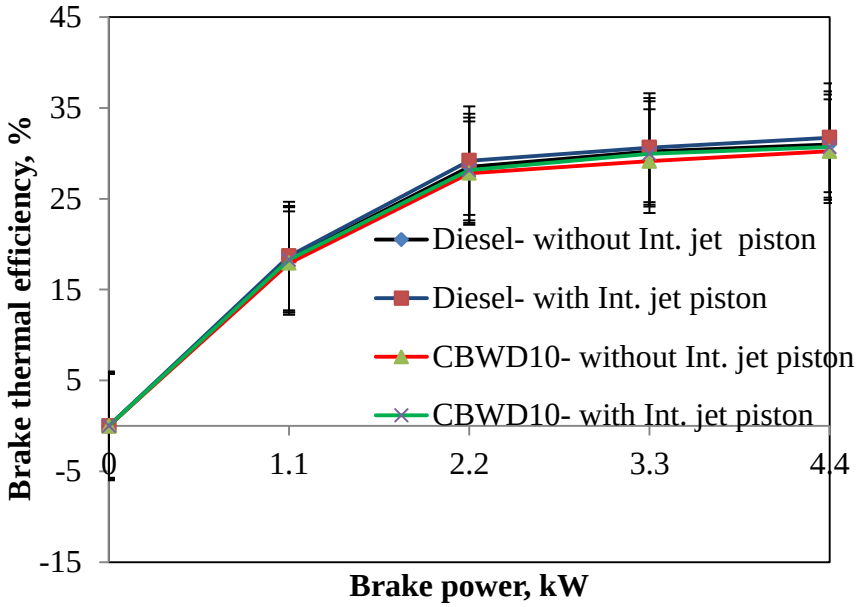

Figure 5.82 Variation of brake thermal efficiency with brake power

5.7.3.2 Brake specific energy consumption

Figure 5.83 portrays the variation of BSEC with brake power for the CBWD10 emulsion and diesel with and without internal jet piston arrangement. The BSEC of diesel and the CBWD10 emulsion decreases with the increases in the brake power with base piston operation. Similar trend is followed by the CBWD10 emulsion and diesel with internal jet piston operations. The value of BSEC for diesel and the CBWD10 emulsion without internal jet piston are found to be about 10.7 MJ/kWh and 12.3 MJ/kWh at full load. Similarly, the BSEC with internal jet piston for diesel and the CBWD10 are found to be by about 10.5 MJ/kWh and 11.1 MJ/kWh respectively, at the full load. It can also be observed from the figure the BSEC is lower by about 2.3% and 9.8% with internal jet piston for diesel and the CBWD10 emulsion compared to that of engine run without internal jet piston. This may be due to better combustion owing to induced turbulence due to squish motion generated with the modified piston. Similar results were indicated by Rajashekhar et al., [234] for the results they obtained in a single cylinder, four stroke, DI diesel engine with modification of piston geometry run on biodiesel.

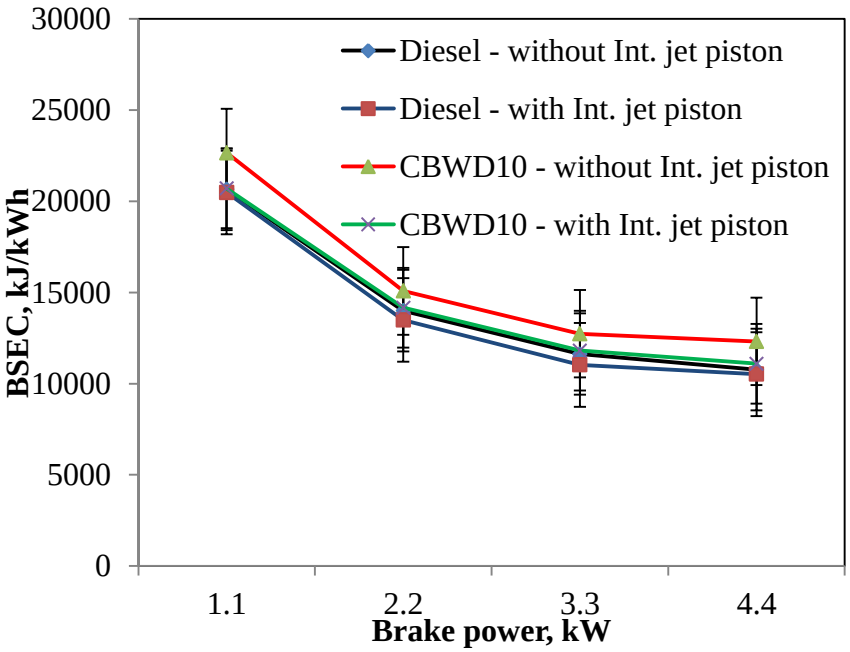

Figure 5.83 Variation of BSEC with brake power

5.7.3.3 Exhaust gas temperature

Figure 5.84 depicts the variation of the exhaust gas temperature for the CBWD10 emulsion and diesel with the brake power for the engine run without and with internal jet piston. The exhaust gas temperature may be regarded as the parameter to determine whether the

combustion is efficient [45]. It can be observed from the figure, that with the increase in the brake power, the exhaust gas temperature increases for diesel and the CBWD10 emulsion. The maximum temperatures of exhaust gas for diesel and the CBWD10 emulsion for the engine run without internal jet piston are found to be about 304^{o}C and 309^{o}C respectively at the full. Similarly, with the internal jet piston the exhaust gas temperature are found to be about 321^{o}C and 327^{o}C for diesel and the CBWD10 emulsion respectively at the full load. It can also be observed that the exhaust gas temperature is higher for the CBWD10 emulsion in the both piston operations compared to that of diesel operation. This may due to higher viscosity and density of the CBWD10 emulsion, and also the more quantity of fuel being consumed.

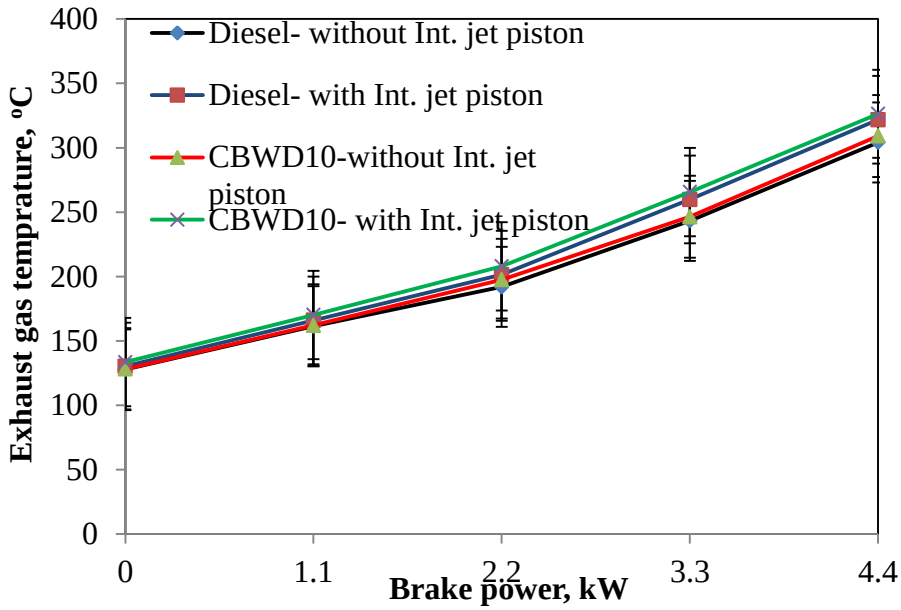

Figure 5.84 Variation of exhaust gas temperature with brake power

5.7.4 Emission analysis

5.7.4.1 CO emission

Figure 5.85 depicts the variation of the CO emission with brake power for diesel and the CBWD10 emulsion for the engine run without and with internal jet piston. It can be observed from the figure, that the CO emission decreases with the increase in the brake power for diesel and the CBWD10 emulsion with both the piston operations. The CO emission for diesel and the CBWD10 emulsion are found to be about 0.008 g/kWh and 0.01 g/kWh at the full load for the engine run without the internal jet piston. Similarly the values of CO emission for diesel and the CBWD10 emulsion with the internal jet piston are found to be by about 0.0053 g/kWh and 0.007 g/kWh at full load, respectively. It can be observed from the

results, the CO emission is lower by about 33% for diesel and lower by about 30% for the CBWD10 emulsion with the internal jet piston operation at full load compared to that of base engine piston. The decrease the CO emission for diesel and the CBWD10 emulsion with the internal jet piston. This may be due to a better mixture formation of the air and fuel by the jets, which leads to complete combustion. This reason is well suited with the reasons stated by Prasad et. al., [235] for the results they have obtained from a DI diesel engine with high swirl-inducing bowls for emission reduction.

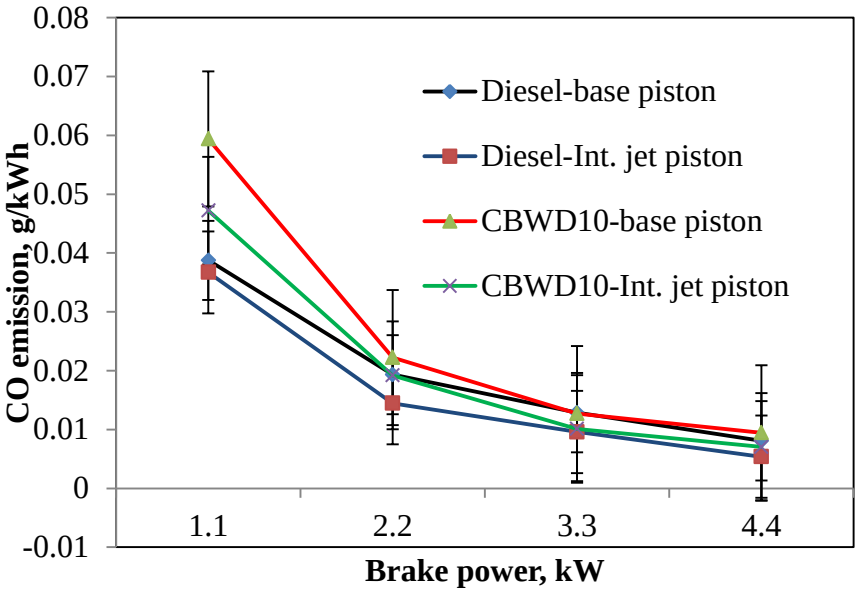

Figure 5.85 Variation of CO emission with brake power

5.7.4.2 HC emission

The variation of HC emission with brake power for diesel and the CBWD10 emulsion for the engine run with the conventional piston (base piston) and internal jet piston is depicted in Figure 5.86. The concentration of HC emission increases with the increase in the engine brake power. It can also be observed from the figure, that the HC emission of the CBWD10 emulsion is higher compared to that of diesel with both the pistons, which may be due to incomplete combustion, because some carbon black particles do not combust properly in the combustion chamber. The HC emission for diesel and the CBWD10 emulsion without the internal jet piston are found to be about 0.025 g/kWh and 0.028 g/kWh respectively, whereas for the internal jet piston is found to be about 0.021 g/kWh and 0.0256 g/kWh at the full load respectively. The increase in the HC emission for the CBWD10 emulsion with the base piston may be due to high viscosity and density of the fuel, which leads to poor mixture

formation of air and the CBWD10 emulsion, and incomplete combustion. The HC emission is reduced by the internal jet piston operation compared to that of the engine without internal jet piston. This may be due to a better combustion with the increase in the turbulence of diesel and the CBWD10 emulsion resulting in a better mixture formation of air and fuel. This reason is good agreement with Bharathi Pratiba et al., [147] for the results they observed in a single cylinder, four stroke, DI diesel engine.

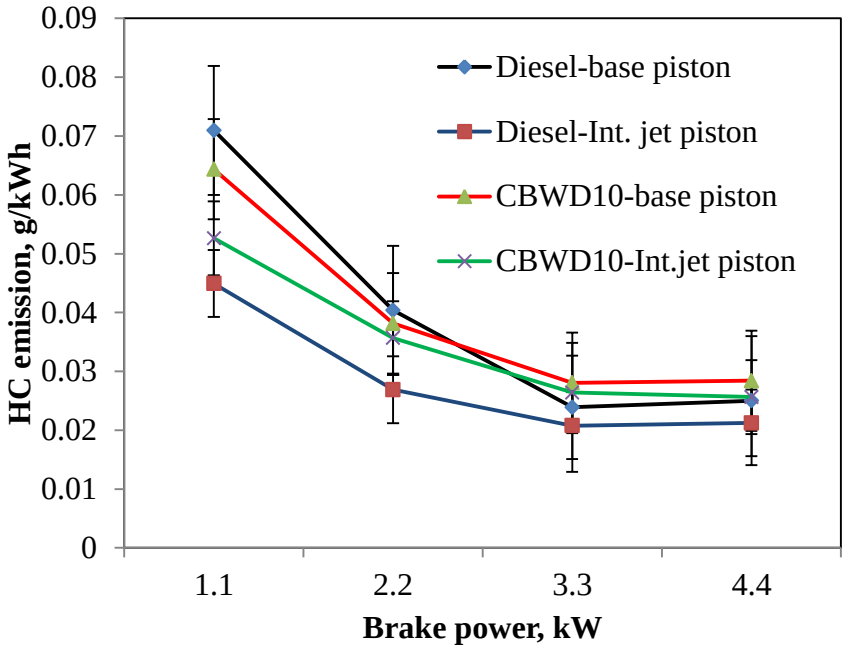

Figure 5.86 Variation of HC emission with brake power

5.7.4.3 NO emission

Figure 5.87 illustrates the variation of NO emission with brake power for diesel and the CBWD10 emulsion, for both the base piston and internal jet piston operations. It can observed from the figure that, the measured NO emissions are found to be lower for the CBWD10 emulsion compared to that of diesel with both the piston, due to the lower combustion temperature caused by the presence of water in the CBWD10 emulsion. Sivasami et al., [236] have given the similar reason for the results they have obtained in a biodiesel-water emulsion in diesel engine for NO emission reduction. The NO emissions of diesel and the CBWD10 emulsion are higher for the internal jet piston than that of the unmodified piston, because the NO emissions formation strongly depends on the in-cylinder temperature. The NO emissions for diesel and the CBWD10 emulsion with conventional piston are found to be about 3 g/kWh and 2.75 g/kWh respectively and the NO emission for diesel and the CBWD10 emulsion with internal jet piston are found to be about 3.13 and 2.86 g/kWh at full

load, respectively. The NO emission for diesel is by about 4.3% higher with the internal jet piston than that of original piston due to high combustion temperature, complete combustion. The higher exhaust gas temperature, which may accelerate the high formation of NO emission. Similarly, for the CBWD10 emulsion the NO emission is by about 4% higher with the internal jet piston than that of original piston operation at full load. This increase in the NO emission may be due to rapid burning of the air which is offered fuel mixture in the diffusion phase combustion as a result of better mixture formation of the fuel and air by the internal jets. Similar reasons were indicated by Rajan and Senthil [232] for the results they have obtained in a biodiesel fuelled in single cylinder, four stroke, DI diesel engine with thermal barrier coated internal jet piston.

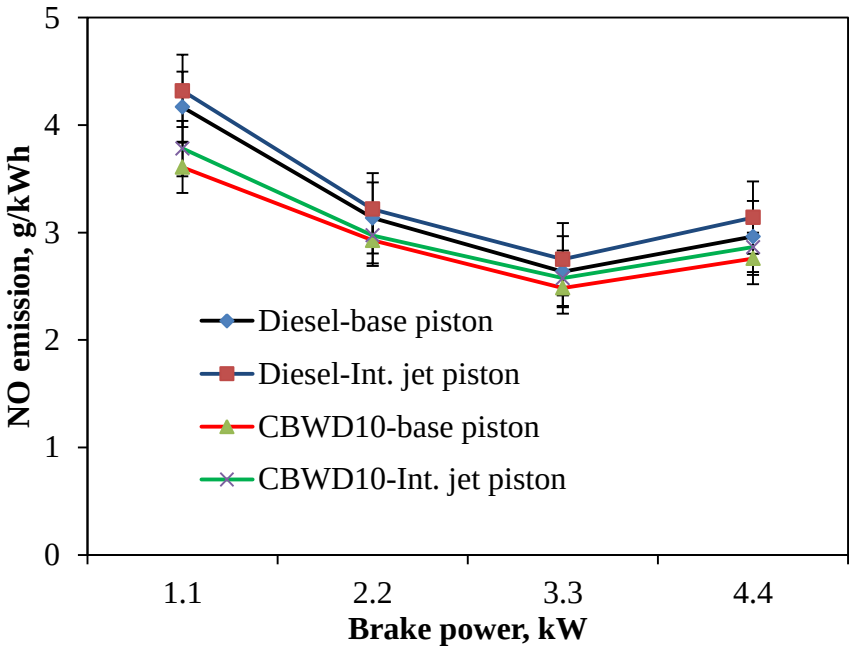

Figure 5.87 Variation of NO emission with brake power

5.7.4.4 Smoke emission

Figure 5.88 portrays the variation of smoke emission with brake power for diesel and the CBWD10 emulsion with the base piston and internal jet piston operations. The smoke opacity generally increases with the increase in the brake power for both the piston experiment. It can be observed from the figure that the smoke opacity for diesel and the CBWD10 emulsion without internal jet piston are found to be about 45% and 49.8 % respectively at full load. Similarly, at full load the smoke opacity with internal jet piston for diesel and the CBWD10 emulsion are found to be about 41.4% and 47.2% respectively. The smoke opacity of the CBWD10 emulsion is found to be higher by about 10.7% than that of diesel with the original

piston due to slow combustion as a result of poor mixture formation of emulsion. It can also be observed from the figure that the smoke opacity with the internal jet piston is found to be lower by about 8% for diesel and is found to be lower by about 5.2% for the CBWD10 emulsion compared to that of base engine piston operation at the full load, respectively. This may be due to turbulence inducement results better atomization, air-fuel mixing and better utilization of oxygen and higher combustion temperature with the internal jet piston. These reasons are in good agreement with the reasons were mentioned by Rajan et al., [237] for the similar results they have obtained in a biodiesel fuelled in, DI diesel engine for reduction of NO and smoke emission with the internal jet piston. The internal jet piston offers an improvement in the combustion process for diesel and the CBWD10 emulsion, resulting in a reduced smoke opacity.

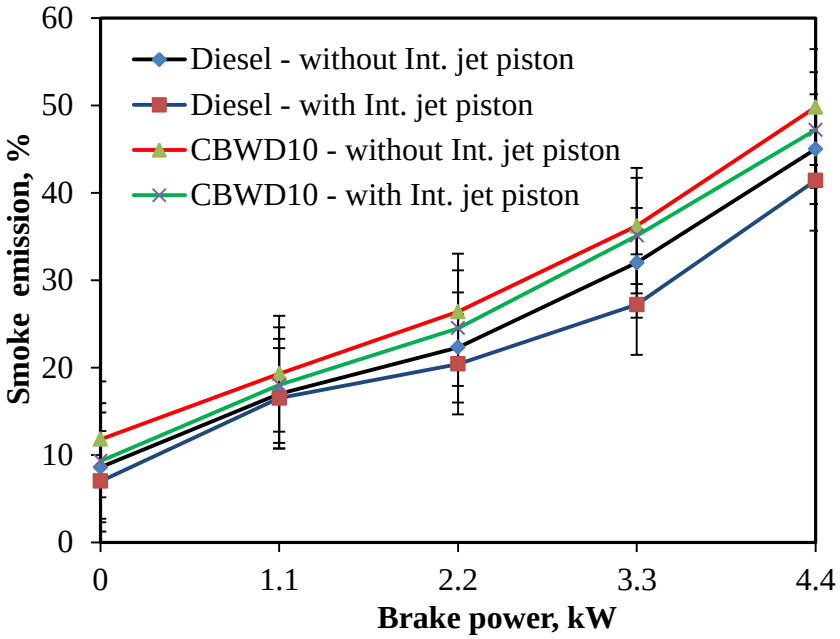

Figure 5.88 Variation of smoke emission with brake power

5.7.5 Summary

It is summarized that a single cylinder DI diesel engine can give a higher efficiency for both diesel and the CBWD10 emulsion operations by providing more turbulence through internal jets. The maximum heat release rate for diesel and the CBWD10 with the internal jet piston were found to be higher by about 3.8% and 1.9% than that of the original piston engine. The turbulence due to internal jets piston resulted in 1.3% improvement in brake thermal efficiency using the CBWD10 compared to that of base engine. The CO and HC emissions were reduced by about 23.5% and 7.2% respectively for the CBWD10 emulsion with the

internal jet piston compared to that of the engine run with the conventional piston. The smoke emissions were reduced by about 5.2%, while the NO emissions were increased by about 6% for the CBWD10 emulsion with the internal jet piston compared to that of the engine run with the conventional piston. Table 5.7.1 provides the values of important engine parameters obtained for diesel and the CBWD10 emulsion with and without internal jet piston at full load.

Table 5.7.1 Values of important engine parameters obtained for diesel and the CBWD10 emulsion with and without internal jet piston (IJP) at full load.

S.No.	**Parameters**	Diesel with IJP	Diesel without IJP	CBWD10 with IJP	CBWD10 without IJP
Combustion parameters					
1	Maximum cylinder pressure, (bar)	80.78	79.2	76.8	75.3
2	Ignition delay, (^{o}CA)	8.98	9.31	9.77	10.11
3	Max. heat release rate, (J/^{o}CA)	56.6	54.5	53.94	53.4
4	Combustion duration, (^{o}CA)	37.35	38.16	38.22	39.52
5	90% Mass fraction burned, (^{o}CA)	391.89	389.47	390.92	388.56
6	Maximum rate of pressure rise, (bar/^{o}CA)	5.62	5.34	5.28	5.1
Performance parameters					
1	Brake thermal efficiency, (%)	31.7	30.9	30.68	30.23
2	Brake specific energy consumption, (kJ/kWh)	10521.75	10772.3	11091.1	12316.91
3	Exhaust gas temperature, (^{o}C)	321.74	304.97	326.36	309.17
Emission Parameters					
1	CO emission, (g/kWh)	0.0053	0.0080	0.0070	0.0094
2	HC emission, (g/kWh)	0.0212	0.025	0.0256	0.0284
3	NO emission, (g/kWh)	3.13	2.96	2.86	2.75
4	Smoke emission, (%)	41.4	45	47.2	49.8

CHAPTER 6

CONCLUSIONS

6.1 General

In this study, the possibilities of using CB obtained from a tyre recycling plant were exposed as an alternative fuel for CI engines. The CB was tested in a single cylinder, four stroke, air cooled, DI diesel in the form of slurry and emulsion. The combustion, performance and emission characteristics of fuelled with Carbon black-diesel slurry (Carbodiesel) and Carbon black-water-diesel emulsion (CBWD) with and without engine modifications, were analysed, compared with those of diesel operation of the same engine. Also, the experimental results of the CBWD10 emulsion was validated using a two zone mathematical model developed with the help of MATLAB program. The conclusions of each technique are given in this section.

On the basis of, the comparison of experimental results and diesel replacement with CB, in all CB blend Carbodiesel slurry and CBWD emulsion from I have chosen Cabodiesel10 and CBWD-10 the optimum blend to be further used as fuel throughout the investigations. Yes, most of the cases CB-5 and CBWD-5 are shown better or little higher results than CB-10 and CBWD-10 cases, but on the basis of fuel replacement is low by 5% of the CB. So, I have choosen CB-10 and CBWD-10 further experiment.

6.2 Rheological behaviour of CBWD emulsion

1. The stability of the CBWD emulsion was calculated from the electrophoretic mobility obtained from electrophoretic light scattering measurements, by measuring the mean zeta potential (ζ) of a sample. It was found that, the CB particles the stable in the CBWD emulsion.
2. The high zeta of the sample indicates the higher stability of the sample due to a high surface charge on the particle, which exhibited stability due to surface charge repulsion.
3. It was found the apparent viscosity decreases with an increase in the shear rate of up to 100 S^{-1} for the CBWD10 emulsion.
4. The apparent viscosity of the CBWD emulsion increases with respect to the shear rate.

6.3 Carbodiesel slurry

6.3.1 Different Carbodiesel slurries

1. The CB obtained from the tyre pyrolysis process can be used as an alternative fuel in stationary diesel engines after proper fuel processing process.
2. The engine was able to run with a maximum blend ratio of 20% of CB in Carbodiesel.
3. The use of Carbodiesel5, Carbodiesel10, Carbodiesel15 and Carbodiesel20 in a diesel engine showed that, it could perform with marginally lower brake thermal efficiency than that of diesel, because of the higher density and lower calorific value.
4. Carbodiesel10 was found to be optimum, based on the performance and emissions of all Carbodiesels.
5. The maximum cylinder pressure and heat release rate for the Carbodiesel10, Carbodiesel15 and Carbodiesel20 were found to be lower by about in the range of 1.5% to 9.7% and 7.1% to 10.6% compared to that of diesel at full load. Because, the all Carbodiesel heating value and cetane number are lower compared to diesel.
6. The CO emissions was found to be higher for Carbodiesel10 by about 23.5% than that of diesel at full load, this may be due to lack of oxygen and poor mixture formation.
7. The HC emission was found to be higher for Carbodiesel10 by about 24.3% than that of diesel at full load. The higher the HC emission is due to the poor atomization of high density fuel that results in incomplete combustion.
8. The smoke emission was found to be higher for Carbodiesel10 by about 11.5% than that of diesel at full load. Higher smoke values may be attributed to the unburned and partially reacted hydrocarbons as well as higher density carbon black particles presents in the Carbodiesel10.
9. The NO emission was found to be lower for Carbodiesels10 by about 6% respectively that compared to diesel at full load, this may be probably due to the lower heat release rate as a poor combustion.
10. A maximum of 10% of diesel can be replaced by Carbodiesel10 when it was used as a fuel in the diesel engine.

6.3.2 Carbodiesel10 with different injection timings

1. The engine was able to run with Carbodiese10, when the injection timing was advanced and retarded.
2. The maximum cylinder pressure for Carbodiesel10 was found to occur earlier for the advanced injection timings and later for retarded injection timing at maximum brake

power. The advanced injection timing, more fuel is accumulated in the combustion chamber and hence a higher maximum pressure is attained.

3. Carbodiesel10 at 26^{o}CA bTDC injection timing exhibited better performance and lower emissions compared to the other injection timings, due to the high heat release rate in the premixed combustion phase.
4. Carbodiesel10 gave a higher brake thermal efficiency of about 5.9% at 26^{o}CA bTDC injection timing respectively, compared to that of the original injection timing. At advanced injection timings peak pressure reaches closer to the TDC, which results in higher effective pressure to do more work and also the earlier start of combustion in advanced injection timing reduce the time of vaporization of fuel.
5. Carbodiesel10 gave a lower BSEC of about 11.9% at the advanced injection timing of 26^{o}CA bTDC compared to that of the original injection timing. The advanced injection timing, the ignition delay is shorter due to early commencement of ignition.
6. The NO emission was found to be higher by about 9.5% at the advanced injection timings than that of original injection timing for Carbodiesel10 at full load. Advancing the injection timings caused an earlier start of combustion relative to the TDC and the higher combustion temperature.
7. At the advanced injection timings of 26^{o}CA bTDC, smoke was found to be lower by about 13.5% than that of the original injection timing at full load.

6.4 CB-water-diesel emulsions

6.4.1 Different CBWD emulsions

1. The engine was able to run with a 5% to 20% of CB in the form of emulsion. There is no abnormal noise noticed during the entire engine operation run with the emulsions.
2. The CBWD10 was found to be optimum, based on the performance and emissions of all the emulsions and on basis of fuel replacement.
3. A maximum 10% of diesel can be replaced by the CBWD10 emulsion when it was used as a fuel in the diesel engine.
4. A maximum cylinder pressure and heat release rate for the CBWD10 emulsion were found to be lower by about 5.3% and 1.8% compared to than that of diesel at full load. This due to lower cetane value, lower heating and poor air-fuel mixing.
5. The use of the CBWD10 emulsion in a diesel engine that, the engine could perform with higher brake specific energy consumption by about 14.2% than that of diesel,

because of higher density and lower calorific value and water percentage was present in it.

6. The NO emission level was found to be lower by about 20% for the CBWD10 emulsion, respectively, compared to diesel at full load. This may be due to lower combustion temperature caused by the lower heat release rate in the premixed combustion

6.4.2 CBWD10 emulsion with different injection timings

1. The engine was able to run on the CBWD10 emulsion with different injection timings. At 26^{o}CA bTDC injection timing gave better performance and emissions than the other injection timings.
2. The maximum cylinder pressure and the heat release rate of the CBWD10 at 26^{o}CAbTDC were 4% and 5% higher than that original injection timing because, advanced injection timing, more fuel is accumulated a higher peak pressure is attained than that of original injection timing.
3. Based on the brake thermal efficiency at the injection timing of 26^{o}CAbTDC, the CBWD10 emulsion gave 2.6 % higher compared to that of original injection timing. Due to the high heat release rate.
4. The CO emission of the CBWD10 emulsion at the advanced injection timing of 26^{o}CA bTDC was found to be by about 16.6% lower compared to than that of original injection timing of the CBWD10 emulsion. The advanced injection timing exhibits a higher cylinder temperature and increased oxidation process between the carbon and oxygen molecules.
5. The HC emission of the CBWD10 emulsion at the advanced injection timing of 26^{o}CA bTDC was found to be by about 25% lower compared to than that of original injection timing of the CBWD10 emulsion. At advanced injection timing causes an earlier start of combustion relative to the TDC. Because of this, the cylinder charge, being compressed as the piston moves to the TDC, had relative higher temperature, and thus lowered the HC emission.
6. The NO emission at the advanced injection timing of 26^{o}CAbTDC was found to be about 7% higher than that of standard condition, and by about 18 % lower than that of diesel. Due to higher temperature at advanced injection timing.
7. The smoke emission was found to be about 11.2% lower at 26^{o}CAbTDC advanced injection timing than that of standard injection timing.

6.4.3 Combined effect of compression ratios, nozzle opening pressures and injection timings

1. The engine was successfully run on the CBWD10 emulsion with varying engine parameters such as compression ratios viz; 16.5, 17.5 and 18.5, different nozzle opening pressures viz; 200, 220 and 240 bar and injection timings viz; 23, 24.5 and 26^{o}CA bTDC.
2. The increase in the heat release rate and the peak pressure increase at the higher compression ratio of 18.5. This may be due to higher combustion temperature and increased air temperature helps in better atomization of fuel, proper air-fuel mixing which contributes to complete combustion.
3. The ignition delay was found to be lower with higher compression ratio. This reduction in the ignition delay period is mainly due to the increased cylinder gas temperature, at higher compression ratio and a higher cetane number of the CBWD10 emulsion, compared to that of diesel.
4. The brake thermal efficiency of the CBWD10 emulsion was 1.7% to 5.1% higher at compression ratio 18.5 with different nozzle opening pressure and injection timing compared to that of diesel. This may be due to the better combustion because finer fuel droplets providing more surface are and better mixing of the fuel-air, and improved fuel spray charatersistics.
5. The exhaust gas temperature of the CBWD10 emulsion was found to be about 3.3% to 9.8% lower at compression ratio 18.5 than that of diesel. At 26^{o}CAbTDC injection timing and 220 bar nozzle injection pressure, the exhaust gas temperature for the CBWD10 emulsion was found to be lower by about 3.3% at full load respectively. Due to the heat release occurring closer to the TDC in the expansion stroke, which might provide enough time for the hot gases to expand and cool down before the exhaust valve are opened.
6. The CO and HC emissions were found to be about 16% and 35% lower at 26^{o}CA bTDC injection timing with 220 bar nozzle opening pressure with a higher compression ratio 18.5 at a full load respectively. This may be increase better and more complete combustion of the fuel.
7. The NO emission of the CBWD10 emulsion was lower for the all compression ratios which is lower in the range of 16 to 20.5% than that of diesel at full load. The NO emission for the CBWD10 emulsion at a compression ratio 18.5 is 5% lower than that

of original compression ratio. Due to the finely dispersed water droplets of the CBWD10 emulsion might absorb heat for its vaporization there, by lowering the in-cylinder temperature of the burned gases, and thus reduce the production of NO emission.

6.5 CBWD10 emulsion without and with internal jet piston

1. The CBWD10 emulsion was successfully tested in the diesel engine with the internal jet piston. Effect of swirl with the turbulence induced on the piston surface showed better results and reduced emissions.
2. The maximum heat release rate for diesel and the CBWD10 emulsion with internal jet piston were found to be higher by about 3.8% and 1.9% than that of the original piston engine. This may be due to shorter ignition delay and the corresponding decrease in the diffusion combustion phase.
3. The turbulence due to internal jets piston resulted in 1.3% improvement in brake thermal efficiency using the CBWD10 compared to the base engine. This may be due to better mixing formation of fuel and air as a result of higher turbulence motion of air in the combustion chamber by the internal jets.
4. The CO and HC emissions were reduced by about 23.5% and 7.2% respectively for the CBWD10 emulsion with the internal jet piston compared to that of the engine run with the conventional piston. This may be due to a better mixing formation of the air and jets.
5. The smoke emission was reduced by about 5.2%, while the NO emission was increased by about 6% for the CBWD10 emulsion with the internal jet piston compared to that of the engine run with the conventional piston. This may be due to turbulence inducement results better atomization, air-fuel mixing and better utilization of oxygen.

6.6 Scope for future work

The following are suggested as future work for the investigations on the use of Carbodiesel and CBWD emulsion

1. Durability test is to be done for checking the longevity of the engine fuelled with CBWD emulsion.
2. Preparation and characterisation the nanoparticles of CB for the better engine performance.

3. Carbodiesels and CBWD emulsion can be used with an internal jet piston operation, with modification of engine such as; different injection timings, nozzle opening pressures and compression ratios.
4. Carbodiesels and CBWD emulsion can be used in engine with EGR method for the reduction of the emissions.
5. The engine is further tested with nanoparticles of CB using an internal jet piston.

Annexure 1

Technical specifications of the XRD

S. No.	Instrument	Description	Unit	Data
1.	X-ray generator	Maximum rated output	kW	3
		Rated tube voltage	kV	20 - 60
		Rated tube current	mA	2 - 60
		Focus size	mm	0.4 x 12 (others: optional)
2.	Goniometer	Scanning mode		θs/θd coupled or θs, θd independent
		Goniometer radius	mm	285
		2θ measuring range	degree	-3 to 162 (maximum)
		Minimum step size	degree	0.0001
3.	Optics	Divergence slit		Fixed or automatic variable
		Scattering slit		Fixed or automatic variable
		Receiving slit		Fixed or automatic variable
		Optics alignment		Automatic alignment of tube height, goniometer, optics and detector
4.	Detector	Detector		Scintillation counter (others: optional)
5.	Dimensions	H x W x D	mm	1600 x 1100 x 800
		Sample height	mm	1050

Annexure 2

Technical specifications of SHIMADZU DTG-60/60H instrument

Model	**SHIMADZU DTG-60/60H**
Balance type	Parallel guide differential top pan type
Description	**Range**
Measured temperature range, °C	Room temperature to 1,100°C
Measurable range, mg	± 500
Measurable range, µV	± 1000
Readability, mg	0.001
Sample quantity, g max	1, in gross weight
Dimensions, mm	W:386 D:590 H:540
Weight, Kg	33
Required power supply	AC100, 120V, 1300VA, 50/60Hz

Annexure 3

Fuel cost for Carbodiesel5

Items	Cost
Diesel - 950 ml	48.45 Ru.
43g CB (equal to 50ml)	0.215 Ru.
0.15 kWh electricity charge	0.90 Ru.
Total fuel Cost	49.56 Ru.

Annexure 4

Technical specifications of Penkin Elmer spectroscopy

Model	**Penkin Elmer spectroscopy, ISO-9001**
Detectors	FR-DTGS Detector
Wavelength range, cm^{-1}	7,800 – 350 with KBr beamsplitter
Resolution, cm^{-1}	0.5 to 64
Signal to noise ratio for KBr optics	30,000/1 rms, 6,000/1 p-p for a 5 second measurement
Wavelength Accuracy, cm^{-1}	0.1 at 3000
Optics	Kinematically mounted, zero alignment optics , with high reflectivity and a low-angle off axis design
Size, mm	475W x 547D x 260H
Weight, Kg	30

Annexure 5

Different types of surfactant

S.No.	Name of the surfactant	Chemical formula	HLB value
1	Span 20 (Sorbitan monolaurate)	$C_{18}H_{34}O_6$	8.6
2	Span 80 (Sorbitan monooleate)	$C_{24}H_{44}O_6$	4.3
3	Tween-20 (polyoxyethylene sorbitan monolaurate)	$C_{58}H_{114}O_{26}$	16
4	Tween 80 (Polysorbate 80)	$C_{64}H_{124}O_{26}$	15
5	Span 80 + Tween 80 mixed	-	6.45

Annexure 6

Technical specifications Zeta potential analyser

Description	**Unit**	**Maximum value or range**
Zeta potential measurement range	mV	-200 to 200
Mobility	cm2/sec .V	-20 to 20
DLS light source:		He-Ne laser 633nm, Max 10mW
Particle size range for zeta potential measurement	µm	0.02-100 (Measurable size changes depending on the particle property and medium.)
Particle size range for particle size distribution measurement	µm	0.1-1 (Measurable size changes depending on the particle property and medium.)
Supply voltage	V DC	0 to 350
Weight	kg	25
Power supply	Hz	AC100V 1A 50/60

Annexure 7

Technical specification of BHOLIN VISCO-88

Description	**Unit**	**Data**
Rotational speeds	rpm	0 - 1000
Shear rate range	S^{-1}	$0 - 2x10^{-4}$
Torque range	mNm	0 - 10
Shear stress range	Pa	$0 - 10^{-4}$
Viscosity range	mPa.s	$5 - 10^{-7}$
Temperature range	°C	-35 to 150
Operating voltage	V	9 (Rechargeable batteries)
Size/weight (instrument excluding measuring geometry)	Cm/ kg	24 (H) x 15 (W) x 23 (D) /1.2
Size (instrument on stand)	cm	55 (maxH) x 24 (W) x 23 (D)
Size/weight (instrument in carrying case)	Cm/ kg	56 x 43cm x 19cm /10.5

Annexure 8

Technical specifications of the diesel engine

S. No.	Description	Unit	Data
1	Model type	-	Kirloskar TAF1
2	Type of injection	-	Direct
3	Rated power	kW	4.4
4	Rated speed	rpm	1500
5	Bore x Stroke	mm	87.5 x 110
6	Compression ratio	-	17.5:1
7	Method of cooling	-	Air cooled with radial fan
8	Piston type	-	Bowl-in-piston
9	Type of fuel injection	-	Pump-line-nozzle injection system
10	Nozzle type	-	Multi hole
11	No. of holes	-	3
12	Number of valves	-	2
13	Needle lift	mm	0.25
14	Spray-hole diameter	mm	0.25
15	Cone angle	deg	110
16	Start of injection	^{o}CA bTDC	23
17	Nozzle opening pressure	bar	200
18	Inlet valve opening	^{o}CA bTDC	4.5
19	Inlet valve closing	^{o}CA aBDC	35.5
20	Exhaust valve opening	^{o}CA bBDC	35.5
21	Exhaust valve closing	^{o}CA bBDC	4.5
22	Connecting rod length	mm	220
23	Weight	kg	163

Annexure 9

Specification of the pressure transducer

S. No.	Description	Unit	Data
1	Model type	-	KIST LER, Switzerland 601 A, air cooled
2	Pressure range	bar	0-100
3	Sensitivity	mV/bar	25
4	Linearity	-	0.1 < + % FS O
5	Acceleration sensitivity	bar/g	< 0.0 01
6	Operating temperature range	^{o}C	-196 to 200
7	Capacitance	PF	5
8	Connector, Teflon insulator	-	M4 x 0.35
9	Weight	g	1.7

Annexure 10

Technical specification of AVL DiGAS anlyser

S. No.	Description	Unit	Data	Accuracy
1	Model type		AVL Digas 444 analyser	
2	CO	%	0-10	< 0.6% vol: ±0.03% vol ≥ 0.6% vol: ± 5% of initial value
3	CO_2	%	0-20	< 10% vol: ±0.05% vol ≥ 10% vol: ± 5% of vol
4	HC	ppm vol.	0-20000	< 200 ppm vol: ± 10 ppm vol ≥ 200 ppm vol: ± 5% of initial value
5	NO	ppm vol.	0-5000	< 500 ppm vol: ± 50 ppm vol ≥ 500 ppm vol: ± 10% of initial value
6	O_2	% vol.	0-22	< 2% vol: ±0.01% vol ≥ 2% vol: ± 5% of vol
7	Operating Temperature	^oC	5-45	
8	Dimensions	mm^3	270 Wx320Dx85H	
9	Weight	Kg	4.5	
10	Power consumption	W	≈25	
11	Power supply	V	110-220	

Annexure 11

Technical specification of AVL 437C smoke meter

S. No.	**Description**	**Unit**	**Data**
1	Measuring range	%	0-100 opacity
2	Accuracy and repeatability	%	±1 of full scale
3	Linearity check	-	48.4%-53.1%/1.54m^{-1}-1.76m^{-1}
4	Alarming signal temperature	^{o}C	Lights up when temperature of measuring chamber is below 70.
5	Measuring chamber length	mm	430±5
6	Measuring chamber heating		Thermostatically controlled
7	Light source	V	Halogen lamp 12
8	Detector	mm	Selenium Photocell dia. 45
9	Weight	kg	24

Annexure 12

MATLAB PROGRAM

Program: **twozone_cbwd.m** (for emissions modelling)
RUN

```
clear all
close all
clc
%values declaration
ga = 0.33;y = 1.33; Vcl = 0.0000401; D = 82.5e-3;
a = 8; l = 2; aw = 3; nw = 5; Mf = 115; Ma = 103;
Tw = 450; R = 8.314; c = 3.4e-8;
dmfb = 0.725986; %at no load
qvs = 42.612e6; %lower heat of combustion

ca=zeros(1,290); p=zeros(1,290); T=zeros(1,290); V=zeros(1,290);
E=zeros(1,290); dW=zeros(1,290); dQ=zeros(1,290); F=zeros(1,290);
q=zeros(1,290); k=zeros(1,290); ht=zeros(1,290); ddd=zeros(1,290);
tu=zeros(1,290); qq=zeros(1,290); bu=zeros(1,290); au=zeros(1,290);
bb=zeros(1,290); ab=zeros(1,290); Tb=zeros(1,290); bbmix=zeros(1,290);
Tbmix=zeros(1,290); wbmix=zeros(1,290); wb=zeros(1,290);
cau=zeros(123,290); W = zeros(1,290);

%IVC
ca(1) = -145;
p(1) = 1.85e5;
T(1) = 350;
V(1)=0.0000401+0.0003305*(1+4-cos(ca(1)*0.017453)-sqrt(16-
(sin(ca(1)*0.017444))^2));
mfinj = 1.459e-3;
mfj = mfinj/12;
Watot = (p(1)*V(1))/(R*T(1)); %ideal gas eqn
afr = Watot/mfinj;
maj = afr/mfj;
Wftot = Watot/afr;            %global AFR=Watot/Wftot
E(1) = ienergy(T(1))*1000;    %calcualte E1


for i=1:123
      ca(i+1) = ca(i) + 1;
      V(i+1)=0.0000401+0.0003305*(1+4-cos(ca(i+1)*0.017453)-sqrt(16-
      (sin(ca(i+1)*0.017444))^2));
      T(i+1)=T(i)*(V(i)/V(i+1))^ga;  %isentropic change
      b(i) = Watot;
      for it = 1:5
            p(i+1) = (V(i)*T(i+1)*p(i))/(V(i+1)*T(i));
            for j = 1:50
                  [fe fed dq]=enerbal(p(i),p(i+1),T(i),T(i+1),V(i),V(i+1));
                  tu(j+1)=tu(j+1) - fe/fed;      %newton raphson method
                  ddd(j+1)=dq;
                  ht(j+1)=-ddd(j+1);
            end
      end
      tu(j)=T(i);
end

%start of combustion
```

```
cau(123) = ca(123);
Tu(123) = T(123);
Tb(123) = T(123);
Vu(123) = V(123);
Vb(123) = 0;
bu(123) = b(123);
bb(123) = 0;

file3 = 'E:/Study/modify.xlsx';
Tbmod = xlsread(file3,'D7:D296');
Tumod = xlsread(file3,'E7:E296');
x = -145:144;
xx = -145:5:144;
Tspl = spline(x,Tbmod,xx);

for ii=123:289
      qq(ii+1)=combsm2(ca(ii+1));
      q=qq(ii+1);
      ca(ii+1)=ca(ii)+1;
      cau(ii+1)=cau(ii+1);
      V(ii+1)=0.0000401+0.0003305*(1+4-cos(ca(ii+1)*0.017453)-sqrt(16-
      sin(ca(ii+1)*0.017453)*sin(ca(ii+1)*0.017453)));
      T(ii+1)=T(ii)*(V(ii)/V(ii+1))^ga;           % ga=1.31

      W(ii) = 1 - exp(-3*(((ca(ii) - (-23))/71)^5));

      Tu(ii+1)=Tu(ii)*(V(ii)/V(ii+1))^ga;
      p(ii+1)=(p(ii)*V(ii)*T(ii+1))/(T(ii)*V(ii+1));

      bu(ii+1)= Watot - maj/Ma;
      wloss = bu(ii) - bu(ii+1);
      au(ii) = bu(ii);
      if ii<=136
            if ii==5
                  au(ii) = bu(ii) - 0.21*wloss;
            elseif ii==6
                  au(ii) = bu(ii) - 0.79*wloss;
            end

            Vu(ii+1) = (bu(ii+1)*R*Tu(ii+1))/p(ii+1);

            for j =1:50
                  [fe fed]=
                  enerbal2(p(ii),p(ii+1),T(ii),T(ii+1),Vu(ii),Vu(ii+1),q);
                  if fed<eps
                        T(ii+1)=T(ii);
                  else
                        T(ii+1)=T(ii+1)-fe/fed;   %newton raphson method
                  end
            end
      end


      %burning zone
      bb(ii+1) = Watot + maj/Mf;
      wgain = bb(ii+1) - bu(ii);
      if ii==5
            bbmix(ii) = bb(ii) + 0.21*wgain;
      elseif ii==6
            bbmix(ii) = bb(ii) + 0.79*wgain;
```

```
      elseif ii==7
            bbmix(ii) = bb(ii) + (mfb/Mf);
      else
            bbmix(ii) = bb(ii);
      end

      Tbmix(ii) = (bb(ii)*Tb(ii) + wgain*Tu(ii))/(bb(ii) + wgain);
      Tb(ii+1) = Tbmix(ii)*((p(ii+1)/p(ii))^(ga/y)) -
      (dmfb*qvs*ga)/(bbmix(ii)*R);
      Vb(ii+1) = (wb(ii)*R*Tb(ii+1))/p(ii+1);

      for j = 1:50
            [fe fed dq]=enerbal(p(i),p(i+1),T(i),T(i+1),V(i),V(i+1));
            tu(j+1)=tu(j+1) - fe/fed;     %newton raphson method
            ddd(j+1)=dq;
            ht(j+1)=-ddd(j+1);
      end
      for j=1:50
            [fe fed
            dq]=enerbal2(p(ii),p(ii+1),T(ii),T(ii+1),V(ii),V(ii+1),q);
            T(ii+1)=T(ii+1)-fe/fed;          %newton raphson method
      end

      ddd(ii+1)=dq;
      ht(ii+1)=qq(ii+1)+ddd(ii+1);
end

file='E:/Study/data/Emulsion10.csv';
file2='E:/test.xlsx';
file3='E:/Study/data/New HR.xlsx';
pres = xlsread(file,'D5343:D5670');
theta = xlsread(file,'B5343:B5670');
heat = xlsread(file2,'N1:N290');
heatsim = xlsread(file2,'O1:O290');
heatr = xlsread(file,'G5380:G5530');
thetar = xlsread(file,'B5380:B5530');
theta3 = xlsread(file3,'J5:J83');
heatrr = xlsread(file3,'L5:L83');
hrsim = xlsread(file3,'K5:K83');
theta3s = -180:1:180;
heatrrs = spline(theta3,heatrr,theta3s);
hrsims = spline(theta3,hrsim,theta3s);
Tspl = spline(ca,Tbmod,theta3s);
pres = pres*1e5;
heatr = heatr*0.01;
thetar = thetar - 360;
theta2 = theta - 360;
theta1 = theta2 - 10;
limit = [-135 135 0 8e6];
limit1 = [-125 125 -10 2000];
limit2 = [-75 75 0 1.1];
limit3 = [-45 45 -10 70];

for ii=1:290
      m11=m11+1;
      if m11<63
            mfc(ii)=mfrt*0.00028*mfb(ii);
      else
            mfc(ii)=mfrt*0.00028*mfb(61);
      end
```

```
end

%%%emissions modelling
phi(1)=-145;
t(1)=350;
p(1)=1.55e5;
v(1)=0.0000401+0.0003305*(1+4-cos(phi(1)*0.017453)-sqrt(16-
sin(phi(1)*0.017453)*sin(phi(1)*0.017453)));

mftot=mfrt*0.028/M;              % mass of fuel in Kmol/cycle.
matot=16*mftot;
E(1)=ienergy(t(1))*matot*1000;      %internal energy in j/mol

for iii=1:122
      phi(iii+1)=phi(iii)+1;
      v(iii+1)=0.0000401+0.0003305*(1+4-cos(phi(iii+1)*0.017453)-sqrt(16-
      sin(phi(iii+1)*0.017453)*sin(phi(iii+1)*0.017453)));
      t(iii+1)=t(iii)*(v(iii)/v(iii+1))^0.33;

      for kkk=1:5
            p(iii+1)=(p(iii)*v(iii)*t(iii+1))/(t(iii)*v(iii+1));
            for jjj=1:50
                  [fe fed dq]=
                  ebalance1(p(jjj),p(jjj+1),t(jjj),t(jjj+1),v(jjj),v(jjj+1)
                  );
                  t(jjj+1)=t(jjj+1)-fe/fed;          %newton raphson method
                  ddd(jjj+1)=dq;
                  ht(jjj+1)=-ddd(jjj+1);             % heat tranfer rate
            end
      end
      tu(jjj)=t(jjj);
      vu(jjj)=v(jjj);
end

aj(4)=0.21*matot;  aj(3)=0.70*matot;
for nnn=1:12
      bju(nnn)=aj(nnn);
end
roa=1.29*273/t(iii);
tu(123)=t(123);    tb(123)=t(123);
vu(123)=v(123);    vb(123)=0;
y(3)=0.1; y(4)=0.1; y(5)=1e-6; y(6)=1e-6;
for mmm=123:289
      phi(mmm+1)=phi(mmm)+1;
      pphii=pphii+1;
      sum=sum+1;
      qq(mmm+1)=combsm2(phi(mmm+1));
      q=qq(mmm+1);
      v(mmm+1)=0.0000401+0.0003305*(1+4-cos(phi(mmm+1)*0.017453)-sqrt(16-
      sin(phi(mmm+1)*0.017453)*sin(phi(mmm+1)*0.017453)));
      t(mmm+1)=t(mmm)*(v(mmm)/v(mmm+1))^0.33;
      p(mmm+1)=(p(mmm)*v(mmm)*t(mmm+1))/(t(mmm)*v(mmm+1));

      for kk2=1:50
            [fe fed dq]=
            ebalancec(p(mmm),p(mmm+1),t(mmm),t(mmm+1),v(mmm),v(mmm+1),q);
            if fed<eps
                  t(mmm+1)=t(mmm);
            else
                  t(mmm+1)=t(mmm+1)-fe(1)/fed(1);  %newton raphson method
```

```
      end
end

K(1)=10^(0.432168*log(t(mmm+1)/1000)+(-0.112464e5)/t(mmm+1)+0.267269e1+(-
0.745744e-4)*t(mmm+1)+(0.242484e-8)*(t(mmm+1)^2));
K(2)=10^(0.310805*log(t(mmm+1)/1000)+(-0.129540e5)/t(mmm+1)+0.321779e1+(-
0.738336e-4)*t(mmm+1)+(0.344645e-8)*(t(mmm+1)^2));
K(3)=10^(-0.141784*log(t(mmm+1)/1000)-
0.213308e4/t(mmm+1)+0.853461+(0.355015e-4)*t(mmm+1)+(-0.310227e-
8)*(t(mmm+1)^2));
K(4)=10^(0.0150879*log(t(mmm+1)/1000)-
0.470959e4/t(mmm+1)+0.646096+(0.272805e-5)*t(mmm+1)+(-0.154444e-
8)*(t(mmm+1)^2));
K(5)=10^((-0.752364*log(t(mmm+1)/1000)+0.124210e5/t(mmm+1)-
2.60286+(0.259556e-3)*t(mmm+1)+(-0.162687e-7)*(t(mmm+1)^2))/100);
K(6)=10^(((-0.415303e-2)*log(t(mmm+1)/1000)+0.148627e5/t(mmm+1)-
0.475746e1+(0.124699e-3)*t(mmm+1)+(-0.900227e-8)*(t(mmm+1)^2))/1e5);

%K(1)=1;K(2)=1;K(3)=1;K(4)=1;K(5)=4.7;K(6)=12.18;
c(1)=K(1)/sqrt(p(mmm+1)/1e5);
c(2)=K(2)/sqrt(p(mmm+1)/1e5);
c(3)=K(3);
c(4)=K(4);
c(5)=K(5)*sqrt(p(mmm+1)/1e5);
c(6)=K(6)*sqrt(p(mmm+1)/1e5);
d(1)=b/a;
d(2)=g/a+0.42/(epss*er*a);
d(3)=delta/a+1.58/(epss*er*a);
for fi=1:10
      D76=0.5*c(1)/sqrt(y(6));
      D103=0.5*c(4)*sqrt(y(4))/sqrt(y(3));
      D84=0.5*c(2)/sqrt(y(4));
      D26=c(5)*sqrt(y(4));
      D94=0.5*c(3)*sqrt(y(6))/sqrt(y(5));
      D24=0.5*c(5)*y(6)/sqrt(y(4));
      D96=0.5*c(3)*sqrt(y(4)/y(6));
      D14=0.5*c(6)*y(5)/sqrt(y(4));
      D104=0.5*c(4)*sqrt(y(3))/sqrt(y(4));
      D15=c(6)*sqrt(y(4));

      A(1,1)=1+D103;
      A(1,2)=D14+D24+1+D84+D104+D94;
      A(1,3)=D15+1;
      A(1,4)=D26+1+D76+D96;
      A(2,1)=0;
      A(2,2)=2*D24+D94-d(1)*D14;
      A(2,3)=-d(1)*D15-d(1);
      A(2,4)=2*D26+2+D76+D96;
      A(3,1)=D103;
      A(3,2)=2*D14+D24+2+D84+D94+D104-d(2)*D14;
      A(3,3)=2*D15+1-d(2)*D15-d(2);
      A(3,4)=D26+D96;
      A(4,1)=2+D103;
      A(4,2)=D104-d(3)*D14;
      A(4,3)=-d(3)*D15-d(3);
      A(4,4)=0;

      y(7)=c(1)*sqrt(y(6));
      y(8)=c(2)*sqrt(y(4));
      y(9)=c(3)*sqrt(y(4)*y(6));
```

```
        y(10)=c(4)*sqrt(y(4)*y(3));
        y(2)=c(5)*sqrt(y(4))*y(6);
        y(1)=c(6)*sqrt(y(4))*y(5);

        f(1)=y(1)+y(2)+y(3)+y(4)+y(5)+y(6)+y(7)+y(8)+y(9)+y(10)-1;
        f(2)=2*y(2)+2*y(6)+y(7)+y(9)-d(1)*y(1)-d(1)*y(5);
        f(3)=2*y(1)+y(2)+2*y(4)+y(5)+y(8)+y(9)+y(10)-d(2)*y(1)-d(2)*y(5);
        f(4)=2*y(3)+y(10)-d(3)*y(1)-d(3)*y(5);

        A(1,5)=-f(1);
        A(2,5)=-f(2);
        A(3,5)=-f(3);
        A(4,5)=-f(4);

        % gauss elimination
        A=rref(A);
        dy(4)=A(4,5);
        dy(3)=A(3,5);
        dy(2)=A(2,5);
        dy(1)=A(1,5);

        y(3)=y(3)+dy(1);
        y(4)=y(4)+dy(2);
        y(5)=y(5)+dy(3);
        y(6)=y(6)+dy(4);

        y(7)=c(1)*sqrt(y(6));
        y(8)=c(2)*sqrt(y(4));
        y(9)=c(3)*sqrt(y(4)*y(6));
        y(10)=c(4)*sqrt(y(4)*y(3));
        y(2)=c(5)*y(6)*sqrt(y(4));
        y(1)=c(6)*y(5)*sqrt(y(4));


        yco2(mmm+1)=y(1);
        yh2o(mmm+1)=y(2);
        yn2(mmm+1)=y(3);
        yo2(mmm+1)=y(4);
        yco(mmm+1)=y(5);
        yh2(mmm+1)=y(6);
        yh(mmm+1)=y(7);
        yo(mmm+1)=y(8);
        yoh(mmm+1)=y(9);
        yno(mmm+1)=y(10);
end
ddd(mmm+1)=dq;
ht(mmm+1)=qq(mmm+1)+ddd(mmm+1);
end
chr(1)=ht(1);pbar(1)=p(1)/1e5;
for n11=1:289
      chr(n11+1)=chr(n11)+ht(n11);pbar(n11+1)=p(n11+1)/1e5;
end

cumsum(yco)
cumsum(yco2)

%plot graphs
subplot(2,2,1)
plot(ca,p)
```

```
hold on
plot(theta1,pres,'red')
axis(limit);
xlabel('Crank angle (deg)')
ylabel('Pressure (Pa)')
subplot(2,2,2)
hold on
plot(ca,Tumod,'b-')
hold on
plot(theta3s,Tspl,'red')
axis(limit1);
xlabel('Crank angle (deg)')
ylabel('Temperature (K)')
subplot(2,2,3)
plot(ca,W)
axis(limit2);
hold on
plot(thetar,heatr,'r-')
xlabel('Crank angle (deg)')
ylabel('mf of fuel burnt')
subplot(2,2,4)
plot(theta3s,hrsims,'red')
hold on
plot(theta3s,heatrrs,'blue')
axis(limit3);
xlabel('Crank angle (deg)')
ylabel('Heat Release rate (W)')
```

FUNCTIONS

```
function [fe fed dq]=enerbal(p1,p2,t1,t2,v1,v2)
matot=28.543*1.18*0.028/170;
s=0.11;
d=87.5e-3;
n=1470;
 E1=ienergy(t1)*matot*1000;
 E2=ienergy(t2)*matot*1000;
       dw=0.5*(p1+p2)*(v2-v1);
       tg=0.5*(t1+t2);
       mua=3.3*1e-7*(tg^0.7);
       mua=mua/(1+0.027*0.94);
       re=(0.0387*n*s*d)/mua;
       lg=1005*mua/0.7 ;                % thermal conductivity
       dq=((0.626/d)*lg*(re^0.6)*(450-tg)+5.67*(1e-8)*(450^4-tg^4))/(6*n);
         % annand formula from rajendraprasad paper
       fe=E2-E1+dw-dq;              %energy balance
       dqd=((0.2626/d)*lg*(re^0.6)*(-1)+5.67*(1e-8)*(-4*tg^3))/(6*n);
       fed=ienergyd(t2)*matot*1000-dqd;
```

```
function [fe fed dq] = enerbal2(p1,p2,t1,t2,v1,v2,q)
M=170;
```

```
afr=40;
mfrt=0.5;  % in kg/hr
n=1470;
matot=afr*mfrt*2.8e-3/M ;s=0.11;d=87.5e-3;
 E1=fienergy(t1)*matot*1000;
 E2=fienergy(t2)*matot*1000;
    dw=0.5*(p1+p2)*(v2-v1);
       tg=0.5*(t1+t2);
       mua=3.3*1e-7*(tg^0.7);
       mua=mua/(1+0.027*0.94);
       re=(0.0387*n*s*d)/mua;
       lg=1005*mua/0.7 ;                % thermal conductivity
       dq=((0.2626/d)*lg*(re^0.6)*(450-tg)+5.67*(1e-8)*(450^4-tg^4))/(6*n);  % annand formula
from rajendraprasad paper
       fe=E2-E1+dw-dq-q;              %energy balance
       dqd=((0.2626/d)*lg*(re^0.6)*(-1)+5.67*(1e-8)*(-4*tg^3))/(6*n);
       fed=fienergyd(t2)*matot*1000-dqd;

-----------
function [fe fed dq] = enerbal3(p1,p2,t1mix,t2,v1,v2,q)
M=170;
afr=28.543;
mfrt=0.5;  % in kg/hr
n=1470;
matot=afr*mfrt*2.8e-3/M ;s=0.11;d=87.5e-3;
 E1mix = fienergy(t1mix)*matot*1000;
 E2 = fienergy(t2)*matot*1000;
    dw=0.5*(p1+p2)*(v2-v1);
       tg=0.5*(t1+t2);
       mua=3.3*1e-7*(tg^0.7);
       mua=mua/(1+0.027*0.94);
       re=(0.0387*n*s*d)/mua;
       lg=1005*mua/0.7 ;                % thermal conductivity
       dq=((0.2626/d)*lg*(re^0.6)*(450-tg)+5.67*(1e-8)*(450^4-tg^4))/(6*n);  % annand formula
from rajendraprasad paper
       fe=E2-E1mix+dw-dq;             %energy balance
       dqd=((0.2626/d)*lg*(re^0.6)*(-1)+5.67*(1e-8)*(-4*tg^3))/(6*n);
       fed=fienergyd(t2)*matot*1000-dqd;

-----------
function h=enthalpy(t)
hn2=8.314*(3.34*t+2.94e-4*t^2+1.95e-9*t^3-6.57e-12*t^4);
ho2=8.314*(3.25*t+6.52e-4*t^2-1.5e-7*t^3+1.54e-11*t^4);
h=0.79*hn2+0.21*ho2;    %internal energy in j/mol

-----------
function hd = enthalpyd(t)
  hn2d=8.314*(3.34 + 2*2.94e-4*t + 3*1.95e-9*t^2 - 4*6.57e-12*t^3);
  ho2d=8.314*(3.25 + 2*6.52e-4*t - 3*1.5e-7*t^2 + 4*1.54e-11*t^3);
  hd=0.79*hn2d+0.21*ho2d;
```

```
----------
function [fe fed] = enthbal(t1bmix,t1b,t1u)
M=170;
afr=28.543;
mfrt=0.5;  % in kg/hr
n=1470;
matot=afr*mfrt*2.8e-3/M;
s=0.11;d=87.5e-3;
 H1bmix = enthalpy(t1bmix)*matot*1000;
 H1b = enthalpy(t1b)*matot*1000;
 H1u = enthalpy(t1u)*matot*1000;
        fe = H1bmix - H1b - H1u;              %energy balance
        fed = enthalpyd(t1bmix)*matot*1000;
end

----------
function uff=fienergy(t)
nf=0.5*3.3/160;
un2=8.314*(3.34*t+2.94e-4*t^2+1.95e-9*t^3-6.57e-12*t^4)-8.314*t;
uo2=8.314*(3.25*t+6.52e-4*t^2-1.5e-7*t^3+1.54e-11*t^4)-8.314*t;
uf=8.314*(6.4*t+5.3e-2*t^2-1.27e-5*t^3+1.06e-9*t^4)-8.314*t;
uff = (0.79-0.79*nf)*un2 + (0.21-0.21*nf)*uo2 + nf*uf;    %internal energy in j/mol

----------
function du=fienergyd(t)
nf=0.5*3.3/160;
un2=8.314*(3.34+2*2.94e-4*t+3*1.95e-9*t^2-4*6.57e-12*t^3)-8.314;
uo2=8.314*(3.25+2*6.52e-4*t-2*1.5e-7*t^2+4*1.54e-11*t^3)-8.314;
uf=8.314*(6.4+2*5.3e-2*t-3*1.27e-5*t^2+4*1.06e-9*t^3)-8.314;
du=(0.79-0.79*nf)*un2+(0.21-0.21*nf)*uo2+nf*uf;
  %internal energy in j/mol

----------
function u=fienergy(t)
un2=8.314*((3.34*(t))+(2.94e-4*(t^2))+(1.95e-9*(t^3))-(6.57e-12*(t^4)))-8.314*t;
uo2=8.314*((3.25*(t))+(6.52e-4*(t^2))-(1.5e-7*(t^3))+(1.54e-11*(t^4)))-8.314*t;
u = 0.79*un2 + 0.21*uo2;    %internal energy in j/mol

----------
function du = ienergyd(t)
un2d=8.314*(3.34+(2*(2.94e-4)*(t))+(3*1.95e-9*(t^2))-(4*6.57e-12*(t^3)))-8.314;
uo2d=8.314*(3.25+(2*6.52e-4*(t))-(3*1.5e-7*(t^2))+(4*1.54e-11*(t^3)))-8.314;
du = 0.79*un2d + 0.21*uo2d;    %internal energy in j/mol
```

LIST OF PATENTS FILES AND PUBLICATIONS

A. Patents under Examination

1. Inventors: Dr. S. Murugan and **Arun Kumar Wamankar**

Title: Process of Producing a Synthetic Fuel (Carbodiesel) from Carbon Black and Use the Same as an Alternative Fuel for CI (Diesel) Engines

Patent No. : Indian patent, File No. 213/ KOL/2013

2. Inventors: Dr. S. Murugan and **Arun Kumar Wamankar**

Title: An Emulsified fuel for Compression Ignition Engine

Patent No. : Indian patent, File No. 1019/KOL/2013

B. List of Publications

(1) International Journal

1. **Arun Kumar Wamankar**, S. Murugan. Experimental investigation of carbon black–water–diesel emulsion in a stationary DI diesel engine. **Fuel Processing Technology, Elsevier publication**, 125; 2014: 258-266.

2. **Arun Kumar Wamankar**, S. Murugam. Effect of injection timings on DI diesel engine fuelled with synthetic fuel blend. **Journal of Energy Institute, Elsevier publication**, 88; 2015: 406-413.

3. **Arun Kumar Wamankar**, S. Murugan. Combustion, performance and emission of a diesel engine fueled with diesel doped with Carbon black. **Energy, Elsevier publication**, 86; 2015: 467-475.

4. **Arun Kumar Wamankar**, S. Murugan. DI diesel engine operated with Carbon-black-water-diesel slurry at different injection timing and nozzle opening pressure. **Journal of Energy Institute, Elsevier publication**, DOI: 10.1016/j.joei.2015.04.003, 2015.

5. **Arun Kumar Wamankar**, S. Murugan. Review on Production, Characterisation and Utilisation of Solid fuels in Diesel Engines. **Renewable and Sustainable Energy Reviews, Elsevier publication**, 51; 2015: 249-262.

6. **Arun Kumar Wamankar**, S. Murugan. Combustion, performance and emission characteristics of a diesel engine with internal jet piston using carbon black-water-diesel emulsion. **Energy, Elsevier publication**, 91; 2015: 1030-1037.

7.**Arun Kumar Wamankar**, Ashok Kumar Satapathy, S. Murugan. Experimental investigation of the effect of compression ratio, injection timing and pressure in a DI diesel engine running on Carbon black-water-diesel emulsion. **Energy, Elsevier publication**, 93;2015:511-520.

REFERENCES

[1] Intergovernmental Panel on Climate Change in 2015. http://www.ipcc.ch.

[2] http://www.esrl.noaa.gov/gmd/ccgg/trends.

[3] Atmospheric greenhouse gas concentration 4 assessments. http:// www.eea.europa.ed.

[4] Ozone depletion. http:// environment.nationalgeographic.com

[5] Mr. Robison's Regents Earth Science website. How is Global Warming Related to the Ozone Hole? http://www.regentsearthscience.com

[6] Boden TA, Marland G, Andres RJ. Global regional and national fossil-fuel CO_2 emissions. Carbon dioxide information analysis center, Oak ridge national laboratory, U.S. Department of Energy, Oak Ridge, U.S.A. 2009.

[7] The global carbon budget 1959–2011. Earth system science data discussions 5th 2012; 2: 1107–1157.

[8] Defra UK. The 2014 government greenhouse gas conversion factors for company reporting. Department for Environment, Food & Rural Affairs, London; 2014.

[9] Global carbon budget 2014. http://www.globalcarbonproject.org

[10] Watson RT, Rodhe H, Oeschger H, Siegenthaler U. Greenhouse gases and aerosols. 1–40. www.ipcc.ch/ipccreports/ chapter_01.pdf.

[11] Solid waste management. http://www.cyen.org

[12] Murugan S, Sai Gu. Research and development activities in pyrolysis-contributions from Indian scientific community-A review. Renew Sustain Energy Rev 2015; 46: 282–295.

[13] Rajeshwari KV, Balakrishnan M. Biochemical methods of conversion. Energy environment technology division, TERI, New Delhi.

[14] Rai GD. Nov-conventional energy sources. Khanna publication, Fifth edition 2011, Delhi.

[15] Angelidaki I, Batstone DJ. Anaerobic digestion: process in Solid waste technology & management 2011.

[16] Thorin E, Boer ED, Belous O, Song H. Waste to Energy- A Review. International Conference on Applied Energy, ICAE 2012, Suzhou, China 2012.

[17] Ray NHS, Mohanty MK, Mohanty RC. Biogas as alternate fuel in diesel engines: A Literature Review. IOSR Journal of Mechanical and Civil Engineering 2013; 9: 23–28.

[18] Singh J, GuSai. Biomass conversion to energy in India–a critique. Renew Sustain Energy Rev 2010; 14: 1367–78.

[19] Fendel A, Firege H. Competition of different methods for recovering energy from waste leading to overcapacities. ISWA World congress, Hamburg, Germany 2010.

[20] Ptasinski KJ. Thermodynamic efficiency of biomass gasification and biofuels conversion. Biofpr 2008; 2: 239–253.

[21] Sharma BK, Moserb BR, Vermillionb KE, Dollb KM, Rajagopalan NK. Production characterization and fuel properties of alternative diesel fuel from pyrolysis of waste plastic grocery bags. Fuel Proce Techno 2014; 122: 79–90.

[22] Brownsort PA. Biomass pyrolysis processes: Review of scope, control and variability. 2009, www.biochar. Org.uk

[23] Bridgwater AV. Czernik S, Piskorz J. An overview of fast pyrolysis. Prog Thermochem biomass convers 2001; 2: 977–997.

[24] Demibas A. Arin G. An overview of biomass pyrolysis. Energy Source Part A 2002; 24: 471–482.

[25] Jahirul MI, Rasul MG, Chowdhury AA, Ashwath N. Biofuels production through biomass pyrolysis - A Technological Review, Energies 2012; 5: 4952–5001.

[26] Cornelissen T, Yperman Y, Reggers G, Schreurs S, Carleer R. Flash co-pyrolysis of biomass with polylactic acid. Part 1: Influence on bio-oil yield and heating value. Fuel 2008; 87: 1031–1041.

[27] Asnani PU. Solid waste management. IIR Reports 2006.

[28] Harnessing Hydrogen from Wastes. Waste to Energy, vol.7, 2013. http://w2es.com/Source/Hydrogen.pdf

[29] Kapdan IK, Kargi F. Bio-hydrogen production from waste materials. Enzyme and Microbial Technology 2006; 38: 569–582.

[30] Messenger B. Tackling tyre waste, waste management world magazine, 22 April 2013.

[31] Murugana S, Ramaswamy MC, Nagarajan G. Assessment of pyrolysis oil as an energy source for diesel engines. Fuel Proces Techno 90; 2009: 67 –74.

[32] Williams PT. Pyrolysis of waste tyres: A Review. Energy Research Institute, University of Leeds, UK .

[33] Aylon E, Colino FA, Navarro M.V, Murillo R, Garcıa T, Mastral AM. Waste Tire Pyrolysis: comparison between fixed bed reactor and moving bed reactor. Ind Eng Chem Res 2008; 47: 4029–4033.

[34] Islam MR, Parveen M, Haniu H, Sarker MRI. Innovation in pyrolysis technology for management of scrap tire: a solution of energy and environment. International Journal of Environmental Science and Development 2010; 1: 258–264.

[35] Unapumnuk K, Keener TC, Lu M. Pyrolysis behavior of tire-derived fuels at different temperatures and heating rates. J Air & Waste Manage Assoc 2006; 56: 618–627.

[36] Ganesan V. Internal combustion engine. Tata McGraw Hill Publication New Delhi 2011.

[37] Soloiu V, Lewis J, Yoshihara Y, Nishiwaki K. Combustion characteristics of a charcoal slurry in a direct injection diesel engine and the impact on the injection system performance. Energy 2011; 36: 4353–4371.

[38] Uzkan T, Horton CE. Combustion of coal-water slurry in a two-cycle diesel engine: effects of fuel amount and timing. J Eng Gas Turbines Power 1990; 112: 376–383.

[39] Bell SR, Caton JA. Coal-fueled diesel engines: analytical evaluations of Institute. Twenty-first Symposium (International) on Combustion 1986; 471: 389–397.

[40] Hsu BD. Progress on the investigation of coal-water slurry fuel combustion in a medium speed diesel engine: part 1-ignition studies. J Eng Gas Turbines Power 1988; 110: 415–422.

[41] Purushothaman K, Nagarajan G. Effect of injection pressure on heat release rate and emissions in CI engine using orange skin powder diesel solution. Energ Convers Manage 2009; 50: 962–969.

[42] Basha JS, Anand RB. An experimental investigation in a diesel engine using carbon nanotubes blended water–diesel emulsion fuel. Proc. Inst Mech Eng Part A: J Power Energy 2011; 225–279.

[43] Tewari P, Doijode E, Banapurmath NR, Yaliwal VS. Experimental investigations on a diesel engine fuelled with multi walled carbon nanotubes blended biodiesel fuels. Int J Emerg Tech Adv Eng 2013; 3; 72–76.

[44] World diesel engine demand in 2015, by region.
http://www.statista.com/statistics/245357/world-diesel-engine-demand-by-region

[45] Heywood JB. Internal combustion engines fundamentals. McGraw Hill Publications: 1988; 491–667.

[46] Suzzi D. Diesel Nozzle Flow and Spray Formation: Coupled Simulations with Real Engine Validation. Institute of Aerospace Thermodynamics, University Stuttgart 2009.

[47] Evaporative Emission Control Technologies for Gasoline Powered Vehicles. Manufacturers of Emission Controls Association, Arlington, VA 2010. www.meca.org

[48] http://www.epa.gov.Nonroad Compression-Ignition Engines-Exhaust Emission Standards.

[49] https://en.wikipedia.org/wiki/Bharat Stage emission standards

[50] https://www.dieselnet.com/standards/us/nonroad.php

[51] Piriou B, Vaitilingoma G, Veyssiere B, Cuq B, Rouau X. Potential direct use of solid biomass in internal combustion engine. Prog Energ Combust 2013; 39; 169–188.

[52] Chen R, Wilson M, Leong YK, Bryant P, Yang H, Zhang DK. Preparation and rheology of biochar lignite char and coal slurry fuels. Fuel 2011; 90: 1689–1695.

[53] Dincer H, Boylu F, Sirkeci AA, Ates G. The effect of chemicals on the viscosity and stability of coal water slurries. Int J Miner Process 2003; 70: 41–51.

[54] Tian-ye GU, Guo-guang WU, Qi-hui LI, Zhi-qiang SUN, Fang ZENG, Guang-you WANG, Xian-liang MENG. Blended coals for improved coal water slurries. J China Univ Mining Tech 2008; 18; 50–54.

[55] Kihm KD, Terracina DP, Caton JA. Spray-tip droplet SMDs of intermittent high-pressure sprays of diesel fuel compared with coal- water slurry sprays, J Inst Energy. 1995; 68; 57–64.

[56] Khodakov GS. Coal water suspensions in power engineering. Therm Eng 2007; 54; 36–47.

[57] Mchale ET. Coal water fuel combustion. Twenty-first Symposium (International) on Combustion Germany 1986; 21; 159–171.

[58] Yuchi W, Li B, Li W, Chen H. Effects of coal characteristics on the properties of coal water slurry. Coal Prepara 2005; 25; 239–249.

[59] Ajay A, Yiannis AL, Combustion of CWF agglomerates from pulverized or micronized bituminous coal, carbon black, and diesel soot. Combust Flame 1994; 98; 326–349.

[60] Deng S, Zhou J. An experimental study of the effect of water content on combustion of coal -tar water emulsion droplets. Energy 2011; 36; 6130–6137.

[61] Burgess AR, Ghaffari R. Pre-ignition phenomena and their effects on overall combustion rates of coal slurry droplets. Twenty-Second Symposium (International) on Combustion, 1988: 2009–2017.

[62] Ken DK, Deignan P. Dynamic surface tension of coal-water slurry fuels. Fuel 1995; 74; 295–300.

[63] Chen X, Zhao L, Zhang XU, Qian C. An investigation on characteristics of coal–water slurry prepared from the solid residue of plasma pyrolysis of coal. Energ Convers Manage 2012; 62; 70–75.

[64] Basha JS, Anand RB. The influence of nanoadditive blended biodiesel fuels on the working characteristics of a diesel engine. J Braz Soc Mech Sci Eng 2013; 35; 257–264.

[65] Fawzi A, Amrousi Al, Ahmed M, Sabagh Al, Magda MO. Physicochemical characterization of emulsion fuel from fuel oil-water-charcoal and surfactants. Fuel 1996; 75; 1193–1198.

[66] Kalpesh V, Shyam D. Review of charcoal-diesel slurry an alternative fuel for compession ignition engine. Int J Adv Engi Res Stud 2012; 1; 143–147.

[67] Zhang G, Qiao X, Miao X, Hong J, Zheng J, Huang Z. Experimental study on the effect of coal to liquid on combustion and emission of heavy-duty diesel engine with exhaust gas recirculation. Appl Therm Eng 2012; 42; 64–70.

[68] Qiang Z, Keming L, Dafeng T. Research on Diesel-water coal slurry blends combustion on diesel engine of Generating Unit. Proc Power Energ Eng Conf 2009.

[69] Qiang Z, Lan-zhu R, Ying T. Effect of fuel supply advance angle on combustion and emission of diesel engine with diesel coal water slurry blend fuel. J Therm Sci Tech 2008; 1; 58–63.

[70] Seshadri AK, Caton JA, Kihn KD. Coal water slurry spray characteristics of a positive displacement fuel injection system. J Eng Gas Turbines Power 1992; 114; 528–533.

[71] Urban CM, Mecredy HE, Ryan TW, Ingalls MN, Jett BT. Coal-water slurry operation in an EMD diesel engine. J Eng Gas Turbines Power 1988; 110; 437–443.

[72] Kishan S, Bell SR, Caton JA. Numerical simulations of two-stroke cycle engines using coal fuels. J Eng Gas Turbines Power 1986; 108; 661–668.

[73] Rao AK, Melcher CH, Wilson RP, Balles EN, Schaub FS, Kimberley JA. Operating results of the cooper- bessemer JS-1 engine on coal-water slurry. J Eng Gas Turbines Power 1988; 110; 431–436.

[74] Hsu BD. Progress on the investigation of coal-water slurry fuel combustion in a medium speed diesel engine: part 2—preliminary full load test. J Eng Gas Turbines Power1988; 110; 423–430.

[75] Hsu BD, Leonard GL, Johnson RN. Progress on the investigation of coal-water-slurry fuel combustion in a medium-speed diesel engine: part 3—accumulator injector performance. J Eng Gas Turbines Power 1989; 111; 516–520.

[76] Hsu BD, Confer GL, Shen ZJ. Progress on the investigation of coal-water slurry fuel combustion in a medium-speed diesel engine: part 5—combustion studies. J Eng Gas Turbines Power 1992; 114; 515–521.

[77] Hsu BD, Branyon DP. Progress on the investigation of coal-water slurry fuel combustion in a medium-speed diesel engine: part 6—in-cylinder combustion photography studies. J Eng Gas Turbines Power 1993; 115; 790–797.

[78] Siebers DL, Dyer TM. The Auto-ignition and combustion of coal-water slurry under simulated diesel engine conditions. J Eng Gas Turbines Power 1986; 108; 654-660.

[79] Hsu BD. Coal-fueled diesel engine development update at GE transportation systems. J Eng Gas Turbines Power 1992; 114; 502–508.

[80] Benedek KR, Menzies KT, Johnson SA, Wilson RP, Rao AK, Schaub FS. Emission characteristics and control technology for stationary coal-fueled diesel engines. J Eng Gas Turbines Power 1989; 111; 507–515.

[81] Dodge LG, Callahan TJ, Ryan TW, Schwalb JA, Benson CE, Wilson RP. Injection characteristics of coal- water slurries in medium-speed diesel equipment. J Eng Gas Turbines Power 1992; 114; 522–527.

[82] Basha JS, Anand RB. Performance, emission and combustion characteristics of a diesel engine using carbon nanotubes blended jatropha methyl ester emulsions. Alexandria Eng J 2014; 53; 259–273.

[83] Basha JS, Anand RB. An experimental study in a CI engine using nanoadditive blended water–diesel emulsion fuel. Int J Green Energy 2011; 8; 332–348.

[84] Patton R, Steele P, Yu F. Coal vs. Charcoal-fueled diesel engines: A review. Energy sources, part a recovery, utilization, and environmental effects 2010; 32; 315–322.

[85] Reddy MH, Rohith M, Vinay P. The effect of orange peel powder extracts in diesel solution on exhaust gas emissions in compression ignition engine. Int J Mech Prod Eng 2013.

[86] Alsaleh A, Sattler, ML. Waste tire pyrolysis influential parameters and product properties. Renew Sust Energ Rev 2014; 1: 120–129.

[87] Martinez JD, Puy N, Murillo R, Garcia T, Navarro, MV, Mastral AM. Waste tire pyrolysis-a review. Excellent review of tire pyrolysis studies concerning factors impacting distribution of gas, liquid, and solid phase pyrolysis products and their physical/chemical properties. Renew Sust Energ Rev 2013; 23:179–213.

[88] Sharuddin SDA, Abnisa F, Ashri WM, Daud W, Aroua MK. A review on pyrolysis of plastic wastes. Energ Convers Manage 2016; 115: 308–326.

[89] Nhlanhla, Nkosi, Edison, Muzenda. A review and discussion of waste tyre pyrolysis and derived products. Proceedings of the World Congress on Engineering Vol II, 2014.

[90] Chaala A, Darmstadt H, Roy C. Acid-base method for the demineralization of pyrolytic carbon. Fuel Process Technol 1996; 46: 1–15.

[91] Wamankar AK, Murugan S. Experimental investigation of carbon black water diesel emulsion in a stationary DI diesel engine. Fuel Process Technol 2014; 125: 258–266.

[92] Wamankar AK, Murugan S. Combustion, performance and emission of a diesel engine fuelled with diesel doped with carbon black. Energy 2015; 86: 467–475.

[93] Shah J, Jan RM, Mabood F, Shahid M. Conversion of waste tyres into carbon black and their utilization as adsorbent. J Chin chemical Soc 2006; 53: 1085–1089.

[94] Wamankar AK, Murugan S. DI diesel engine operated with carbon-black-water-diesel slurry at different injection timing and nozzle opening pressure. J Energ Inst 2015; 1–14.

[95] Basics of X-ray Diffraction, Thermo ARL, ARL Applied Research Laboratories S.A., Thermo ARL-CH publication.

[96] Pilusa J, Muzenda E. Beneficiation of pyrolitic carbon black. International journal of chemical, nuclear, metallurgical and materials engineering 2013; 7: 1–10.

[97] Calderon L, Fernando, Schmitt, Veronique, Bibette, Jerome. Emulsion science basic principles. Springer publication, 2007.

[98] http://www.molecularrecipes.com/emulsions/emulsion-types

[99] http://petrowiki.org/Stability of oil emulsions

[100] Strassner, JE. Effect of pH on Interfacial Films and Stability of Crude Oil-Water Emulsions. J Pet Technol 1968, 20: 303–312.

[101] Cassiday L. Emulsions: making oil and water mix 2014. http://www.aocs.org

[102] Reddy CP. Studies on droplet size measurement and engine performance usingnon-edible oils as alternate fuels, National Confrence on IC Engine and Combu, 1994; 197–204.

[103] Measuring Zeta Potential Laser Doppler Electrophoresis, Technical note. www.malvern.co.uk

[104] http://laser.spbu.ru/en/research-eng/dzeta-eng.html

[105] Swain P, Panda D. Rheology of coal-water mixture. Fuel Sci Technol 1996; 9: l–14.

[106] Mishra SK, Senapati PK, Panda D. Rheological behavior of coal-water slurry. Energy Sources 2010; 24: 159-167.

[107] Ting AP, Luebbers RH. Viscosity of suspensions of spherical and other isodimensional particles. AIChE Journal 2004; 3: 111–116.

[108] Ugwu KE, Ofomatah AC, Eze SI. Influence of solid concentration on the flow characteristics and settling rate of coal-water slurries. Journal of Energy and Natural Resources 2013; 2: 21–24.

[109] https://en.wikipedia.org/wiki/Data_acquisition

[110] Shahabuddinn M, Liaquat AM, Masjuki HH, Kalam MA, Mofijur M. Ignition delay, combustion and emission characteristics of diesel enginefueled with biodiesel. Renew Sust Energ Rev 2013; 21: 623–632.

[111] Belagura VK, Chitiminib VR. Influence of static injection timing on combustion, emission and performance characteristics of DI diesel engine fuelled with honge oil methyl ester. International Journal of Ambient Energy 2012; 33: 65–74.

[112] http://www.redpowermagazine.com/forums/topic/52088-what-is-static-timing.

[113] Murugan S, Ramaswamy MC, Nagarajan G. A comparative study on the performance emission and combustion studies of a DI diesel engine using distilled tyre pyrolysis oil–diesel blends. Fuel 2008; 87: 2111–2121.

[114] Pundir BP. IC Engines: Combustion and Emissions. Alpha Science International Limited, Publication 2010; 1-504.

[115] Applied thermal engineering, Unit-7 IC engine testing.

[116] Appendix 1 Technologies available for measuring NOX. http://uk-air.defra.gov.u

[117] www.avl.com/-/avl-smoke-meter

[118] Coleman HW, Steele JWG. Experimentation and uncertainty analysis for engineers. John Willey & Sons 2nd ed. New York: 1989.

[119] Nwafor OMI, Rice G, Ogbonna AI. Effect of advanced injection timing on the performance of rapeseed oil in diesel engines. Renew Energ 2000; 21: 433–444.

[120] Hariram V, Mohan GK. The effect of injection timing on combustion, performance and emission parameters with AOME blends as a fuel for compression ignition engine. European Journal of Scientific Research 2012; 79: 653–665.

[121] Mani M, Nagarajan G. Influence of injection timing on performance, emission and combustion characteristics of a DI diesel engine running on waste plastic oil. Energy 2009; 34: 1617–1623.

[122] Rakopoulos CD, Antonopoulos KA, Rakopoulos DC. Development and application of multi-zone model for combustion and pollutants formation in direct injection diesel engine running with vegetable oil or its bio-diesel. Energ Convers Manage 2007; 48: 1881–1901.

[123] Ganesan, V. Computer simulation of Compression-Ignition engine processes, University Press(India) Ltd., Hyderabad, India, 2000.

[124] Patil S. Thermodynamic modelling for performance analysis of compression ignition engine fuelled with biodiesel and its blends with diesel. International Journal of Recent Technology and Engineering 2013; 1: 134–138.

[125] Awad S, Varuvel EG, Loubar K, Tazerout M. Single zone combustion modeling of biodiesel from wastes in diesel engine. Fuel 2013; 106: 558–568.

[126] Rakopoulos CD, Antonopoulos KA, Rakopoulos DC, Hountalas DT. Multi-zone modeling of combustion and emissions formation in DI diesel engine operating on ethanol–diesel fuel blends. Energ Convers Manage 2008; 49: 625–643.

[127] Rakopoulos CD, Antonopoulos KA, Rakopoulos DC. Multi-zone modeling of diesel engine fuel spray development with vegetable oil, bio-diesel or diesel fuels. Energ Convers Manage 2006; 47: 1550–1573.

[128] Rakopoulos CD, Kosmadakis GM, Pariotis EG. Critical evaluation of current heat transfer models used in CFD in-cylinder engine simulations and establishment of a comprehensive wall-function formulation. Appl Energ 2010; 87: 1612–1630.

[129] Harch CA, Rasul MG,. Hassan NMS, Bhuiya MMK. Modelling of engine performance fuelled with second generation biodiesel. Procedia Engineering 2014; 90: 459–465.

[130] Ottikkutti P, Gerpen JV, Cui KR. Multizone modeling of a fumigated diesel engine, SAE 1991; 1–21.

[131] Ramos JI. Internal Combustion Engine Modeling, Hemisphere Publishing Corporation, New York, 1989.

[132] Sahin Z, Durgun O. Multi-zone combustion modeling for the prediction of diesel engine cycles and engine performance parameters. Appl Therm Eng 2008; 28: 2245–2256.

[133] Lakshminarayanan PA, Aghav YV. Modelling diesel combustion, Pg. 59, Mechanical engineering series, DOI 10.1007/978-90-481-3885-2_5, Springer, New York, London; 2009.

[134] Lakshminarayanan PA, Aghav YV. Modelling diesel combustion, Pg.79, Mechanical engineering series, DOI 10.1007/978-90-481-3885-2_6, Springer, New York, London; 2009.

[135] Way RJB. Methods for determination of composition and thermodynamic properties of combustion products for internal combustion engine calculations. Proceedings of the Institute of Mechanical Engineers 1977; 190: 687–697.

[136] Lavoie GA, Heywood JB, Keck JC. Experimental and theoretical study of nitric oxide formation in internal combustion engines. Combustion Science and Technology 1970; 1: 313–326.

[137] Hiroyasu H, Yoshimatsu A, Arai M. Mathematical model for predicting the rate of heat release and exhaust emissions in IDI diesel engines. In Diesel Engines for Passenger Cars and Light Duty Vehicles, Institute of Mechanical Engineers, paper 1982; 102: 207–213.

[138] Bari S, Yu CW, Lim TH. Effect of fuel injection timing with waste cooking oil as a fuel in a direct injection diesel engine. Proceedings of the institution of mechanical engineers Part D Journal of automobile engineering 2004; 218: 93–104.

[139] Agarwa AK, Srivastava DK, Dhar A, Maurya RK, Shukla PC, Singh AP. Effect of fuel injection timing and pressure on combustion, emissions and performance characteristics of a single cylinder diesel engine. Fuel 2013; 111: 374–383.

[140] Roberts M. Benefits and challenges of variable compression ratio (VCR), Paper Number 03P-227, SAE 2002.

[141] Brevick JE. Variable compression ratio piston. US Patent 5755192, 1998-05-26.

[142] Aoyama S, Fujimoto H, Moteki K. Variable compression ratio mechanism of reciprocating internal combustion engine. European Patent 1170482, 2002-01-09.

[143] Saito T, Daisho Y, Uchida N, Ikeya N. Effects of combustion chamber geometry on diesel combustion. SAE Technical Paper 861186, 1986, doi:10.4271/861186.

[144] Lin L, Shulin D, Jin X, Jinxing W, Hong GX. Effects of combustion chamber geometry on in-cylinder air motion and performance in DI diesel engine. SAE Technical Paper 2000-01-0510, 2000, doi:10.4271/2000-01-0510.

[145] Rajan K, Senthil Kumar KR. Performance and emissions characteristics of a diesel engine with internal jet piston using biodiesel. Int J Environ Stud 2010; 67: 557–566.

[146] Konno M, Chikashisa T, Murayama T. Reduction of smoke and NOx by strong turbulence generated during the combustion process in DI diesel engine. SAE Technical Paper 920467, 1992, doi:10.4271/920467.

[147] Bharathi Pratiba VV, Prasanthi G. Influence of in cylinder air swirl on diesel engine performance and emission. Int J Appl Eng Technol 2011; 1: 113–118.

[148] Kamimoto T, Osaka S, Matsuoka S. An air cell DI diesel engine and its soot emission characteristics. SAE Technical Paper 831297, 1983, doi:10.4271/831297.

[149] Kurtz EM, Foster DE. Exploring the limits of improving DI diesel engine emissions by increasing in-cylinder mixing. SAE Technical Paper 982677, 1998, doi:10.4271/982677.

[150] Montajir R, Tsunemoto H, Minami T. Fuel spray behavior in a small DI diesel engine: effect of combustion chamber geometry. SAE Technical Paper 2000-01-0946, 2000, doi:10.4271/2000-01-0946.

[151] Jaichandar S, Annamalai K. Influences of re-entrant combustion chamber geometry on the performance of Pongamia biodiesel in a DI diesel engine. Energy 2012; 44: 633–640.

[152] Senthil MK, Ramesh A, Nagalingam B. Complete vegetable oil fueled dual fuel compression ignition engine. SAE: paper no: 2001-28-0067.

[153] Balamurugan T, Nalini R. Experimental investigation on performance, combustion and emission characteristics of four stroke diesel engine using diesel blended with alcohol as fuel. Energy 2014; 78: 356–363.

[154] Muralidharan K, Vasudevan D, Sheeba KN. Performance, emission and combustion characteristics of biodiesel fuelled variable compression ratio engine. Energy 2011; 36: 5385–5393.

[155] Behera P, Murugan S. Combustion, performance and emission parameters of used transformer oil and its diesel blends in a DI diesel engine. Fuel 2013; 104: 147–154.

[156] Mohammed ELK, Medhat A, Nemit-allah. Experimental investigations of ignition delay period and performance of a diesel engine operated with Jatropha oil biodiesel. Alexandria Engineering Journal 2013; 52: 141–149.

[157] Mani M, Subash C, Nagarajan G. Performance, emission and combustion characteristics of a di diesel engine using waste plastic oil. Appl Therm Eng 2009; 29: 2738–2744.

[158] Elango T, Senthil TK. Combustion and emission characteristics of a diesel engine fuelled with Jatropha and diesel oil blends. Therm Sci 2011; 15: 1205–1214.

[159] Subramanian KA, Ramesh A. Experimental investigation on the use of water diesel emulsion with oxygen enriched air in a DI diesel engine. SAE Paper 2001: 201–205.

[160] Prakash R, Singh RK, Murugan S. An experimental investigation on a diesel engine fueled by biodiesel and its emulsions with wood pyrolysis oil. Int J Green Energy 2013; 9: 749–765.

[161] Mendera KZ, Spyra A, Smereka M. Mass fraction burned analysis. Journal of KONES Internal Combustion Engines 2002.

[162] Prabhahar M. Experimental studies on biodiesel (Pongamia Oil) fuelled direct injection diesel engine with different techniques. 2012.

[163] Sastry GRK. Bio-diesel: dio-degradable alternative fuel for diesel engine. Read worthy publication Ltd. 2008.

[164] Prabhu L, Sathish SK, Prabhahar M, Rajan K. Combustion, performance and emission characteristics of diesel engine with neem oil methyl ester and its diesel blends. Am J Appl Sci 2013; 10: 810–818.

[165] Ibrahim TN. Experimental study of vegetable oil diesel blends on the performance of compression ignition engine. J Eng Sci 2011; 4: 33–44.

[166] Altun S, Bulut H, Cengiz O. The comparison of engine performance and exhaust emission characteristics of sesame oil–diesel fuel mixture with diesel fuel in a direct injection diesel engine. Renew Energ 2008; 33: 1791–1795.

[167] Devan PK, Mahalakshmi NV. Study of the performance, emission and combustion characteristics of a diesel engine using poon oil-based fuels. Fuel Process Technol 2009; 90: 513–519.

[168] Ramadhas AS, Jayaraj S, Muraleedharan C. Characterization and effect of using rubber seed oil as fuel in the compression ignition engines. Renew Energ 2005; 30: 795–803.

[169] Rao GLN, Sampath S, Rajagopal K. Experimental studies on the combustion and emission characteristics of a diesel engine fuelled with used cooking oil methyl ester and its diesel blends. International Journal of Mechanical, Aerospace, Industrial, Mechatronic and Manufacturing Engineering 2008; 2: 90–96.

[170] Rao PS, Srinivas K. Experimental analysis of single cylinder diesel engine fuelled with Methyl Ester of Palm Kernel oil blending with eucalyptus oil. International Journal of Engineering Research and Applications 2012; 2: 90–95.

[171] Venkatraman M, Devaradjane G. Effect of compression ratio injection timing and injection pressure on a DI diesel engine for better performance and emission fueled with diesel diesel biodiesel blends. Int J Appl Eng Res 2010; 1: 288–298.

[172] Xue J, Grift TE, Hansen AC. Effect of biodiesel on engine performances and emissions. Renew Sust Energ Rev 2011; 15: 1098–1116.

[173] Banapurmatha NR, Tewaria PG and Hosmath RS. Performance and emission characteristics of a DI compression ignition engine operated on Honge, Jatropha and Sesame oil methyl esters. Renew Energ 2008; 33: 1982–1988.

[174] Sahoo PK and Das LM. Combustion analysis of Jatropha, Karanja and Polanga based biodiesel as fuel in a diesel engine. Fuel 2009; 88: 994–999.

[175] Caresana F. Impact of biodiesel bulk modulus on injection pressure and injection timing. Fuel 2011; 90: 477–485.

[176] Seppo AN, Tommi PJP, Mika JL. Effect of injection timing, EGR and EGR cooling on the exhaust particle number and size distribution of an off-road diesel engine. SAE 1998.

[177] Gumus M, Sayin C, Canakci M. Effect of fuel injection timing on the injection, combustion, and performance characteristics of a direct-injection (DI) diesel engine fueled with canola oil methyl esterifies diesel fuel blends. Energy fuels 2010; 24: 3199–3213.

[178] Yadav SPR, Saravanan, Kannan M. Influence of injection timing on DI diesel engine characteristics fueled with waste transformer oil. Alexandria Engineering Journal 2015.

[179] Kannan GR, Anand R. Effect of injection pressure and injection timing on DI diesel engine fuelled with biodiesel from waste cooking oil. Biomass Bioenergy 2012; 46: 343–352.

[180] Sathish Kumar PS, Mahalingam S. Effect of injection timing on performance and emission analysis of single cylinder diesel engine fuelled with dual bio-fuels. International Journal of Advanced Mechanical Engineering. 4; 2014: 487–496.

[181] Lakshmanan T, Nagarajan G. Experimental investigation of timed manifold injection of acetylene in direct injection diesel engine in dual fuel mode. Energy. 2010; 35: 3172–3178.

[182] Pandian M, Sivapirakasam SP, Udayakumar M. Influence of injection timing on performance and emission characteristics of naturally aspirated twin cylinder CIDI engine using bio-diesel blend as fuel. International Journal of Recent Trends in Engineering 2009; 1: 113–117.

[183] Challen B, Baranescu R. Diesel Engine Reference Book, Butterworth and Heinemann Publishing, England, 1999.

[184] Sequera AJ, Parthasarathy RN and Gollahalli SR. Effects of fuel injection timing in the combustion of biofuels in a diesel engine at partial loads. Journal of energy resources technology 133; 2011.

[185] Sayin C, Ilhan M, Canakci M, Gumus M. Effect of injection timing on the exhaust emissions of a diesel engine using diesel methanol blends, Renew. Energy 2009; 34: 1261–1269.

[186] Zuohua H. Combustion behaviors of a compression ignition engine fuelled with diesel/ methanol blends under various fuel deliveries advance angles. Int J Bio Res Tech 2004; 95: 331–341.

[187] Chiosa A, Scarpete D, Buturca RC. An overview on combustion and performance characteristics of diesel engine using diesel-water emulsion. Termotehnica Supliment 2013; 1: 102–107.

[188] Prakash R, Singh RK, Murugan S. Experimental studies on combustion, performance and emission characteristics of diesel engine using different biodiesel bio oil emulsions. J Energ Inst 2014; 88: 64–75.

[189] Salmani MH, Rehman S, Zaidi K , Hasan AK. Study of ignition characteristics of microemulsion of coconut oil under off diesel engine conditions. Engineering Science and Technology, an International Journal 2015; 18: 318–324.

[190] Kannan GR, Anand R. Experimental investigation on diesel engine with diestrol-water micro emulsions. Energy 2011; 36: 1680–1687.

[191] Singh NK. Experimental investigations of diesel emulsions as fuel in small direct injection compression ignition engines. Int J Mech Eng 2012; 2: 39–44.

[192] Murugan S, Ramaswamy MC, Nagarajan G. The use of tyre pyrolysis oil in diesel engines. Waste Management 2008; 28: 2743–2749.

[193] Sadhik Basha J, Anand RB. Effects of nanoparticle blended water–biodiesel emulsion fuel on working characteristics of a diesel engine. J Global Warming 2010; 2: 330–346.

[194] Alahmer A, Yamin J, Sakhrieh A, Hamdan MA. Engine performance using emulsified diesel fuel. Energ Convers Manage 2010; 51: 1708–1713.

[195] Chauhan BC, Kumar N, Jun YD, Lee KB. Performance and emission study of preheated Jatropha oil on medium capacity diesel engine. Energy 2010; 35: 2484–2492.

[196] Odaka M, Koike N, Tsukamoto Y, Kazuysawa, Koichi Y. Effects of EGR with a supplemental manifold water injection to control exhaust emissions from heavy-duty diesel powered vehicles. Society of Automotive Engineers. SAE 910739, 1991.

[197] Nadeem M, Rangkuti C, Anuar K, Haq MRU, Tan IB, Shah SS. Diesel engine performance and emission evaluation using emulsified fuels stabilized by conventional and surfactant. Fuel 2006; 85: 2111–2119.

[198] Li-ming X, Xing-hu LI, Chu-jiang CAI, Zhi-gang SHEN. Performances and emissions of a petroleum coke oil slurry engine. J Cent South Univ 2012; 19: 3342−3350.

[199] Horlock JH, Winterbone DE. The Thermodynamics and Gas Dynamics of Internal Combustion Engines. Clarendon Press: Oxford, 1986.

[200] Ganapathy T, Gakkhar RP, Murugesan K. Influence of injection timing on performance, combustion and emission characteristics of Jatropha biodiesel engine. Appl Energ 2011; 88: 4376–4386.

[201] Scarpete ED. Diesel-water emulsion, an alternative fuel to reduce diesel engine emissions a review. Journal of Machines, technologies Materials 2013; 7: 13–16.

[202] Raheman H, Ghadge SV. Performance of diesel engine with biodiesel at varying compression ratio and ignition timing. Fuel 2008; 87: 2659–2666.

[203] Alahmer A. Influence of using emulsified diesel fuel on the performance and pollutants emitted from diesel engine. Energ Convers Manage 2013; 73: 361–369.

[204] Zhang G, Qiao X, Miao X, Hong J, Zheng J. Effects of highly dispersed spray nozzle on fuel injection characteristics and emissions of heavy-duty diesel engine. Fuel 2012; 102: 66–73.

[205] Kannan GR, Anand R. Experimental evaluation of DI diesel engine operating with diestrol at varying injection pressure and injection timing. Fuel Process Technol 2011; 92: 2252–2263.

[206] Abdel-Rahman AA. On the emissions from internal-combustion engines. Int. J. Energy Research 2002; 22: 483–513.

[207] Gumus M, Sayin C, Canakci M. The impact of fuel injection pressure on the exhaust emissions of a direct injection diesel engine fueled with biodiesel–diesel fuel blends. Fuel 2012; 95: 486–494.

[208] Prasad PV, Prasad BD, Prakash RH. Effect of injection timing on performance and emission characteristics of 4S-single cylinder DI diesel engine using PME blend as fuel. International Journal of Engineering Research & Technology 2013; 2: 3201–3207.

[209] Canakci M. Idealized engine emissions resulting from the combustion of isooctane supplemented with hydrogen. MSc Thesis, Vanderbilt University, Tennessee 1996.

[210] Armas O, Ballesteros R, Martos FJ, Agudelo JR. Characterization of light duty diesel engine pollutant emissions using water emulsified fuel. Fuel 2005; 84: 1011–1018.

[211] Canakci M. Combustion characteristics of a turbocharged DI compression ignition engine fueled with petroleum diesel fuels and biodiesel. Bioresource Technolo 2007; 98: 67–75.

[212] Muralidharan K, Vasudevan D. Performance, emission and combustion characteristics of a variable compression ratio engine using methyl esters of waste cooking oil and diesel blends. Appl Energ 2011; 88: 3959–3968.

[213] Mohammed ELK, Medhat AN. Studying the effect of compression ratio on an engine fuelled with waste oil produced biodiesel/diesel fuel. Alexandria Engineering Journal 2013; 52: 1–11.

[214] Sukumar P, Jegan R, Balasubbramanian K, Nagarajan G. Effect of injection pressure on performance, emission and combustion characteristics of high linolenic linseed oil methyl ester in a DI diesel engine. Renew Energy 2009; 34: 1227–1233.

[215] Senthilkumar R, Manimaran R. Performance, emission, combustion, compression ratio, injection timing and injection pressure on a single cylinder CI engine operated with mahua methyl ester. Int J Engi Sci Res Technol 2014; 3: 387–399.

[216] Selvan VAM, Anand RB, Udayakumar M. Combustion characteristics of diesohol using biodiesel as an additive in a direct injection compression ignition engine under various compression ratios. Energy Fuels 2009; 23: 5413–5422.

[217] Sharma R, Singh RR, Vishwakarma SK. Experimental study of the effect of fuel injector nozzle holes on direct injection diesel engine. J Mech Civil Eng 2013; 7: 67–74.

[218] Hirkude J, Padalkar AS. Experimental investigation of the effect of compression ratio on performance and emissions of CI engine operated with waste fried oil methyl ester blend. Fuel Process Technol 2014; 128: 367–375.

[219] Kassaby MEL, Nemit_allah MA. Studying the effect of compression ratio on an engine fuelled with waste oil produced biodiesel/diesel fuel. Int J Amb Energ 2013; 52: 1–11.

[220] Jaichandar S, Annamalai K. Combined impact of injection pressure and combustion chamber geometry on the performance of a biodiesel fueled diesel engine. Energy 2013; 55: 330–339.

[221] Subba Reddy CV, Eswara Reddy C, Hemachandra Reddy K. Effect of fuel injection pressures on the performance and emission characteristics of diesel engine with biodiesel blends cotton seed oil methyl ester. IJRRAS 2012; 13: 139–149.

[222] Bora BJ, Saha UK, Chatterjee S, Veer V. Effect of compression ratio on performance combustion and emission characteristics of a dual fuel diesel engine run on raw biogas. Energ Convers Manage 2014; 87: 1000–1009.

[223] Radivoje B, Pesic S, Milojevi T, Stevan P, Veinovi. Benefits and challenges of variable compression ratio at diesel engines. Therm Sci 2010; 14: 1063–1073.

[224] Venkanna BK, Wadawadagi SB, Venkataramana Reddy C. Effect of Injection Pressure on Performance, Emission and Combustion Characteristics of Direct Injection Diesel Engine Running on Blends of Pongamia Pinnata Linn Oil (Honge oil) and Diesel Fuel. CIGRE Journal 2009; 6: 1–17.

[225] Anbazhagan R, Srinivasan V. Effect of compression ratio on performance and exhaust emission characteristics of diesel engine powered by Jatropha curcas oil. J Inno Resea Sol 2013; 1: 9–15.

[226] Cenk S, Gumus M. Impact of compression ratio and injection parameters on the performance and emissions of a DI diesel engine fueled with biodiesel-blended diesel fuel. Appl Therm Eng 2011; 31: 3182–3188.

[227] Hariharan VS, Vijayakumar Reddy K. Effect of injection pressure on diesel engine performance with Sea lemon oil. Indian Journal of Science and Technology 2011; 4: 907–909.

[228] Gnanamoorthi V, Devaradjane G. Effect of compression ratio on the performance, combustion and emission of DI diesel engine fueled with ethanol diesel blend. J Energ Insti 2015; 88: 19–26.

[229] Choi CY, Reitz RD. An experimental study on the effects of oxygenated fuel blends and multiple injection strategies on DI diesel engine emissions. Fuel 1999; 11: 03–17.

[230] Prabhahar M, Rajan K. Performance and combustion characteristics of a diesel engine with titanium oxide coated piston using Pongamia methyl ester. Journal of Mechanical Science and Technology 2013; 27: 1519–1526.

[231] Sameca N, Kegla B, Dibble RW. Numerical and experimental study of water/oil emulsified fuel combustion in a diesel engine. Fuel 2002; 81: 2035–2044.

[232] Rajan K, Senthil Kumar KR. Combustion and emission characteristics of a biodiesel fuelled diesel engine with the effect of thermal barrier coated internal jet piston. Second International Conference on Sustainable Energy and Intelligent System, Dr. M.G.R. University, Chennai, 2011; 184–189.

[233] Jaichandar S, Annamalai K. Effects of open combustion chamber geometries on the performance of pongamia biodiesel in a DI diesel engine. Fuel 2012; 98: 272–279.

[234] Rajashekhar CR, Chandrashekar TK, Umashankar C, Rajagopal HK. Studies on effects of combustion chamber geometry and injection pressure on biodiesel combustion. Transactions of the Canadian Society for Mechanical Engineering 2012; 36: 429–438.

[235] Prasad BVVSU, Sharma CS, Anand TNC, Ravikrishna RV. High swirl-inducing piston bowls in small diesel engines for emission reduction. Appl Energ 2011; 88: 2355–2367.

[236] Sivasami K, Selladurai V, Devadasan SR, Rajan K. Reduction of NOx and Smoke Emission with the effect of Biodiesel-Water Emulsion Mixture Fuel in a Diesel Engine. International Journal of Engineering and Technology 2013; 5: 4378–4387.

[237] Rajan K, Senthil Kumar KR. Reduction of NOx and smoke emission on a diesel engine with internal jet piston using bio-diesel with exhaust gas recirculation technique. Int J design Manuf Technol 2012; 6: 41–47.

CURRICULUM VITAE

ARUN KUMAR WAMANKAR

At. Post. Kolgaon,
Th. Dist. Betul-460001
Madhay Pradesh
Mail: arun.wamankar@gmail.com, wamankar_arun@yahoo.co.in
Contact No. : +91-9438503593(M).

Academic Qualifications

- Masters in Thermal engineering with C.G.P.A of 7.4 from National Institute of Technology, Rourkela Odisha, 2009.

- Bachelor Degree in Mechanical Engineering from Indira Gandhi engineering college Sagar (M.P.) affiliated by RGPV University with 65.6% in 2005.

Academic Experience

- Two years six months of teaching experience (09.07.2009–30.12.2011) as Assistant Professor in Department of Mechanical Engineering, Technocrats Institute of Technology Bhopal, M.P.

List of Patents files and Publications

(1) Patent

1) Inventors: Dr. S.Murugan and **Arun kumar Wamankar**
   Title: Process of Producing a Synthetic Fuel (Carbodiesel) from Carbon Black and Use the Same as an Alternative Fuel for CI (Diesel) Engines.
   Patent No.: Indian patent, File No. 213/ KOL/2013
2) Inventors: Dr. S.Murugan and **Arun kumar Wamankar**
   Title: An Emulsified fuel for Compression Ignition Engine.
   Patent No.: Indian patent, File No. 1019/KOL/2013

(2) International Journal

1) **Arun Kumar Wamankar**, S. Murugan. Experimental investigation of carbon black–water–diesel emulsion in a stationary DI diesel engine. **Fuel Processing Technology, Elsevier publication**, 125 (2014) 258–266.
2) **Arun Kumar Wamankar**, S. Murugan. Effect of injection timings on DI diesel engine fuelled with synthetic fuel blend. **Journal of Energy Institute, Elsevier publication**, 88 (2015) 406-413.

3) **Arun Kumar Wamankar**, S. Murugan. Combustion, performance and emission of a diesel engine fueled with diesel doped with Carbon black. **Energy, Elsevier publication**, 86 (2015) 467–475.
4) **Arun Kumar Wamankar**, S. Murugan. DI diesel engine operated with Carbon-black-water-diesel slurry at different injection timing and nozzle opening pressure. **Journal of Energy Institute, Elsevier publication**, DOI: 10.1016/j.joei.2015.04.003, 2015.
5) **Arun Kumar Wamankar**, S. Murugan. Review on Production, Characterisation and Utilisation of Solid fuels in Diesel Engines**. Renewable and Sustainable Energy Reviews, Elsevier publication**, 51 (2015) 249–262.
6) **Arun Kumar Wamankar**, S. Murugan. Combustion, performance and emission characteristics of a diesel engine with internal jet piston using carbon black- water- diesel emulsion. **Energy, Elsevier publication**, 91 (2015) 1030–1037.
7) **Arun Kumar Wamankar**, Ashok Kumar Satapathy, S. Murugan. Experimental investigation of the effect of compression ratio, injection timing & pressure in a DI diesel engine running on Carbon black-water-diesel emulsion. **Energy, Elsevier publication**, 93 (2015) 511–520.

(3) Papers published in proceedings of International conference

1) Vinay Shrivastava, Abhishek Jha, **Arun kumar Wamankar** and S. Murugan. Design and fabrication of small scale downdraft gasifier for power generation. **Procedia Engineering, Elsevier publication**, 51 (2013) 600–608.

(4) National Journal

1) Prashant Vyas, Satyashree Ghodke, **Arun Wamankar**. Carbon dioxide as a natural refrigerant: an overview. **Journal of Information, Knowledge and Research in Mechanical Engineering**, 01 (2011) 65 -72.
2) Prashant Vyas, Satyashree Ghodke, **Arun Wamankar**. Optimization of natural refrigerants carbon dioxide (R744) and ammonia (R717) in cascade refrigeration system using genetic algorithm. **Journal of Information, Knowledge and Research in Mechanical Engineering**, 01 (2011) 73-79.